


2010-01-01

Computer-Aided Detection Of Sleep Apnea And Sleep Stage Classification Using HRV And EEG Signals

Edson F. Estrada

University of Texas at El Paso, edsonfco@gmail.com

Follow this and additional works at: https://digitalcommons.utep.edu/open_etd

 Part of the [Biomedical Commons](#), [Electrical and Electronics Commons](#), [European Languages and Societies Commons](#), and the [Scandinavian Studies Commons](#)

Recommended Citation

Estrada, Edson F., "Computer-Aided Detection Of Sleep Apnea And Sleep Stage Classification Using HRV And EEG Signals" (2010). *Open Access Theses & Dissertations*. 2482.
https://digitalcommons.utep.edu/open_etd/2482

This is brought to you for free and open access by DigitalCommons@UTEP. It has been accepted for inclusion in Open Access Theses & Dissertations by an authorized administrator of DigitalCommons@UTEP. For more information, please contact lweber@utep.edu.

COMPUTER-AIDED DETECTION OF SLEEP APNEA AND SLEEP STAGE CLASSIFICATION USING HRV AND EEG SIGNALS

EDSON F. ESTRADA

Department of Electrical and Computer Engineering

APPROVED:

Homer Nazeran, Ph.D., Chair

Patricia A. Nava, Ph.D., Co-Chair

Scott Starks, Ph.D.

Humberto Ochoa, Ph.D.

Luis Carcoba, Ph.D.

Patricia D. Witherspoon, Ph.D.
Dean of the Graduate School

COMPUTER-AIDED DETECTION OF SLEEP APNEA AND SLEEP STAGE
CLASSIFICATION USING HRV AND EEG SIGNALS

By

EDSON F. ESTRADA, M.S. EE

DISSERTATION

Presented to the Faculty of the Graduate School of

The University of Texas at El Paso

In Partial Fulfillment

of the Requirements

for the Degree of

Doctor of Philosophy

Department of Electrical and Computer Engineering

THE UNIVERSITY OF TEXAS AT EL PASO

DICEMBER 2010

Acknowledgements

I would like to express my gratitude to the following people for their support and assistance in developing this dissertation.

I want to acknowledge the inspiration I received from my advisor, Dr. Homer Nazeran, who taught me by his example to strive for excellence in both teaching and research. I would have been lost without him. I owe a great deal of gratitude to my examiners, Dr. Patricia Nava, Dr. Scott Starks, Dr. Humberto Ochoa (external examiner) and Dr. Miguel Carcoba (external examiner) for immensely helpful comments, criticisms and suggestions. I want to thank the soon to be Dr. Gustavo Sierra for his time and interest in evaluating the scientific quality of my work. I am thankful to Ms. Juliette Caire and GEAR UP program for providing me with the opportunity to learn so many things working as a Research Assistant during my doctoral studies and let me be part of the GEAR UP Family over the last eight years. I would like to acknowledge support of CONACYT Scholarship for the support provided. I wish to thank friends Carlos Torres and Graciela Ramirez for helping me through the difficult times, and for all the emotional support, entertainment, and caring they provided. I am indebted to my UACJ colleagues for providing a stimulating and enjoyable work environment when navigating through the doctoral research work. I wish to thank Galindo's Family. They provided me a second family and gave all the possible support when I moved to El Paso and Juarez. I had a lot of fun with them. I am grateful to my brothers and my sister; they know we all together are realizing this dream. Lastly, and most importantly, I wish to thank my parents, Mario F. Estrada and Maria T. Meneses. They supported me incessantly throughout all these years; they have been my best teachers. They have taught me real life stuff. They have encouraged me in so many ways to pursue my life dreams. It is to them that I dedicate again this dissertation with heart-felt gratitude.

Quiero agradecer a mis padres, Ellos han sido mis mejores maestros, me han enseñado las cosas de la vida. Me alentaron de muchas maneras para alcanzar mis sueños. A ellos les dedico de nuevo esta disertación.

Abstract

Sleep is a circadian rhythm essential for human life. Many events occur in the body during this state. In the past, significant efforts have been made to provide clinicians with reliable and less intrusive tools to automatically classify the sleep stages and detect apnea events. A few systems are available in the market to accomplish this task. However, sleep specialists may not have full confidence and trust in such systems due to issues related to their accuracy, sensitivity and specificity. The main objective of this work is to explore possible relationships among sleep stages and apneic events and improve on the clinical accuracy, sensitivity and specificity of algorithms for sleep classification and apnea detection. Electroencephalograms (EEGs) and Heart Rate Variability (HRV) signals will be assessed using advanced signal processing approaches. In this research work, we present a compendium of features extracted from EEG and Heart Rate Variability (HRV) data acquired from twenty five patients (21 males and 4 females) suffering from sleep apnea (age: 50 ± 10 years, range 28-68 years undergoing polysomnography). Polysomnographic data were available online from the Physionet database. Results show that trends detected by these features could distinguish between different sleep stages at a very significant level ($p < 0.01$). This study showed that inclusion of HRV features as inputs to the classifier system increased the performance of the ANN system by improving the accuracy by 5.8 % when considering data from all 25 subjects whereas for sensitivity, specificity, and geometric mean the increments were 7.5%, 2.1%, and 5.2% respectively. The work presented here contributes to the ultimate goal of the project, which is to find novel and more reliable tools to assess sleep quality and sleep breathing disorders by means of less invasive techniques requiring minimal number of sensors.

Table of Contents

Acknowledgements	iii
Abstract	v
List of tables.....	xi
List of figures.....	xii
Chapter 1. Introduction to Sleep Stage Classification and Sleep Apnea.....	1
1.1 Sleep.....	1
1.2 Polysomnogram and Biosignals.....	1
1.3 Electroencephalogram.....	2
1.3.1 Brain Rhythms.....	4
1.3.2 Sleep Stages and R & K Rules.....	5
1.3.3 American Academy of Sleep Medicine 2007 Sleep Scoring Manual.....	7
1.4 Electrocardiogram.....	8
1.4.1 The ANS and its Influence on Hear Rate.....	11
1.4.2 Hear Rate Variability.....	11
1.5 Sleep Disorders.....	12
1.5.1 Sleep Apnea.....	13
1.5.2 Apnea-Hypopnea Index.....	14
Chapter 2. Research Topic.....	16
2.1 Problem Definition.....	16
2.2 Significance.....	16
2.3 Hypothesis, Research Question Variables.....	20
2.4 Objective.....	20
2.5 Proposed Solution.....	20

Chapter 3. Previous Work on EEG and HRV Feature Extraction and Sleep Stage

Classification.....	23
3.1 General Overview.....	23
3.2 EEG and HRV Feature Extraction.....	25
3.2.1 Relative Percent Spectral Energy Band (RPSEB).....	25
3.2.2 Hjorth Parameters.....	26
3.2.3 Harmonic Hjorth Parameters.....	27
3.2.4 Itakura Distance	28
3.2.5 Wavelets.....	29
3.2.6 Empirical Mode Decomposition.....	30
3.2.7 Nonlinear Features.....	32
3.2.7.1 Detrended Fluctuation Analysis (EEG and HRV)	32
3.2.7.2 Correlation Dimension (EEG and HRV).....	33
3.2.7.3 Approximate Entropy (EEG and HRV).....	34
3.3 HRV Features.....	35
3.3.1 Time Domain Features.....	35
3.3.2 Frequency Domain Features.....	35
Chapter 4. Materials and Biosignal Conditioning.....	37
4.1 Materials.....	37
4.2 EEG Filtering and Denoising.....	37
4.2.1 Discrete Wavelet Transform.....	38
4.2.2 Denoising.....	42
4.2.2.1 Threshold Filter.....	42
4.2.2.2 Threshold Value λ	43

4.2.2.3 Methods.....	44
4.2.2.4 Results.....	46
4.3 ECG Filtering and Denoising.....	47
Chapter 5. EEG Feature Extraction.....	48
5.1 Boxplots.....	48
5.2 Relative Percent Spectral Energy Band.....	49
5.2.1. Parameter Selection.....	51
5.3 Hjorth Parameters.....	51
5.3.1. Parameter Selection.....	52
5.4 Harmonic Parameters.....	52
5.4.1. Parameter Selection.....	53
5.5 Itakura Distance.....	53
5.5.1. Parameter Selection.....	55
5.6 Wavelets.....	55
5.6.1. Parameter Selection.....	56
5.7 Empirical Mode Decomposition.....	56
5.7.1 Parameters Selection.....	57
5.8 Detrended Fluctuation Analysis.....	57
5.8.1 Parameters Selection.....	58
5.9 Correlation Dimension.....	58
5.9.1 Parameter Selection.....	60
5.10 Approximate Entropy.....	61
5.10.1 Parameter Selection.....	61
Chapter 6. HRV Signal Derivation and HRV Features Extraction.....	62
6.1 Hear Rate Variability Signal Derivation.....	62

6.2 Time Domain Features.....	64
6.2.1 Parameter Selection.....	64
6.3 Frequency Domain Features.....	64
6.3.1 Parameter Selection.....	65
6.4 Nonlinear Features Parameters.....	65
6.4.1 Detrended Fluctuation Analysis.....	65
6.4.2 Correlation Dimension.....	65
6.4.3 Approximate Entropy.....	66
6.5 Results.....	67
Chapter 7. Relationship Between EEG and HRV Features.....	69
7.1 Correlation between EEG vs. EEG Features, EEG and HRV Features.....	69
7.2 EEG and HRV features vs. Sleep Stages.....	70
7.3 EEG and HRV Features vs. Respiratory Events by Sleep Stage.....	71
7.4 Results.....	73
Chapter 8. Neural Network Design.....	77
8.1 EEG and HRV Feature Preprocessing.....	77
8.1.1 Feature Smoothing.....	77
8.1.2 Feature Normalization.....	78
8.1.3 Principal Component Analysis.....	79
8.2 Neural Network Designing.....	79
8.2.1 Feedforward Artificial Neural Networks.....	79
8.2.2 Back Propagation.....	81
8.3 Experiment Design.....	82

8.4 Results.....	83
Chapter 9. Conclusions and Future Work.....	95
9.1 Conclusions.....	95
9.2 Future Directions.....	99
References.....	103
Acronym List.....	117
Appendix 1. Subjects.....	121
Appendix 2. EEG Sleep Stages Reflected in Brain Rhythms.....	131
Appendix 3. 44 Features Extracted from Subject 2.....	137
Appendix 4. 44 Features Extracted from all Subjects. Normalized values.....	145
Appendix 5. Correlation between Extracted Features.....	152
Appendix 6. EEG and HRV ANOVA One-way Analysis from Power Analysis.....	155
Appendix 7. Features Vs. Respiratory Events – Anova One-way.....	170
Vita.....	303

List of Tables

Table 1.1 R & K Rules.....	6
Table 1.2 R & K Rules and 2007 AASM Manual.....	8
Table 1.3 Apnea-Hypopnea Index.....	14
Table 4.1 Denoising Performances.....	46
Table 5.1 Spectral Energy Bands.....	51
Table 5.2 Parameters and Method Selected.....	51
Table 5.3 Parameters and Method Selected.....	52
Table 5.4 Parameters and Method Selected.....	53
Table 5.5 Parameters and Method Selected.....	55
Table 5.6 Parameters and Method Selected.....	56
Table 5.7 Parameters and Method Selected.....	57
Table 5.8 Parameters and Method Selected.....	58
Table 5.9 Parameters and Method Selected.....	60
Table 5.10 Parameters and Method Selected.....	61
Table 6.1 Parameter Selection.....	64
Table 6.2 Parameter Selection.....	65
Table 6.3 Parameter Selection.....	65
Table 6.4 Parameter Selection.....	65
Table 6.5 Parameter Selection.....	66
Table 7.1 Population of Extracted Features.....	68
Table 7.2 Power Analysis for Correlation Test.....	70
Table 7.3 Power Analysis for ANOVA Test (6 groups).....	71
Table 7.4 Power Analysis for ANOVA Test (3 Groups).....	72

Table 7.5 Features with Statistical Differences for all three Breathing Condition.....	75
Table 8.1 Codification of Sleep Stages AASM.....	80
Table 8.2 Training Confusion Matrix (25 Hidden Neurons).....	84
Table 8.3 Training Confusion Matrix (35 Hidden Neurons).....	84
Table 8.4 Training Confusion Matrix (35 Hidden Neurons-Smoothed Features-EEG+HRV Features).....	86
Table 8.5 Testing Confusion Matrix (35 Hidden Neurons-EEG+HRV Features).....	87
Table 8.6 Testing Confusion Matrix (35 Hidden Neurons-Smoothed Features-EEG+HRV Features).....	87
Table 8.7 Training Confusion Matrix (35 Hidden Neurons-Smoothed Features-Only EEG Features).....	89
Table 8.8 Testing Confusion Matrix (35 hidden neurons-smoothed features- Only EEG Features)....	89
Table 8.9 Training Confusion Matrix (All Subjects- 35 Hidden Neurons-Smoothed Features- EEG+HRV features).....	91
Table 8.10 Training Confusion Matrix (All Subjects- 35 Hidden Neurons-Smoothed Features-Only EEG Features).....	91
Table 8.11 Testing Confusion Matrix (All Subjects- 35 Hidden Neurons-Smoothed Features- EEG+HRV Features).....	92
Table 8.12 Testing Confusion Matrix (All Subjects- 35 Hidden Neurons-Smoothed Features-Only EEG Features).....	93
Table 8.13 Training Confusion Matrix (All Subjects- 35 Hidden Neurons-Smoothed Features- PCA EEG+HRV Features).....	94

List of Figures

Figure. 1.1 Piramydal neuron and generation of dipole.....	3
Figure 1.2 A) Frontal View of 10-20 EEG Electrode Placement System, B) Sagittal view.....	4
Figure 1.3 EEG Rhythms and Sleep Stages.....	5
Figure 1.4 The 12-lead Electrocardiogram Standard.....	8
Figure 1.5 A) Electric Conductive System of the Heart. B) The different waveforms for each of the specialized cells found in the heart are shown.....	10
Figure 1.6 PSN and SNS of heart's innervations.....	11
Figure 2.1 Proposed Methodology.....	22
Figure 4.1 a) DWT algorithm, b) IDWT algorithm.....	41
Figure 4.2 a) DWT tree, b) WPT tree.....	41
Figure 4.3 a) Hard thresholding, b) Soft thresholding.....	43
Figure 4.4 Denoising process based on DWT.....	45
Figure 4.5 EEG (right) and PSD (left). a) Original EEG, b) Noisy EEG, c) De-noised EEG.....	47
Figure 5.1 Visual representation of $C_m(r)$ integral in a tridimensional embedding space using the sphere counting method.....	60
Figure 6.1 HRV EHT Extraction.....	63
Figure 7.1 Exploratory experiment of relation among variables.....	68
Figure 7.2 the effect of the sample size on the power variable.....	70
Figure 7.4 the effect of the sample size on the power variable.....	71
Figure 7.4 the effect of the sample size on the power variable.....	72
Figure 7.5 Different Pearson correlation values. a) $r \sim 1$, b) $r \sim -1$ and c) $r = 0$	74
Figure 8.1 a) Raw feature b) Smoothed feature.....	78

Figure 8.2 a) Raw feature b) Smoothed feature.....	78
Figure 8.3 Feedforward Neural Network block diagram.....	80
Figure 8.4 ROC plots for training a) 25 hidden neurons, b) 35 hidden neurons.....	85
Figure 8.5 ROC plots for training 35 hidden neurons-smoothed features-EEG+HRV features.....	86
Figure 8.6 ROC plots for testing a) 35 hidden neurons-EEG+HRV features, b) 35 hidden neurons-smoothed features-EEG+HRV features.....	88
Figure 8.7 ROC plots for a) Training: 35 hidden neurons-smoothed features-Only EEG Features, b) Testing: 35 hidden neurons-smoothed features-Only EEG Features.....	90
Figure 8.8 ROC plots for training a) EEG+HRV features, b) Only EEG Features.....	92
Figure 8.9 ROC plots for testing a) EEG+HRV features, b) Only EEG Features.....	93
Figure 9.1 ANFIS target output vs. targeted training data (average testing error 0.3635).....	99
Figure 9.2 Probabilities of sleep stage change.....	100
Figure 9.3 Simulated hypnogram trial 1 (Stage 1=1, Stage 2=2, Stage 3=3, Stage 4=4, Awake=5, REM=6).....	101
Figure 9.4 Simulated hypnogram trial 2 (Stage 1=1, Stage 2=2, Stage 3=3, Stage 4=4, Awake=5, REM=6).....	101
Figure 9.5 Simulated hypnogram trial 3 (Stage 1=1, Stage 2=2, Stage 3=3, Stage 4=4, Awake=5, REM=6).....	102

Chapter 1. Introduction to Sleep Stage Classification and Sleep Apnea

1.1 Sleep

Sleep state is part of a circadian rhythm essential for human life. Many events occur in the body during this state: blood pressure decreases, the heart rate slows down, muscles enter a state of relaxation, and the body's metabolic rate decreases. This state is mainly characterized by reduction of body movements and a decreased alertness of environment. It is believed that this process provides the body the opportunity to repair muscles and other tissues, replace aging or dead cells, etc. Also, sleep stage gives the brain a chance to organize and fix memories. Dreams are thought to be a part of this process. The main difference between rest and sleep lies in the brain, which controls the sleep stage [1-3].

1.1 Polysomnogram and Biosignals

Polysomnography is a sleep disorder diagnostic test, performed in a sleep center where a large number of physiological variables are measured and recorded during sleep. Hence, the biosignals acquired provide an overall view of the body behavior during sleep. The recordings are scored offline by a qualified physician or sleep specialist technician to determine whether or not a person suffers from a sleep disorder. The raw biosignals, signals that are obtained directly by electrodes and then amplified, are comprised of: Electroencephalogram (EEG) for brain monitoring using the 10-20 standard positions for electrode placement, Electromyogram (EMG) to measure motor unit recruitment at the muscle level; Electrooculogram (EOG) for eye movements, and Electrocardiogram (ECG) which allows the assessment of heart function using the 12-lead standard technique. A variety of other biosignals are also recorded in

polysomnography, where tracings are acquired using more sensors such as thermoresistors or infrared sensors to derive more signals such as airflow, respiratory effort, oxygen saturation, temperature, and body position. A full review of an overnight polysomnography procedure may be found in [4].

1.2 Electroencephalogram

The electroencephalogram (EEG) reveals the electrical activity of the brain through placement of electrodes on the skull. The use of EEG in the field of medicine has been a very important marker in the detection of brain disorders such as epileptic seizure events and assessment of sleep disorders [5].

Unlike other biosignals such as EMG or ECG, EEG signals do not originate from the action potentials of the continuous polarization and depolarization of neurons. This is because the electrical activity of a single neuron cannot be measured noninvasively due to the presence and thickness of different tissue layers (fluids, bone, and skin) that attenuates the action potential's intensity as it travels to the electrode. EEG signals originate, and can be measured, from the coordinated (can also noncoordinated) activity of millions of cortical neurons that produce an electric field sufficiently large enough to be detected and amplified by the acquisition equipment.

This electric field is mainly formed by the dipoles caused by the currents flowing during the dendrites' presynaptic excitation and postsynaptic excitatory potentials (Fig. 1.1). Moreover, the generation of excitatory and inhibitory postsynaptic potentials (EPSPs and IPSPs respectively) occurs when specific postsynaptic receptors are activated by the release of excitatory and inhibitory neurotransmitters. Negative deflections or negative potentials at the cortical surface are directly related to EPSPs. A radially oriented dipole is created when the

EPSPs are generated as a result of excitatory synaptic inputs. Then, a closed current pathway is formed through the following elements: circuit cytoplasmic core of the dendrites, cell body of the cell, and the synaptic sites via the conducting extracellular medium. This current flow makes the extracellular medium surrounding the cell body to act as a source with positive polarity and the upper part of the apical dendritic tree to behave as a sink with negative polarity. Finally, positive deflections are related to IPSPs and therefore they are created by deep excitatory or superficial inhibitory inputs. [6]

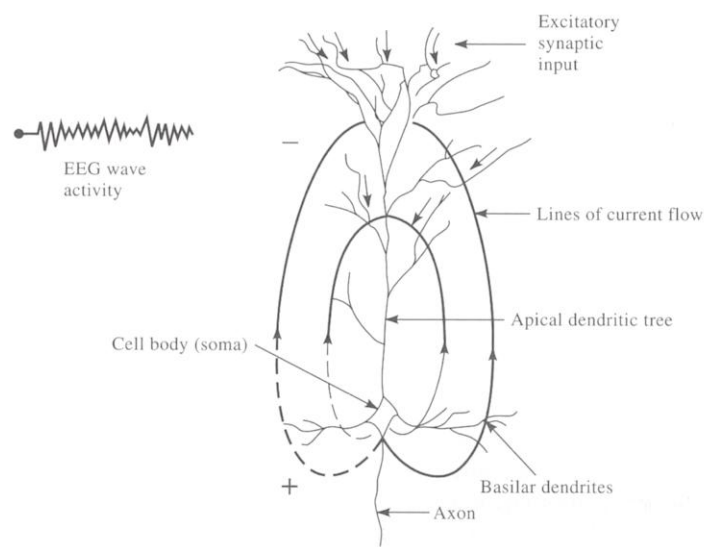


Figure. 1.1 Pyramidal neuron and generation of dipole.

Interestingly, the EEG amplitude is a result of the degree of synchronization in the cortical neurons and their respective excitatory fields. A spatio-temporal constructive collaboration is often referred to as a synchronous rhythm and large EEG amplitude. Similarly, waveforms of low amplitude are the result of a destructive collaboration or asynchronous behavior of pyramidal cells in the cortex.

Finally, this repetitive and stationary association of electric fields is referred as EEG rhythms; however, the frequency of EEG waveforms is also controlled by input from the

thalamus. This specific region of the brain is composed of pacemaker cells which possess an intrinsic capability to yield a self-supported firing pattern [5]. The 10-20 System or International 10-20 System is a globally recognized technique to describe and apply the location of scalp electrodes for EEG signal acquisition (Figure 1.2).

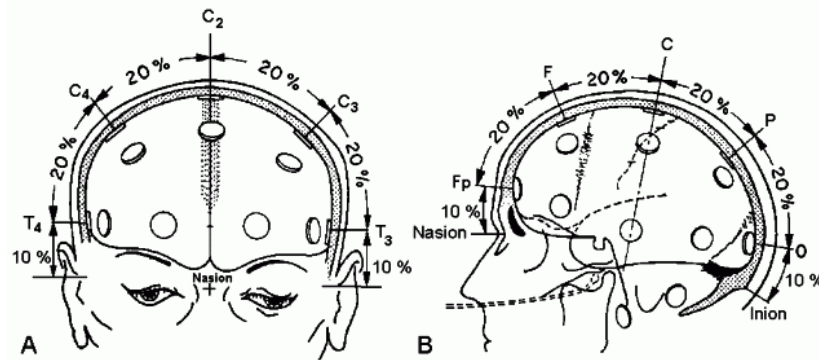


Figure 1.2 A) Frontal view of 10-20 EEG electrode placement system, B) Sagittal view.

The different types of EEG waveforms and their relationship with the sleep stages will be described in the following sections.

1.2.1 Brain Rhythms

Electric recordings from the exposed surface of the brain or from the outer surface of the head demonstrate continuous oscillating electric activity within the brain. The frequencies of brain waves and their characteristics are highly dependent on the degree of activity of the cerebral cortex [6-8]. Brain activity is divided into four main rhythms known as alpha, beta, theta, and delta waves. First, alpha waves occur during relaxed states with eyes closed. These are regular rhythms of 8 to 12 Hz with higher amplitudes than beta waves. Their amplitude is approximately 20 – 200 μV . Secondly, beta waves are defined as low voltage (around 5 μV) and high frequency waves (20 to 40 Hz). Then, theta waves are typically of even greater amplitude and slower frequency than alpha waves. Their frequency range is normally between 5 and 8 Hz.

Finally, delta rhythms which are the slowest EEG waves, generally have the highest amplitude EEG waveforms observed (about 300 μV) with a frequency range of 0.5 to 3 Hz. They occur in deep sleep. There are two other types of activities present on EEG recordings: K-complexes which are sharp, high voltage transient waves that occur spontaneously and last more than 0.5 seconds, and sleep spindle waves which are synchronized bursts of waves having a frequency of 12 to 15 Hz and last for 0.5 to 1.5 seconds (Figure 1.3).

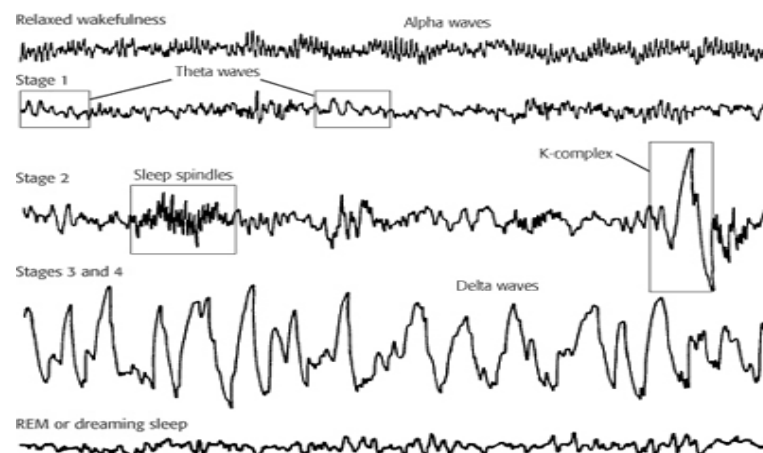


Figure 1.3 EEG Rhythms and Sleep Stages.

1.2.2 Sleep Stages and R & K Rules

In the early 1960's, the Association for the Psychophysiological Study of Sleep (APSS) created a committee of sleep researchers in order to create a standard system for visually scoring stages of sleep [9]. This standard was rapidly implemented after its publication in 1968 under the auspices of the UCLA Brain Information Service as 'A Manual of Standardized Terminology, Techniques and Scoring System for Sleep Stages of Human Subjects'. The R&K standardized scoring system was named after Alan Rechtschaffen and Anthony Kales, editors and co-chairpersons of the committee. The proposal to standardize recording techniques and scoring criteria was intended to increase the comparability of results reported by different investigators.

This method of scoring implies a visual screening on polysomnogram recordings, yielding an epoch-by-epoch approach. The standard time period of observation is 30 seconds for any tracing (e.g. EEG). The epoch-by-epoch approach does not imply that each epoch is considered in isolation. There are many cases where the stage assigned to a particular epoch depends in part on the polygraphic features of preceding and succeeding epochs.

Epoch classification depends mainly on EEG, EOG and EMG signals. Thus, the gold standard for sleep stage classification defines two groups for depth of sleep. First, Non-Rapid Eye Movement Stage (N-REM) that is sub-divided in four stages: Stage 1, Stage 2, Stage 3, and Stage 4. Second, Rapid Eye Movement Stage (REM), that has high ocular activity present in the EOG recordings. Table 1.1 summarizes the R&K standards, EEG and EOG rhythms as well as EMG electrical activity.

Table 1.1 R&K Rules.

	Stage	Awake	Stage 1	Stage 2	Stage 3	Stage 4	REM
Patterns							
EEG	Delta (0.5-4 Hz)	No	No	No	Yes 20%-50%	Yes More than 50%	No
	Theta (4-8 Hz)	No	Yes	Yes	No	No	No
	Alpha (8-12 Hz)	Yes	Yes	Yes	No	No	Yes
	Beta (12-40 Hz)	Yes	No	No	No	No	Yes
	Sleep spindles K-Complexes	No	No	Yes	Don't care	Don't care	No
EOG : REM Signal		Yes	Eye Slow Movements	No	No	No	Yes
EMG: Muscle Tone		Yes	Don't care	Don't care	Don't care	Don't care	No

According to R&K rules, there is a predominance of certain brain waves for each sleep stage, rather than a simple presence or absence of these rhythms. Appendix 2 shows the dominance of these brain waves for each sleep stage by the decomposition and reconstruction of

brain rhythms based on an analysis of Wavelet Packet Tree and the bank of filters that this method utilizes to obtain approximate and detail components for each level, as was done in [10].

1.2.3 American Academy of Sleep Medicine 2007 Sleep Scoring Manual

The Manual of Standardized Terminology, Techniques, and Scoring System for Sleep Stages of Human Subjects (R&K Rules) still works extremely well; however, an update and revision was long overdue. Forty seven years later, the American Academy of Sleep Medicine appointed task forces to review the current literature to strengthen standard associated with the five basic processes related to computerized polysomnography:

1. Data acquisition (recording)
2. Data display (viewing)
3. Data manipulation (scoring and editing)
4. Data reduction (parameters for reporting)
5. Data filing (storage)

Eight different task forces were assembled to address the various issues. These groups were required to follow certain philosophies: the rules should be compatible with published evidence, they should be based on biologic principles, they should be applicable to both normal and abnormal sleep, and they should be easy to use by clinicians, technologists, and scientists [11, 12].

The key changes in scoring include the following:

Table 1.2 R&K Rules and 2007 AASM Manual.

R & K	2007 AASM
Stage wake	Stage W
Stage 1	Stage N1
Stage 2	Stage N2
Stage 3	Stage N3
Stage 4	
REM	Stage R

As it can be observed that Stages 3 and 4 in the previous R&K rules were abbreviated to stage N3 in the new rules, as no physiologic or clinical basis exists for a difference between Stages 3 and 4. Also, the change in abbreviations is to distinguish between the old and the new classification systems.

1.3 Electrocardiogram

The Electrocardiogram (ECG) is a description of the electrical activity of the heart. This most popular biosignal is recorded by placing bioelectrodes on the body surface. Similar to EEG recording, different topologies are used to record the ECG signal. Moreover, the well-accepted standard 12-lead electrocardiogram is a representation of the heart's electrical activity recorded from different perspectives (Figure 1.4).

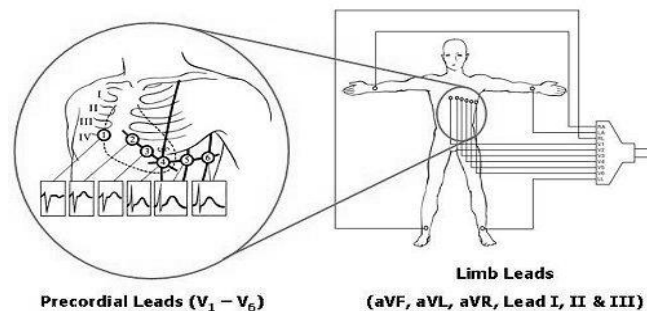


Figure 1.4 The 12-lead electrocardiogram standard.

In a formal description, the ECG is produced by the action potential of cardiac cells during the contraction of the heart, whose main function is to pump oxygenated blood throughout the body. To accomplish this purpose, the heart is divided into two mirrored-synchronized sides: the left and right sections. Each side consists of two chambers, the blood-reception chambers are known as the atria and the blood-propulsion chambers are known as the ventricles. The transfer of blood between the different chambers is controlled by specialized valves that are opened or closed during the synchronized contraction of the heart [5, 6].

In this sense, the ECG describes the different electrical phases of the cardiac cycle and the spatio-temporal superposition of the action potentials of millions of cardiac cells. Moreover, the activation of the muscular walls of the chambers of the heart is initiated by a series of electrical events through the specialized conduction system of the heart (Figure 1.5 A). This process is described as follows:

1. The rhythmic cardiac impulse originates in pacemaking cells in the sinoatrial (SA) node.
2. The electric impulse passes from the SA node to both atria in a synchronized fashion through specialized conducting pathways.
3. Thus, the impulse is conducted to the atrioventricular node (AV) throughout three specialized pathways known as: anterior, middle and posterior inter-nodal tracts.
4. Here the Bachmann's bundle originates from the anterior internodal tract leading to the left atrium.
5. Later on, the impulse conduction is delayed in the AV node before it continues into the Bundle of His.

6. Finally, the contraction of the ventricles is achieved by the conduction of the impulse through the right bundle branch, the common left bundle branch, the anterior and posterior division of the left bundle branch and the purkinje network.

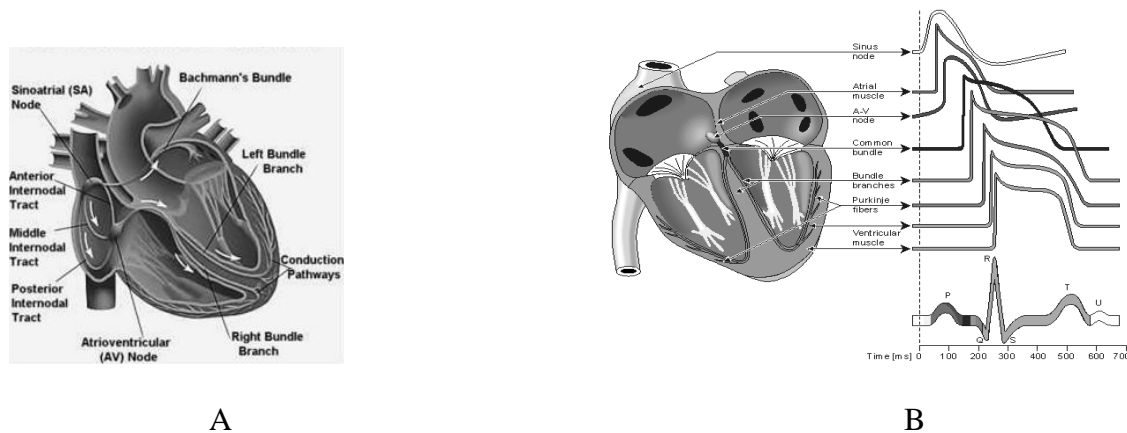


Figure 1.5 A) Electric conductive system of the heart. B) The different waveforms for each of the specialized cells found in the heart are shown.

The superposition of the action potentials generated from this process is known as the typical ECG waveform: the P-Q-R-S-T waveform (Figure 1.5 B). Where, the P wave is produced by atrial depolarization, the QRS complex primarily by the ventricular depolarization, and the T wave by ventricular repolarization.

Therefore, the frequency of heart pumping or heart rate (HR) may be defined as the number of P-Q-R-S-T waveforms packed in a period of time. Unlike other signals, HR is not expressed in Hertz frequency units but in beat-per-minutes (b.p.m.). This unit expresses the number of heart contractions during a one-minute period.

The SA node is the natural pacemaker, which determines the heart rate. However, SA firing rate is not only determined by its natural activation rate but also by the external control of the Autonomic Nervous System (ANS) and hormonal influences.

1.3.1 The ANS and its influence on Hear Rate

The Autonomic Nervous System is composed of two subsystems, which operate in an antagonistic fashion with each other: the sympathetic nervous system (SNS) which dominates when there is a demand for physical activity or stress and the parasympathetic nervous system (PNS), which governs during resting conditions [5].

Both subsystems innervate the same organs and regulate the correct balance of the internal organ environment such as the heart (Figure 1.6). Thus, the Heart Rate Variability signal (HRV) is the result of the antagonistic interactions between the two ANS subsystems.

The dynamic and smooth interplay between the parasympathetic and sympathetic ANS subsystems determines the modification of the "baseline" heart rate. Hence, an increment in activity of PNS will decrease the heart rate, whereas an increase in SNS activity will increase the heart rate.

The importance of studying and understanding the ECG has been improved with the design of new state-of-the-art technologies based on ECG's variability patterns.

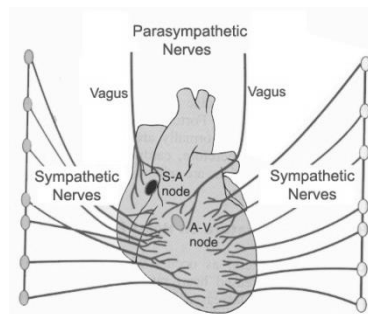


Figure 1.6 PSN and SNS heart's innervations.

1.3.2 Heart Rate Variability

In recent years, Heart Rate Variability (HRV) analysis has attracted a lot of interest in the medical research community due to its feasibility as an indicator and a promising noninvasive

marker to understand and monitor the activity or status of the autonomous nervous system (Parasympathetic and Sympathetic nervous systems). Moreover, signal processing of the HRV and features extracted from this signal have been used to identify various cardiac-related diseases [13]. Detection of apnea events from the HRV signal have also been explored [14, 15].

The HRV signal is derived from the raw ECG signal by accurate detection of the QRS complexes. It is comprised of detecting the time interval between successive R-peaks. The raw peak-to-peak measurement (R-R, sometimes called N-N) interval is then used for time domain and nonlinear analysis. As R-R peaks do not occur at evenly-spaced time periods, there is a need to interpolate the raw signal and apply uniform sampling when a frequency domain analysis is to be carried out.

Time domain analysis of the HRV signal yields statistical information about heart rate tendencies such as: Maximum, minimum, mean, standard deviation of N-N intervals, as well as Histograms and Poincare plots ($N-N_i$ vs. $N-N_{i+1}$ plots). Moreover, frequency domain analysis provides three main spectral components of the HRV signal: Very Low Frequencies (VLF), Low Frequencies (LF), and High Frequencies (HF). Approximate entropy (ApEn) and detrended fluctuation analysis (DFA) explore the complexity of the HRV signal by means of nonlinear dynamics methods [16, 17].

1.4 Sleep Disorders

According to the International Classification of Sleep Disorders [12] there are more than 80 different sleep disorders. These can be divided into four major categories: dyssomnias (disturbances in the amount, timing, or quality of sleep), parasomnias (abnormal events occur during sleep), sleep disorders associated with medical and psychiatric disorders. This

classification is useful in helping clinicians arrive at a useful differential diagnosis and leads the way towards understanding the etiology and pathophysiology of sleep disorders.

1.4.1 Sleep Apnea

Sleep Apnea is defined as cessation of breathing for 20 seconds or longer (or for a shorter period of time if accompanied by bradycardia, cyanosis, or pallor). Basically, apnea can be subdivided into three different categories. The first category is Obstructive Sleep Apnea (OSA), which is due to complete closure (collapse) of the throat. This is most likely to happen during sleep when the soft tissue at back of the throat is most relaxed. Nine out of ten patients with sleep apnea have this type of apnea. This type of sleep apnea is also present in children. The second category of sleep apnea is known as Central Sleep Apnea (CSA), which is associated with problems in the central nervous system. In CSA, the part of the brain that controls breathing does not start or maintain the breathing process properly. Therefore, the muscles used in breathing do not get the activation signal from the brain. Either the brain does not send the signal, or the signal gets interrupted. It is the least common form of apnea and often has a neurological cause. The third, and last, category is mixed apnea, a combination of central and obstructive apnea.

OSA, which is the most common form of apnea, occurs when mechanical or structural abnormalities in the upper airway cause interruptions in breathing during sleep. When the throat muscles collapse, the muscles of the diaphragm struggle harder and harder against the blocked passage without success. At this time, carbon dioxide builds up in the bloodstream and after a minute or more, the brain screams out for oxygen. The subject then suddenly struggles to wake up and the tongue and throat muscles tighten, allowing oxygen to flow into the lungs. The apnea event lasts between 10 seconds to 60 seconds in the worse scenarios. Instead of being alarmed and

staying awake, the victim immediately goes back to sleep again. This cycle is repeated several times during one night [8, 12]. As a consequence of the quality of sleep being compromised by the apnea events, the sleep debt increases. This makes the subject suffer from the most common apnea related symptoms such as extreme fatigue, high blood pressure, drowsiness, etc. In worst case, it can lead to fatal heart attacks and strokes.

The gold standard indicator to diagnose OSA is the oxygen saturation (SaO_2) and airflow variables. During an apneic event both measurements decrease significantly.

1.4.2 Apnea-Hypopnea index

The apnea-hypopnea index (AHI) has been used traditionally for obtaining and diagnosing the intensity of OSA events present in patients with suspicion of sleep breathing disorders. It's computation is straightforward defined as the sum of apneas and hypopneas per hour of sleep [18]. Moreover, the typical classification of this index according to severity of OSA is shown in table 1.3.

Table 1.3 Apnea-Hypopnea index.

AHI (Seconds)	OSA Condition
Less than 5	Normal
5-15	Mild
15-30	Moderate
Above 30	Severe

Despite the ease of obtaining this indicator, its usefulness has been questioned by the scientific community because of the lack of criteria in the definition of hypopnea events, and the validation of the instrumentation used. Therefore, its usefulness to evaluate sleepiness, muscle dysfunction or other markers related to sleep breathing disorders [19] is questionable. However, in order to unify the criteria for the severity OSA assessment, other markers based on pulse

oxygen saturation has been developed and modeled to predict AHI in a more controlled manner. Measurements validated are the Δ index, the average of the absolute differences of oxygen saturation between successive 12-s intervals; desaturation events per hour to 2%, 3%, and 4% levels; and cumulative time spent below 90%, 88%, 86%, 84%, 82%, and 80% saturation [20].

Chapter 2. Research Topic

2.1 Problem Definition

In the past, significant efforts have been made to provide physicians with reliable and less invasive tools to automatically classify the sleep stages [21, 22, 23], not only by our research group but globally. A few systems are available in the market to accomplish this task. However, sleep specialists and technicians are not convinced about their use because of the lack of accuracy of the equipment. Therefore, visual scoring is still preferred over automatic methods. Also, these systems are not ready for in-home environments, yet due to the high cost and complexity of the systems (polysomnography based scheme). Although similar attempts have been made to diagnose Sleep Apnea, the diagnosing of sleep apnea and sleep stage classification have been treated as isolated problems. Therefore, the possible effects of apneic events on sleep stages are not well ascertained. The literature shows a tendency to link the HRV signal and its corresponding sleep stages, but there is a lack of information on how HRV trends can be used as markers for sleep stage classification and vice versa (how brain rhythms are related to apneic events).

2.2 Significance

Studies have shown that sleep-related problems affect more than 50 to 70 million Americans [24]. In 2005, the National Sleep Foundation (NSF) indicated that: the Annual Sleep America Poll included a representative sample of the U.S. adult population and out of the 1,506 respondents, 26% met the Berlin questionnaire criteria, indicating a high risk of OSA. Furthermore, the risk of OSA increased at the age of 64 [25]. In addition, it was concluded that as many as one in four American adults could benefit from the early detection of OSA. Other epidemiologic data establishes that more than 18 million American adults have sleep apnea.

During childhood there is a prevalence of two or three percent. In 2005, the Sleep in America Poll [25], found that eight percent of responders experience or have been observed to have pauses in their breathing during sleep at least three nights per week.

Lack of sleep reduces alertness, impairs judgment, and affects tempers. Impairments to alertness and judgment due to sleep deprivation not only lead to a loss of productivity at school or work, but also contribute to increased accident rates. This translates in a loss of billions of dollars annually. The National Highway Traffic Safety Administration (NHTSA) estimated that there are 100,000 to 150,000 automotive accidents each year, of which four percent are caused by drowsy driving. According to the NSF, respondents in the 2008 Sleep America Poll [26], answered that 29 percent fell asleep or become very sleepy at work during the last month of the survey, and 36 percent have fallen asleep or nodded off while driving in the past year.

The 2009 Sleep America Poll was conducted using a random sample of 1,000 adults at least 18 years old who were interviewed by phone, and found that more than one-half of adults (54%), potentially 110 million licensed drivers experienced driving drowsy conditions at least once in the past year [27].

In early 90's the National Center on Sleep Disorders Research (NCSDR) was established within the National Heart, Lung, and Blood Institute (NHLBI) via a provision of the National Institute of Health Revitalization Act of 1993. By 1996, the NCSDR was committed to the development of a National Sleep Disorders Research Plan [28]. This plan would boost existing sleep research programs and create new programs applying state-of-the-art techniques and methods to establish a solid pathway towards understanding the problem and its solution. These new methods should be applicable to children and adults. Section III in the 2003 National Sleep Disorders Research Plan revision discusses the significance of the analysis for sleep-wake stages.

It points out that since 1960 when the R&K rules were created to classify sleep-wake stages, the scheme has been useful and considered as the gold standard for diagnosis. However, the rules have the weakness of being not being able to detect and quantify micro arousals or slight disruption of sleep.

The National Sleep Disorders Research Plan also highlights the quantification of breathing abnormalities during sleep, such as sleep apnea, which presents a challenge that must be addressed. The NCRS recommends essential directives on sleep-wake stage research topics, allowing the medical community by means of new and sophisticated computer-based signal processing methodologies (both linear and non- linear approaches), to timely diagnose and treat patients in an early stage of the disorder. Also, these new methods must adhere to the design of portable ambulatory systems, to measure sleep, and other physiologic variables at home while providing highly accurate measurements. One of the major limitations in diagnosing Sleep Breathing Disorders (SBD) is the need for relatively complex, and costly procedures, in addition to bulky and expensive equipment such as those currently required for overnight polysomnography.

Statistics in México provided by the Platino Research Group, part of the National Institute of Respiratory Diseases (INER-Instituto Nacional de Enfermedades Respiratorias), indicate a significant sleep apnea prevalence in a population of adults, aged 40 or older: a telephone survey showed 2.2 percent of women and 4.4 percent of men exhibited symptoms of sleep apnea. These tendencies were similar to those found in the United States by 1993: a prevalence of 2% for women and 4% of men of the total population [29]. Mexico City's last census, in 2005, estimated a total population of 26 million adult, aged 40 or older: 14 million women population and 12 million men [30]. Considering that Mexico City's statistics may be

similar for the whole country, this may lead us to an estimation of about 1 million of Mexicans suffering from sleep apnea disorder.

Moreover, a large part of the subjects suffering from sleep apnea have not been diagnosed and therefore lack the appropriate treatment. That is because statistics are calculated from score-based surveys and not from the actual medical facilities' statistics. Another factor leading to under-reporting is that only a sample of the total population is surveyed. In addition, the Mexican Institute of Social Security (IMSS – Instituto Mexicano del Seguro Social) states that sleep apnea is one of more than 80 sleep disorders that affect 4 million Mexicans and more importantly, is related to the top ten mortal diseases, such as cardiopathies, breathing disorders, arrhythmias, high blood pressure and arterial thrombosis [31]. Another study by the IMSS found that 35 million Mexicans aged 30 to 60 suffered from snoring, which led IMSS to consider an important public health issue. Snoring is related to heart problems, neurologic problems, and high blood pressure due of lack of oxygen flow [32]. In recent years, the IMSS has conducted a 1,489 polysomnogram studies, an average of 362 examinations per year. Despite the efforts of medical institutes, personnel and equipment availability are not enough to reach populations as large as the statistics cited above.

As described above sleep apnea is not an isolated problem. For example, the Official Mexican Norm for the integral treatment of obesity [33] ascertained co-morbidity among obesity and other diseases including sleep apnea (arterial hypertension, cardiovascular problems, Type II diabetes, hypoventilation, osteoarthritis, and others). Sleep Breathing Disorders (SBD) may contribute to the development of insulin resistance and other components of Metabolic Syndrome [34]. Therefore, in order to start an efficient and integral treatment of obesity, sleep problems must be identified and treated as well.

2.3 Hypothesis, Research Question, and Variables

The *hypothesis* to be tested in this research is: The relationships between sleep stages and apneic events can be used to consolidate sleep classification and apnea detection algorithms.

The following *questions* will be addressed in this work:

- Are there relationships between sleep stages and apneic events?
- Can these relationships be used to strengthen classification or apnea detection algorithms?

The independent variables are: Biosignal tracings, manual scoring, and apnea events annotations.

The dependent variables are: EEG and HRV feature statistical correlation, statistical differences, system performance, accuracy, sensitivity, and specificity.

2.4. Objective

To find and establish relationships between sleep stages and apneic events and increase the accuracy, sensitivity, specificity and geometric mean of sleep classification algorithms for apnea detection using minimum number of sensors.

2.5 Proposed Solution

The proposed method to assess the research questions and hypothesis is shown in figure 2.1. First, the analysis starts with a preprocessing block designed to condition and filter undesired frequencies from the raw biosignals. Then, EEG signals are ready for the proposed feature extraction algorithms. On the other hand, HRV must be derived from ECG signals before corresponding feature extraction algorithms can be applied. Once the HRV signal is derived, time-domain and nonlinear algorithms can be applied, whereas frequency domain analysis needs the computation of an evenly spaced (sampled) HRV by using interpolation methods. After

features are extracted from EEG and HRV signals, feature vectors are formed and re-arranged using manual scoring and apneic event indicators enabling the computation of statistics such as mean and standard deviation and statistical trends for sleep stages. Hence, significant differences will be established at $p < 0.05$ level using the t- (Student) test (for two means) and ANOVA (for multiple means). Then features will be fed into a classifier system to calculate its discriminative capacity based on performance measures such as accuracy, sensitivity, specificity and geometric mean [35]. Thus, the performance will be assessed using the following concepts:

$$Accuracy = \frac{True\ Positives + True\ negatives}{Positives + Negatives} \quad (2.1)$$

$$Specificity = \frac{number\ of\ True\ Negatives}{number\ of\ True\ Negatives + number\ of\ False\ Positives} \quad (2.2)$$

$$Sensitivity = \frac{number\ of\ True\ Positives}{number\ of\ True\ Positives + number\ of\ False\ Negatives} \quad (2.3)$$

$$Geometric\ Mean = \sqrt{Specificity \times Sensitivity} \quad (2.4)$$

The Receiver Operating Curve (ROC) is a visual performance metric constructed when plotting the sensitivity vs. specificity for a performance metric. The more a ROC tends towards the left and top edges of the plot, the better the classification [36]

Alpha level is set at .01 to maintain a low level probability to make a type I error, and to be 99% confident that the mean difference is not due to random sampling error or just by chance.

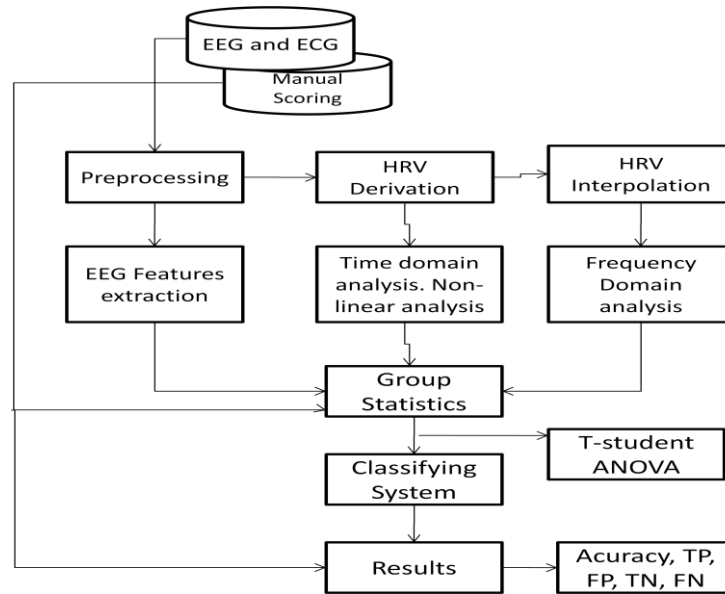


Figure 2.1 Proposed Methodology.

The following chapter details the proposed algorithms for EEG and HRV signals feature extraction that can be useful for achieving the objective: To find and establish relationships between sleep stages and apneic events and increase the performance of sleep classification algorithms for apnea detection

Chapter 3. Previous Work on EEG and HRV Feature Extraction and Sleep Stage Classification

This chapter describes the previous work related to this investigation carried out by other researchers in recent years. It also includes a description of the set of features extracted from the EEG and HRV signals and how these features have been used in the field of automatic sleep stage classification and the detection of apneic events. For simplicity and easier flow of concepts, the mathematical theory and parameters underlying each feature are described in Chapters 5 and 6.

3.1 General Overview

In 2001, Agarwal et al. [37] presented a computer-assisted sleep staging method tested on four patients. The method used the principles of segmentation and self-organization based on primitive sleep-related features to classify sleep stages by means of EEG, EOG, and EMG records. The overall performance on a stage-by-stage basis of the computer versus manual scoring yielded an accuracy of 72.5%-93.4%, an average specificity of 76%, and a sensitivity of 76%. Similar results can be found in research by Oropesa et al. [22], which used wavelet transform and a neural network (NN) as the classifier system. In 2003, Penzel et al. [38] focused on the current problems of automatic sleep scoring applied to sleep apnea. This work showed difficulty to distinguish between sleep stage 1 and REM sleep due to similar EEG tracing (EOG is then indispensable); similarly, wakefulness and REM sleep were difficult to separate and success depended on the quality of the EMG signal. Finally, sleep stage 2 was difficult to assess due to the possibility of change in the nature of sleep spindles among patients.

Classification of sleep stages has not been limited to adult populations. In 2002, Heiss [39] attempted to assess sleep recordings obtained from eight infants between 6 and 13 months of age. A neuro-classifier system was applied to the extracted patterns. This system achieved a performance of 80% accuracy. A more complex classifier system was designed by Übeyli [40] in 2009. Features were comprised of Lyapunov exponents and classification was carried out by using an adaptive neuro-fuzzy inference system (ANFIS). Only the EEG tracing was used to assess sleep stages. After training the ANFIS, accuracies up to 99% were obtained for selected data. In addition to classical biosignal study, other noninvasive sleep stage classification methods have been tried. Komatsu et al. [41], in 2006, by means of a pneumatic heartbeat method obtained accuracy up to 36 percent. Although theoretically interesting, this level of performance, with such low accuracy, is not reliable for clinical use. It does, however, increase the corpus of knowledge in the area.

There has been considerable amount of research on the analysis of HRV and sleep apnea. Penzel et al. [42] compared the HRV derived from the sleep recordings of 67 sleep apnea patients (experimental group) with the recordings of 14 healthy subjects (control group). Analysis of HRV was performed by applying a nonlinear method called detrended fluctuation analysis (DFA). Results showed significant differences among DFA's sleep stages for both groups. Khandoker et al. [43] studied the interaction between EEG and ECG recordings during and after apenic events. Ten OSA patients participated in this study. A coherence analysis was performed on EEG and ECG during N-REM and REM sleep. Major findings described a significant difference between coherence values in normal breathing subjects and those values in OSA patients (both N-REM and REM stages). They concluded that findings could be useful in detecting OSA events or OSA-related arousal to classify sleep stages. In recent years, simple

ways to assess sleep apnea have also been developed. Balakrishnan et al. [44] developed an index called Sleep Index to evaluate the quality of normal sleep and OSA. The index computation was based on the amount of time spent in each sleep stage. The proposed index range would assign low values to OSA subjects and higher values to normal breathing subjects. Statistical differences between both groups were found, suggesting the index may be used as a single number indicator reflecting the quality of sleep.

Zilinskas et al. [23] analyzed the heart rate features as being the main goal to the development of an automatic diagnostic sleep system. To design the system, authors attempted to classify the stages by means of three methods: ANN, SVM, and Quadratic Classification Function (QCF). However, their contributions and conclusions were not supported by accuracy rates values. The authors concluded that the best classification was achieved by the SVM system.

3.2 EEG and HRV Feature Extraction

3.2.1 Relative Percent Spectral Energy Band (RPSEB)

The spectral energy band is the energy ratio contained in a well-defined range of EEG frequencies [5, 6]. This band is defined based on information in the brain rhythms alpha, beta, theta, and delta. Its calculation requires power spectrum density (PSD). The decomposition of the EEG PSD into regions is the first step in this frequency domain calculation. The segmentation of the EEG signal is based on conventional clinical limits of brain wave rhythms (such as alpha, beta and so on). Moreover, the measurement of the relative energy or normalized energy within a certain region (energy band divided by the total energy) is preferred over the absolute measurements because relative measurements are less affected by factors such as electrode impedance, amplification factor, and skull thickness [5].

In 1977, when the EEG paper records was preferred over computer to find trends, Gotman et al. [45] with the aid of a digital computer studied these frequency domain features to describe abnormalities present in brain-injured patients. They computed the alpha, beta, delta, and theta RPSEB's and also the ratio of slow wave activity defined as $(\text{delta} + \text{theta}) / (\text{alpha} + \text{beta})$. They concluded that this ratio was a promising marker to find abnormalities in brain waves patterns. Moreover, as markers defined in the frequency domain were not readily available to the human EEG technician upon a simple temporal observation, such methods provided more analytical tools to assess brain condition.

Matthis et al. [46] analyzed 23 EEGs of a 9-year-old girl with an inoperable brain tumor, they concluded that RPSEB parameters were as powerful when describing EEG rhythms as the Hjorth parameters, slope parameters or the zero crossing features.

3.2.2 Hjorth Parameters

Hjorth parameters, in use since 1970, are the three time domain parameters have been used to describe the EEG rhythm activity. These parameters are also known as the normalized slope descriptors because they may be computed by means of the first and second signal derivatives. Each descriptor corresponds to its counterpart in the frequency domain: Activity ($m0$) is an estimate of the mean power contained in the signal; the second descriptor is called Mobility ($m2$) which is an approximation of the mean frequency; and the complexity descriptor, which quantifies the bandwidth of the signal ($m4$) [47, 48, 49]. Computation of these parameters involves discrete derivatives of the epoch to be analyzed. Vourkas et al. [50] performed a study on mental task discrimination based on Hjorth parameters. In their study, EEG signals from 20 different subjects were recorded during three mental tasks (baseline EEG and EEG rhythms

during two mathematical mental computations). When Hjorth descriptors were used as input to a feedforward artificial neural network, and the system achieved 100% accuracy when the number of hidden units was greater than 15. In 1987, Bankman et al. [51] characterized the behavior of EEG tracings and measured the “depth of anesthesia”. Eleven subjects were under an anesthesia procedure when data were recorded continuously while halothane concentration was changed stepwise from 1.2 to 2.6 percent and down again at the end of the surgery. They found that Activity and Mobility markers increased during the administration of the anesthesia whereas Mobility and mean frequency of EEG patterns decreased. Moreover Activity and Mobility parameters were inversely correlated to Mobility for this particular study. Other applications of Hjorth’s parameters include EMG analysis [52].

3.2.3. Harmonic Hjorth Parameters

The three parameters based on the estimation of the power spectrum density (PSD) of the signal. The harmonic Hjorth parameters [53], are the frequency-domain versions of the Hjorth parameters. Specifically, they are the center frequency (f_c), the bandwidth ($f\sigma$), and the value at the central frequency. Hence, the computation of the PSD may be based on parametric or non-parametric methods.

Van Hese et al. [47], in 2000, utilized the harmonic Hjorth parameters to implement an automatic sleep scoring system by means of cluster analysis. The proposed method was applied to only one EEG recording. In that research paper, the behavior of Harmonic parameters was described graphically using a 3-D scatter plot. It was observed that central frequency matched the EEG frequency rhythms present in sleep stages (e.g. alpha, delta, theta, and beta waves). It was also inferred that the awake stage possessed the widest bandwidth, whereas slow wave

stages (SWS) had narrower spectrum. The SWS had the highest value at the center frequency index, possibly because synchronized brain activity possesses larger energy signal contents. Despite of the evidence of these trends, the authors did not present a statistical method to assess significant differences among sleep stages. Even though the results of the K-means classification were presented graphically, they did not provide a system performance measurement.

Center frequency is also known as the mean frequency [54]. This feature is widely used to assess muscle fatigue from superficial EMG signals in a non-invasive fashion.

3.2.4. Itakura Distance

In 1974, Fumitada Itakura [55] introduced this measure based on autoregressive (AR) modeling coefficients. He presented a system focused on speech recognition, where a word was recognized as the reference word (baseline) when the comparison of the test word and the baseline word produced minimum prediction residue. In other words, the distance between the two AR models became close to zero.

Kong et al. [56, 57] applied the generalized Itakura distance to EEG signals to quantify changes in the brain activity, especially those changes associated with brain injury. In experiments, EEG data from a sleeping uninjured piglet was recorded, and taken as a baseline to compare with EEG segments of the same piglet under the following conditions: 30 minutes of hypoxia, 5 minutes of room air, and seven minutes of asphyxia, followed by four hours of room air recovery. Findings showed that the Itakura distance among EEG epochs at asphyxia stage and normal state increased significantly, indicating a drastic change in brain activity. Moreover, the distance decreased during the recovery process, and approached a zero value. A similar

experiment utilizing autoregressive moving average (ARMA) processes was performed by Löfgren et al. [58].

Since 2004, our research group has applied the Itakura distance as a feature to identify similarity between EEG and EOG tracings among different sleep stages and have demonstrated that it may be used for automatic sleep stage classification [59, 60].

In this research, the Itakura distance will be used to measure the similarity (by Auto Regressive process modeling) of a baseline EEG epoch (Awake, Stage 1, Stage 2, Stage 3, Stage 4, and REM) with the rest of the epochs in the EEG vector [61].

3.2.5 Wavelets

The non-parametric (e.g. Fourier Transform) and parametric methods (e.g. ARMA) have been widely used for signal processing and power spectrum density estimation. Both methods are powerful tools to analyze stationary signals and determine their frequency content; however, such methods have the disadvantage of not providing any localization in time. As a consequence, alternative methods based on Fourier Transform have been developed to overcome this limitation. Short Time Frequency Transform (STFT) was introduced as a method based on analyzing the signal frequency content over short periods of times by windowing the original time series. As a consequence of window application, the frequency resolution is always fixed throughout the signal.

A more advanced version of these time-frequency transform methods is known as Wavelet Transform (WT), where the shifting window is called the “mother wavelet” and it is scaled to constant, relative values. Furthermore, wavelets offer certain advantages over classical PSD estimation techniques for the analysis of the EEG signal by adapting the window width in

function on the frequency content; time-frequency decomposition of EEG epochs using the Wavelet transform offers an optimal compromise for time domain resolution [22].

In general terms, the one-dimensional (1-D) Wavelet decomposition could be considered as a generated pair of quadrature mirrored FIR filter banks. These filters are related to the scaling function and the mother wavelet. A discrete wavelet transform (DWT) is the decomposition of the original time series into the approximate component (A) and the detailed component (D). These two signals are the output of the time series through a decimator low and high pass filters. The 1-D DWT tree is formed when the approximation level is decomposed into further levels. A wavelet package transform (WPT) tree is a special case where approximate and detailed components are further decomposed in subsequent levels.

Oropesa et al. [22] utilized the filter banks created by the WPT to analyze the energy content of the well-defined brain frequency band rhythms of the EEG sleep stages. The energy band was calculated by combining nodes and leaves of the WPT tree corresponding to the brain rhythms. Then the energy coefficients were fed into a neural network obtaining an accuracy of 77% for a testing set of 590 epochs. Other uses of wavelets are related to image compression, and image and signal denoising.

3.2.6 Empirical Mode Decomposition

This state-of-the art method for analyzing nonlinear and non-stationary data has been developed in recent years. This is known as Empirical Mode Decomposition (EMD) method [62]. The key point of the EMD method is the generation of a collection of Intrinsic Mode Functions (IMF). This decomposition is based on the extraction of the energy contained within various intrinsic time scales. IMF's are components that possess a well-behaved Hilbert

Transform that allow the computation of instantaneous frequency. Moreover, an intrinsic mode function is a construct that satisfies two conditions:

- A) The number of extremes and the number of zero crossings must be equal or at most differ by one.
- B) At any given instant, the mean value of the envelope defined by the local maxima and the envelope defined by the local minima is zero.

It seems that EMD possesses advantages over other methods utilized to quantify non-stationary signals [63]. For example, the Fast Fourier Transform does not have the capability to track the time location of events. A wavelet analysis may solve this temporal location of non-stationary events. However, it is not an adaptive process and therefore a “mother” wavelet is used for all data.

Even though of this technique was developed recently, the main disadvantage is the lack of a clear mathematical theory and foundations that are needed to provide a strong support of this relative easy-to-compute method [64]

As it is a relatively new, only a few projects have used this method to analyze EEG signals. Sweneg-Rear et al. [65] applied the EMD method on EEG records for a synchronization analysis. EEG records were collected during imagined finger movements, and two EEG channels were used for this trial. Four IMF's were extracted and their corresponding PSD's were computed. From the graph in the article it could be observed that IMF1 lies in frequency ranges of less than 15 Hz, IMF2 has a wider frequency content (0-40 Hz), IMF3 less than 10 Hz and IMF4 has less than 5 Hz. This filterbank is studied more thoroughly in [62]. In the case of Fractional Gaussian Noise, EMD can be interpreted as a filter bank of overlapping bandpass filters for modes of indices $K > 2$. The first mode corresponds to a half-band high pass filter.

Similar to wavelet denoising, DE-Xian [63] implemented an EEG preprocessing method based on the EMD method. Also, Diaz [64] utilized the EMD method to discriminate mental tasks. For each IMF this research group computed traditional features such as RMS value, normalized Shannon entropy, central frequency and maximum frequency. An accuracy of 66-68% was achieved utilizing different classification systems.

3.2.7 Nonlinear Features

3.2.7.1. Detrended Fluctuation Analysis (EEG and HRV)

Detrended Fluctuation Analysis (DFA) is a nonlinear method capable of identifying scaling behavior and detrend long range correlations [66]. Thus, EEG time series are assumed to conform to fluctuations whose scaling behavior reflect neurophysiologically important information [67]. This method computes the integral time series $Y(k)$ of the original data series $X(t)$. Then $Y(k)$ is divided into “boxes” of size n . For each box a linear regression is computed. Thus the average fluctuation of a box is calculated by subtracting the local linear regression from the “boxed” series. Finally, in the log-log plot of the average fluctuation versus the variable n , the slope of that characteristic behavior is known as the α scaling exponent.

Alpha values of 0.5 represent scaling exponents corresponding to integrating series such as a random walk. For the case of $\alpha=1$, the time series corresponds to $1/f$ noise. On the other hand, a value of 1.5 indicates Brownian noise behavior. In [68] DFA was applied to the EEG time series (MIT-BIH polysomnography database). The authors were able to establish that the scaling exponent alpha was larger at deep sleep stages (1.2) than those during light sleep (approximately 1). Statistical differences we assessed by ANOVA and $p<0.01$.

Other uses of DFA on EEG time series include the study presented by Lee et al. [69]. They analyzed the trends of the EEG signal during waking and hypnosis states. A Student t-test was used to find statistical differences between the two means ($p < 0.05$).

Penzel et al. [42] investigated the effect of sleep stages and sleep autonomic activity by analyzing the HRV signal, in 2003. The DFA was used to describe the scaling behavior and to detect long range correlations on 14 healthy subjects, 33 patients with moderate sleep apnea and 31 patients with severe sleep apnea. The results showed that deep sleep alpha values were smaller (around 0.82) than those values found in light sleep (1.21). Also the alpha scaling value of healthy subjects was significantly different ($p < 0.05$) from alpha values for moderate and severe groups.

3.2.7.2 Correlation Dimension

Correlation Dimension (CD) is a nonlinear dynamics method, which quantifies the dimensionality of the underlying physiological processes generating the biosignals with respect to their geometrical reconstruction in phase space [70]. The correlation integral $C(r)$ using the Grassberger-Procaccia algorithm is the most common method applied to the EEG time series. The study of nonlinear dynamic analysis has been developed as a state-of-the-art method for the study of complex time series in the past four decades. For the constructed m space it estimates the number of data points within a radius r of the data point X_m .

Acharya et al. [71] demonstrated that CD has its highest value for the awake stage due to desynchronization of alpha waves present in the EEG signals. In addition, the CD value increased during REM stage. The changes that occurred among the stages were attributed to the signal variability. Statistical differences in this study were assessed via ANOVA analysis

($p < 0.01$). Similar conclusions were made by other authors [70,72]. Ferri et al. used the CD feature for a nonlinear analysis of EEG signals in children with epilepsy [73,74].

In recent years, there has been an increasing interest in nonlinear analysis of HRV signal. As the R-R tachogram may have a nonlinear nature and exhibit a complex behavior, the CD measures the geometry of the cloud of points in the well-known phase space. Carvajal et al. [75] presented an analysis of CD in HRV signals as a means to discriminate healthy subjects and patients suffering from a dilated cardiomyopathy condition.

3.2.7.3 Approximate Entropy

Approximate Entropy (ApEn) is a “regularity statistic” method that quantifies the unpredictability of fluctuations in time series such as the EEG or HRV signals [76]. In this way, a given stochastic signal will have very small ApEn values (close to zero). On the other hand, a random signal having nonregularity will present a large ApEn value. Typically this value lies between zero and two.

In 2005, Achary et al. [71] derived this feature for EEG signals downloaded from the Physionet sleep database. This research group found the statistical difference ($p < 0.01$) among sleep stages. Moreover, ApEn values were higher due to highly active cortex and desynchronized brain activity. Thus, during stage 4 the ApEn values had the lowest values due to the high synchronization of delta waves.

Beside conventional time and frequency domain features, new variables to determine HRV signal behavior have become available. Approximate entropy (ApEn) which assesses the irregularity on R-R times series was studied by Virtanen et al. [77]. The trends found suggested that ApEn values were smaller on SWS and larger values were reported in awake stage

3.3 HRV Features

3.3.1. Time-domain Features

Time domain features on the HRV signal are based on statistical measurements as the maximum and minimum R-R interval, mean RR, SDNN (standard deviation of R-R intervals) and variance. Changes of sleep stages trends have been reported on the HRV's statistical time domain features [78].

3.3.2 Frequency-domain Features

When speaking of frequency domain features of the HRV signal, we have markers similar to RPSEB described in section 3.2.1. For this particular signal, the studies generalize only three subbands to be analyzed over the PSD: Very Low Frequencies (VLF), Low Frequencies (LF) from 0.05 to 1.45 Hz and High Frequencies (HF) within a range of 0.15 to 0.50 Hz. Moreover, there exists strong evidence that relates the presence of HF component to vagal (parasympathetic) activity. Also, HF components are decreased by parasympathetic antagonists. On the other hand, LF is reduced by both sympathetic and parasympathetic antagonists, which may indicate that LF components are related to both ANS subsystems. In this sense the LF/HF ratio is used as a marker of ANS balance control. The frequency-domain methods provide easier access to interpret physiological results when compared to the time-domain methods on short-term recordings (2-5 minutes). Yang et al. [79] explored the relationship and correlation between the changes of ANS and the depth of sleep by means of continuous power spectral analysis. Based on the analysis of ten healthy subjects, they concluded that SWS (sleep stage 3 and stage 4) was associated with an increase in HF component and HRV presence. Inversely, LF component increased during that stage whereas the LF/HF was significantly and negatively

related to the delta RPSEB feature. In addition, cardiac sympathetic regulation is negatively related to the depth of sleep. Similar trends have been concluded by other authors [80, 81].

Chapter 4. Materials and Methods

4.1. Materials

Data were available on the Physionet website for downloading in EDF format. Subjects were randomly selected over a 6-month period from patients referred to the Sleep Disorders Clinic at St Vincent's University Hospital, Dublin, for possible diagnosis of obstructive sleep apnea, central sleep apnea or primary snoring [82]. Subjects had to be above 18 years of age, with no known cardiac disease, autonomic dysfunction, and should have been not on medication known to interfere with heart rate. Twenty-five subjects (21 males and 4 females) were selected (age: 50 ± 10 years, range 28-68 years; BMI: 31.6 ± 4.0 kg/m², range 25.1 - 42.5 kg/m²; AHI: 24.1 ± 20.3 , range 1.7-90.9). The 10-20 standard electrode placement system was used for EEG recording. Polysomnograms were obtained using the Jaeger-Toennies system. Signals recorded were: EEG (C3-A2), EEG (C4-A1), left EOG, right EOG, submental EMG, ECG (modified lead V2), oro-nasal airflow (thermistor), ribcage movements, abdomen movements (uncalibrated strain gauges), oxygen saturation (finger pulse oximeter), snoring (tracheal microphone) and body position. A sample rate of 128 Hz was used for EEG, EOG, and ECG tracings, whereas EMG was sampled at 32 Hz. Each epoch was analyzed to indentify the number of apneas, hypopneas, EEG arousals, oxyhemoglobin desaturation, and disturbances in cardiac rate and rhythm. A full description of subject demographic, sleep scoring and apneic events of each study is presented in Appendix 1.

4.2. EEG Filtering and Denoising

EEG signals are easily contaminated with artifacts, the most common noise sources influencing the quality of the EEG signals are EMG signals, electrode movements, 60 Hz

powerline interference and uniform or Gaussian white noise. Some noise sources (for example white noise) are difficult to remove by typical bandpass finite impulse response (FIR) filters or infinite impulse response (IIR) filtering. The reason for this inefficacy is that the power spectral density (PSD) of white noise fully overlaps with the PSD of the EEG signals and this makes it almost impossible to separate a clean EEG signal from the contaminating noise components.

A novel solution to denoise non-stationary natural signals is based on the shrinkage properties of Discrete Wavelet Transform (DWT) coefficients, as proposed by Dohono et al. [83]. This method has been used to denoise not only non-stationary EEG signals but also ECG signals as is described in section 4.3. In order to better understand the fundamental of DWT-based signal denoising, this section covers the mathematical basis of this transform that will be also used as an EEG feature extraction method and will be described further in subsequent sections.

4.2.1. Discrete wavelet transform

In order to understand the basis of wavelet theory, let's start with an extension of Fourier Transform (FT) method known as the Short Time Fourier Transform (STFT). The FT is a powerful tool to study the frequency content of a given signal. However, it lacks information about the time of occurrence (time resolution) of frequency changes, which is crucial in nonstationary signal analysis. This issue is resolved by analyzing the frequency content of segments of the signal over a short period of time using a shifting window. Thus the STFT is computed as:

$$STFT(f(w, s)) = \int g^*(t - s)f(t)e^{-j\omega t} dt \quad (4.1)$$

Where $g(t-s)$ is the shifting window in time domain. In STFT analysis, the time and frequency resolution is fixed as a result of using a fixed window to split the signal.

The Continuous Wavelet Transform (CWT) is a method based on the STFT's window-shifting process. The CWT differs from the STFT by scaling a self-styled “mother wavelet” or window.

Thus the CWT is defined by:

$$CWT(f(a, b)) = \int f(t) \psi_{a,b}(t) dt \quad (4.2)$$

$$\text{Where} \quad \psi_{a,b}(t) = \frac{1}{\sqrt{a}} \psi\left(\frac{t-b}{a}\right), a \in \mathbb{R}^+, b \in \mathbb{R} \quad (4.3)$$

Here, the $\psi_{a,b}(t)$ is the well-known wavelet window function with parameters a and b . Thus, the time resolution depends now on the scaling “ a ” parameter and the translation parameter “ b ”. Several set of mother wavelets have been designed for wavelet transform analysis, such as the Mexican hat (sombbrero) function, Harr, Symlet and Daubechies to name only a few of them [84].

The discrete transform of the CWT or DWT is achieved by taking discrete values of the parameters a and b .

$$DWT_{m,n}(f) = a_0^{-m/2} \int f(t) \psi(a_0^{-m}t - nb_0) dt \quad (4.4)$$

When a_0 and b_0 values are set to 2 and 1, respectively, the DWT can be described as the output produced by two quadrature mirror filters (QFT), where g is a highpass FIR filter and h is a lowpass FIR filter given as:

$$g(h) = (-1)^n h(1 - n) \quad (4.5)$$

In this equation, filter h is related to the scaling function, whereas filter g is related to the mother wavelet.

$$\phi(x) = \sum_n h(n) \sqrt{2} \phi(2x - n) \quad (4.6)$$

$$\psi(x) = \sum_n g(n) \sqrt{2} \phi(2x - n) \quad (4.7)$$

Thus the QMF outputs are characterized as:

$$H_L = \sum_n h(n - 2L)x(n) \quad (4.8)$$

$$G_L = \sum_n g(n - 2L)x(n) \quad (4.9)$$

As it can be observed, the signal $x(n)$ is lowpass filtered by convolving with $h(n-2L)$ and highpass filtered by convolving with $g(n-2L)$, therefore transforming the original signal into two subbands of bandwidth: $[0-F_{N/2}]$ and $[F_{N/2}-F_N]$ respectively (Figure 4.1 a). Moreover, H_L output is commonly known as the approximation (*A*) component and represents the lower resolution components. In this context, G_L is known as the detailed (*D*) decomposition containing the high resolution components. The DWT tree is formed when the decomposition process is only applied to the *A* component at each corresponding decomposition level. During this process the time resolution decreases by a factor of two at each level. However, the frequency resolution increases and is reflected in each coefficient of A_L (Figure 4.2 a).

The reconstruction of the signal is achieved by applying the inverse procedure without loss of information. This technique is identified as the Inverse Discrete Wavelet Transform (IDWT) and differs from the DWT in the order that it implies upsampling and filtering the *A* and *D* subband components (Figure 4.1 b).

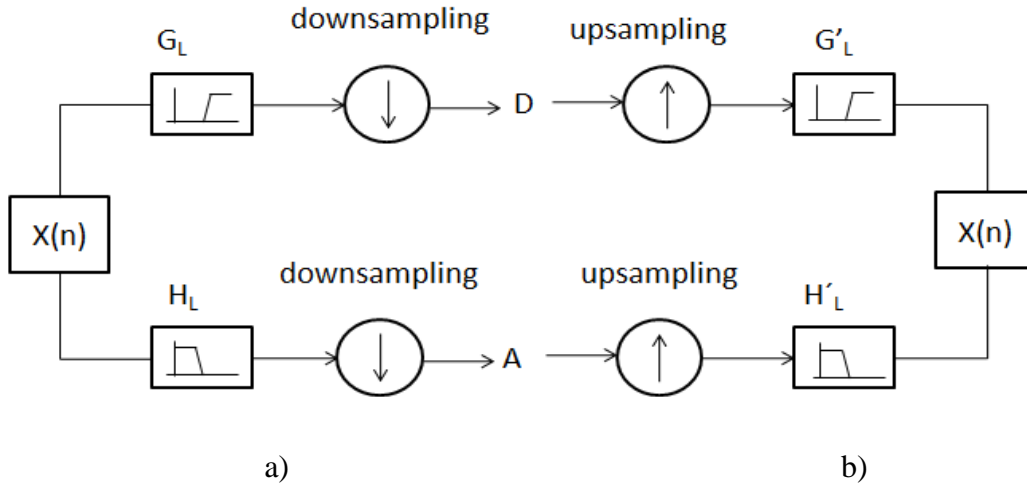


Figure 4.1 a) DWT algorithm, b) IDWT algorithm.

The Wavelet Packet Transform (WPT) is produced when the QMF filters are applied on both the A and the D components. The WPT tree is a special case of the DWT and defines a neat set of filters, which leads to a huge library of frequency subbands producing an excellent resolution on the signal undergoing the decomposition process (Figure 4.2 b).. On the other hand, the cost of computing this filterbank has a high computational complexity of the order $O(N(\log(N)))$.

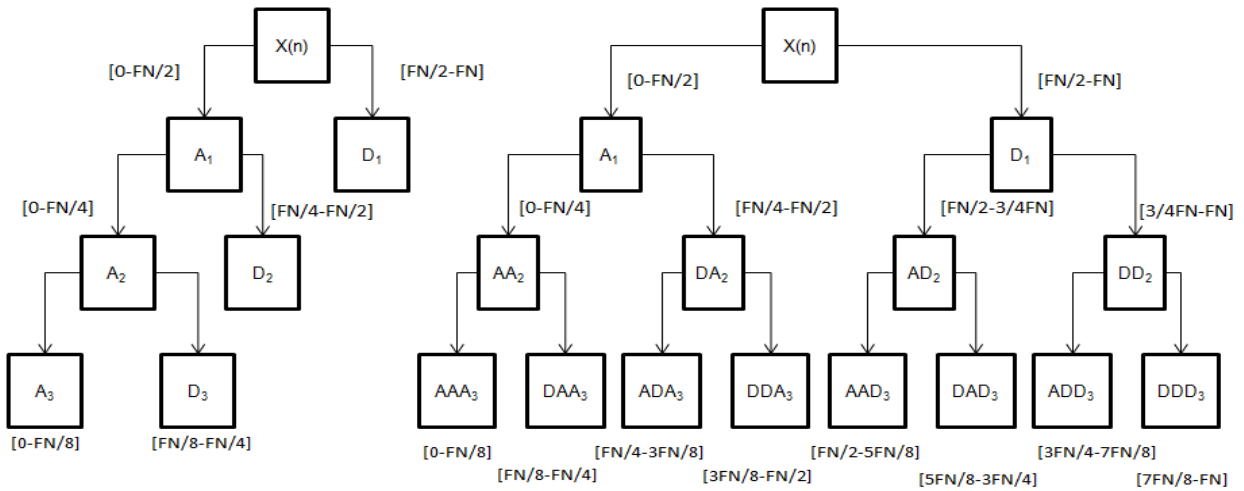


Figure 4.2 a) DWT tree, b) WPT tree.

4.2.2. Denoising

As stated before, EEG is a biosignal, which is easily contaminated with artifacts. In recent years, a number of methods based on removing undesired wavelet coefficients, under the hypothesis that those coefficients are related to noise sources have become very popular. In these methods the signal is decomposed into its wavelet coefficients by applying the DWT. After selecting a pre-defined threshold value, coefficients that contribute to noise components are discriminated and zeroed out by using a threshold discrimination filter.

4.2.2.1. Threshold filter

The detailed coefficients d_k^l are modified according to a threshold value λ and a threshold coefficient filter. In a general sense, the wavelet denoising method considers the absolute value of d_k^l , smaller than λ are considered noise, whereas larger values are considered as coefficients that contribute to the signal information rather than the noise information.

A hard-thresholding rule (Figure 4.3 a) is defined as follow:

$$d_k^{\wedge l} = \begin{cases} 0 & |d_k^l| < \lambda \\ d_k^l & |d_k^l| \geq \lambda \end{cases} \quad (4.10)$$

Where $d_k^{\wedge l}$ is the modified detailed wavelet coefficient k at level l .

An alternative shrinkage function, the soft-thresholding rule (Figure 4.3 b) is defined by:

$$d_k^{\wedge l} = \begin{cases} 0 & |d_k^l| < \lambda \\ \text{sgn}(d_k^l)(|d_k^l| - \lambda) & |d_k^l| \geq \lambda \end{cases} \quad (4.11)$$

Where $\text{sgn}(d_k^l)$ is the mathematical sign function.

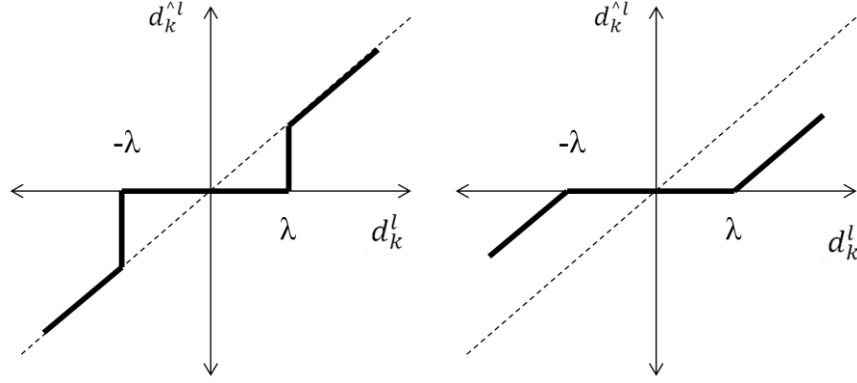


Figure 4.3 a) Hard thresholding, b) Soft thresholding.

Hard thresholding is preferred. However, this method produces artifacts on the reconstructed signal due to the discontinuous nature of the filtering. This issue is overcome by the soft thresholding method. However, the main disadvantage here is that the coefficients are shrunk towards zero and consequently the reconstructed signal will have lower amplitude than the original signal amplitude [85].

4.2.2.2 Threshold value λ

There are a variety of methods to determine the threshold value λ [85]. One of the most commonly used is the Universal threshold value which depends on the number of samples N in the signal.

$$\lambda = \sqrt{2 \log(N)} \quad (4.12)$$

The method known as SURE (Stein's Unbiased Risk Estimation) is calculated by minimizing the risk function:

$$\lambda = \sqrt{NV(k_{\min})} \quad (4.13)$$

Where $NV(k)$ is a data vector to the second power.

$$R(k) = \frac{N - 2k + \sum_{j=1}^k NV(j) + (N - K)NV(N - K)}{n} \quad (4.14)$$

The Heuristic SURE selects the lowest value of the two previous thresholds. The last thresholding method discussed in this work is the Minimax, in which λ value is defined as a data series as follow:

$$\lambda = 0.3936 + 0.1829 \left(\frac{\log(N)}{\log(2)} \right) \quad (4.15)$$

4.2.2.3 Methods

In order to find and test the best denoising threshold and threshold-filtering rule, the data used in this section was collected from an EEG online database provided by Dr. Ralph Andrzejak with the Epilepsy Center at the University of Bonn, Germany [86].

This database is comprised of EEG records of both healthy and epileptic subjects. The groups are identified as follows: Group H (healthy subjects), Group E (epileptic subjects during a seizure-free interval), and Group S (epileptic subjects during seizure). Each group contains 100 single channel EEG segments of 23.6 sec duration each sampled at 173.61 Hz. Here the signal was resampled to match the EEG's sampling frequency described in section 4.1 to a rate of 128 Hz. The rationale for using this specific database for identifying the denoising parameters was that it has been previously chosen by several researchers who tested their novel denoising methods and reported their results based on this data [87]. Due to nature of this research, group H was the only dataset used, from which 20 EEG epochs were selected to create $y(n)$ EEG noisy signals by adding a white noise signal ($E[x]=0, \sigma = 20$) and a 50 Hz powerline noise as follow:

$$y(n) = x(n) + w(n) + s(n) \quad (4.16)$$

The first step to clean up $y(n)$ was to eliminate $s(n)$ by applying a WPT decomposition and zeroing out the WPT coefficients of those EEG's subbands where no brain's rhythm content was supposed to be present (0 to 0.5 Hz and frequencies above 40 Hz). According to the Nyquist theorem, the maximum frequency contained in the EEG signal is 64 Hz for a sampling frequency

of 128 Hz ($F_N=64$ Hz). To achieve a resolution of 0.5Hz on each subband, the number of levels required was computed as follows:

1. The number of required subbands :

$$Terminal\ nodes = \frac{F_N}{Frequency\ Resolution} = \frac{64Hz}{0.5Hz} = 128 \quad (4.17)$$

2. The number of terminal nodes was twice each level of decomposition

$$Terminal\ nodes = 2^l \quad (4.18)$$

3. Thus the number of levels required was 7:

$$128 = 2^7 \quad (4.19)$$

Therefore, a WPT Dauchabies of second order (db2) and 7 levels decomposition was used. After bandpassing the non-desired frequency content by zeroing out the proper terminal node coefficients, the signal was reconstructed using the Inverse Wavelet Packet Transform (IWPT).

In the next step, the EEG signal was decomposed again using a DWT Dauchabies of second order (db2) and 7 levels. After that, the hard thresholding and soft thresholding rules were applied to the EEG bandpassed noisy record and the threshold values λ were computed by the Universal, SURE, Heuristic SURE and Minmax methods (Figure 4.4).

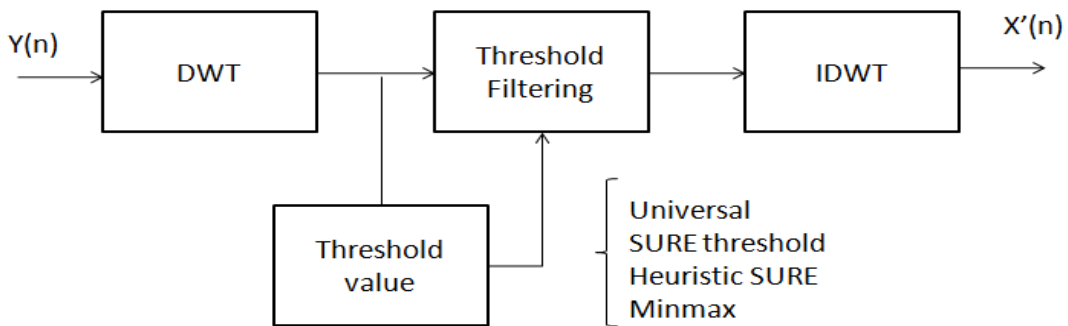


Figure 4.4 Denoising process based on DWT.

The criteria utilized to evaluate the denoising performance were the Mean Squared Error (MSE) and the Signal-to Noise-Ratio (SNR) values calculated from the reconstructed de-noised EEG signal $\hat{x}(n)$ and the original EEG $x(n)$ signal as follows:

$$MSE = \frac{1}{N} \sum_{i=1}^N [x(n) - \hat{x}(n)]^2 \quad (4.19)$$

and,

$$SNR = 10 \log \left| \frac{\sum_n \hat{x}^2(n)}{\sum_n [x(n) - \hat{x}(n)]^2} \right| \quad (4.20)$$

4.2.2.4 Results

The results of the different combination of denoising parameters are described in table 4.1, and Figure 4.5 shows an example on a denoised epoch.

Table 4.1 Denoising Performances

	Soft thresholding (mean values)				Hard thresholding (mean values)			
	SURE	Heuristic SURE	Universal	Minmax	SURE	Heuristic SURE	Universal	Minmax
MSE	117.64	117.19	111.30*	111.75	117.49	117.45	117.68	117.52
SNR	11.71	11.73	11.99 ⁺	11.96	11.72	11.72	11.71	11.71

*MSE lowest value, ⁺ SNR highest value

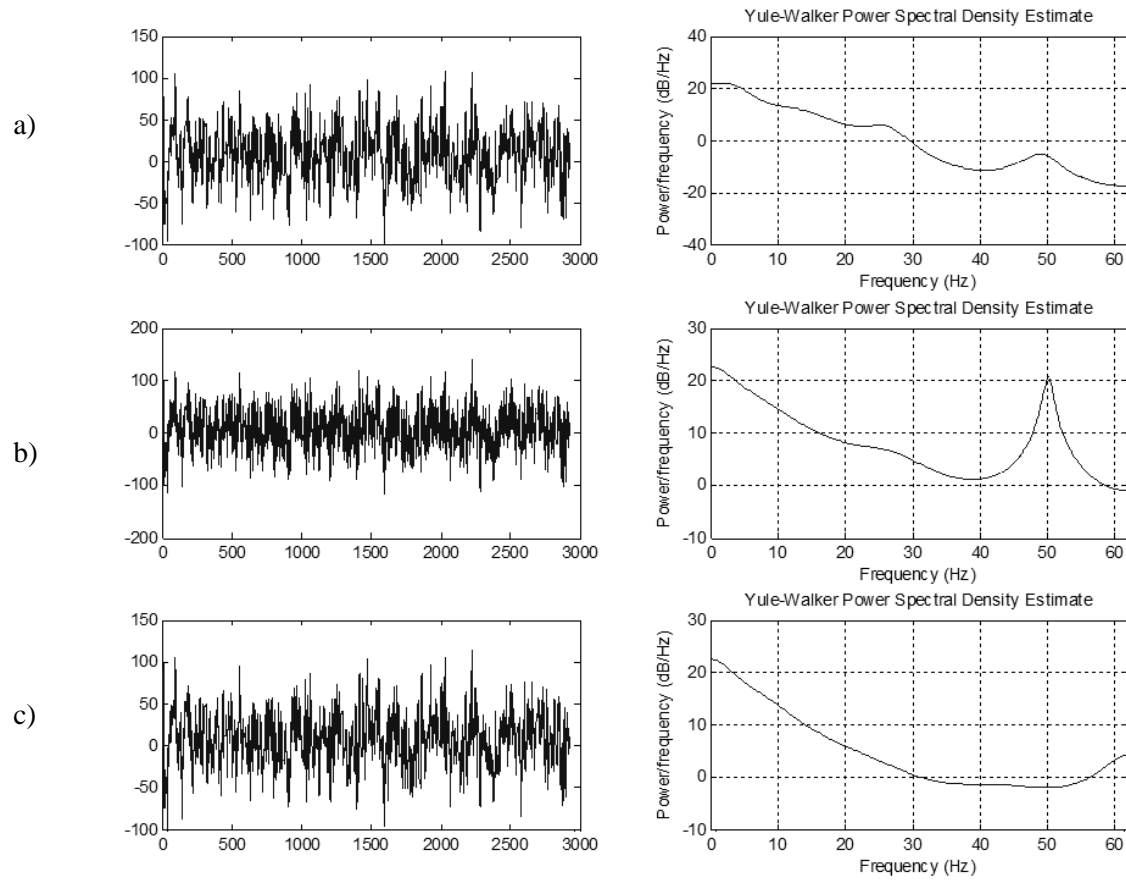


Figure 4.5 EEG (right) and PSD (left). a) Original EEG, b) Noisy EEG, c) De-noised EEG.

4.3. ECG Filtering and Denoising

The method described in previous section was utilized to filter and denoise the ECG signals. An advantage of bandpass filtering was that EEG and ECG signals used were sampled using the same sampling frequency (128 Hz). Thus the same filterbank was used to filter the ECG signal as well. In this particular case, the denoising method was based on the parameters described in [88]. Reddy et al., in their results achieved a better denoising performance ($MSE=8.8397$, $SNR= 14.9290$) by utilizing a Universal soft threshold, db5 and a 7-level DWT decomposition. The same parameters were used in this research.

Chapter 5. EEG Feature Extraction

5.1. Boxplots

, In this study it was used a technique known as boxplot to observe the distribution of the features extracted and to make visual comparisons based on the depth of sleep. A boxplot depicts the relationship among the median, upper quartile and lower quartile to describe the skewness of a distribution.

In this context, the upper and lower quartiles are defined as the 75th and 5th percentiles of the sample. In other words, the limits $\frac{3}{4}$ and $\frac{1}{4}$ are separated in the ordered sample. Boxplots are useful to judge the distribution symmetry. For example, if the distribution is symmetric, both the upper and the lower quartile must be equally spaced from the median line. A positively skewed distribution may be observed when the upper quartile is further from the median line than the lower quartile. Consecutively, the distribution is considered negatively skewed when the lower quartile is more separated from the median than the upper quartile value. [89].

In addition a boxplot is useful to visualize the spread of a sample. It can also be helpful to detect possible outlier values. A full boxplot construction will include:

- A vertical line bar or whisker from the upper quartile to the largest non outlying value contained in the sample.
- A vertical bar from the lower quartile to the smallest non outlying value in a sample.
- Identification of outlying values in the sample by a “+” or “*” symbol. Thus, an outlying value is labeled as a value x such that either:
 - o $x > \text{upper quartile} + 1.5 (\text{upper} - \text{lower quartile})$ OR
 - o $x < \text{lower quartile} - 1.5 (\text{upper} - \text{lower quartile})$

5.2. Relative Percent Spectral Energy Band

This frequency-domain feature requires the estimation of the EEG epoch's power spectrum $P(f)$. The $P(f)$ can be estimated using non-parametric methods such as Fast Fourier Transform (FFT) or spectral averaging methods (e.g. Welch's method). However, parametric-based methods have shown to provide smoother $P(f)$ estimations and improved smoothed spectrum profiles for short signal segments [46]. For this reason, an autoregressive (AR) parametric method was deployed to compute the $P(f)$ of EEG epochs. As it will be pointed out in later sections, this method was utilized as the standardized method to compute power spectrum densities of EEG and ECG signals as needed. Thus, a description of the autoregressive AR processes is presented first.

The autoregressive $AR(p)$ process is a special case of an Autoregressive Moving Average $ARMA(p,q)$ process when $q = 0$ [90] and the model order is p . The $AR(p)$ process is generated when unit variance white noise $w(n)$ is passed through an all pole filter of the form:

$$H(z) = \frac{b(0)}{1 + \sum_{k=1}^p a_p(k)z^{-k}} \quad (5.1)$$

The autocorrelation sequence of this process satisfies the Yule-Walker equations:

$$r_x(k) + \sum_{l=1}^p a_p(l)r_x(k-l) = |b(0)|^2; \quad k \geq 0 \quad (5.2)$$

where the autocorrelation function is defined by:

$$r_x(k) = \frac{1}{N} \sum_{n=0}^{N-1-k} x(n+k)x^*(n); \quad k = 0, 1, \dots, p \quad (5.3)$$

Hence, solving for these equations we can obtain the $a_p(l)$ coefficients. $b(0)$ can be found as follows:

$$|b(0)|^2 = r_x(0) + \sum_{k=1}^p a_p(k) r_x(k) \quad (5.4)$$

Using the estimates of the model coefficients, it is possible to estimate the Power Spectrum:

$$|H(z)|^2 \Big|_{z=e^{j\omega}} \approx \hat{p}_e(e^{j\omega})^w \frac{|\hat{b}(0)|^2}{\left|1 + \sum_{k=1}^p \hat{a}_p(k) e^{-jk}\right|^2} \quad (5.5)$$

where the power spectrum estimation $P(f)$ is defined as follows:

$$\hat{P}(f) = \hat{P}_e(e^{j2\pi f}) \quad (5.6)$$

The selection of the model order is a very important decision. If the order p is too low, the power spectrum of the signal would not be appropriately modeled. On the other hand, if the order is too high, the power spectrum could contain spurious peaks. Several criteria have been developed to find the correct model order. The Akaike information criterion establishes that AR processes require a model order from 8 to 12 in order to model delta, alpha, theta and beta rhythms [91].

For this analysis, the total power content (TPC) of $P(f)$ was computed (from 0.5 to 45 Hz). Then, $P(f)$ was divided into seven different energy bands (see Table 5.1), and the respective power energy bands (PEB) were calculated. The relative percent spectral energy band (RPEB) was then expressed as:

$$RPEB = \frac{PEB}{TPC} \times 100 \quad (5.7)$$

Table 5.1 Spectral Energy Bands.

Band energy		Bandwidth (Hz)
Delta 1	(δ_1)	0.5-2.5
Delta 2	(δ_2)	2.5-4
Theta 1	(θ_1)	4-6
Theta 2	(θ_2)	6-8
Alpha	(α)	8-12
Beta 1	(β_1)	12-20
Beta 2	(β_2)	20-45

5.2.2 Parameters Selection

The following parameters were used:

Table 5.2 Parameters and method selected.

Parameter	Description	Value/Method
PDS	Power Density Spectrum	AR Modeling (Yule-walker)
p	Model order	9
N	Epoch length	30 sec., Fs=128 Hz, 3840 samples

5.3 Horth Parameters

By definition, activity (m_0), mobility (m_2) and complexity (m_4) are represented by the following formulas:

$$m_2 = \int_{-\infty}^{\infty} w^2 S(w) dw = \frac{1}{T} \int_{t-T}^t \left(\frac{df}{dt} \right)^2 dt \quad (5.8)$$

$$m_4 = \int_{-\infty}^{\infty} w^4 S(w) dw = \frac{1}{T} \int_{t-T}^t \left(\frac{d^2 x}{dt^2} \right)^2 dt \quad (5.9)$$

where m_n in the spectral moment of order n , $S(w)$ in the power density spectrum in radians and $x(t)$ is the EEG signal as a function of continuous time.

Their computation in discrete time involves the variance (σ_0) of $x(n)$ (the segment of the EEG signal to be analyzed) as well as the variance of the first and second derivatives of $x(n)$ (σ_1 and σ_2 , respectively). These measures are described by the following formulas:

$$Act i v i o \sigma_0^2 \quad (5.10)$$

$$Mobility = \frac{\sigma_1}{\sigma_0} \quad (5.11)$$

$$Comp l e x \sqrt{\left(\frac{\sigma_2}{\sigma_1}\right)^2 - \left(\frac{\sigma_1}{\sigma_0}\right)^2} \quad (5.12)$$

Given that Hjorth parameters are based on variances, the computational cost is affordable compared to other methods.

5.3.1 Parameters Selection

The following parameters were used:

Table 5.3 Parameters and method selected.

Parameter	Description	Value/Method
$x'[n]$ and $x''[n]$	Discrete derivatives	$x'[n]=x[n]-x[n-i]$
N	Epoch length	30 sec., Fs=128 Hz, 3840 samples

5.4 Harmonic Parameters

The calculation of harmonic Hjorth parameters requires power spectrum estimation $P(f)$ of the epoch and they are defined as follows:

$$f_c = \int_{f_L}^{f_H} fP(f)df / \int_{f_L}^{f_H} P(f)df \quad (5.13)$$

$$f_\sigma = \sqrt{\int_{f_L}^{f_H} (f - f_c)^2 P(f)df / \int_{f_L}^{f_H} P(f)df} \quad (5.14)$$

$$Pf_c = P(f_c) \quad (5.15)$$

Since the computation of $P(f)$ involves discrete values, the above formulas were approximated using summations as follows:

$$f_c = \sum_{f=f_L}^{f_H} f \hat{P}(f) / \sum_{f=f_L}^{f_H} \hat{P}(f) \quad (5.16)$$

$$f_\sigma = \sqrt{\sum_{f=f_L}^{f_H} (f - f_c)^2 \hat{P}(f) / \sum_{f=f_L}^{f_H} \hat{P}(f)} \quad (5.17)$$

$$Pf_c = \hat{P}(f_c'). \quad (5.18)$$

In the above formulas, the f index spans from 0.5 to 45 Hz.

5.4.1 Parameters Selection

The following parameters were used:

Table 5.4 Parameters and method selected.

Parameter	Description	Value/Method
PDS	Power Density Spectrum	AR Modeling (Yule-walker)
p	Model order	9
	Discrete integration method	Trapezoidal
N	Epoch length	30 sec., Fs=128 Hz, 3840 samples

5.5 Itakura Distance

Itakura distance is used widely in speech processing applications to measure the distance between 2 AR processes [92, 93]. Here the Itakura distance was used to measure the similarity of a baseline EEG epoch (Awake, Stage1, Stage2, Stage 3, Stage 4, REM) with the rest of the epochs in the EEG vector. If we let the baseline epoch $x(n)$ be an AR process given by $a_x = [1 - a_1 - a_2 \dots - a_p]$ and the segment $y(n)$ to be compared to it given by $a_y = [1 - a_1 - a_2 \dots - a_p]$, then the minimum mean square error (MMSE) for the baseline process is:

$$MSE_{x,x} = a_x^T R_x(p) a_x \quad (5.19)$$

where $R_x(p)$ is the autocorrelation matrix for the baseline epoch of size $p+1$:

$$R_x(p) = \begin{bmatrix} r_x(0) & r_x(1) & \dots & r_x(p) \\ r_x(1) & r_x(0) & \dots & \\ \dots & \dots & \dots & \\ r_x(p) & \dots & \dots & r_x(0) \end{bmatrix} \quad (5.20)$$

Similarly the MSE of the other processes passing through the baseline model will be:

$$MSE_{x,y} = a_y^T R_x(p) a_y \quad (5.21)$$

The Itakura distance of the baseline to the other epochs is defined as:

$$d_{I_{x,y}} = 1 - \left(\frac{\frac{M}{S_{x,y}}}{\frac{\bar{M}}{\bar{S}_{x,x}}} \right)^E = 1 - \left(\frac{a_y^T R_x(p) a_y}{a_x^T R_x(p) a_x} \right)^E \quad (5.22)$$

The closer to a_x the parameter set a_y is, the smaller the $MSE_{x,y}$, since a_x is obtained to produce the minimum squared error. A distance closer to zero indicates a ratio closer to one, thus a closer match between the baseline $x(n)$ and segment $y(n)$. Furthermore, an analysis of how well $y(n)$ is modeled via the AR parameters of $x(n)$ can be done, thus the new Itakura distance is:

$$d_{I_{y,x}} = 1 - \left(\frac{\frac{M}{S_{y,x}}}{\frac{\bar{M}}{\bar{S}_{y,y}}} \right)^E = 1 - \left(\frac{a_x^T R_y(p) a_x}{a_y^T R_y(p) a_y} \right)^E \quad (5.23)$$

Combining $d_{I_{x,y}}$ and $d_{I_{y,x}}$, we obtain the symmetric Itakura distance as:

$$d'_{I_{x,y}} = \frac{1}{2} (d_{I_{x,y}} + d_{I_{y,x}}) \quad (5.24)$$

The Awake stage segment is set as the baseline and it is compared versus the subsequent epochs. Itakura distances obtained with different AR model orders reveal that regardless of the model order “ p ”, Itakura distance changes significantly when brain activity changes [61].

5.5.1 Parameters Selection

The following parameters were used:

Table 5.5 Parameters and method selected.

Parameter	Description	Value/Method
PDS	Power Density Spectrum	AR Modeling (Yule-walker)
p	Model order	9
	Discrete integration method	Trapezoidal
N	Epoch length	30 sec., Fs=128 Hz, 3840 samples
a_x	Baseline	sleep epoch scored as Awake Stage

5.6 Wavelets

The WPT of depth 7 was designed following the wavelet theory presented in section 4.2. Thus the energy mean quadratic values were computed from the following bands (or combination of terminal nodes) as described in detail in [22].

- E1: K complexes + Delta (0.5-1.55Hz)
- E2: Delta (1.5-3.0 Hz)
- E3: Theta (3.0-8.5 Hz)
- E4: Alpha (8.5-11.0 Hz)
- E5: Spindles (11.0-15.5 Hz)
- E6: Beta 1 (15.5-22.0 Hz)
- E7: Beta 2 (22.0-37.5 Hz)

And six more ratio energy features:

- E8: Total Energy of the seven previous bands
- E9: Percent Delta Activity Ratio (E1+E2)/E8
- E10: Percent Alpha Activity Ratio E4/E8
- E11: Percent K-complexes and Sindle Activity Ratio (E1+E5)/E8
- E12: Ratio alpha/theta activity Ratio E4/E3
- E13: Ratio delta/theta activity Ratio (E1+E2)/E3

Finally, the energy mean quadratic is calculated as follows:

$$Energy = \frac{\sum_{i=1}^N (c(n) - \overline{c(n)})^2}{N} \quad (5.25)$$

5.6.1. Parameters Selection

The following parameters were used:

Table 5.6 Parameters and method selected.

Parameter	Description	Value/Method
<i>Wavelet</i>	Wavelet family	Db2
<i>l</i>	Number of levels	7
N	Epoch length	30 sec., Fs=128 Hz, 3840 samples

5.7 Empirical Mode Decomposition

The algorithm for Empirical Mode Decomposition (EMD) is described as follows:

1. First, the computation of all extreme points (peaks and valleys) of $x(t)$ is computed.
2. In order to construct $x(t)$ envelopes $e_{max}(t)$ and $e_{min}(t)$, the maxima and minima outliers are interpolated.
3. The signal $m(t)$ is computed by averaging the envelopes: $(e_{max}(t) + e_{min}(t))/2$.
4. Finally, the detailed signal $d(t)$ is calculated by subtracting $m(t)$ from $x(t)$.

5. Iterations are performed on the residual signal $m(t)$.

As discussed in [60] this algorithm requires to be refined by a “sifting” process which summarizes the first iterating step 1 to 4 leading the detailed signal $d(t)$. The sifting process terminates when the stop criterion (e.g. $d(t)$ has a mean value close to zero) is reached. In this research the EMD algorithm was applied to EEG signals and the first six Intrinsic Mode Functions (IMF) functions were extracted using the freeware matlab toolbox *emd.m* available online in [94]. Then the center frequency (f_c) of each IMF function was calculated as described equation 5.16.

5.7.1. Parameters Selection

The following parameters were used:

Table 5.7 Parameters and method selected.

Parameter	Description	Value/Method
<i>IMF</i>	Number of IMF functions	6
Fc	Center frequency	Described in section 5.3
N	Epoch length	30 sec., Fs=128 Hz, 3840 samples

5.8 Detrended Fluctuation Analysis

This method has been devised to detrend variability in a sequence of events [95]. The DFA computation involved the calculation of the summed series:

$$y(k) = \sum_{t=1}^k \{X(t) - E[X]\} \quad (5.26)$$

where $y(k)$ is the k-th value of the summed series, $X(t)$ represents the sequence (epoch to be evaluated) at time t, and $E[X]$ the average of the entire time series $\{X(t)\}$. The summed series was divided into sub sequences of length m and a least squares fit was performed on each of the data

segments, providing the detrends for the individual segments. Detrending was carried out by subtracting the local trend $y_m(k)$ in each segment. The root-mean-square fluctuation of the resulting series was then:

$$F(m) = \left\{ \frac{1}{L} \sum [y(k) - y_m(k)]^2 \right\}^{1/2} \quad (5.27)$$

A linear relationship on a log-log plot indicates the presence of power law (fractal) scaling. Under such conditions, the fluctuations can be characterized by a scaling exponent α , the slope of the line relating $\log F(m)$ to $\log m$.

5.8.1 Parameters Selection

The following parameters were used:

Table 5.8 Parameters and method selected.

Parameter	Description	Value/Method
$y_m(k)$	Local trend	Linear regression
M	Number of Boxes	10-20
N	Epoch length	30 sec., Fs=128 Hz, 3840 samples

5.9 Correlation Dimension

In order to compute the correlation dimension (D2) of a time series $x(n)$, the embedding dimension m is set to construct a K number of points in the corresponding embedding space [96-97]. Let's consider the following time series with length N:

$$\vec{x} = \{P_1, P_2, P_3, P_4, \dots, P_N\} \quad (5.28)$$

Consequently, the points are formed as follow:

$$\vec{X}_1 = \{P_1, P_2, \dots, P_m\} \quad (5.29)$$

$$\vec{X} = \{P_1, P_2, \dots, P_m\}$$

$$\begin{aligned}
\overrightarrow{X_3} &= \{P_{(1+2\tau)}, P_{(2+2\tau)}, \dots, P_{(m+2\tau)}\} \\
&\dots \\
\overrightarrow{X_K} &= \{P_{(1+(K-1)\tau)}, P_{(2+(K-1)\tau)}, \dots, P_{(m+(K-1)\tau)}\}
\end{aligned} \tag{5.30}$$

Where the number of K sub-vectors are defined by the dimensionality of the space m and the time lag τ :

$$K = (K - m) / \tau + 1 \tag{5.31}$$

Then, the correlation integral $Cm(r)$ is calculated by finding the ratio of the total X_K pairs and those pairs that have an Euclidean distance less than a radius r . The value of r starts at 0 and it ends at the maximum distance found in the X_K pairs.

$$Cm(r) = \frac{1}{N_p} \sum_{i=1}^K \sum_{j=1}^K \Theta\left(r - \|X_i - X_j\|\right) \Big|_{r=0 \rightarrow \max\|X_i - X_j\|} \tag{5.32}$$

Where Θ is the Heaviside function defined as:

$$\begin{aligned}
\Theta(x) &= 1, x \geq 0 \\
\Theta(x) &= 0, x < 0
\end{aligned} \tag{5.33}$$

And, N_p as the numbers of different X_K pairs:

$$N_p = K(K-1)/2 \tag{5.34}$$

Let's consider a tridimensional embedding space $m=3$ and a set of points $K=6$ (Figure 5.1). The integral $Cm(r)$ can be represented as a growing sphere with radius r . This is sometimes called the sphere counting method. As the radius is increased up to its maximum value, the number of points contained within the sphere increases and eventually all points are embedded in it. Thus, $Cm(r)$ behaves as a monotonic increasing function with values from 0 to 1.

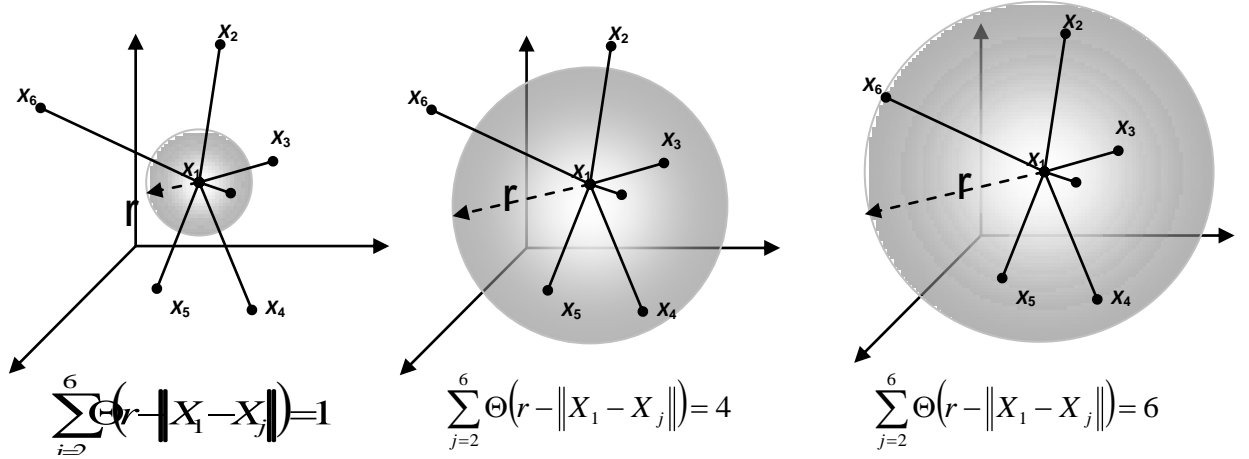


Figure 5.1 Visual representation of $Cm(r)$ integral in a tridimensional embedding space using the sphere counting method.

Grassberger and Procaccia showed that $Cm(r)$ behaves as a power law of r :

$$Cm(r) = \alpha r^{D2} \quad (5.35)$$

The correlation dimension $D2$ is defined as the slope within the scaling region of the curve

$\log_2(Cm(r))$ vs. $\log_2(r)$:

$$D2 = \lim_{r \rightarrow 0} \left[\frac{\log_2(Cm(r))}{\log_2(r)} \right] \quad (5.36)$$

5.9.1 Parameters Selection

The following parameters were used:

Table 5.9 Parameters and method selected.

Parameter	Description	Value/Method
τ	Time lag	2
M	Constructed phase space	10-20
N	Epoch length	500 first samples for each epoch

5.10 Approximate Entropy

The ApEn feature was computed using the correlation integral $C_{m,i}(r)$ defined by Pincus [76], that establishes the self-similarity of a m-constructed space from the time series $X[n]$ of length N given a filter factor of “ r ”:

$$C_{m,i}(r) = \frac{\text{Number of } x(j) \text{ such that } d[x(i), x(j)] \leq r}{N-m+1} \quad (5.37)$$

That can be defined by the Heaviside function $\Theta(x)$ as:

$$C_{m,i}(r) = \frac{\sum \Theta(r - d[x(i), x(j)])}{N-m+1} \quad (5.38)$$

Furthermore, ApEn is defined as:

$$ApEn = \Phi^m(r) - \Phi^{m+1}(r) \quad (5.39)$$

And

$$\Phi^m(r) = \frac{1}{N-(m-1)} \sum_{i=1}^{N-(m-1)} \ln C_{m,i}(r) \quad (5.40)$$

Finally,

$$ApEn = \frac{1}{N-(m-1)} \sum_{i=1}^{N-(m-1)} \ln C_{m,i}(r) - \frac{1}{N-m} \sum_{i=1}^{N-m} \ln C_{m+1,i}(r) \quad (5.41)$$

5.10.1 Parameters Selection

The following parameters were used:

Table 5.10 Parameters and method selected.

Parameter	Description	Value/Method
r	Filter Factor	0.2 σ
m	Constructed phase space	2
N	Epoch length	500 first samples for each epoch

Chapter 6. Derivation of HRV Signals and HRV Features Extraction

6.1 Derivation of Heart Rate Variability Signal

As was mentioned before, HRV refers to the signal derived from the QRS complexes of the ECG signal, which displays the beat to beat modulation of the heart rate largely controlled by the ANS, as a result of the balance between the PNS and SNS subsystems. As the HRV signal is a non-invasive marker of possible irregular behavior of the ANS control associated with SDB, the accurate detection of the R peaks and correct derivation of the HRV signal are highly important.

In a previous work our group presented a robust approach for determination of the QRS complexes based on an Enhanced Hilbert Transform (EHT) algorithm [98]. It has also been shown by others that by applying the first derivative of the ECG signal followed by the conjugation of its Hilbert Transform (HT) resulted in an effective method to detect and differentiate R peaks from T and P waves with a high degree of accuracy [99, 100]. In these works, transformed ECG signals values that were greater in amplitude than a predefined threshold were selected as possible peak regions. Hence, the threshold was set equal to the RMS value of the signal. Then the R-peaks were detected by comparing the amplitude of the ECG signal of the selected possible peak region samples. The samples with larger amplitude were then considered as the R-peaks and those amplitude and sample positions were stored in a separate array to generate the HRV signal. In our EHT method we compared and analyzed the R-R intervals looking for possible missing peaks. The rule used to determine missing R-peaks was defined as follow:

“If an $R-R_i$ interval was greater than 130% of the previous $R-R_{i-1}$ interval, the QRS complex was considered missing”.

The correction of the HRV signal was based on an updated moving average of previous R-R intervals. The peak amplitude was determined as the average of adjacent $R-R_{i-1}$ and $R-R_{i+1}$ whereas the position in time was determined by the moving average predictor.

After derivation of the HRV signal, it was ready for time domain or nonlinear time series analysis. However, in the case of frequency domain analysis the derivation of the HRV signal required an extra step to resample the R-R intervals and thus obtain an equally sampled signal with a defined sampling frequency. Cubic spline functions were used to interpolate the discrete HRV signal and construct a continuous-time signal. Consequently, the new equally sampled HRV signal was computed by sampling the continuous signal at a sampling rate of 2 Hz. Then the HRV signal was decimated and low pass filtered to 1 Hz allowing the computation of PSD estimations from 0 to 0.5 Hz (Figure 6.1) [98].

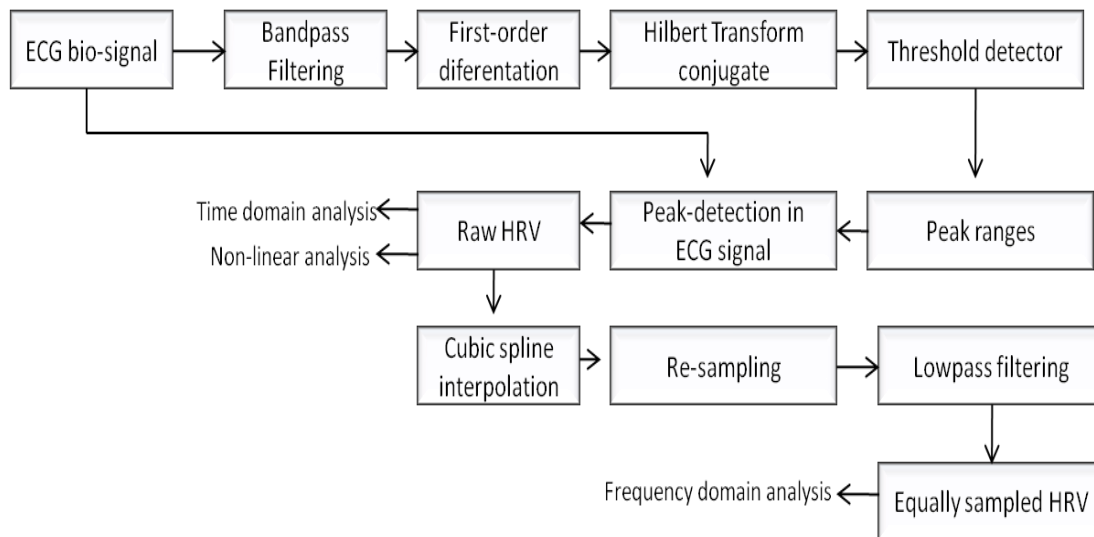


Figure 6.1 EHT-based derivation of the HRV signal.

6.2 Time-domain Features

The mean RR and the standard deviation of RR (SDNN) intervals were computed using the following formulas:

$$\text{meanRR} = \frac{\sum_{i=1}^n \text{RR}_i}{n} \quad (6.1)$$

and

$$\text{SDNN} = \sqrt{\frac{1}{n} \sum_{i=1}^n (\text{RR}_i - \text{meanRR})^2} \quad (6.2)$$

6.2.1 Parameter Selection

The following parameters were used:

Table 6.1 Parameter Selection.

Parameter	Description	Value/Method
N	Epoch length	Variable, depends on the number of QRS complexes present in 5-minute ECG tracings

6.3 Frequency-domain Features

In this research, the HF in nomal units (HF_{n.u.}) and LF_{n.u.} were extracted from the interpolated HRV signal discussed in section 6.1. The PDS was computed by means of a non-parametric AR modeling. HF_{n.u.} and LF_{n.u.} features were computed as follow:

$$\text{HF}_{n.u.} = \frac{HF}{(\text{Total Power} - \text{VLH})} \quad (6.3)$$

and

$$\text{LF}_{n.u.} = \frac{LF}{(\text{Total Power} - \text{VLH})} \quad (6.4)$$

6.3.1 Parameter Selection

Table 6.2 Parameter Selection.

Parameter	Description	Value/Method
PDS	Power Density Spectrum	AR Modeling (Yule-walker)
p	Model order	9
N	Epoch length	Variable, depends on the number of QRS complexes present in 5-minute ECG tracings

6.4. Nonlinear Features

6.4.1 Detrended Fluctuation Analysis

The algorithm used to compute the scaling alpha value is described in section 5.8. The following parameters were used for this computation:

Table 6.3 Parameter Selection.

Parameter	Description	Value/Method
$y_m(k)$	Local trend	Linear regression
m	Number of Boxes	10-20
N	Epoch length	Variable, depends on the number of QRS complexes present in 5-minute ECG tracings

6.4.2 Correlation Dimension

The algorithm used to compute the CD feature is described in section 5.9. The following parameters were used to compute the CD:

Table 6.4 Parameter Selection.

Parameter	Description	Value/Method
τ	Time lag	2
m	Constructed phase space	10-20
N	Epoch length	Variable, depends on the number of QRS complexes present in 5-minute ECG tracings

6.4.3 Approximate Entropy

The algorithm used to compute the ApEn feature is described in section 5.10. The following parameters were used to compute approximate entropy:

Table 6.5 Parameter Selection.

Parameter	Description	Value/Method
r	Filter Factor	0.25 σ
m	Constructed phase space	2
N	Epoch length	500 first samples for each epoch

6.5 Results

Preliminary results and the trends of EEG and HRV features for one subject are presented in Appendix 3 as an example., It was observed that tendencies for both sets of features were similar to those trends found in the literature [21, 22, 45-50, 56, 60, 69, 72-79]. In the following chapter, the relationship between EEG and HRV features for all subjects will be described.

Chapter 7. Relationships between EEG and HRV Features

The complex relationships and similarities between EEG and HRV features are described in this chapter from different points of view and analysis. The behavior of each feature vector within the different specific sleep stages or respiratory events is also analyzed and explained. This analytical knowledge could strongly impact the development of future automatic sleep stage classification or sleep apnea detection systems.

A common oversight when designing a classifier system is that the input vectors are pre-processed (e.g. normalized, transformed) and fed to the system without analyzing and understanding the behavioral patterns of features and their impact on classifier performance. Hence the accuracy of the system is mainly dependent on its architecture and parameters, and any attempt to improve its performance is achieved by trying to adjust its structural components only. In addition, the feature extraction/classification system output will be described by a pointless black-box overall behavior and this may not translate into a practical opportunity to implement the system into a final reliable product. Furthermore, this is a critical stage of the research that helps us deeply understand the character of the problem and gain valuable insight into the quality of the extracted features which in turn play an essential role in determination of the failure or success of the classifier system.

Trend analysis was performed for all the features extracted from 25 subjects as described in chapters 5 and 6. Table 7.1 shows the total number (e.i. sample size) of features extracted for this study. Due to the large amount of data, the sample size to be analyzed was determined guided by a power analysis in order to avoid Type II errors and avoid accepting false significant statistical differences in this study [101]. The sample size was calculated using the computational

program *G. Power 3.1*. Alpha was set to 0.01, effect size to 0.5, power to 0.8 ($1 - \beta = 0.8$), and the required numbers of sleep stages (groups) to 6.

Table 7.1 Population of extracted features.

Stage	Number of samples	Respiratory Events Distribution		
		Normal Breathing	Hypopnea	Apnea
Awake	4,707	4584	107	16
Stage 1	3,403	3156	221	26
Stage 2	6,985	6634	312	39
Stage 3	673	657	13	3
Stage 4	1,990	1966	15	9
REM	3,016	2706	274	36
Totals	20,774	19703	942	129

The power analyses were designed to study the associations between the extracted features. Figure 7.1 provides an exploratory model to investigate the relationships among various features, sleep stages and respiratory events and guide the statistical analyses that will be described in later sections.

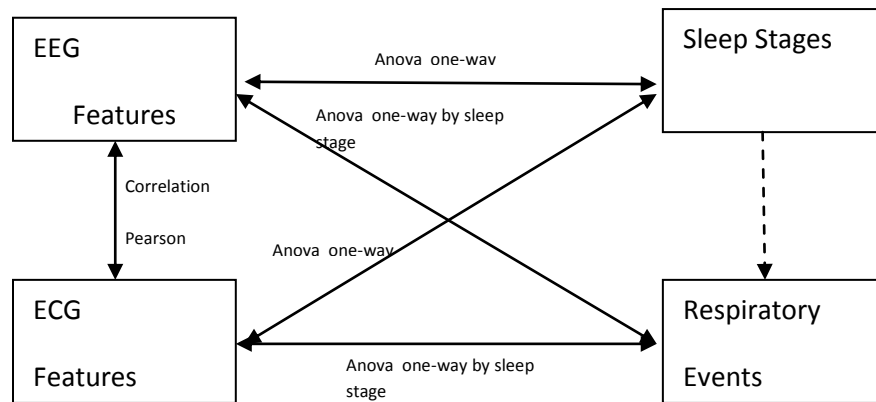


Figure 7.1 Exploratory model to investigate the relationships among study variables.

7.1 Correlations between EEG vs. EEG Features, EEG vs. HRV Features, and HRV vs. HRV Features

First, to study the connections between EEG and HRV features, a correlation study based on the computation of the Pearson coefficient “ r ” was performed in this experiment. The Pearson coefficient r ranges from +1 to -1. A correlation of +1 means that there is a perfect positive linear relationship between variables whereas a value of -1 implies a perfect negative linear relationship. A zero value is given when there is no relationship between the variables. The Pearson coefficient between two continuous variables X and Y can be calculated with the following formula:

$$r_{xy} = \frac{\sum x_i y_i - n \bar{x} \bar{y}}{(n-1) s_x s_y} \quad (7.1)$$

Moreover, the number of trials performed was based on the number of the possible different feature pairs and thus allowed the construction of the well-known correlation matrix. Considering that 44 features were extracted, the number of different pairs was 44x44. However, a correlation matrix is a symmetric matrix along the principal diagonal and the correlation of the pair “feature A” vs. “feature B” is the same as the pair “feature B” vs. “feature A”. Moreover, the correlation of a feature vs. itself produces a r value of 1. Therefore, a total of 924 $([44 \times 44] / 2 - 44)$ correlations were computed. Table 7.2, shows the number of samples required to achieve significant differences based on the parameters involved. Figure 7.2 shows the effect of the sample size on the power variable.

Table 7.2 Power analysis for correlation test.

t tests – Correlation: Point biserial model		
Analysis: A priori: Compute required sample size		
Input:	Tail(s)	= Two
	Effect size $ \rho $	= 0.5
	α err prob	= 0.01
	Power (1- β err prob)	= 0.80
Output:	Noncentrality parameter δ	= 3.6055513
	Critical t	= 2.7154087
	Df	= 37
	Total sample size	= 39
	Actual power	= 0.8069446

Samples were obtained from the total population randomly without replacement.

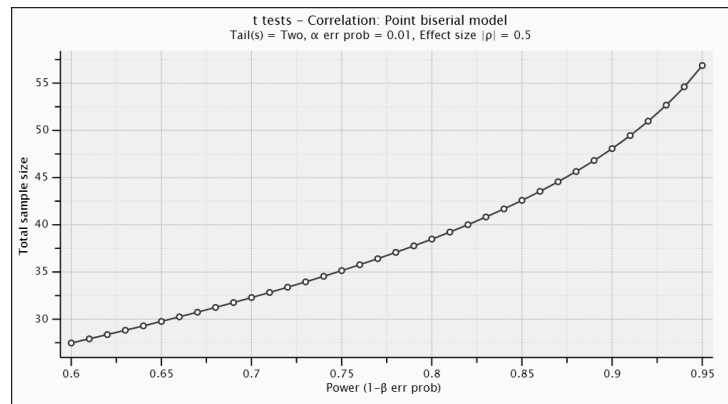


Figure 7.2 the effect of the sample size on the power variable.

7.2 EEG and HRV Features vs. Sleep Stages

The objective of this experiment was to determine if the extracted feature vectors and their central measurements based on the sleep stages were significantly different. The best statistical tool to analyze these behaviors was the one-way ANOVA test due to the nature of the dependent continuous variables (i.e. features vectors) and the independent categorical variable (i.e. sleep stage). A detailed procedure to compute the ANOVA's p significant value can be found in [89]. A total of 44 analyses were performed and the power analysis to determine the sample size given that there were 6 groups to compare (Awake, Stage 1, Stage2, Stage 3, Stage 4

and REM) is given in table 7.3. Figure 7.3 shows the effect of the sample size on the value of the power coefficient.

Table 7.3 Power analysis for ANOVA test (6 groups).

F tests – ANOVA: Fixed effects, omnibus, one-way		
Analysis:	A priori: Compute required sample size	
Input:	Effect size f	= 0.5
	α err prob	= 0.01
	Power (1- β err prob)	= 0.80
	Number of groups	= 6
Output:	Noncentrality parameter λ	= 21.0000000
	Critical F	= 3.2614145
	Numerator df	= 5
	Denominator df	= 78
	Total sample size	= 84
	Actual power	= 0.8346766

Samples were obtained from the total population randomly without replacement.

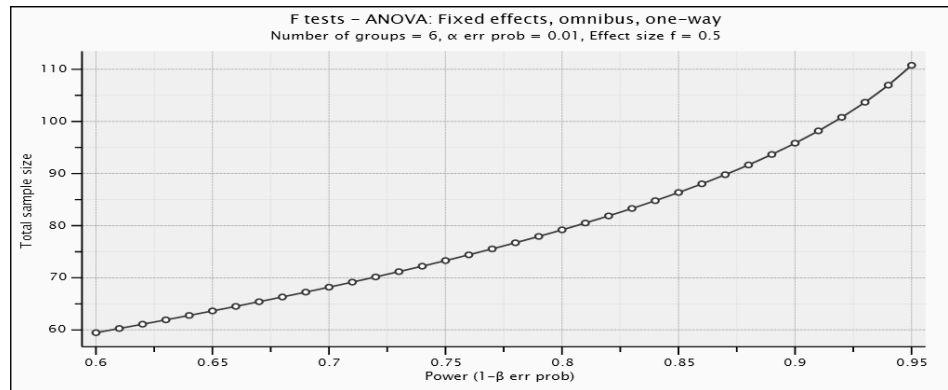


Figure 7.3 The effect of the sample size on the power variable.

7.3 EEG and HRV features vs. Respiratory Events by Sleep Stage

The purpose of this statistical analysis was to determine if the respiratory events (i.e. normal breathing, hypopnea and apnea) have an effect on the feature vectors. As will be discussed in the next section there are statistical differences among sleep stages and feature vectors. For this particular reason, the analysis in this section was performed by sleep stages.

Therefore, a total of $44 \times 6 = 264$ different experiments were carried out. One way ANOVA was used, where the dependent variable was given by each feature and the independent categorical variable was based on the respiratory events. Table 7.1 shows the population of samples given by each sleep stage. Finally, the sample size was 63 based on the power analysis and the three different groups to analyze (Figure 7.4).

Table 7.4 Power analysis for ANOVA test (3 groups).

F tests – ANOVA: Fixed effects, omnibus, one-way		
Analysis:	A priori: Compute required sample size	
Input:	Effect size f	= 0.5
	α err prob	= 0.01
	Power (1- β err prob)	= 0.80
	Number of groups	= 3
Output:	Noncentrality parameter λ	= 15.7500000
	Critical F	= 4.9774320
	Numerator df	= 2
	Denominator df	= 60
	Total sample size	= 63
	Actual power	= 0.8240667

Samples were obtained from the total population randomly without replacement.

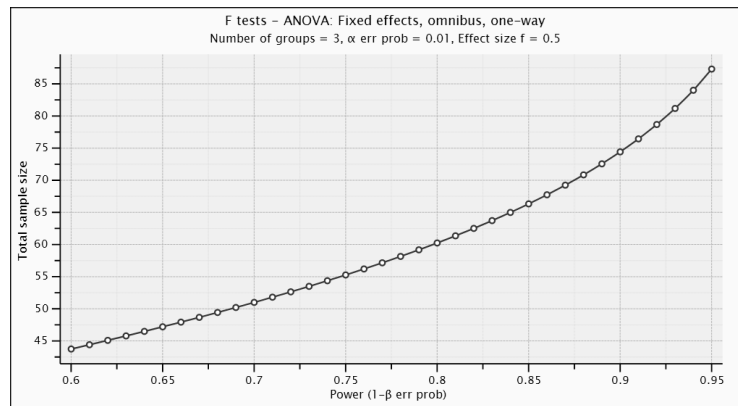
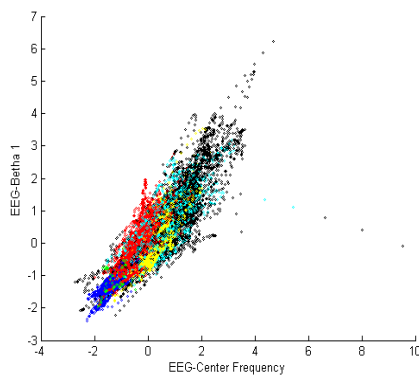


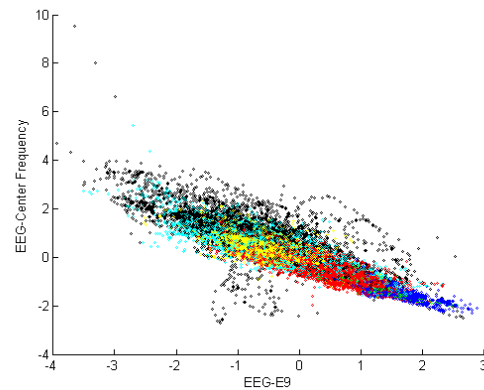
Figure 7.4 The effect of the sample size on the power variable.

7.4 Results

Results highlighted the strong correlations ($r > 0.9$ and $p > 0.01$) between different pairs of features. To name a few examples in the analysis of EEG vs. EEG features, Percent Delta Activity Energy (E9) was strongly correlated to RPEB delta 1 (fd1) whereas Spindles energy band (E5) was directly related to RPEB alpha (fal). It was also observed that harmonic parameters central frequency (fc) and bandwidth (fs) were correlated to features RPEB beta 1 (fb1) and RPEB beta 2 (fb2), respectively. The fb1 feature was significantly related to alpha (E4), beta 2 (E7) and percent alpha activity (E10) energies. An interesting correlation is given by the pair of E9 and fc that displayed a negative correlation between them. This behavior was also observed in the features mobility (m2) vs. complexity (m4). In addition some IMF's vector characteristics (IMF2,3) were related to RPEB beta 2 (fb2) and E7. Expanding on the IMF features it is important to highlight that the IMF1 is the only IMF that is not related to the other IMFs. Moreover, the pairs IMF2-IMF3, IMF3-IMF4 and IMF4-IMF5 are robustly correlated. The effect of the correlation value and the relationship of the variables can be seen in Figures 7.5 a, b, c.



a)



b)

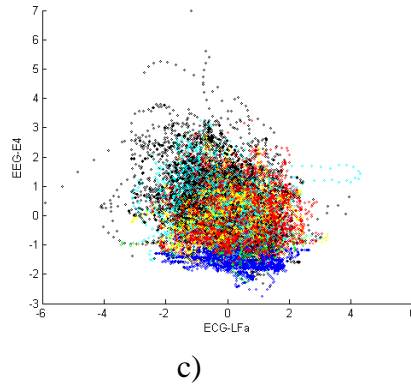


Figure 7.5 Different Pearson correlation values. a) $r \sim 1$, b) $r \sim -1$ and c) $r = 0$.

When analyzing the HRV features against themselves the weak correlations among them were noticeable. Only a few pair of variables showed high correlation values. For example the CD feature was correlated ($r=0.79$, $p<0.01$) positively to the ApEn variable. Result showed a perfect negative correlation ($r=-1$, $p<0.01$) between HFn.u. and LFn.u. more likely because the computation of both features are based on the ratio of HRV total power content. In addition, DFA was not strongly related to any other feature.

Exploring the correlations among EEG and HRV pairs of features, the results showed weak correlations ($r \sim 0.3$ $p<0.01$) on most of the EEG features compared with HRV features. The meanRR value was weakly correlated to RPEB delta 2 (fd2), HRV-ApEn to fd2 and HRV-DFA to fb2 feature. Moreover, the Hjorth features were correlated to meanRR. In contrast, LFn.u. HFn.u. HRV features were not associated to any other EEG feature ($r<0.3$, $p>0.01$).

Now if we consider these relationships from the point of view of the classifier system, the situation where two inputs having a strong correlation value may represent a disadvantage because both features are providing the same information to the classifier. Thus, features having zero or close to zero Pearson coefficients values are preferred because their information is not

redundant or duplicated, that is both feature elements are orthogonal (Figure 7.5c). The correlation matrix discussed here can be found in Appendix 5.

The relationships and statistical differences between features and sleep stages by means of one-way ANOVA analysis further highlighted and predicted the effectiveness of each feature vector on providing valuable information to the classifier system. A value of $p > 0.01$ meant that none of the six sleep stage mean values were significantly different enough to be segregated by a classifier. Samples taken from the population shown that a few features did not comply with the $p < 0.01$ criterion: E8, HRV-ApEn, LFn.u., HFn.u. and meanRR. Appendix 4 shows boxplots for the total number of features proposed in this research whereas the sampled features and one-way ANOVA analysis results are documented in Appendix 6.

The last set of one-way ANOVA analyses (recorded in Appendix 7) performed on EEG and HRV features vs. respiratory events by sleep stage showed which features were likely to be affected by the breathing condition. From the total of 264 trials only a few features complied with the $p < 0.01$ criterion. These feature vectors for sleep stages are displayed in the Table 7.5.

Table 7.5 Features with statistical differences for all three breathing conditions.

Awake	Stage 1	Stage 2	Stage 3	Stage 4	REM
<ul style="list-style-type: none"> • Delta 1 • Beta 2 • m2 • E2, E5, E6, E9 • <u>ApEn</u> • CD • IMF3, IMF5, IMG6 	<ul style="list-style-type: none"> • Delta 1 • Bandwidth • m2, m4 • E1, E2, E3, E4, E7, E8, E9 • <u>ApEn</u> • IMF5, IMG6 	<ul style="list-style-type: none"> • Beta 2 • m2 • Itakura Distance • <u>ApEn</u> • IMF3, IMF6 	<ul style="list-style-type: none"> • Beta 1 • Beta 2 • Center Frequency • m4 • E6, E7, E10, E12 • Itakura Distance • <u>ApEn</u> • IMF3 	<ul style="list-style-type: none"> • Theta 2 • Beta 1 • E3, E4, E7, E9, Itakura Distance • <u>ApEn</u> • CD • IMF3, IMF5 	<ul style="list-style-type: none"> • DFA

It is observed in Appendix 7 that in REM stage, DFA is the only sleep feature that changes significantly given a normal, hypopnea or apnea breathing condition ($p > 0.01$). The EEG-ApEn indicated a significant difference for the breathing condition mentioned for most of the sleep stages except REM stage. Thus, a reflection of the neurological status and ANS activity is reflected by means of the EEG-ApEn feature.

Chapter 8. Neural Network Design

8.1 EEG and HRV Feature Preprocessing

As explained in Chapter 7, understanding the behavior of the input features is highly important for the success of the classifier system. Once these relationships and trends are well explored and established, the next logical step is to process the features to a desirable format that will produce an enhanced performance on the overall system. Preprocessing the feature vectors is as important as filtering the raw EEG and ECG signals. In some sense the feature characteristics are “contaminated” and depict a noise-like tendency. Also, the features must be normalized to be able to control and minimize inter-subject variability within the biosignals (make them subject-invariant).

8.1.1 Feature Smoothing

In this research, the first step to preprocess the input feature vectors was to filter or smooth the feature behavior. Although somewhat controversial given the fact that it somehow changes the values of the features, this allows us to eliminate the erratic behavior of features and results in generation of smoother characteristics that are compatible with the natural (smooth) changes in sleep states during the night (Figure 8.1). Filtering input features have been attempted before by other authors using moving average filters to improve the behavior and performance of their classifier systems [102, 103].

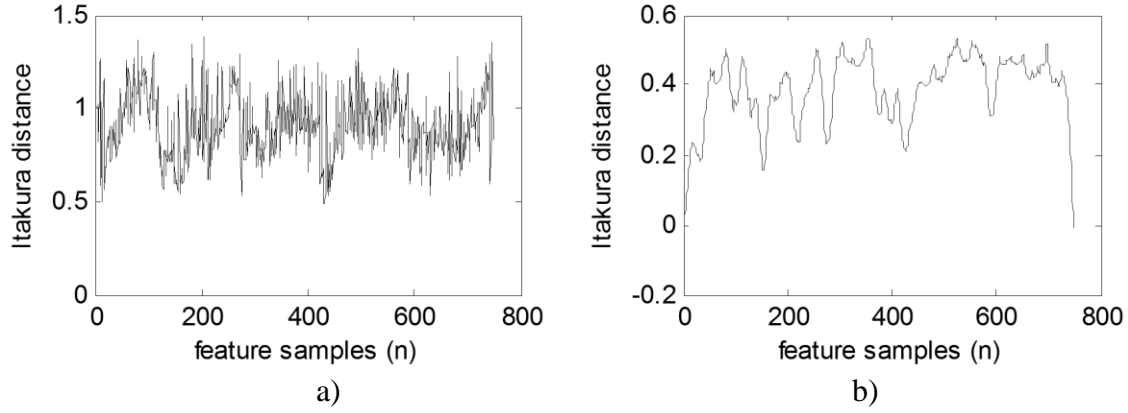


Figure 8.1 a) Raw feature b) Smoothed feature.

This study used a Savitzky-Golay filtering technique to smooth out the inputs features. This type of filter is based on moving polynomial local regression functions of order n over a region of size m that are used to interpolate and de-noise signals [104]. Also, another advantage to smooth out the features is that it minimizes the effect of outlier values as seen in Figure 8.2.

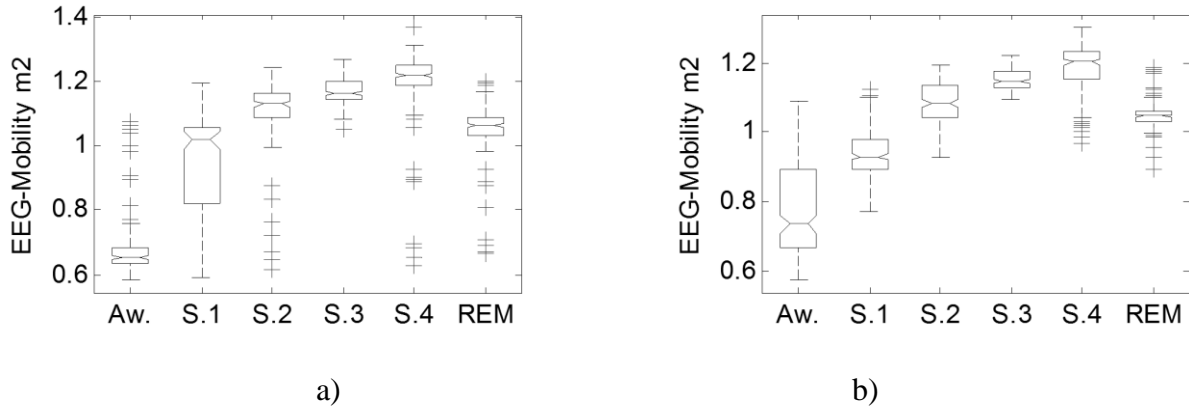


Figure 8.2 a) Raw feature b) Smoothed feature.

8.1.2 Feature Normalization

Features vectors were normalize in order to construct a larger dataset containing feature values from all subjects. The objective of feature normalization is to minimize the inter-subject variability by adjusting vector values to result in more reliable and robust behavior. Here, feature vector normalization was achieved by removing any trends contained in the characteristics

analyzed. First, the mean was removed from all feature vectors. Then, data distribution was normalized by dividing the feature vector by its corresponding σ scalar value:

$$F_{Normalized} = \frac{F - \bar{X}_F}{\sigma_f} \xrightarrow{yields} N(0,1) \quad (8.1)$$

8.1.3 Principal Component Analysis

The objective of this step was to transform the set of correlated features and project them into a m-dimesional space where they have the maximum variability possible and they are uncorrelated. This orthogonal transformation is achieved by means of the computation of the characteristic eigenvalues and eigenvectors. A full description of this method can be found in [105].

8.2 Neural Network Design

8.2.1 Feedforward Artificial Neural Network

Once the input features are ready to be fed into a classifier system, an advanced system was required to process and classify the feature vectors. A “mini brain” capable of learning from an appropriate set of inputs with the best accuracy was designed to facilitate the automated sleep staging based on EEG and HRV features [106]. To accomplish this objective an Artificial Neural Network (ANN) was designed as the classifier system.

This section covers the mathematical background on the Feedforward ANN topology and the backpropagation training technique. In a general sense, the ANN has two manners of operation: training and testing. For training purposes, a group of data samples from EEG and HRV features were input into the classifier and the obtained output was compared vs. the scoring

sleep stage vector (“gold standard”). Thus, the error between the desired output and obtained output was minimized by adjusting the weight values in the ANN to produce better results. For testing, after all weights were estimated, a different group of data samples from EEG and HRV features were input again into the classifier in order to study the overall performance of the classifier system.

A Feedforward Artificial Neural Network architecture with back propagation algorithm was used in training, evaluating, and implementing the neural network (a block diagram is presented in Figure 8.3). It consisted of obtaining a specific output pattern or set of patterns (matrix approach) from a pre-processed input pattern or set of patterns. Moreover, at the output training vectors associated with the input vectors are given in Table 8.1.

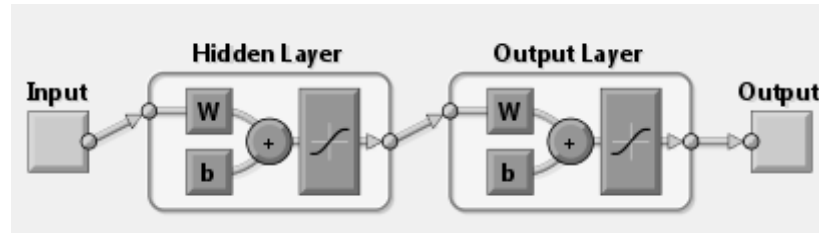


Figure 8.3 Feedforward Neural Network block diagram.

Table 8.1 Codification of Sleep Stages AASM.

Sleep Stage	Training Vector Value
W	[0 0 0 0 1]
N1	[0 0 0 1 0]
N2	[0 0 1 0 0]
N3	[0 1 0 0 0]
R	[1 0 0 0 0]

The feedforward ANN starts with a normalized input matrix, in which the bias value, +1, is inserted in each row then, it is multiplied by an input-hidden weights matrix, and thus the bipolar activation function is applied to all elements of the matrix, obtaining the hidden matrix:

$$H = f(\hat{I} \times W_{IH}) \quad (8.2)$$

Same procedure was applied to the hidden-output matrix:

$$O = f(\tilde{H} \times W_{HO}) \quad (8.3)$$

Finally, outputs were obtained by a threshold value and the activation function. Please expand on this or give a reference.

8.2.2 Back Propagation

This algorithm was used for training the ANN. Its purpose was to obtain all weight matrices incremented by means of the calculation of a matrix defined as the difference between the output matrix and the target matrix. This comparison makes the training more efficient. Also, the learning rate and momentum values helped to improve the training process. First output error information term was calculated as:

$$\delta_O = E \cdot f'(\tilde{H} \times W_{HO}) \quad (8.4)$$

Then, the following equation was used to calculate the correction hidden-output weight matrix considering learning rate and momentum of last correction.

$$\Delta W_{HO} = \alpha \delta_O \times \tilde{H} + \mu \Delta \hat{W}_{HO} \quad (8.5)$$

Similarly, hidden error information was calculated, where output error was back propagated to the hidden layer. This hidden error information was computed by:

$$\delta_H = (\delta_O \times W_{HO}) \cdot f'(\tilde{I} \times W_{IH}) \quad (8.6)$$

Finally, equation (8.7) was used to calculate the correction input-hidden weight matrix.

$$\Delta W_{IH} = \alpha \delta_H \times \tilde{I} + \mu \Delta \hat{W}_{IH} \quad (8.7)$$

In this way, weights were updated. The processes of feedforward and back propagation were repeated until the stop condition was satisfied. A typical stop condition is when the mean square error is less than a constant number.

8.3 Experimental Design

In these experiments, the ANN parameters were fixed in order to be able to evaluate the effect of the HRV inclusion in the Automatic Sleep Classifier System and be able to achieve the main goal of this work. The training algorithm and the testing procedure were implemented by employing the Matlab Neural Network Pattern Recognition Toolbox. Moreover, weight and bias values were updated according to the scaled conjugate gradient method. In addition, from the total possible data samples (Table 7.1), 50% of the data were designated for training purposes, and 50% for testing. Thus, the following exploratory trials were designed and tested:

- a) Determination of number of Hidden Neurons
 - Data from one subject (#006) – all features (44 Input features)
- b) Evaluation on performance of raw features vs. smoothed features
 - Data from one subject (#006) – all features (44 Input features)
- c) Evaluation on performance of EEG features vs. EEG+HRV features
 - Data from one subject (#006) – all features (38 EEG Input features and 6 HRV features)
- d) All Subjects-Evaluation on performance of EEG features vs. EEG+HRV features

- Data from 25 subjects – all features (38 EEG Input features and 6 HRV features)

e) PCA using transformed EEG+HRV features

The output training and testing vectors were codified in order to match only one output neuron (Table 8.1) based on the AASM sleep stage classification standards [12]. Performance of the ANN was measured using the accuracy, sensitivity (Se) and specificity (Sp), geometric mean (GM) values and ROC plots.

8.4 Results

a) Determination of Number of Hidden Neurons

The objective of this experiment was to estimate the number of hidden neurons to achieve the best system performance. Here, raw EEG and HRV features from only one subject were employed to train and test the classifier system. The number of neurons was increased from 20 to 45 in steps of five neural units. Tables 8.2 and 8.3 show the training confusion matrixes for a 25 and a 35 hidden-neuron topology. Accordingly to AASM standards the abbreviations for the sleep stages are: Awake (W), Stage 1 (N1), Stage 2 (N2), Stages 3 and 4 (N3) and REM (R).

Table 8.2 Training Confusion Matrix (25 hidden neurons).

		Target					Geometric		
		R	N3	N2	N1	W	Sensitivity	Specificity	Mean
Output	R	84	0	10	7	0	83.2%	95.3%	89.1%
	N3	5	115	12	1	0	86.5%	96.0%	91.1%
	N2	3	7	24	9	0	55.8%	93.0%	72.1%
	N1	3	1	1	66	5	86.8%	91.7%	89.2%
	W	1	1	0	7	41	82.0%	98.3%	89.8%
Accuracy		87.50%	92.74%	51.06%	73.33%	89.13%			

Total Sensitivity	78.9%
Total Specificity	94.9%

Total Accuracy	81.9%
Total Geometric Mean	86.5%

Table 8.3 Training Confusion Matrix (35 hidden neurons).

		Target					Geometric		
		R	N3	N2	N1	W	Sensitivity	Specificity	Mean
Output	R	91	0	6	7	1	86.7%	98.1%	92.2%
	N3	1	120	7	2	0	92.3%	98.3%	95.3%
	N2	3	4	32	7	0	69.6%	95.6%	81.5%
	N1	0	0	2	72	4	92.3%	94.0%	93.2%
	W	1	0	0	2	41	93.2%	98.4%	95.8%
Accuracy		94.79%	96.77%	68.09%	80.00%	89.13%			

Total Sensitivity	86.8%
Total Specificity	96.9%

Total Accuracy	88.3%
Total Geometric Mean	91.7%

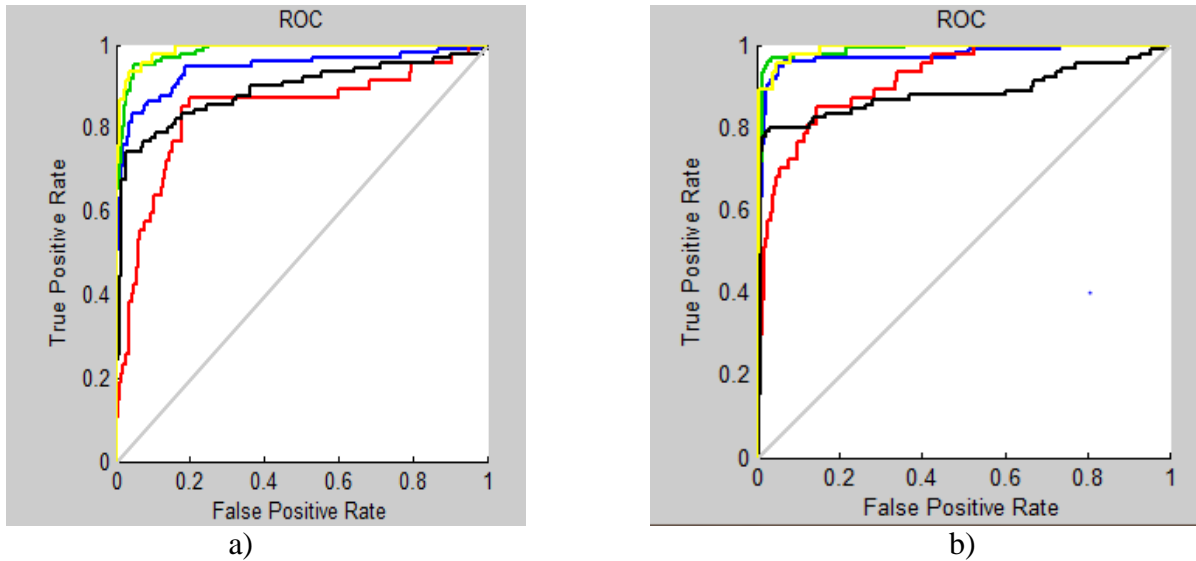


Figure 8.4 ROC plots for training a) 25 hidden neurons, b) 35 hidden neurons.

In ROC plots the following colors were used to identify each sleep stage: yellow (W), black (N1), red (N2), green (N3), and blue (R).

Results showed that better performances were achieved by using 35 neurons in the hidden layer. More than 35 neurons did not improve the overall classifier performance. Therefore, 35 neurons were used during the training and testing procedures in further experiments.

b) Evaluation of Performance of Raw Features vs. Smoothed Features

As described before, it is important to smooth out the erratic behavior of the feature vectors in order to train the ANN system more efficiently, therefore improving the overall performance and achieving a higher discrimination capacity (accuracy, sensitivity, and specificity). That hypothesis was tested in this trial, training confusion Tables 8.3 and 8.4 and

testing confusion tables 8.5 and 8.6 show the increase in accuracy by smoothing the features using a Savitzky-Golay filter of 3rd order and a length of n=31.

Table 8.4 Training Confusion Matrix (35 hidden neurons-smoothed features-EEG+HRV features).

Output	Target					Sensitivity	Specificity	Geometric Mean
	R	N3	N2	N1	W			
	R	94	0	0	0	100.0%	99.3%	99.6%
	N3	0	121	3	0	97.6%	98.8%	98.2%
	N2	2	2	40	9	74.1%	97.9%	85.2%
	N1	0	0	4	81	85.3%	97.0%	90.9%
	W	0	1	0	0	35	97.2%	96.8%
Accuracy	97.92%	97.58%	85.11%	90.00%	76.09%			

Total Sensitivity	90.8%	Total Accuracy	92.1%
Total Specificity	98.0%	Total Geometric Mean	94.3%

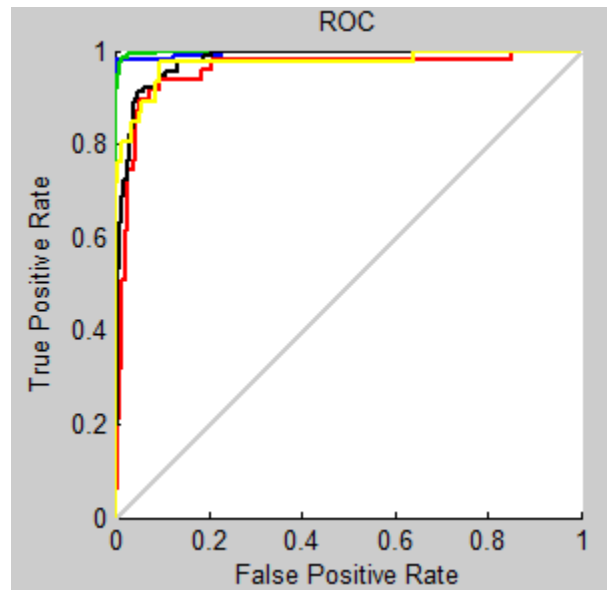


Figure 8.5 ROC plots for training 35 hidden neurons-smoothed features-EEG+HRV features.

Table 8.5 Testing Confusion Matrix (35 hidden neurons-EEG+HRV features).

		Target					Geometric		
		R	N3	N2	N1	W	Sensitivity	Specificity	Mean
Output	R	89	4	7	12	2	78.1%	97.1%	87.1%
	N3	0	112	12	0	0	90.3%	94.6%	92.4%
	N2	2	7	21	5	1	58.3%	91.8%	73.2%
	N1	4	1	7	67	10	75.3%	91.4%	82.9%
	W	1	0	1	7	33	78.6%	95.7%	86.7%
Accuracy		92.71%	90.32%	43.75%	73.63%	71.74%			

Total Sensitivity	76.1%	Total Accuracy	79.5%
Total Specificity	94.1%	Total Geometric Mean	84.6%

Table 8.6 Testing Confusion Matrix (35 hidden neurons-smoothed features-EEG+HRV features).

		Target					Geometric		
		R	N3	N2	N1	W	Sensitivity	Specificity	Mean
Output	R	93	0	1	1	0	97.9%	98.9%	98.4%
	N3	0	116	2	1	1	96.7%	96.8%	96.7%
	N2	2	5	35	6	4	67.3%	96.1%	80.4%
	N1	1	1	5	81	7	85.3%	96.5%	90.7%
	W	0	2	5	2	34	79.1%	96.4%	87.3%
Accuracy		96.88%	93.55%	72.92%	89.01%	73.91%			

Total Sensitivity	85.2%	Total Accuracy	88.6%
Total Specificity	97.0%	Total Geometric Mean	90.9%

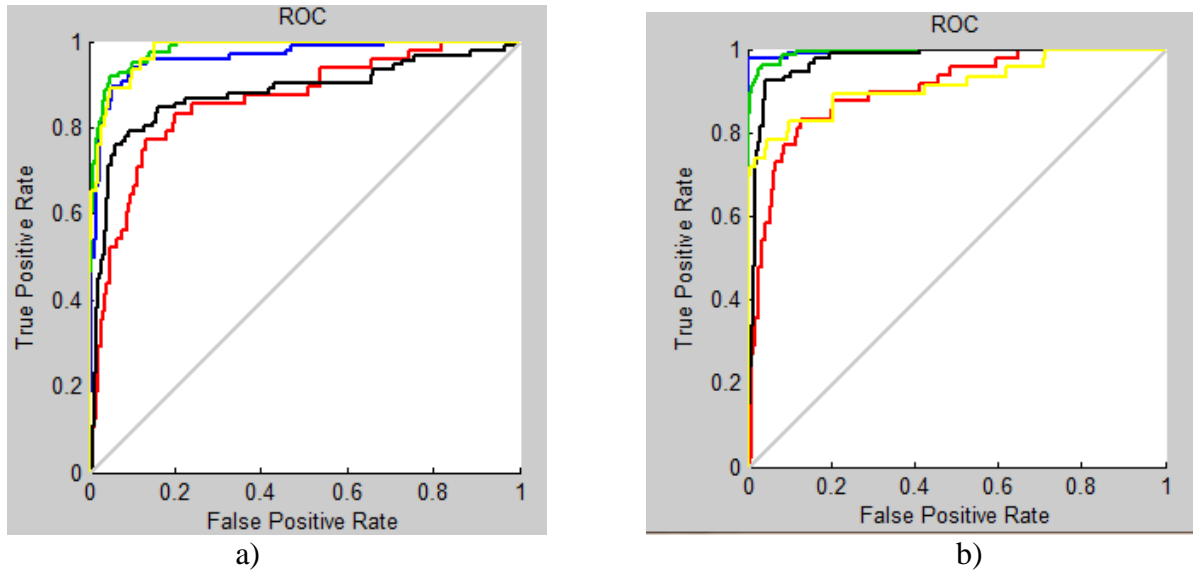


Figure 8.6 ROC plots for testing a) 35 hidden neurons-EEG+HRV features, b) 35 hidden neurons-smoothed features-EEG+HRV features.

A 3.8% improvement in accuracy ($\Delta Se=4.0\%$, $\Delta Sp=1.1\%$ and $GM=2.6\%$).was achieved in the training stage whereas the improvement in accuracy for testing was 9.1% ($\Delta Se=9.1\%$, $\Delta Sp=2.9\%$ and $\Delta GM=5.4\%$).

c) Evaluation of Performance of EEG Features without HRV Features

The objective of this trial was to determine if the removal of HRV features from the set of input vectors would decrease the ANN classifying capabilities. In this exploratory trial, the effects of removing the HRV features are reported in confusion Tables 8.7 for training and 8.8 for testing.

Table 8.7 Training Confusion Matrix (35 hidden neurons-smoothed features-Only EEG Features).

		Target						
		R	N3	N2	N1	W	Sensitivity	Specificity
Output	R	93	0	0	0	0	100.0%	98.9%
	N3	0	117	3	0	0	97.5%	97.2%
	N2	2	7	38	9	0	67.9%	97.3%
	N1	1	0	6	80	14	79.2%	96.6%
	W	0	0	0	1	32	97.0%	95.9%
Accuracy		96.88%	94.35%	80.85%	88.89%	69.57%		

Total Sensitivity	88.3%	Total Accuracy	89.3%
Total Specificity	97.2%	Total Geometric Mean	92.6%

Table 8.8 Testing Confusion Matrix (35 hidden neurons-smoothed features- Only EEG Features).

		Target						
		R	N3	N2	N1	W	Sensitivity	Specificity
Output	R	92	0	2	0	0	97.9%	98.5%
	N3	0	118	4	0	1	95.9%	97.5%
	N2	1	6	30	8	3	62.5%	94.7%
	N1	3	0	12	81	12	75.0%	96.4%
	W	0	0	0	2	30	93.8%	95.3%
Accuracy		95.83%	95.16%	62.50%	89.01%	65.22%		

Total Sensitivity	85.0%	Total Accuracy	86.7%
Total Specificity	96.5%	Total Geometric Mean	90.6%

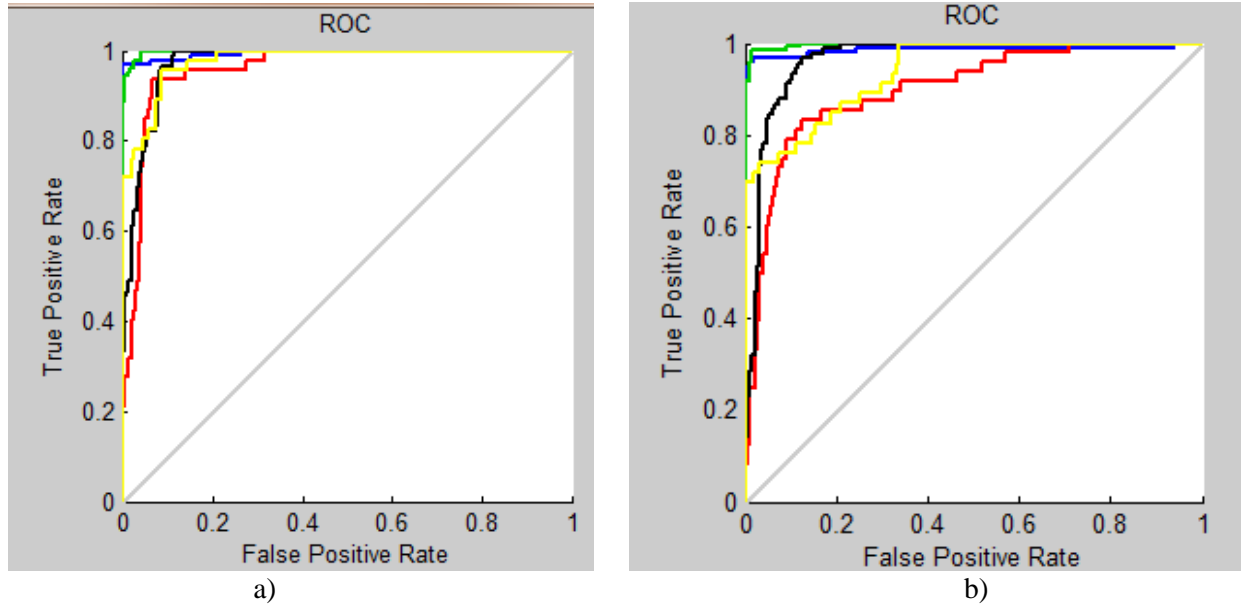


Figure 8.7 ROC plots for a) Training: 35 hidden neurons-smoothed features-Only EEG Features, b) Testing: 35 hidden neurons-smoothed features-Only EEG Features.

It is observed that by including the HRV features the ANN had an improvement of 2.8% in accuracy ($\Delta Se=2.5\%$, $\Delta Sp=0.8\%$ and $\Delta GM=1.7\%$) for training and 1.9% increment in accuracy ($\Delta Se=0.2\%$, $\Delta Sp=0.5\%$ and $\Delta GM=0.3\%$) for testing.

d) All Subjects-Evaluation of performance of EEG Features vs. EEG+HRV Features

In this trial, the experiment evaluation was identical to the trial described in part C. but the data from all 25 subjects were considered for the designing and testing of the ANN system. Results are shown in Tables 8.9 and 8.10 for training and Tables 8.11 and 8.12 for testing, respectively.

Table 8.9 Training Confusion Matrix (All Subjects- 35 hidden neurons-smoothed features- EEG+HRV features).

		Target						
		R	N3	N2	N1	W	Sensitivity	Specificity
Output	R	1236	0	104	96	54	83.0%	96.0%
	N3	0	1091	121	25	25	86.5%	96.6%
	N2	150	235	3047	504	282	72.2%	91.5%
	N1	68	1	143	778	309	59.9%	88.4%
	W	54	4	77	298	1683	79.5%	90.2%
Accuracy		81.96%	81.97%	87.26%	45.74%	71.53%	Geometric Mean	

Total Sensitivity	76.2%	Total Accuracy	75.4%
Total Specificity	92.5%	Total Geometric Mean	84.0%

Table 8.10 Training Confusion Matrix (All Subjects- 35 hidden neurons-smoothed features-Only EEG Features).

		Target						
		R	N3	N2	N1	W	Sensitivity	Specificity
Output	R	1111	0	149	190	90	72.1%	93.9%
	N3	3	1054	156	32	28	82.8%	95.7%
	N2	198	266	2989	605	336	68.0%	89.4%
	N1	86	0	68	375	201	51.4%	83.8%
	W	110	11	130	499	1698	69.4%	89.4%
Accuracy		73.67%	79.19%	85.60%	22.05%	72.16%	Geometric Mean	

Total Sensitivity	68.7%	Total Accuracy	69.6%
Total Specificity	90.4%	Total Geometric Mean	78.8%

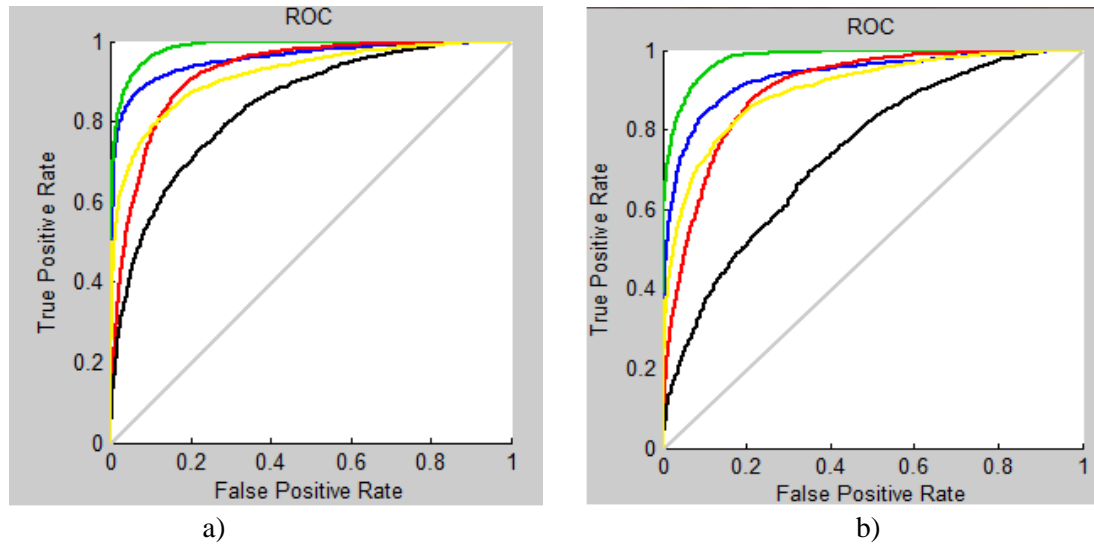


Figure 8.8 ROC plots for training a) EEG+HRV features, b) Only EEG Features.

Table 8.11 Testing Confusion Matrix (All Subjects- 35 hidden neurons-smoothed features-EEG+HRV features).

		Target						
Output		R	N3	N2	N1	W	Sensitivity	Specificity
	R	1240	0	130	83	54	82.3%	96.1%
	N3	1	1069	119	16	18	87.4%	96.2%
	N2	135	251	3032	510	271	72.2%	91.1%
	N1	72	12	130	745	330	57.8%	88.0%
	W	60	0	82	348	1681	77.4%	90.0%
Accuracy		82.23%	80.26%	86.80%	43.77%	71.41%		

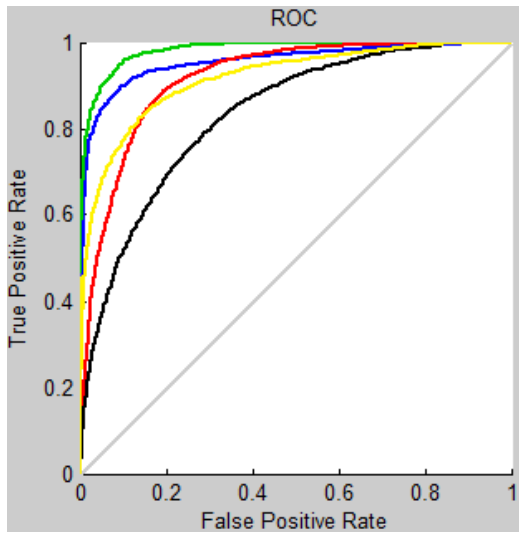
Total Sensitivity	75.4%	Total Accuracy	74.8%
Total Specificity	92.3%	Total Geometric Mean	83.4%

Table 8.12 Testing Confusion Matrix (All Subjects- 35 hidden neurons-smoothed features-Only EEG Features).

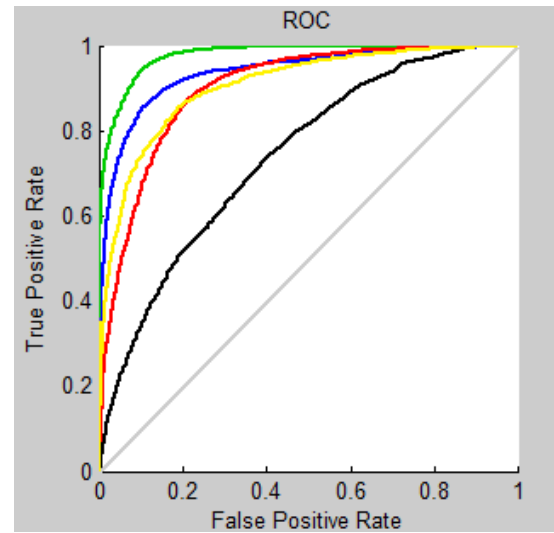
	Target					Sensitivity	Specificity	Geometric Mean
	R	N3	N2	N1	W			
Output	R	N3	N2	N1	W			
R	1137	0	175	195	96	70.9%	94.2%	81.8%
N3	3	1055	177	21	24	82.4%	95.7%	88.8%
N2	172	264	2943	596	305	68.8%	88.5%	78.0%
N1	79	1	65	336	213	48.4%	83.4%	63.5%
W	117	12	133	554	1716	67.8%	89.6%	77.9%
Accuracy	75.40%	79.20%	84.25%	19.74%	72.90%			

Total Sensitivity	67.7%
Total Specificity	90.3%

Total Accuracy	69.2%
Total Geometric Mean	78.2%



a)



b)

Figure 8.9 ROC plots for testing a) EEG+HRV features, b) Only EEG Features.

An improvement of 5.8% in accuracy was achieved when using EEG+HRV feature vectors to train the ANN classifier whereas for sensitivity, specificity, and geometric mean the increments were 7.5%, 2.1%, and 5.2% respectively. Moreover, an increment of 5.5% in accuracy was obtained when testing the ANN ($\Delta Se=7.7\%$, $\Delta Sp=2\%$ and $GM=5.2\%$). In addition,

ROC plots for testing and training depict better performances in both cases when including HRV features, the more each ROC tends the left and top edges of the plot, the better the classification.

e) PCA using Transformed EEG+HRV Features

Finally, a PCA analysis was applied to both EEG and HRV features to eliminate inter-feature correlations. Thus, the PCA provided a new set of features ordered from higher to lower variability. In this trial all transformed features were used to train and test the ANN. However, only variables with higher variability were considered to train the ANN as it can be seen in section 9.2.

Table 8.13 Training Confusion Matrix (All Subjects- 35 hidden neurons-smoothed features- PCA on EEG+HRV features).

Output	Target						Sensitivity	Specificity
	R	N3	N2	N1	W			
	R	2529	0	237	206	115	81.9%	96.5%
	N3	1	2212	234	56	40	87.0%	96.8%
	N2	276	437	6160	956	509	73.9%	91.8%
	N1	103	7	269	1604	570	62.8%	88.9%
	W	107	7	135	581	3473	80.7%	91.0%
	Accuracy	83.85%	83.06%	87.56%	47.13%	73.78%		
							Total Accuracy	76.7%

Chapter 9. Conclusions and Future Work

9.1 Conclusions

The research described in this dissertation investigated quantitative relationships between sleep stages and apneic events by using EEG and ECG signals. Moreover, in the process of establishing the connection between the EEG and HRV features many useful findings emerged.

First, with reference to EEG signal filtering/denoising, it was concluded that the best combination of thresholding rule and threshold value was based on soft thresholding coefficient filtering and the Universal threshold value when denoising this biosignal. This set of parameters could also be applied to denoise EEG epochs for all deep stages. The results showed that by using such parameters no matter what the EEG signal content, the denoising algorithm always produced the best achievable outcomes.

It was also concluded from the HRV features, that the Enhanced Hilbert Transform (EHT) method was a robust technique for R-peak detection from the ECG signal, and therefore it had a high impact on the quality of the extracted features. Statistical analysis demonstrated that 38 out of the 44 features extracted from both the EEG and HRV signals could produce statistically significant parameters for the classifier system ($p < 0.01$) to use and distinguish between different sleep stages. Moreover, it was shown that the Empiric Mode Decomposition (EMD) technique could be used to extract useful information from EEG signals based on the spectrum analysis of the first six IMF functions. However, an in depth study is required to understand the utility of the EMD technique in EEG signal processing and feature extraction in a more comprehensive way.

The tendencies revealed from the extracted EEG and HRV features were in agreement with those reported in the literature as discussed before [21, 22, 45-50, 56, 60, 69, 72-79]. Therefore, it is reasonable to expect that the selected values of the different parameters used to extract the features in each method are valid and adequate. This agreement provides further validation of the approaches taken in this work.

In this work, the correlations (relationships) between EEG and HRV signal features were comprehensively explored and this impacted the success of the classifier system in a positive way. EEG and HRV signal features were weakly correlated, which may mean that HRV signal features provide a different type of information to the neural network than the EEG signal features. However, some EEG signal features showed a higher correlation value amongst themselves, which may indicate that they provide inputs with duplicated information to the classifier system.

The statistical power analysis performed in this work strongly supports the significance of differences found between EEG/HRV across the six R&K sleep stages ($p < 0.01$). This finding justifies the conclusion that at least one sleep stage condition is statistically different and its inclusion as input to the classifier will positively affect the overall system performance.

A novel perspective presented in this work is that the HRV signal features and therefore the related neurological changes were studied under different breathing conditions (e.i. normal breathing, hypopnea, and apnea). Thus, the statistical analysis highlighted those feature changes with significant importance ($p < 0.01$). None of the 44 presented features were affected by the breathing conditions across all sleep stages. Only trends in the EEG-ApEn feature values were significant in Awake, Stage 1, Stage 2, Stage 3 and Stage 4. On the other hand, EEG-DFA feature was the only feature with statistical differences in the REM stage. Using more data, a set

of experiments should be carried out to investigate the interaction between the EEG-ApEn feature and known breathing conditions to determine if this feature could be used to assess such conditions by means of the EEG signal as a reflection of the neurological status and ANS activity.

Additional information acquired from features' behavior may prove beneficial in development of algorithms based on HRV characteristics by taking into consideration the different trends encountered during different sleep stages that could impact the overall detection performance of the classifier.

Finally, this study showed that inclusion of HRV features as inputs to the classifier system increased the performance of the ANN system by improving the accuracy by 5.8 % when considering data from all 25 subjects whereas for sensitivity, specificity, and geometric mean the increments were 7.5%, 2.1%, and 5.2% respectively. Thus the combination of the information from EEG and HRV features led to a more powerful automatic sleep stage classifier system.

With the promising results reported in this research, the development of dedicated EEG/HRV sleep stage databases should be considered in future investigations. The parameters used when developing the database should include targeted standards where sleep epochs and apneic events are scored within the same time frame (e.g. 30 seconds). This will enable the biomedical engineering community to establish new directions in the development of apenic event detection algorithms and sleep stage classification systems based on EEG and ECG biosignals. Moreover, the recently introduced AASM scoring rules should be studied in the existing sleep databases in order to have consistent results with the new regulations and thus be able to transfer and integrate the knowledge accumulated over the years into the R&K rules for development of better automatic sleep classification systems.

Recent literature on this research topic further validates the approach pursued in this work. Malarvili et al. [107] proposed a system for automatic seizure detection by means of fusion of EEG and HRV features. They discussed that such features capture the changes in these physiological signals, which are indicative of the neurological changes and the performance of the automatic system. Similarly, Sakai et al. [108] were able to record simultaneous EEG and ECG signals on the same tracing by using a dedicated set of electrodes. This recording was achieved by applying the reference EEG electrode to a non-cephalic region (i.e. thorax). These authors used a wavelet shrinkage technique to separate the recorded EEG from ECG signals. They were able to successfully perform spectral analysis on the EEG signal, compute all its frequency bands, and detect the R-peaks from the separated ECG signal.

To summarize, the work presented here contributes to the ultimate goal of the ongoing sleep research, which strives to find novel and more reliable tools to assess sleep quality and sleep breathing disorders by means of less invasive computer-aided classification techniques with minimal set of electrodes.

9.2 Future Directions

A few ideas are presented in this section that are important to be investigated and addressed in future research projects:

- a) Perform an investigation into different topologies for the classification system based on the extracted features and selection of those valuable features, which represent the sleep stages and apneic events with larger variances.

During the exploration for development of the neural network system used in this thesis, an Adaptive Neuro-Fuzzy Inference System (ANFIS) was briefly examined as an alternative approach to address the classification problem and its solution. The system was designed using data from only one subject. By applying the PCA analysis on the 44 proposed features, the three more important orthogonally-transformed set of features were used to train the set of rules of the FIS. The training method was based on a back propagation technique. Moreover, each input was modeled by 6 triangular membership functions. Figure 9.1 shows the preliminary results obtained for this pilot investigation.

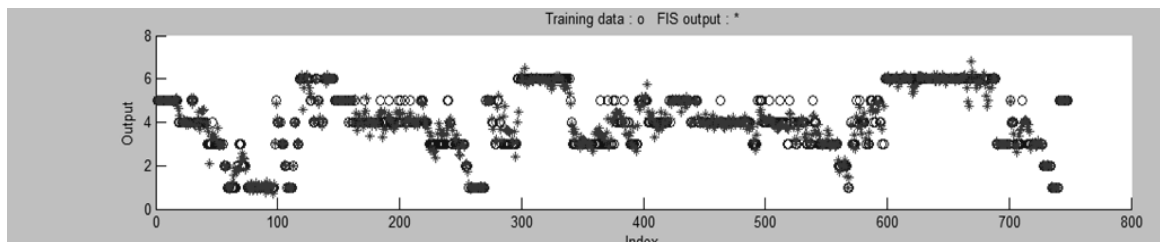


Figure 9.1 ANFIS target output vs. targeted training data (average testing error 0.3635).

- b) Perform an investigation into human sleep transition behavior. As stated in the feature preprocessing section, the changes from a sleep stage to a different stage do not exhibit a random behavior in humans and in some sense, those changes are “predictable”. For the 20,774 data points used in this study, we computed the probability to change from a

stage(i) to a stage (i+1) based on the total number overnight transitions. Figure 9.2 shows these interesting probabilities. As it can be predicted, the probability of continuing in the same stage will be always higher than those probabilities associated with changing to other stages. It is important to point out that the probabilities presented were computed from a population of subjects suffering from sleep breathing disorders. Therefore, a study of the probabilities of changes on healthy subjects should be carried out. Different variables should be taken into consideration (e.g. age, gender, medical condition, time and so on) in order to strengthen the prediction model.

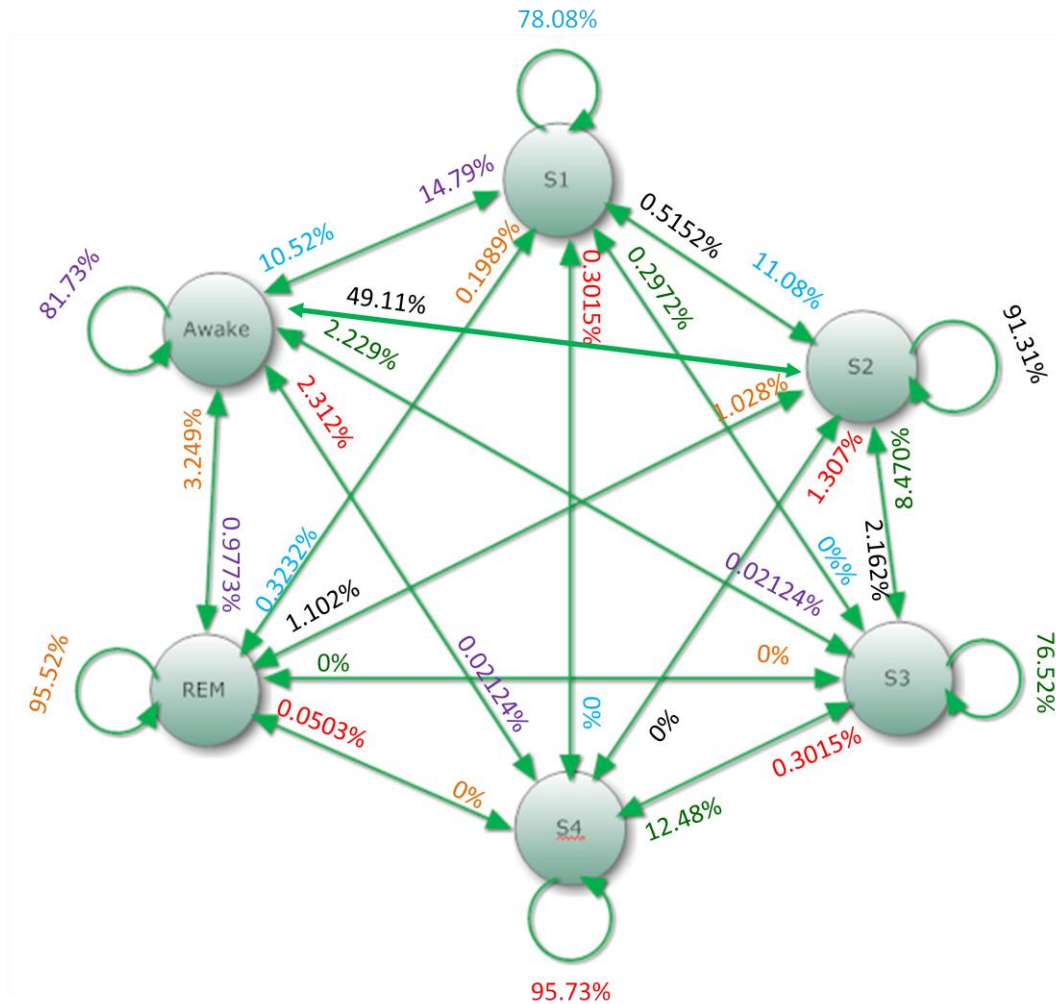


Figure 9.2 Probabilities of sleep stage change.

More importantly, this information may be used as an input for the classifier system. Moreover, a dedicated output monitor system may be designed to screen out the classifier outputs and identify those suspicious sleep changes having a minimal probability to occur (e.g. REM stage to Stage 4 in the above proposed model).

To finalize this proposed approach, a small experiment was performed on the presented probabilities of change. A trial of 1000 changes was computed in a theoretical experiment where the modeled subject started in the awake stage. The surprising results produced hypnogram-behavior plots (Figures 9.3, 9.4 and 9.5) where changes were very similar to changes observed in humans sleep behavior. Moreover, these probabilities mimicked profiles of persons suffering from a sleep breathing disorder, having several awake periods during the night.

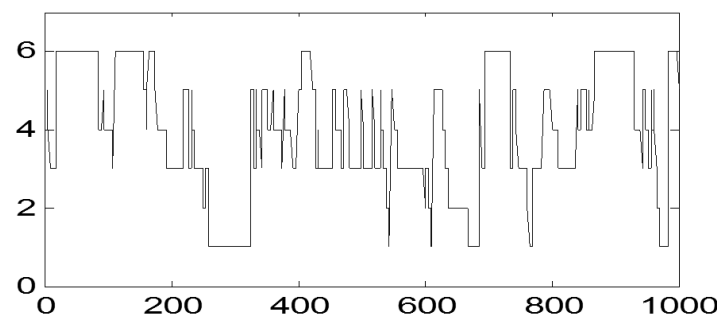


Figure 9.3 Simulated hypnogram trial 1 (Stage 1=1, Stage 2=2, Stage 3=3, Stage 4=4, Awake=5, REM=6)

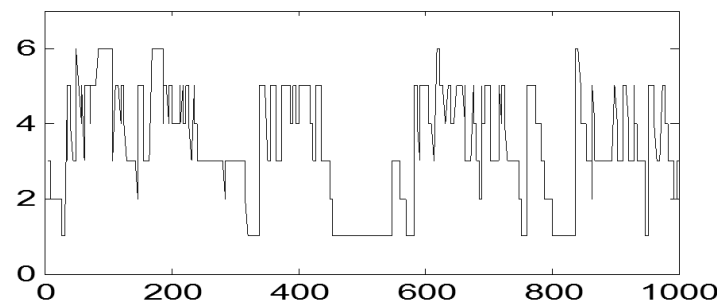


Figure 9.4 Simulated hypnogram trial 2 (Stage 1=1, Stage 2=2, Stage 3=3, Stage 4=4, Awake=5, REM=6)

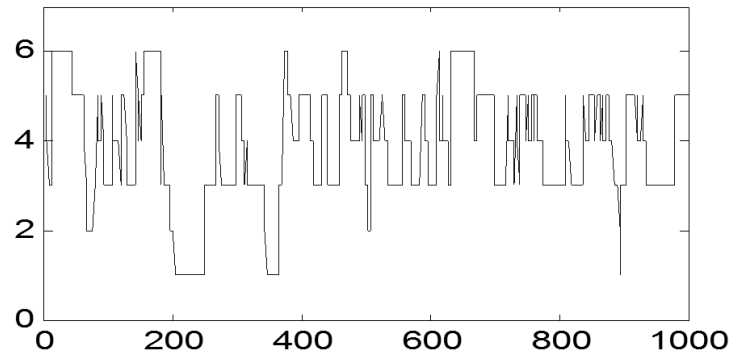


Figure 9.5 Simulated hypnogram trial 3 (Stage 1=1, Stage 2=2, Stage 3=3, Stage 4=4, Awake=5, REM=6).

- c) Development of a comprehensive EEG/HRV sleep database to enable sleep researchers to comprehensively explore novel feature extraction algorithms and classifier systems and disseminate and share their findings based on a common database.

References

- [1] W. B. Mendelson, *Human sleep : research and clinical care*. New York: Plenum Medical Book Co., 1987.
- [2] E. Edelson, *Sleep*. New York: Chelsea House, 1992.
- [3] J. A. Hobson, *The dreaming brain*. New York: Basic Books, 1988.
- [4] E. T. Chang and G. M. Shiao, "Craniofacial abnormalities in Chinese patients with obstructive and positional sleep apnea," *Sleep Med*, vol. 9, pp. 403-10, May 2008.
- [5] L. Sörnmo and P. Laguna, *Bioelectrical signal processing in cardiac and neurological applications*. Amsterdam ; Boston: Elsevier Academic Press, 2005.
- [6] J. G. Webster and J. W. Clark, *Medical instrumentation : application and design*, 4th ed. Hoboken, NJ: John Wiley & Sons, 2010.
- [7] K. E. Misulis, *Essentials of clinical neurophysiology*, 2nd ed. Boston: Butterworth-Heinemann, 1997.
- [8] W. C. Dement and C. C. Vaughan, *The promise of sleep : a pioneer in sleep medicine explores the vital connection between health, happiness, and a good night's sleep*. New York: Delacorte Press, 1999.
- [9] A. Rechtschaffen and A. Kales, *A manual of standardized terminology, techniques and scoring system for sleep stages of human subjects*. Allan Rechtschaffen and Anthony Kales, editors. Los Angeles: U. S. National Institute of Neurological Diseases and Blindness, Neurological Information Network, 1960.
- [10] H. Adeli, S. Ghosh-Dastidar, and N. Dadmehr, "A wavelet-chaos methodology for analysis of EEGs and EEG subbands to detect seizure and epilepsy," *IEEE Trans Biomed Eng*, vol. 54, pp. 205-11, Feb 2007.

- [11] S. Miano, M. C. Paolino, R. Castaldo, and M. P. Villa, "Visual scoring of sleep: A comparison between the Rechtschaffen and Kales criteria and the American Academy of Sleep Medicine criteria in a pediatric population with obstructive sleep apnea syndrome," *Clin Neurophysiol*, vol. 121, pp. 39-42, Jan 2010.
- [12] American Academy of Sleep Medicine., *The international classification of sleep disorders : diagnostic and coding manual*, 2nd ed. Westchester, Ill.: American Academy of Sleep Medicine, 2005.
- [13] "Heart rate variability. Standards of measurement, physiological interpretation, and clinical use. Task Force of the European Society of Cardiology and the North American Society of Pacing and Electrophysiology," *Eur Heart J*, vol. 17, pp. 354-81, Mar 1996.
- [14] H. Nazeran, Y. Pamula, and K. Behbehani, *Heart Rate Variability (HRV): Sleep Disordered Breathing*: John Wiley & Sons, Inc., 2006.
- [15] A. Gradziel, K. Ung, Y. Pamula, and H. Nazeran, "Heart Rate Variability Analysis of Sleep Disordered Breathing in Children," in *Proceedings of the World Congress on Medical Physics and Biomedical Engineering*, Sydney, Australia, 2003.
- [16] R. J. Storella, H. W. Wood, K. M. Mills, J. K. Kanters, M. V. Hojgaard, and N. H. Holstein-Rathlou, "Approximate entropy and point correlation dimension of heart rate variability in healthy subjects," *Integr Physiol Behav Sci*, vol. 33, pp. 315-20, Oct-Dec 1998.
- [17] Y. Rong-Guan, S. Jiann-Shing, H. Yin-Yi, W. Yu-Jung, and T. Shih-Chun, "Detrended Fluctuation Analyses of Short-Term Heart Rate Variability in Surgical Intensive Care Units," *Biomedica Engineering Applications, Basis & Communications*, vol. 18, p. 67.72, 2006.

- [18] C. Sullivan and D. Rapoport, "The apnea-hypopnea index is a useless metric of sleep disordered breathing: pro-con," in *Annual Meeting of the American Thoracic Society*, Atlanta, GA, May 2002.
- [19] W. H. Tsai, W. W. Flemons, W. A. Whitelaw, and J. E. Remmers, "A comparison of apnea-hypopnea indices derived from different definitions of hypopnea," *Am J Respir Crit Care Med*, vol. 159, pp. 43-8, Jan 1999.
- [20] U. J. Magalang, J. Dmochowski, S. Veeramachaneni, A. Draw, M. J. Mador, A. El-Solh, and B. J. Grant, "Prediction of the apnea-hypopnea index from overnight pulse oximetry," *Chest*, vol. 124, pp. 1694-701, Nov 2003.
- [21] J. Virkkala, R. Velin, S. L. Himanen, A. Varri, K. Muller, and J. Hasan, "Automatic sleep stage classification using two facial electrodes," *Conf Proc IEEE Eng Med Biol Soc*, vol. 2008, pp. 1643-6, 2008.
- [22] E. Oropesa, H. L. Cycon, and M. Jobert, "Sleep Stage Classification using Wavelet Transform and Neural Network," *International Computer Science Institute*, 1999.
- [23] A. Zilinskas, J. Zilinskas, and A. Varoneckas, "Computer Aided System for Analysis of Heart Rate Data Oriented to Development of Automatic Diagnostics of Sleep," in *International Conference on Computer Systems and Technologies*, 2005, pp. II.3-1- II.3-6.
- [24] HHS, "National Sleep Institutes of Health Publication No. 03-5209 " U.S. Department of Health and Human Services 2003.
- [25] NFS. (April, 2009). *2005 Sleep in America Poll Results*. National Sleep Foundation.
Available: <http://www.sleepfoundation.org>

- [26] NFS. (April, 2009). *2008 Sleep in America Poll Results*. National Sleep Foundation.
Available: <http://www.sleepfoundation.org>
- [27] NFS. (April, 2009). *2009 Sleep in America Poll Results*. National Sleep Foundation.
Available: <http://www.sleepfoundation.org>
- [28] NIH. (April, 2009). *2003 National Sleep Disorders Research Plan National Center on Sleep Disorders Research*. Available:
http://www.nhlbi.nih.gov/health/prof/sleep/res_plan/sleep-rplan.pdf
- [29] INER. (April, 2009). *Resumen Apnea del Sueño, Instituto Nacional de Enfermedades Respiratorias* Available: www.iner.salud.gob.mx/descargas/resumenapneasueno.pdf
- [30] INEGI. (April, 2009). *Censo 2005*. Available:
<http://www.inegi.org.mx/inegi/default.aspx?s=est&c=10202>
- [31] IMSS, "La apnea del sueño afecta a más de cuatro millones de personas en México, Comunicado No. 314," Instituto Mexicano del Seguro Social 2007.
- [32] IMSS, "Roncar no significa dormir bien, 35 millones de mexicanos sufren esta enfermedad, Comunicado No. 333," Instituto Mexicano del Seguro Social 2007.
- [33] DOF, "NOM-174-SSA1-1998, Para el manejo integral de la obesidad," 1998.
- [34] S. Redline, A. Storfer-Isser, C. L. Rosen, N. L. Johnson, H. L. Kirchner, J. Emancipator, and A. M. Kibler, "Association between metabolic syndrome and sleep-disordered breathing in adolescents," *Am J Respir Crit Care Med*, vol. 176, pp. 401-8, Aug 15 2007.
- [35] V. García, J. S. Sánchez, and R. A. Mollineda, " Exploring the Performance of Resampling Strategies for the Class Imbalance Problem," in *Proceedings of 23rd International Conference on Industrial Engineering and Other Applications of Applied Intelligent Systems, IEA/AIE 2010, LNAI 6096*, 2010, pp. 541-549.

- [36] T. Fawcett, "An introduction to ROC analysis," *Pattern Recognition Letters*, vol. 27, pp. 861-874, 2006.
- [37] R. Agarwal and J. Gotman, "Computer-assisted sleep staging," *IEEE Trans Biomed Eng*, vol. 48, pp. 1412-23, Dec 2001.
- [38] T. Penzel, K. Kesper, V. Gross, H. F. Becker, and C. Vogelmeier, "Problems in automatic sleep scoring applied to sleep apnea," in *Engineering in Medicine and Biology Society, 2003. Proceedings of the 25th Annual International Conference of the IEEE*, 2003, pp. 358-361 Vol.1.
- [39] J. E. Heiss, C. M. Held, P. A. Estevez, C. A. Perez, C. A. Holzmann, and J. P. Perez, "Classification of sleep stages in infants: a neuro fuzzy approach," *IEEE Eng Med Biol Mag*, vol. 21, pp. 147-51, Sep-Oct 2002.
- [40] E. D. Übeyli, "Automatic detection of electroencephalographic changes using adaptive neuro-fuzzy inference system employing Lyapunov exponents," *Expert Systems with Applications*, vol. 36, pp. 9031-9038, 2009.
- [41] E. Komatsu, Y. Kurihara, and K. Watanabe, "Sleep Stage Estimation by Non-invasive Bio-measurement," in *SICE-ICASE, 2006. International Joint Conference*, 2006, pp. 1494-1499.
- [42] T. Penzel, A. Bunde, J. Heitmann, J. W. Kantelhardt, J. H. Peter, and K. Voigt, "Sleep stage-dependent heart rate variability in patients with obstructive sleep apnea," in *Computers in Cardiology 1999*, 1999, pp. 249-252.
- [43] A. H. Khandoker, C. K. Karmakar, and M. Palaniswami, "Analysis of coherence between sleep EEG and ECG signals during and after obstructive sleep apnea events," *Conf Proc IEEE Eng Med Biol Soc*, vol. 2008, pp. 3876-9, 2008.

- [44] G. Balakrishnan, D. Burli, K. Behbehani, J. Burk, and E. Lucas, "Comparison of a Sleep Quality Index between Normal and Obstructive Sleep Apnea Patients," *Conf Proc IEEE Eng Med Biol Soc*, vol. 2, pp. 1154-7, 2005.
- [45] J. Gotman, D. R. Skuce, C. J. Thompson, P. Gloor, J. R. Ives, and W. F. Ray, "Clinical applications of spectral analysis and extraction of features from electroencephalograms with slow waves in adult patients," *Electroencephalogr Clin Neurophysiol*, vol. 35, pp. 225-35, Sep 1973.
- [46] P. Matthis, D. Scheffner, and C. Benninger, "Spectral analysis of the EEG: comparison of various spectral parameters," *Electroencephalogr Clin Neurophysiol*, vol. 52, pp. 218-21, Aug 1981.
- [47] P. Van Hese, W. Philips, J. De Koninck, R. Van de Walle, and I. Lemahieu, "Automatic detection of sleep stages using the EEG," in *Engineering in Medicine and Biology Society, 2001. Proceedings of the 23rd Annual International Conference of the IEEE*, 2001, pp. 1944-1947 vol.2.
- [48] B. Hjorth, "EEG analysis based on time domain properties," *Electroencephalography and Clinical Neurophysiology*, vol. 29, pp. 306-310, 1970.
- [49] B. Hjorth, "The physical significance of time domain descriptors in EEG analysis," *Electroencephalography and Clinical Neurophysiology*, vol. 34, pp. 321-325, 1973.
- [50] M. Vourkas, S. Micheloyannis, and G. Papadourakis, "Use of ANN and Hjorth parameters in mental-task discrimination," in *Advances in Medical Signal and Information Processing, 2000. First International Conference on (IEE Conf. Publ. No. 476)*, 2000, pp. 327-332.

- [51] I. Bankman and I. Gath, "Feature extraction and clustering of EEG during anaesthesia," *Medical and Biological Engineering and Computing*, vol. 25, pp. 474-477, 1987.
- [52] M. Mouzé-Amady and F. Horwat, "Evaluation of Hjorth parameters in forearm surface EMG analysis during an occupational repetitive task," *Electroencephalography and Clinical Neurophysiology/Electromyography and Motor Control*, vol. 101, pp. 181-183, 1996.
- [53] K. Donohue and C. Scheib. (May, 2005). *EEG Fractal Response To Anesthetic Gas Concentration*. Available: www.engr.uky.edu/~donohue/eeg/pre1/EEGpre2.html
- [54] S. Karlsson and B. Gerdle, "Mean frequency and signal amplitude of the surface EMG of the quadriceps muscles increase with increasing torque--a study using the continuous wavelet transform," *J Electromyogr Kinesiol*, vol. 11, pp. 131-40, Apr 2001.
- [55] F. Itakura, "Minimum prediction residual principle applied to speech recognition," *Acoustics, Speech and Signal Processing, IEEE Transactions on*, vol. 23, pp. 67-72, 1975.
- [56] K. Xuan, L. Xuesong, and N. V. Thakor, "Detection of EEG changes via a generalized Itakura distance," in *Engineering in Medicine and Biology Society, 1997. Proceedings of the 19th Annual International Conference of the IEEE*, 1997, pp. 1540-1542 vol.4.
- [57] K. Xuan, V. Goel, and N. Thakor, "Quantification of injury-related EEG signal changes using Itakura distance measure," in *Acoustics, Speech, and Signal Processing, 1995. ICASSP-95., 1995 International Conference on*, 1995, pp. 2947-2950 vol.5.
- [58] N. Löfgren and et al., "Spectral distance for ARMA models applied to electroencephalogram for early detection of hypoxia," *Journal of Neural Engineering*, vol. 3, p. 227, 2006.

- [59] E. Estrada, H. Nazeran, P. Nava, K. Behbehani, J. Burk, and E. Lucas, "EEG feature extraction for classification of sleep stages," in *Engineering in Medicine and Biology Society, 2004. IEMBS '04. 26th Annual International Conference of the IEEE*, 2004, pp. 196-199.
- [60] E. Estrada, H. Nazeran, F. Ebrahimi, and M. Mikaeili, "EEG signal features for computer-aided sleep stage detection," in *Neural Engineering, 2009. NER '09. 4th International IEEE/EMBS Conference on*, 2009, pp. 669-672.
- [61] I. A. Rezek and S. J. Roberts, "Parametric model order estimation: a brief review," in *Model Based Digital Signal Processing Techniques in the Analysis of Biomedical Signals (Digest No. 1997/009), IEE Colloquium on the Use of*, 1997, pp. 3/1-3/6.
- [62] P. Flandrin, G. Rilling, and P. Goncalves, "Empirical mode decomposition as a filter bank," *Signal Processing Letters, IEEE*, vol. 11, pp. 112-114, 2004.
- [63] D.-x. Zhang, X.-p. Wu, and X.-j. Guo, "The EEG Signal Preprocessing Based on Empirical Mode Decomposition," in *Bioinformatics and Biomedical Engineering, 2008. ICBBE 2008. The 2nd International Conference on*, 2008, pp. 2131-2134.
- [64] P. F. Diez, V. Mut, E. Laciari, A. Torres, and E. Avil, "Identificación de estados mentales del EEG mediante Descomposición Empírica en Modos," presented at the XVII Congreso Argentino de Bioingeniería, VI Jornadas de Ingeniería Clínica, Ciudad de Rosario, 2009.
- [65] C. M. Sweeney-Reed, A. O. Andrade, and S. J. Nasut, "Empirical Mode Decomposition of EEG Signals for Synchronisation Analysis," presented at the IEEE EMBSS UKRI Postgraduate Conference on Biomedical Engineering and Medical Physics Southampto, 2004.

- [66] R. C. Hwa and T. C. Ferree, "Fluctuation Analysis of Human Electroencephalogram," *Nonlinear Phenomena in Complex Systems*, vol. 5, pp. 302-307, 2002.
- [67] M. Ignaccolo, M. Latka, W. Jernajczyk, P. Grigolini, and B. West, "The dynamics of EEG entropy," *Journal of Biological Physics*, vol. 36, pp. 185-196, 2010.
- [68] J. M. Lee, D. J. Kim, I. Y. Kim, K. S. Park, and S. I. Kim, "Detrended fluctuation analysis of EEG in sleep apnea using MIT/BIH polysomnography data," *Comput Biol Med*, vol. 32, pp. 37-47, Jan 2002.
- [69] L. Jun-Seok, K. Sae-Byul, Y. Byung-Hwan, S. David, C. Ju-Yeon, C. Jun-Ho, K. eok-Hyeon, L. Jang-Han, and K. Sun-Il, "Fractal Analysis of EEG During Waking and Hypnosis: Laterality and Regional Differences," *Psychiatry Investigation*, vol. 2, pp. 53-60, 2005 2005.
- [70] N. Burioka, G. Cornelissen, F. Halberg, and D. T. Kaplan, "Relationship between correlation dimension and indices of linear analysis in both respiratory movement and electroencephalogram," *Clin Neurophysiol*, vol. 112, pp. 1147-53, Jul 2001.
- [71] R. Acharya U, O. Faust, N. Kannathal, T. Chua, and S. Laxminarayan, "Non-linear analysis of EEG signals at various sleep stages," *Computer Methods and Programs in Biomedicine*, vol. 80, pp. 37-45, 2005.
- [72] P. Achermann, R. Hartmann, A. Gunzinger, W. Guggenbühl, and A. A. Borbély, "All-night sleep EEG and artificial stochastic control signals have similar correlation dimensions," *Electroencephalography and Clinical Neurophysiology*, vol. 90, pp. 384-387, 1994.

- [73] R. Ferri, M. Elia, S. A. Musumeci, and C. J. Stam, "Non-linear EEG analysis in children with epilepsy and electrical status epilepticus during slow-wave sleep (ESES)," *Clin Neurophysiol*, vol. 112, pp. 2274-80, Dec 2001.
- [74] R. Ferri, S. Pettinato, L. Nobili, M. Billiard, and F. Ferrillo, "Correlation dimension of EEG slow-wave activity during sleep in narcoleptic patients under bed rest conditions," *International Journal of Psychophysiology*, vol. 34, pp. 37-43, 1999.
- [75] R. Carvajal, N. Wessel, M. Vallverdú, P. Caminal, and V. , Andreas, "Correlation dimension analysis of heart rate variability in patients with dilated cardiomyopathy," *Computer Methods and Programs in Biomedicine*, vol. 78, pp. 133-140, 2005.
- [76] G. B. Moody. (October, 2010). *Approximate Entropy (ApEn)*, *Physio Toolkit*. Available: <http://physionet.org/physiotools/ApEn>
- [77] I. Virtanen, E. Ekholm, P. Polo-Kantola, and H. Huikuri, "Sleep stage dependent patterns of nonlinear heart rate dynamics in postmenopausal women," *Auton Neurosci*, vol. 134, pp. 74-80, Jul 31 2007.
- [78] G. Brandenberger, J. Ehrhart, and M. Buchheit, "Sleep stage 2: an electroencephalographic, autonomic, and hormonal duality," *Sleep*, vol. 28, pp. 1535-40, Dec 1 2005.
- [79] C. C. Yang, C. W. Lai, H. Y. Lai, and T. B. Kuo, "Relationship between electroencephalogram slow-wave magnitude and heart rate variability during sleep in humans," *Neurosci Lett*, vol. 329, pp. 213-6, Aug 30 2002.
- [80] M. Tsunoda, T. Endo, S. Hashimoto, S. Honma, and K. I. Honma, "Effects of light and sleep stages on heart rate variability in humans," *Psychiatry Clin Neurosci*, vol. 55, pp. 285-6, Jun 2001.

- [81] M. Ako, T. Kawara, S. Uchida, S. Miyazaki, K. Nishihara, J. Mukai, K. Hirao, J. Ako, and Y. Okubo, "Correlation between electroencephalography and heart rate variability during sleep," *Psychiatry Clin Neurosci*, vol. 57, pp. 59-65, Feb 2003.
- [82] C. Heneghan. (October, 2010). *St. Vincent's University Hospital / University College Dublin Sleep Apnea Database*. Available: <http://www.physionet.org/pn3/ucddb/>
- [83] D. L. Donoho, "Wavelet Shrinkage and W.V.D.: A 10-minute tour " in *Progress in Wavelet Analysis and Applications*, 1993.
- [84] I. Daubechies, *Ten lectures on wavelets*. Philadelphia, Pa.: Society for Industrial and Applied Mathematics, 1992.
- [85] C. Guarnizo Lemus, "Análisis de reducción de ruido en señales EEG orientado al reconocimiento de patrones," *Revista Tecnológicas*, vol. 21, pp. 67-80, Diciembre, 2008.
- [86] K. Lehnertz. *EEG Download Page*. Available: <http://www.meb.uni-bonn.de/epileptologie/science/physik/physik.htm>
- [87] A. Subasi, "EEG signal classification using wavelet feature extraction and a mixture of expert model," *Expert Systems with Applications*, vol. 32, pp. 1084-1093, 2007.
- [88] G. U. Reddy, M. Muralidhar, and S. Varadarajan, "ECG De-Noising using improved thresholding based on Wavelet transforms," *International Journal of Computer Science and Network Security*, vol. 9, pp. 221-225, 2009.
- [89] B. Rosner, *Fundamentals of biostatistics*, 7th Ed. ed. Boston, MA: Cengage Learning, 2010.
- [90] M. H. Hayes, *Statistical digital signal processing and modeling*. New York: John Wiley & Sons, 1996.

- [91] S. Y. Tseng, R. C. Chen, F. C. Chong, and T. S. Kuo, "Evaluation of parametric methods in EEG signal analysis," *Med Eng Phys*, vol. 17, pp. 71-8, Jan 1995.
- [92] J. Muthuswamy and N. V. Thakor, "Spectral analysis methods for neurological signals," *J Neurosci Methods*, vol. 83, pp. 1-14, Aug 31 1998.
- [93] K. Xuan, A. Brambrink, D. F. Hanley, and N. V. Thakor, "Quantification of injury-related EEG signal changes using distance measures," *Biomedical Engineering, IEEE Transactions on*, vol. 46, pp. 899-901, 1999.
- [94] P. Flandrin. (October, 2010). *EMD Software*. Available: www.ens-lyon.fr/~flandrin/software.html
- [95] R. Hwa and T. Ferree. (2001). *Fluctuation Analysis of Human Electroencephalogram*. Available: <http://arxiv.org/abs/physics/0105029>
- [96] A. Casaleggio, M. Morando, S. Pestelli, and S. Ridella, "Study of the correlation dimension of ECG signals based on MIT-BIH Arrhythmia Data Base ECGs," in *Computers in Cardiology 1989, Proceedings.*, 1989, pp. 401-404.
- [97] A. Casaleggio, M. Rabbia, C. Lamberti, and G. Bortolan, "Study of the influence of waveform variations on the ECG correlation dimension," in *Computers in Cardiology 1991, Proceedings.*, 1991, pp. 601-604.
- [98] S. Chatlapalli, H. Nazeran, V. Melarkod, R. Krishnam, E. Estrada, Y. Pamula, and S. Cabrera, "Accurate derivation of heart rate variability signal for detection of sleep disordered breathing in children," *Conf Proc IEEE Eng Med Biol Soc*, vol. 1, pp. 538-41, 2004.

- [99] N. M. Arzeno, D. Zhi-De, and P. Chi-Sang, "Analysis of First-Derivative Based QRS Detection Algorithms," *Biomedical Engineering, IEEE Transactions on*, vol. 55, pp. 478-484, 2008.
- [100] D. Benitez, P. A. Gaydecki, A. Zaidi, and A. P. Fitzpatrick, "The use of the Hilbert transform in ECG signal analysis," *Comput Biol Med*, vol. 31, pp. 399-406, Sep 2001.
- [101] F. Faul, E. Erdfelder, A. Buchner, and A. G. Lang, "Statistical power analyses using G*Power 3.1: tests for correlation and regression analyses," *Behav Res Methods*, vol. 41, pp. 1149-60, Nov 2009.
- [102] B. Chakraborty, R. Kaustubha, A. Hegde, and A. Pereira, "Acoustic seafloor sediment classification using self-organizing feature maps," *Geoscience and Remote Sensing, IEEE Transactions on*, vol. 39, pp. 2722-2725, 2001.
- [103] W. A. Ahmd, "Data preprocessing for neural networks," in *Students Conference, 2002. ISCON '02. Proceedings. IEEE*, 2002, pp. 6-6.
- [104] B. C. H. Turton, "A novel variant of the Savitzky-Golay filter for spectroscopic applications," *Measurement Science and Technology*, vol. 3, p. 858, 1992.
- [105] J. Mohamad-Saleh and B. S. Hoyle, "Improved Neural Network Performance Using Principal Component Analysis on Matlab," *International Journal of the Computer, the Internet and Management*, vol. 16, pp. 1-8, 2008.
- [106] L. V. Fausett, *Fundamentals of neural networks : architectures, algorithms, and applications*. Englewood Cliffs, NJ: Prentice-Hall, 1994.
- [107] M. B. Malarvili and M. Mesbah, "Combining newborn EEG and HRV information for automatic seizure detection," in *Engineering in Medicine and Biology Society, 2008. EMBS 2008. 30th Annual International Conference of the IEEE*, 2008, pp. 4756-4759.

- [108] M. Sakai and W. Daming, "Wavelet shrinkage applications of EEG-ECG-based human-computer interface," in *Computer and Information Technology, 2008. CIT 2008. 8th IEEE International Conference on*, 2008, pp. 538-543.

Acronym List

A	Approximation (wavelet coefficients)
AASM	American Association of Sleep Medicine
AHI	Apnea Hypopnea Index
ANFIS	Adaptive Neuro-Fuzzy Inference System
ANN	Artificial Neural Network
ANOVA	Analysis of Variance
ANS	Autonomic Neural System
ApEn	Approximate Entropy
APSS	Association for the Psychophysiological Study of Sleep
AR	Autoregressive (spectral estimation modeling)
ARMA	Autoregressive Moving Average (spectral estimation modeling)
AV node	Atrioventricular Node
Aw	Awake Stage, R&K Standards
CD	Correlation Dimension
CSA	Central Sleep Apnea
D	Detailed (wavelet coefficients)
Db	Daubechies (wavelet family)
DFA	Detrended Fluctuation Analysis
DWT	Discrete Wavelet Transform
ECG	Electrocardiogram (A recording of the electrical activity of the heart)
EDF	European Data Format
EEG	Electroencephalogram (A recording of the electrical activity of the brain)

EHT	Enlaced Hilbert Transform
EMD	Empirical Mode Decomposition
EMG	Electromyogram (A recording of the electrical activity of the muscles)
EOG	Electrooulogram (A recording of the electrical activity of ocular muscles)
EPSP	Excitatory Postsynaptic Potential
FFT	Fast Fourier Transform
FIR	Finite Impulse Response
FN	False Negative
FP	False Positive
fs	Sample (Sampling) Frequency
FT	Fourier Transform
GM	Geometric Mean
HF	High Frequencies (components in HRV signal spectrum)
HF _{n.u.}	High Frequencies normalized units
HRV	Heart Rate Variability
IDWT	Inverse Discrete Wavelet Transform
IIR	Infinite Impulse Response
IMF	Intrinsic Mode Function
IPSP	Inhibitory postsynaptic potential
LF	Low Frequencies (components in HRV signal spectrum)
LF _{n.u.}	Low Frequencies normalized units
m_0	Activity
m_2	Mobility

m ₄	Complexity
MSE	Mean Square Error
MMSE	Minimum Mean Square Error
N1	Stage 1, AASM Standards
N2	Stage 2, AASM Standards
N3	Stage 3, AASM Standards
NN	Neural Network
N-REM	Non Rapid Eye Movement (sleep stage)
OSA	Obstructive Sleep Apnea
PCA	Principal Component Analysis
PNS	Parasympathetic Nervous System
PSD	Power Spectrum Density
QMF	Quadrature Mirror Filter
R	REM Stage, AASM Standards
REM	Rapid Eye Movement sleep (stage, R&K Standards)
R&K Rules	Rechtschaffen and Kales (Sleep Classification) Rules
RMS	Root Mean Square
ROC	Receiver Operating Characteristic
RPSEB	Relative Power Spectral Energy Band
S1	Stage 1, R&K Standards
S2	Stage 2, R&K Standards
S3	Stage 3, R&K Standards
S4	Stage 4, R&K Standards

SA node	Sinoatrial Node
SBD	Sleep Breathing Disorder
SDNN	Standard Deviation for N-N intervals
Se	Sensitivity
SNR	Signal-to-Noise Ratio
SNS	Sympathetic Nervous System
Sp	Specificity
STFT	Short Time Fourier Transform
SURE	Stein's Unbiased Risk Estimation
TN	True Negative
TP	True Positive
TPC	Total Power Content
VLF	Very Low Frequencies
W	Awake Stage, AASM Standards
WPT	Wavelet Packet Tree

Appendix 1. Subjects information and Hypnograms

Table A1.1 Subjects General Information and demographics

Study Number	Height (cm)	Weight (kg)	Gender	PSG Date	PSG AHI	BMI	Age	Epworth Sleepiness Score	Study Duration (hr)	Sleep Efficiency (%)
UCDDB002	172	100.3	M	10/09/02	23	33.9	54	16	6.2	84
UCDDB003	179	102	M	29/01/03	51	31.8	48	13	7.3	81
UCDDB005	176	100.4	M	20/01/03	13	32.4	65	19	6.9	63
UCDDB006	185	103.5	M	18/02/03	31	30.2	52	3	6.7	89
UCDDB007	183	84	M	26/02/03	12	25.1	47	15	6.8	90
UCDDB008	145	59.8	F	02/10/02	5	28.4	63	1	6.4	64
UCDDB009	180	101.5	M	04/09/02	12	31.3	52	19	7.7	80
UCDDB010	174	119	M	08/10/02	34	39.3	38	2	7.6	92
UCDDB011	188	101	M	21/01/03	8	28.6	51	8	7.5	60
UCDDB012	179	97.5	M	12/02/03	25	30.4	51	16	7.2	85
UCDDB013	153	80	F	03/02/03	16	34.2	62	10	6.8	61
UCDDB014	177	91	M	30/09/02	36	29.0	56	5	6.4	79
UCDDB015	170	83.9	M	19/02/03	6	29.0	28	2	7.6	77
UCDDB017	176	117	M	25/01/03	12	37.8	53	7	6.6	87
UCDDB018	171	77	M	29/01/03	2	26.3	35	10	6.8	60
UCDDB019	178	97.8	M	10/02/03	16	30.9	49	18	7.1	92
UCDDB020	179	108.8	M	19/02/03	15	34.0	52	11	6.3	78
UCDDB021	161	87	F	25/02/03	13	33.6	41	13	7.6	82
UCDDB022	166	80.7	M	03/02/03	7	29.3	34	4	6.6	58
UCDDB023	165	89	F	28/01/03	39	32.7	68	13	7.2	67
UCDDB024	172	99.9	M	05/02/03	24	33.8	54	19	7.6	83
UCDDB025	174	128.6	M	13/01/03	91	42.5	52	24	5.9	77
UCDDB026	175	84	M	05/02/03	14	27.4	49	9	7.0	87
UCDDB027	182	93	M	10/02/03	55	28.1	45	10	7.4	86
UCDDB028	172	88.9	M	30/09/02	46	30.1	50	13	6.0	68
			21	Mean	24.1	31.6	50.0	11.2		
			4	Sd	20.3	4.0	9.5	6.2		
				Min	1.7	25.1	28.0	1.0		
				Max	90.9	42.5	68.0	24.0		

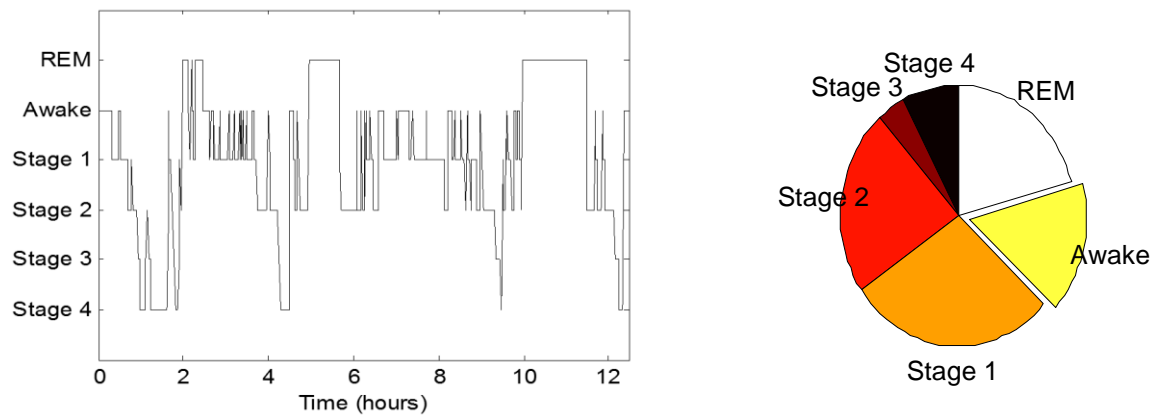


Figure A1.1 Hypnogram subject UCDDB02 and sleep stages distribution.

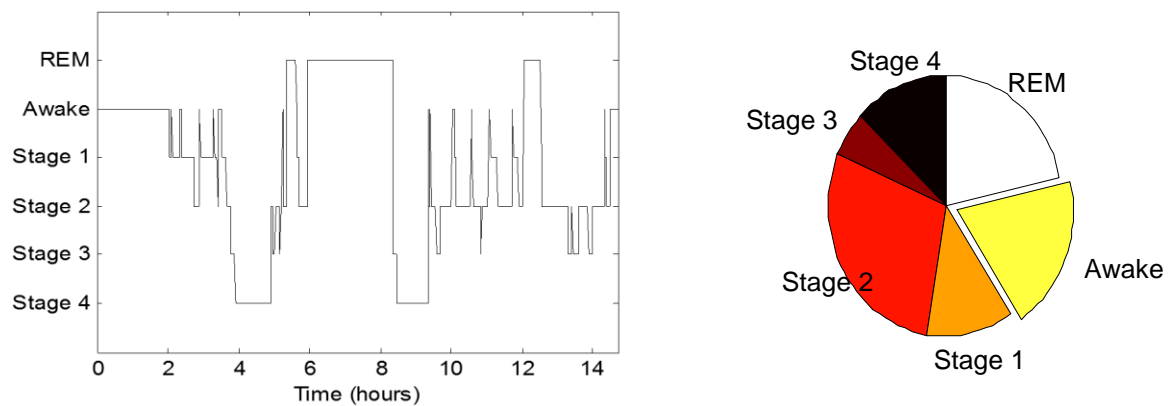


Figure A1.2 Hypnogram subject UCDDB003 and sleep stages distribution.

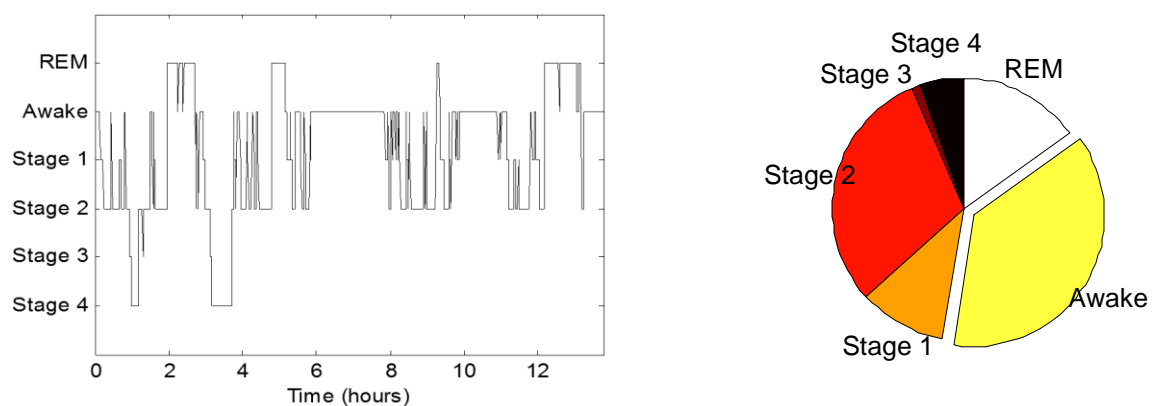


Figure A1.3 Hypnogram subject UCDDB005 and sleep stages distribution.

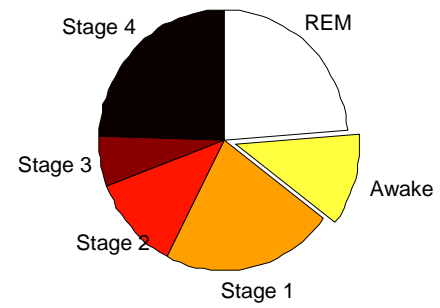
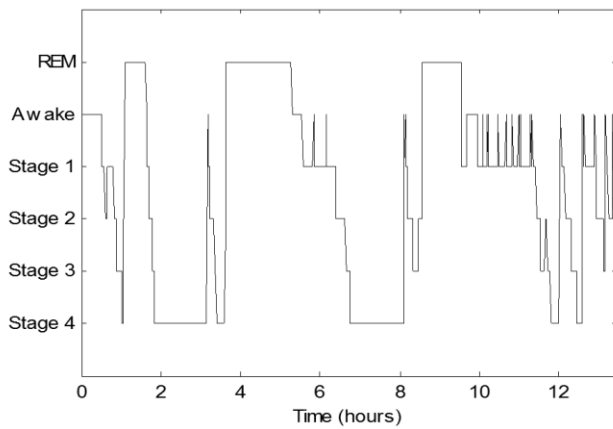


Figure A1.4 Hypnogram subject UCDDDB006 and sleep stages distribution.

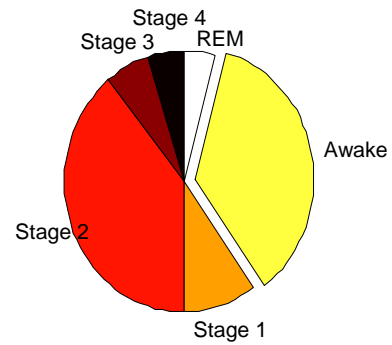
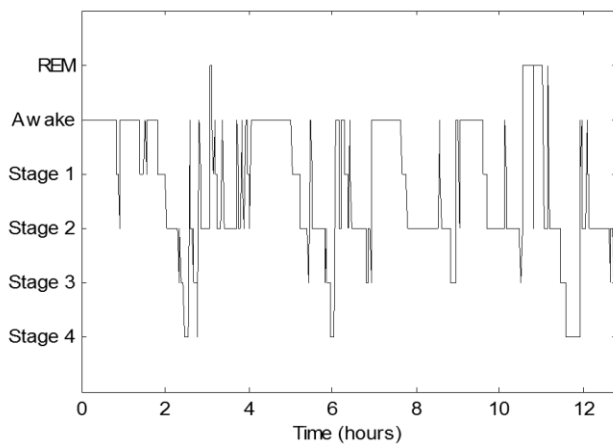


Figure A1.5 Hypnogram subject UCDDDB007 and sleep stages distribution.

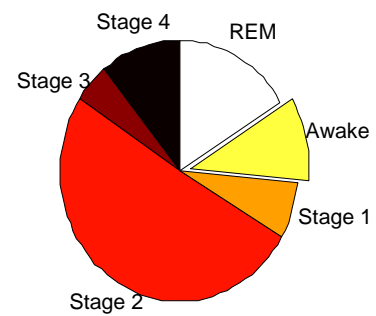
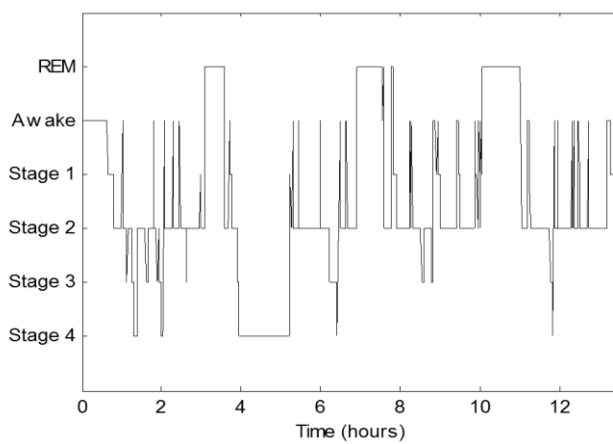


Figure A1.6 Hypnogram subject UCDDDB008 and sleep stages distribution.

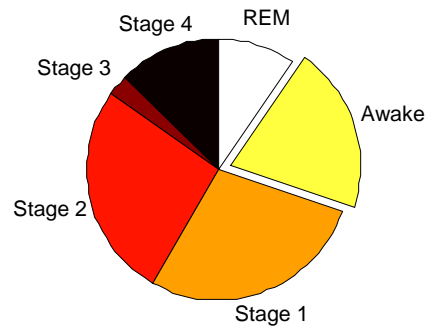
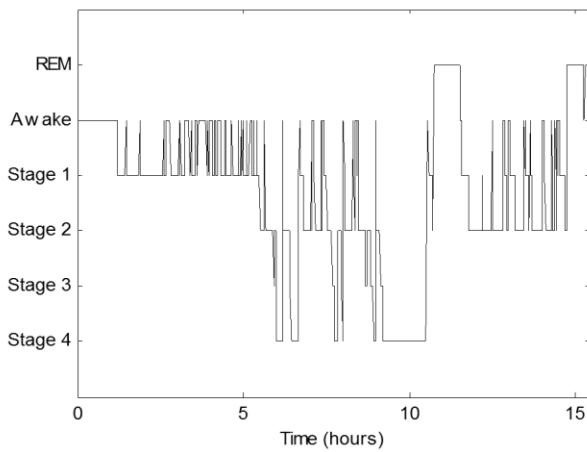


Figure A1.7 Hypnogram subject UCDDB009 and sleep stages distribution.

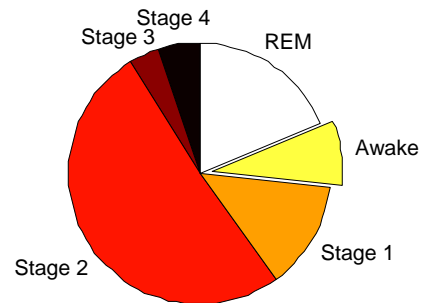
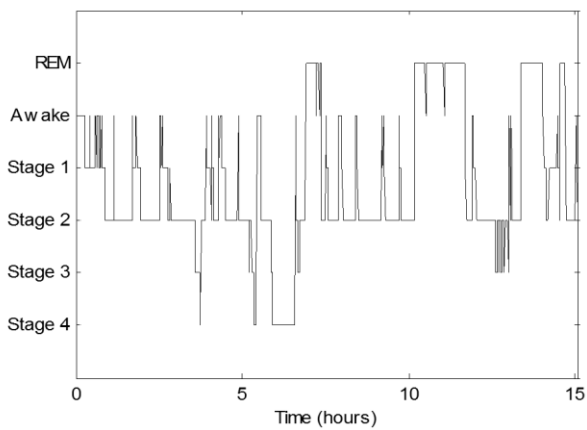


Figure A1.8 Hypnogram subject UCDDB010 and sleep stages distribution.

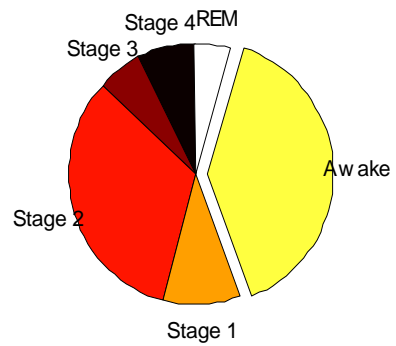
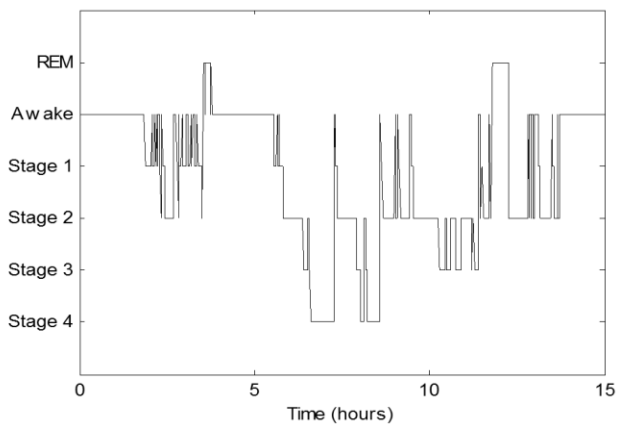


Figure A1.9 Hypnogram subject UCDDB011 and sleep stages distribution.

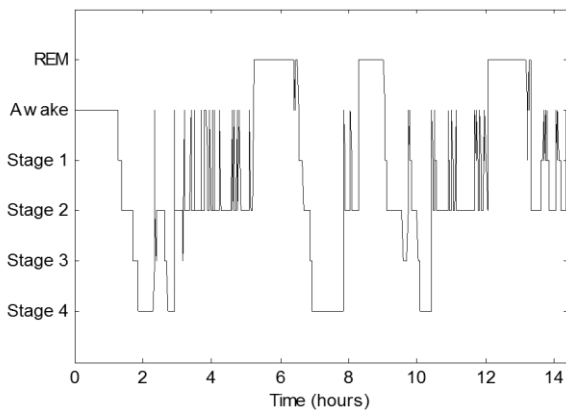


Figure A1.10 Hypnogram subject UCDDB012 and sleep stages distribution.

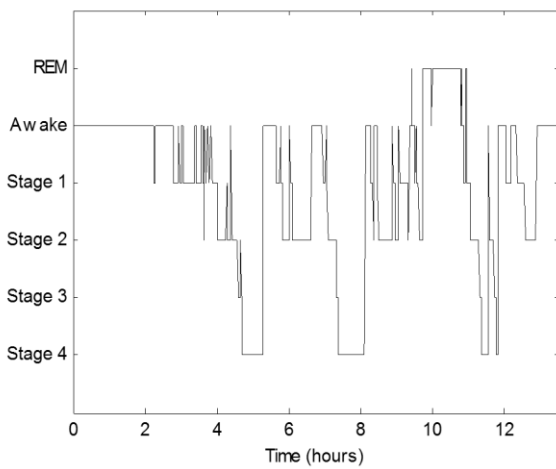
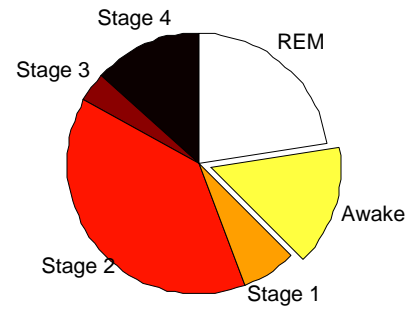


Figure A1.11 Hypnogram subject UCDDB013 and sleep stages distribution.

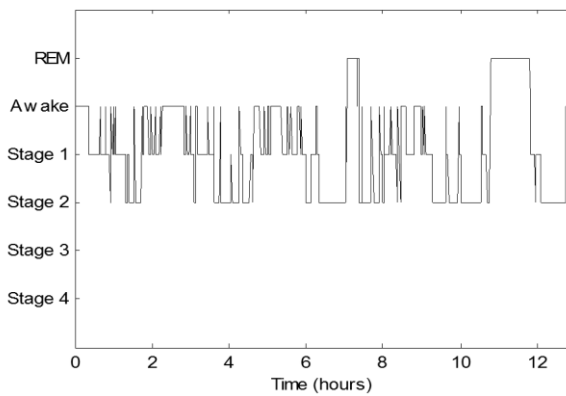
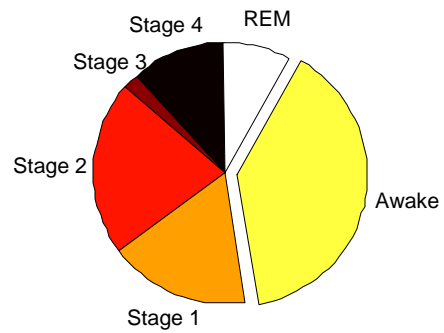
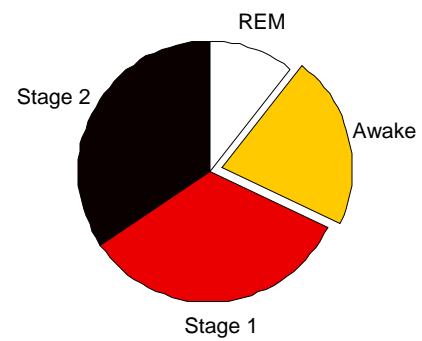


Figure A1.12 Hypnogram subject UCDDB014 and sleep stages distribution.



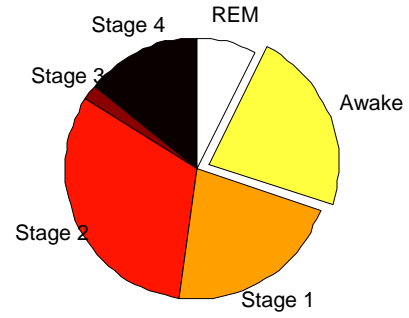
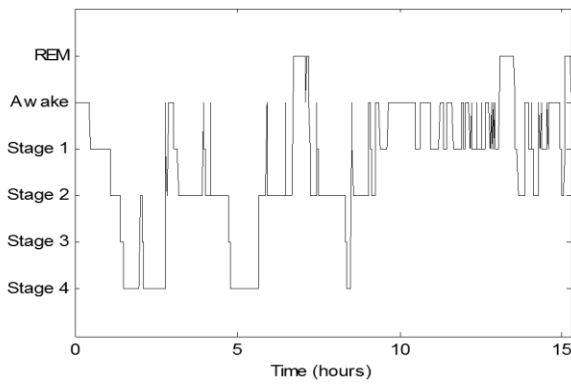


Figure A1.13 Hypnogram subject UCDDB015 and sleep stages distribution.

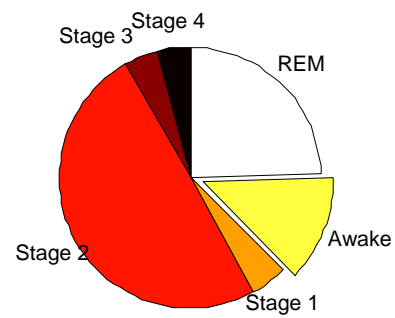
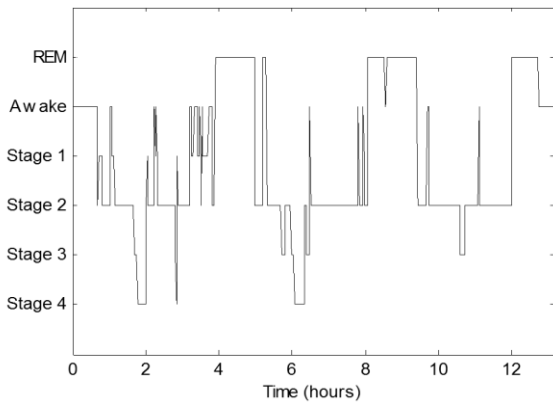


Figure A1.14 Hypnogram subject UCDDB017 and sleep stages distribution.

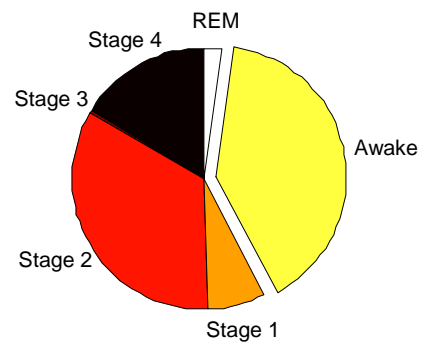
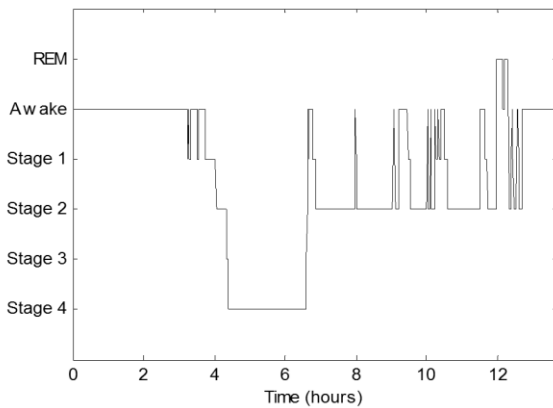


Figure A1.15 Hypnogram subject UCDDB018 and sleep stages distribution.

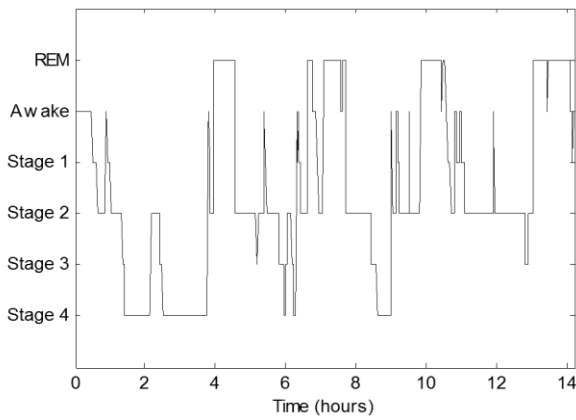


Figure A1.16 Hypnogram subject UCDDB019 and sleep stages distribution.

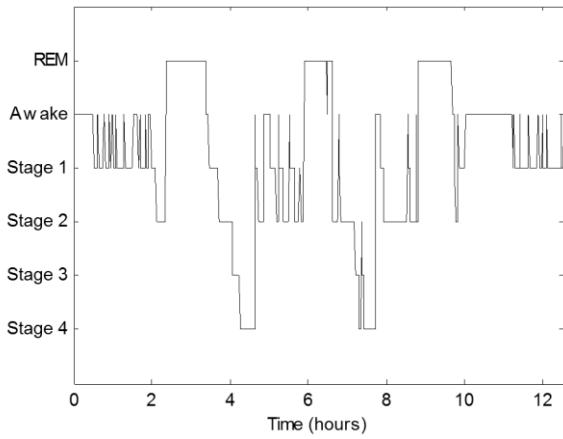
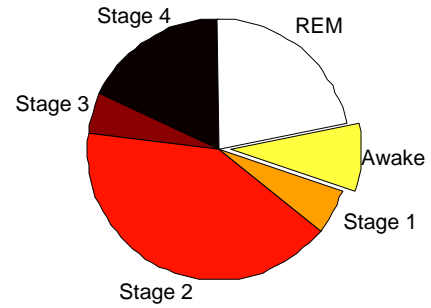


Figure A.17 Hypnogram subject UCDDB020 and sleep stages distribution.

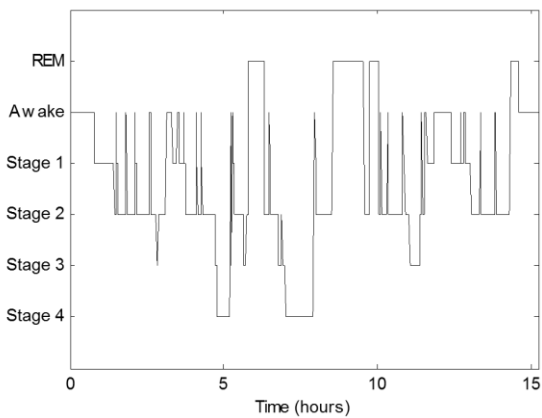
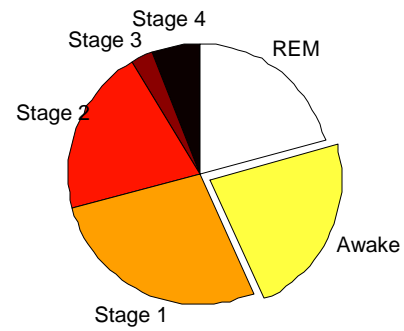
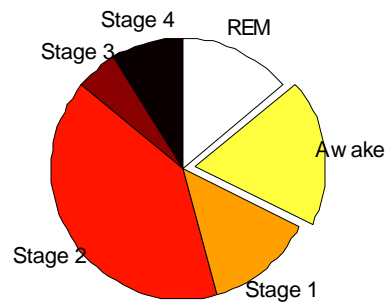


Figure A1.18 Hypnogram subject UCDDB021 and sleep stages distribution.



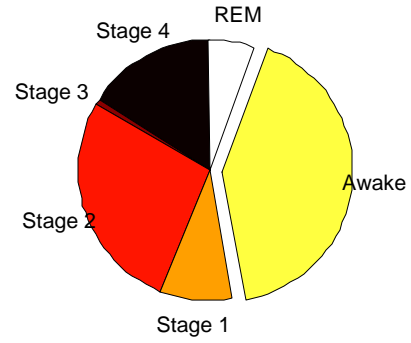
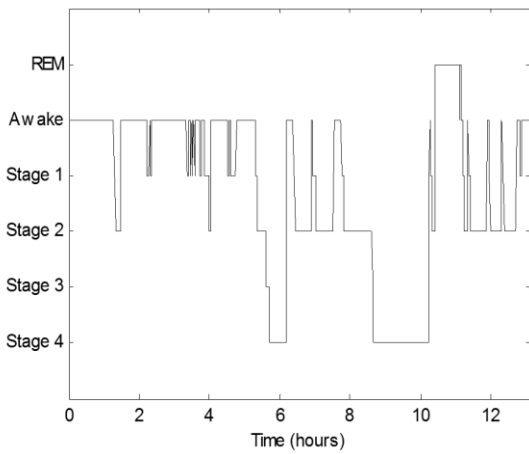


Figure A1.19 Hypnogram subject UCDDB022 and sleep stages distribution.

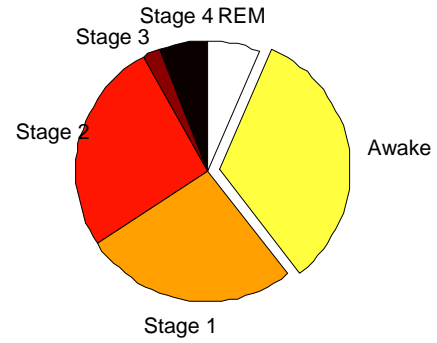
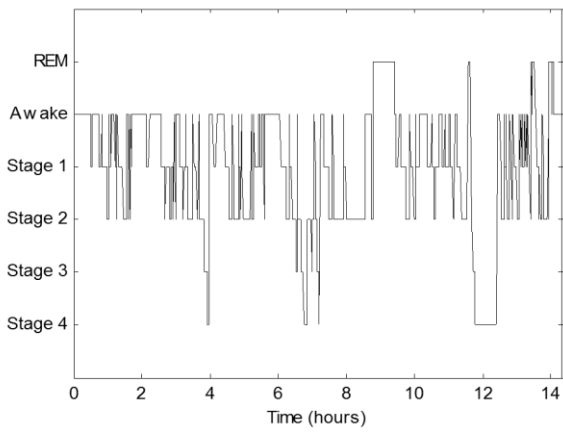


Figure A1.20 Hypnogram subject UCDDB023 and sleep stages distribution.

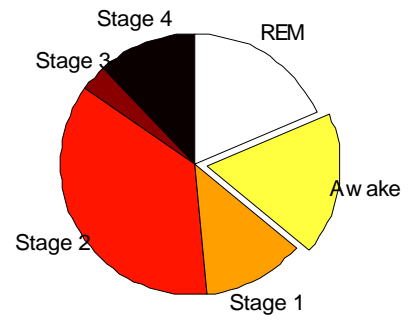
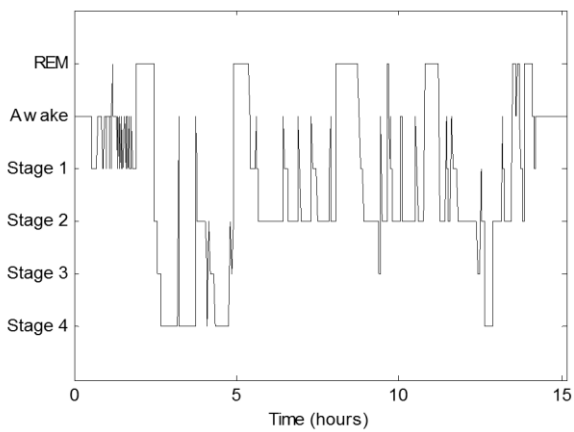


Figure A1.21 Hypnogram subject UCDDB024 and sleep stages distribution.

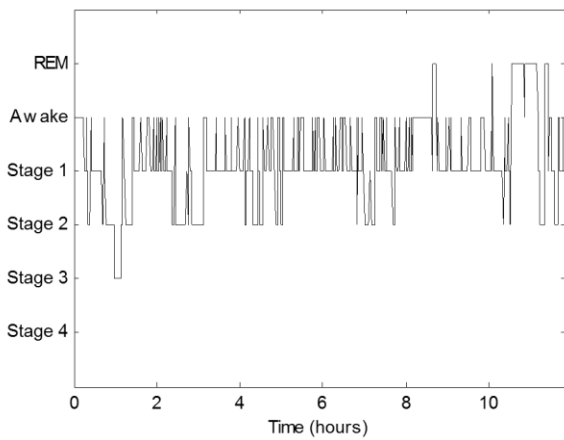


Figure A1.22 Hypnogram subject UCDDB025 and sleep stages distribution.

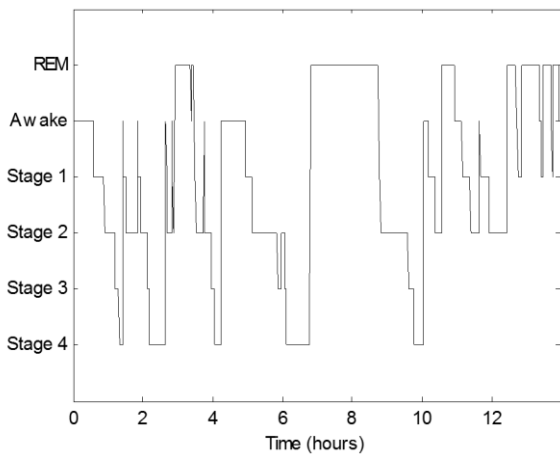
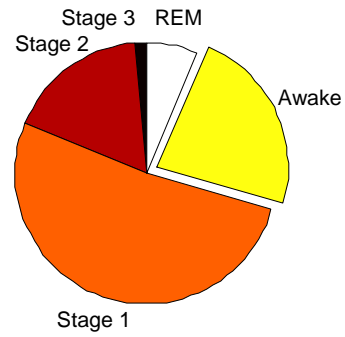


Figure A1.23 Hypnogram subject UCDDB026 and sleep stages distribution.

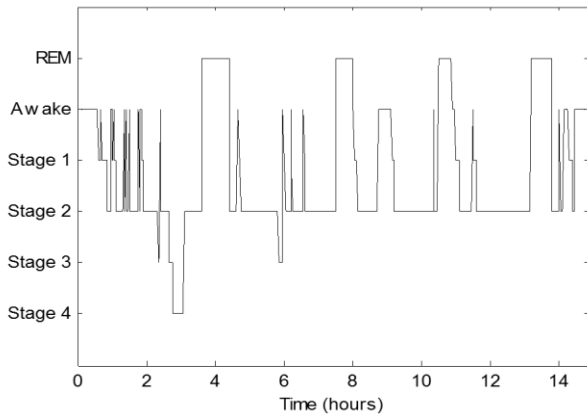
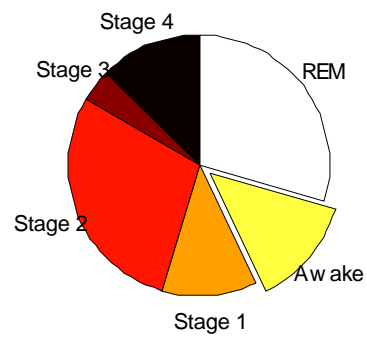
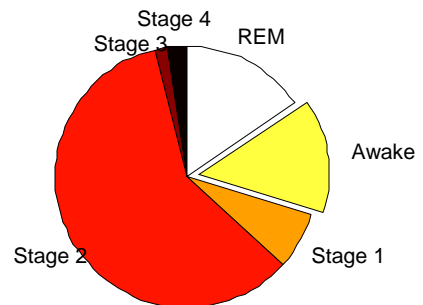


Figure A1.24 Hypnogram subject UCDDB027 and sleep stages distribution.



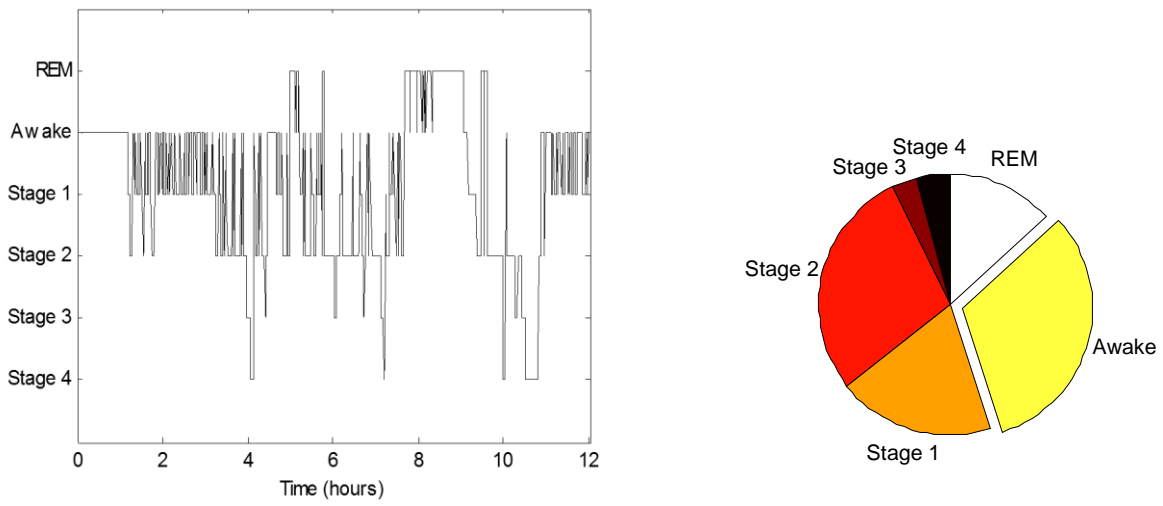


Figure A1.25 Hypnogram subject UCDDB028 and sleep stages distribution.

Appendix 2

EEG sleep stages decomposed in brain rhythms using a 7-level WPT, db4.

Original Signal is labeled “Den”

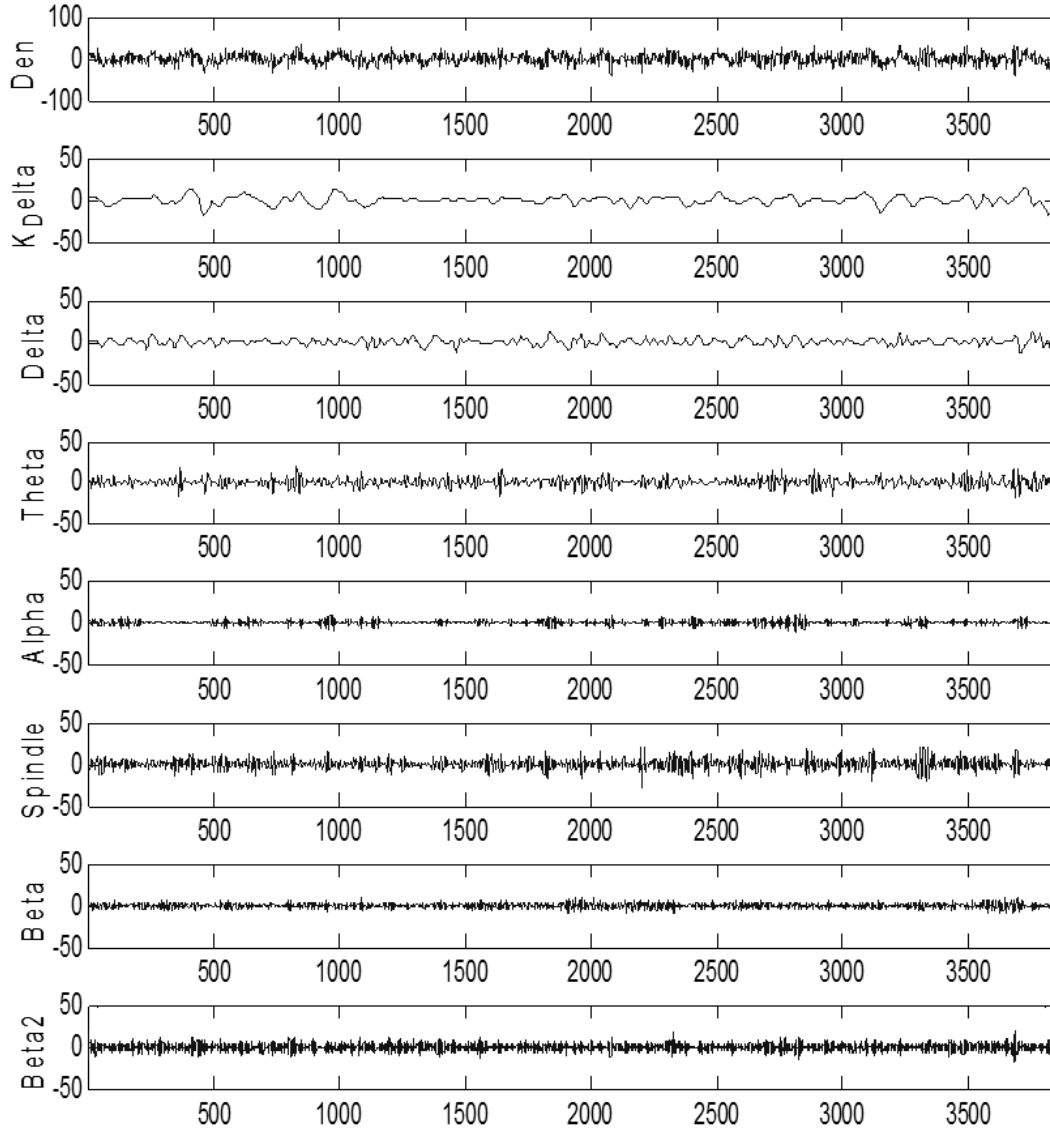


Figure A2.1 Awake stage

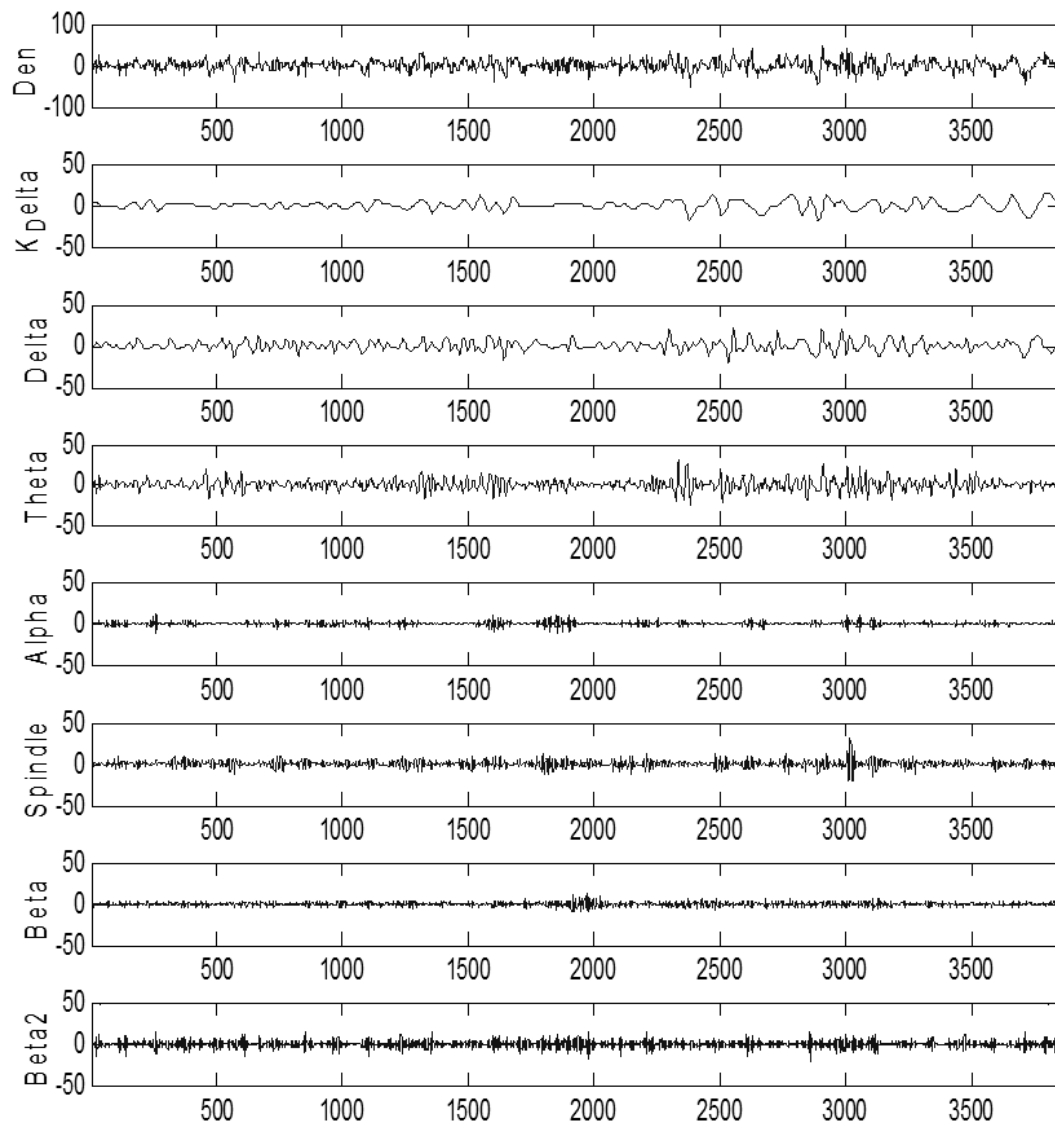


Figure A2.2 Stage 1

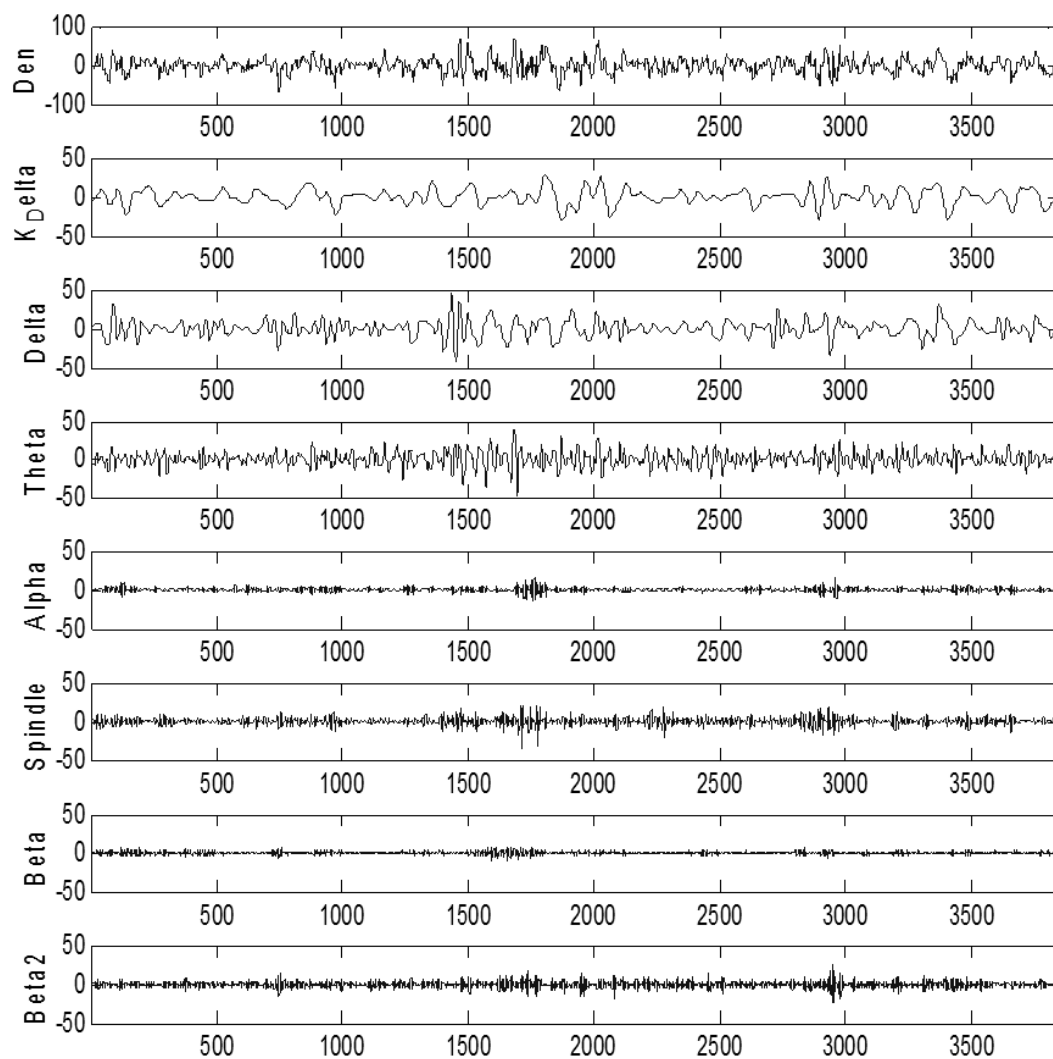


Figure A2.3 Stage 2

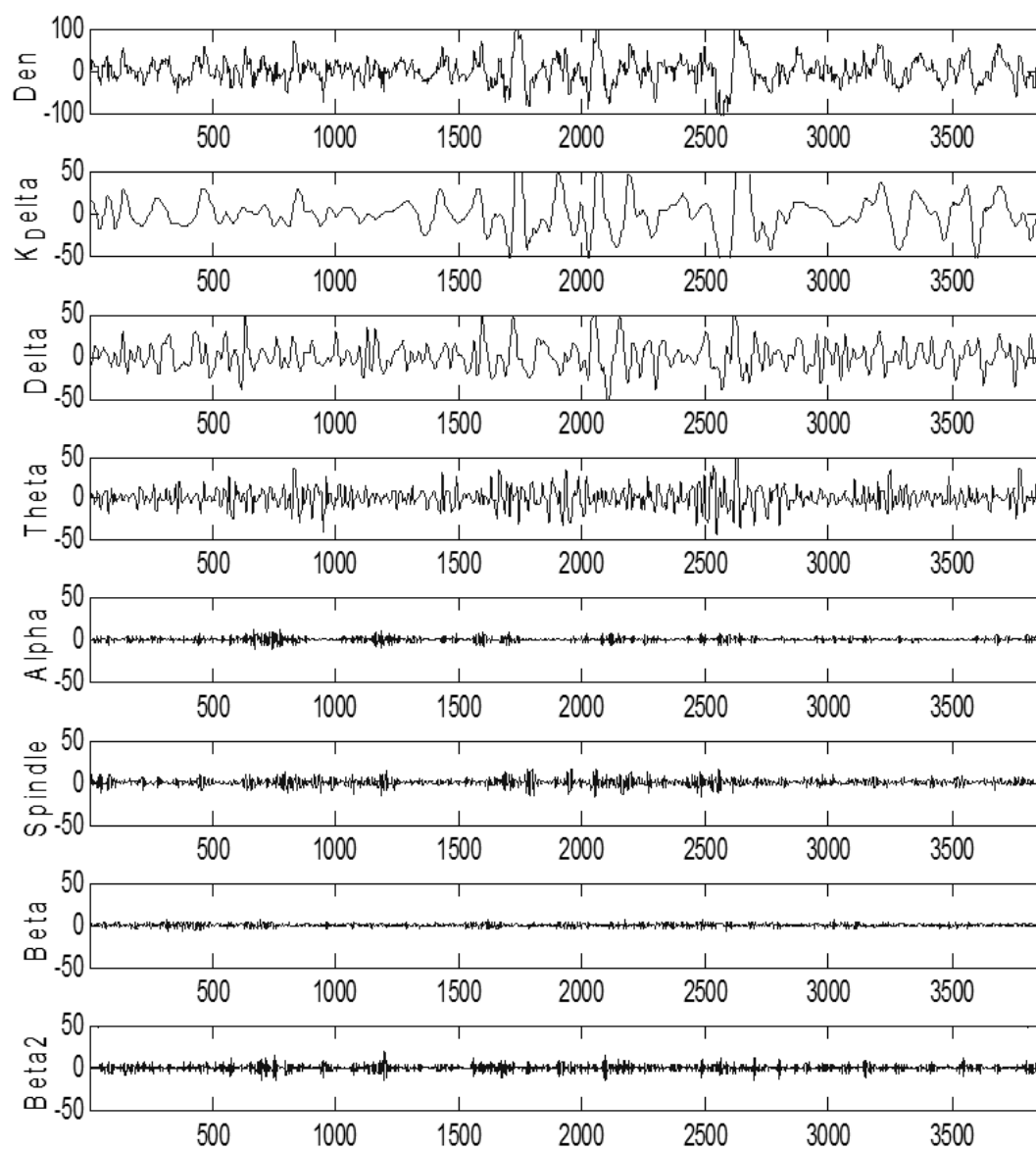


Figure A2.4 Stage 3

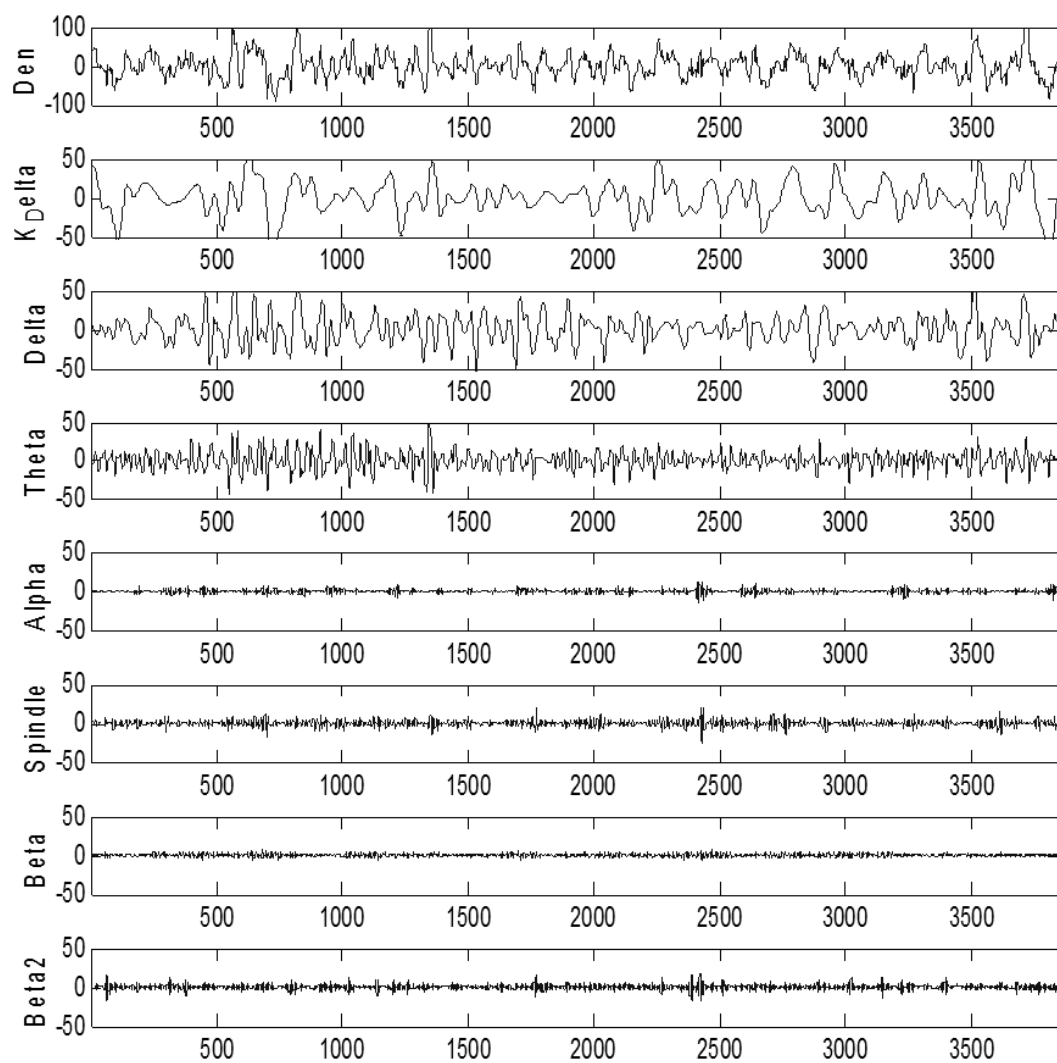


Figure A2.5 Stage 4

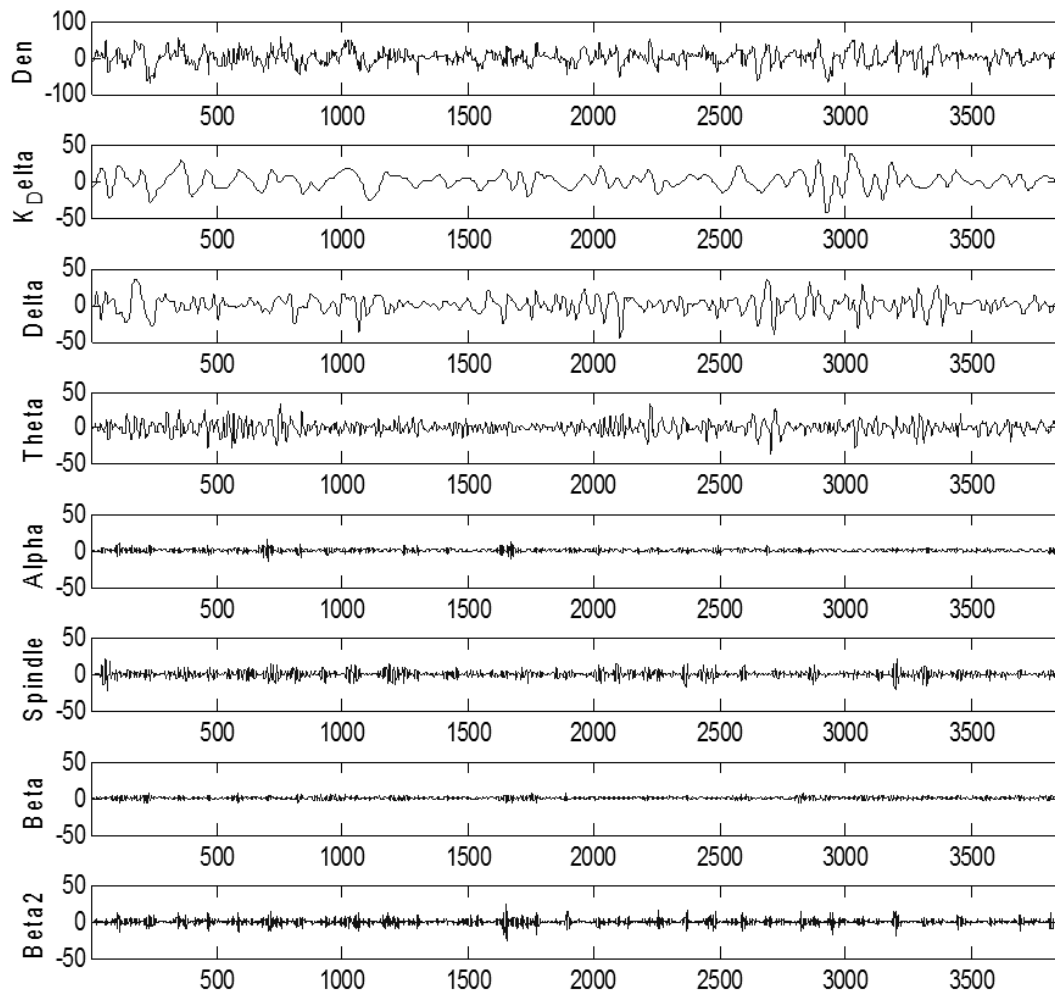
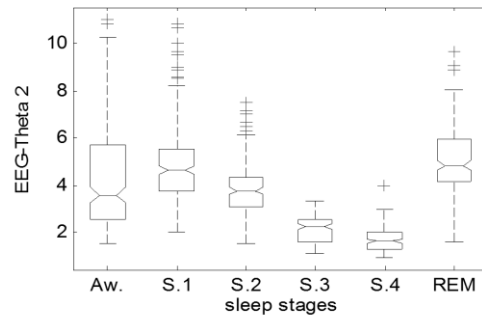
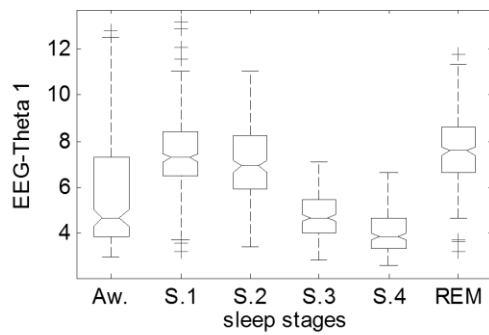
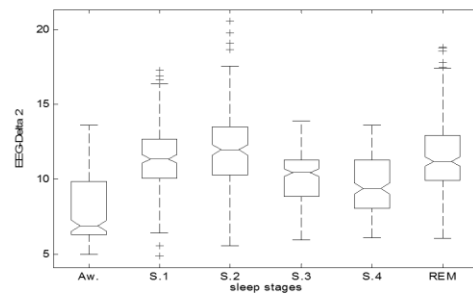
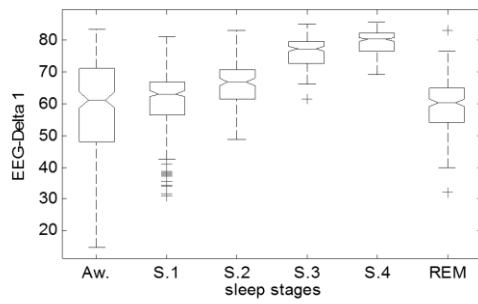
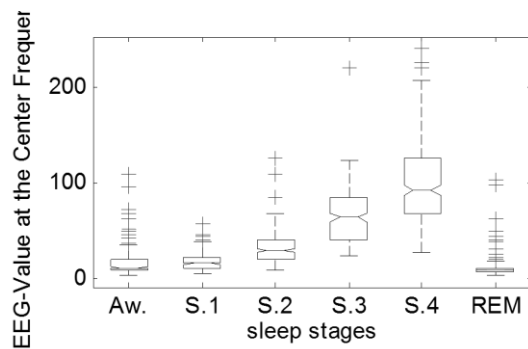
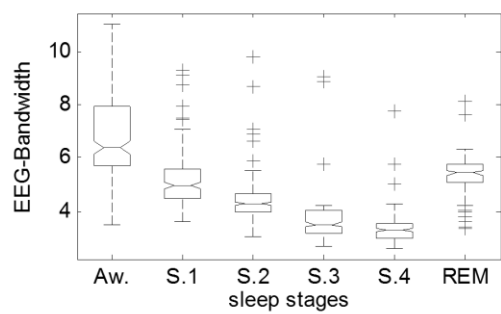
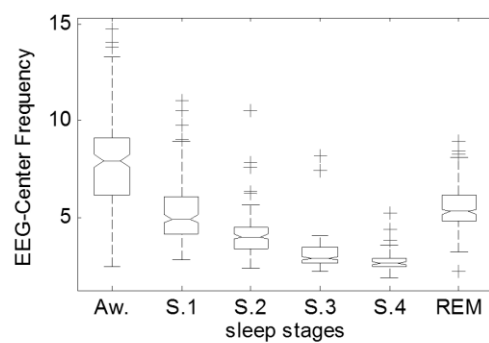
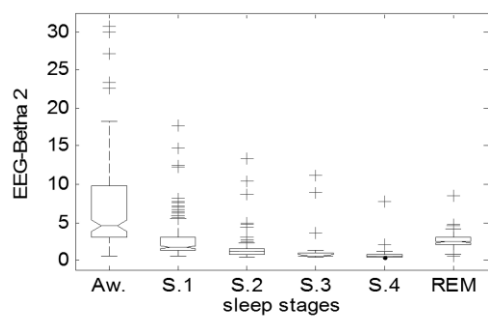
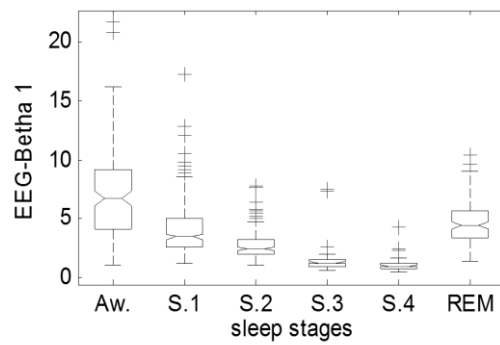
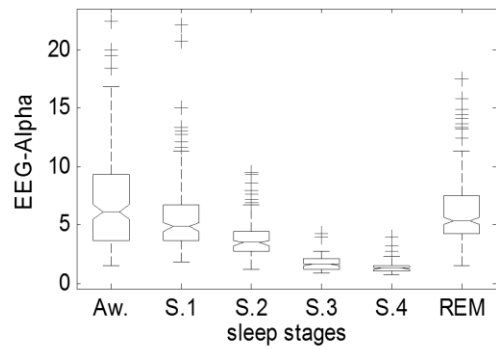


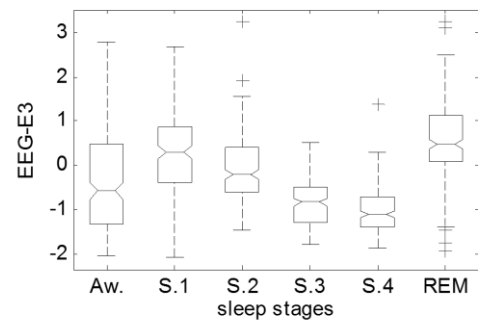
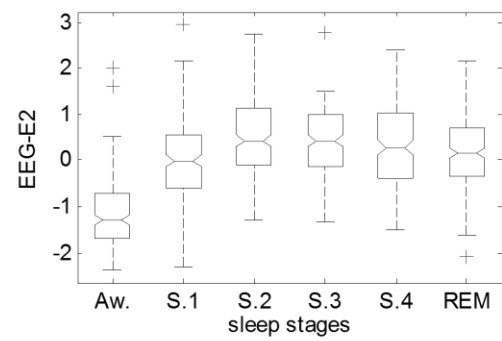
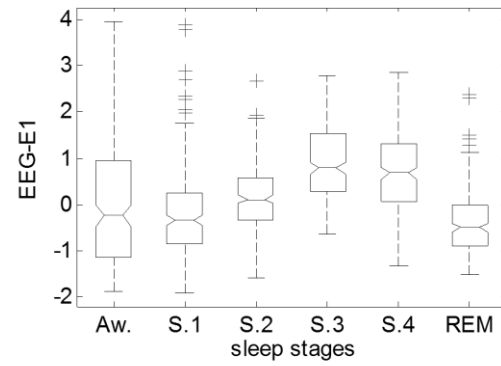
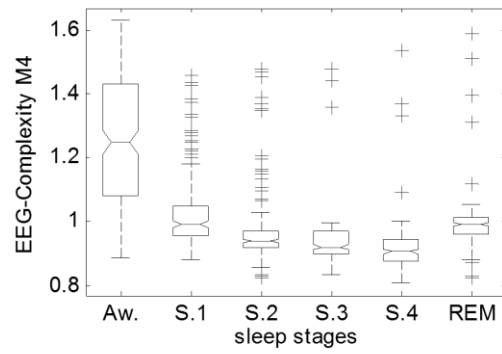
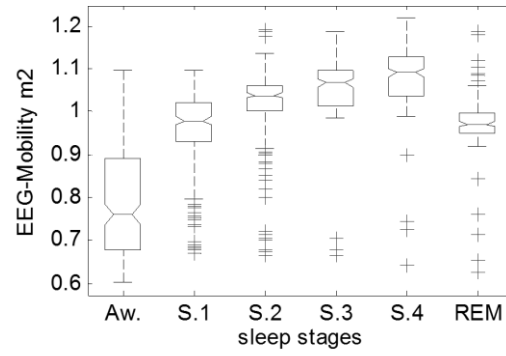
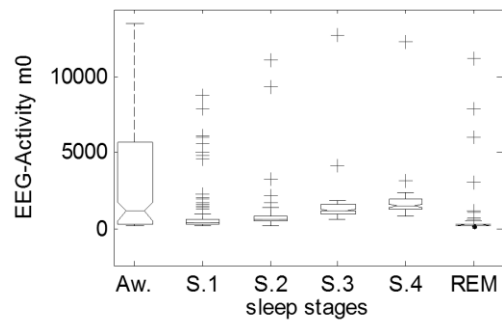
Figure A2.6 REM Stage

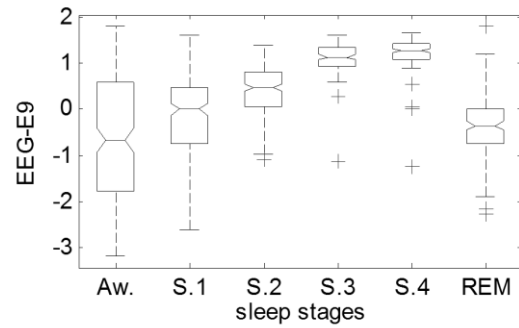
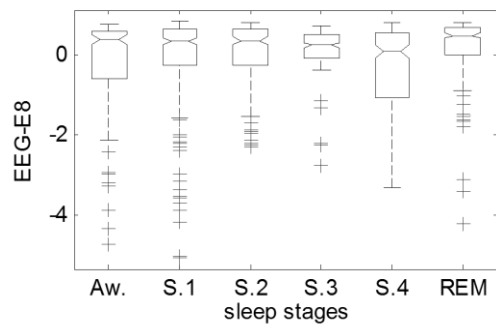
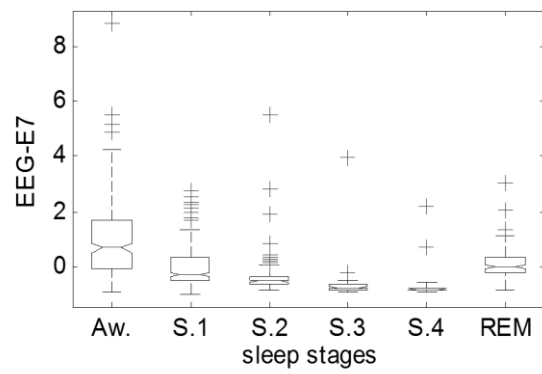
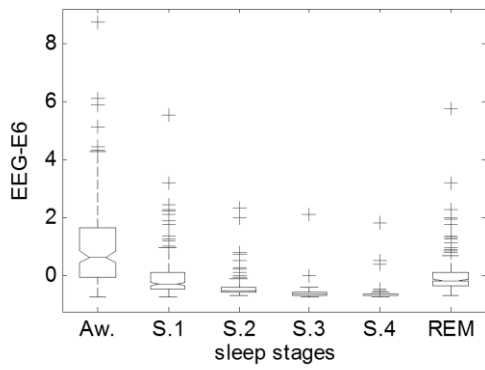
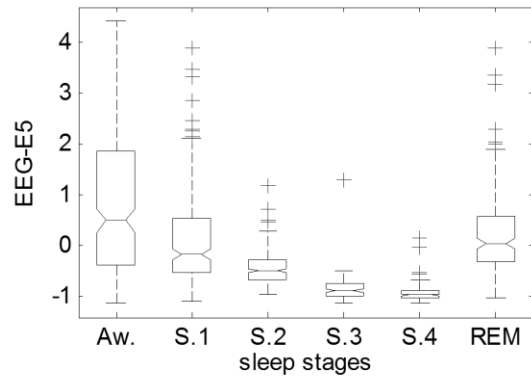
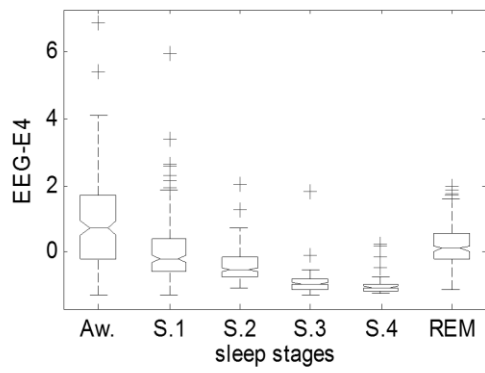
Appendix 3. Proposed 44 features extracted from subject #2

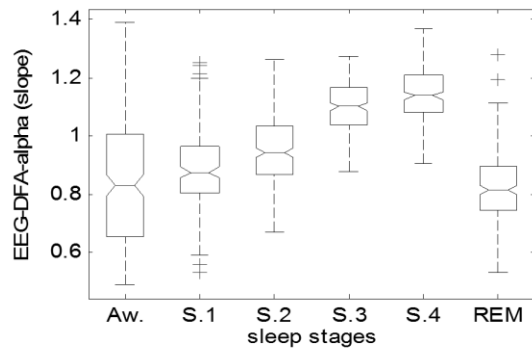
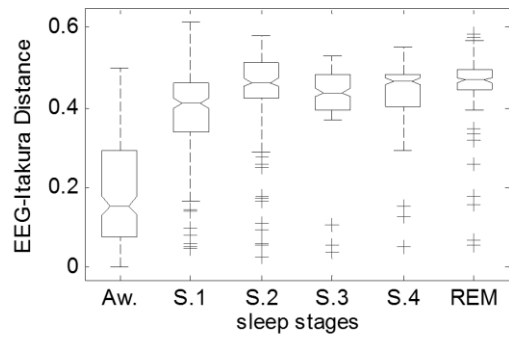
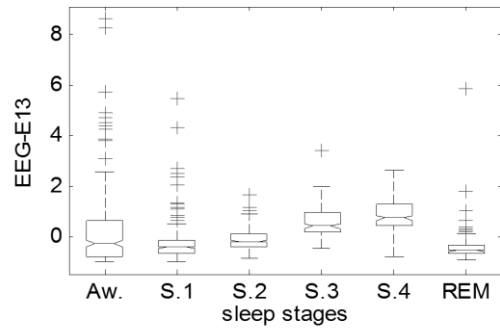
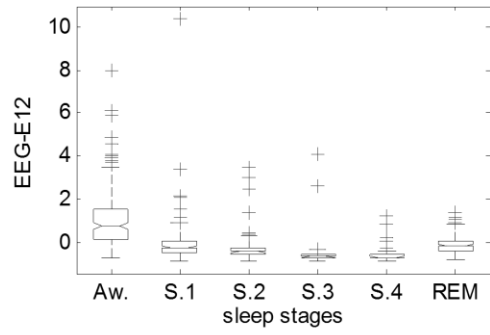
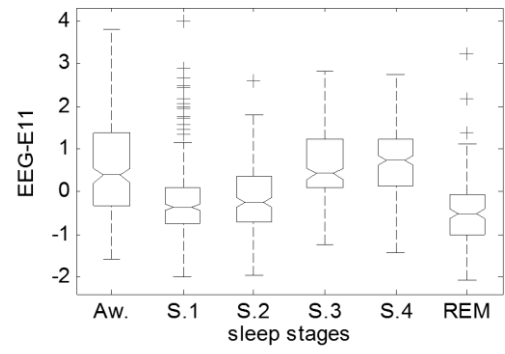
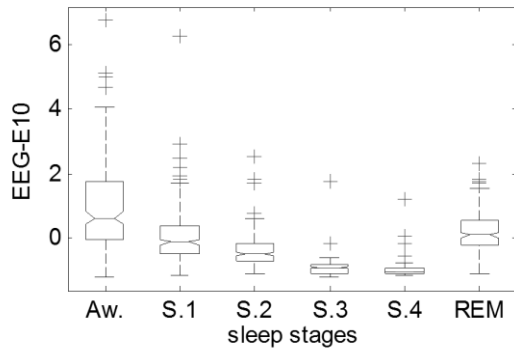
In this appendix all 44 features, computed from subject #2's data, are presented in boxplots. Each boxplot depicts the behavior of one feature for EEG or HRV feature extraction algorithms. The horizontal axis represents the six different sleep stages whereas the vertical axis represents the distribution of the labeled feature across the sleep stages.

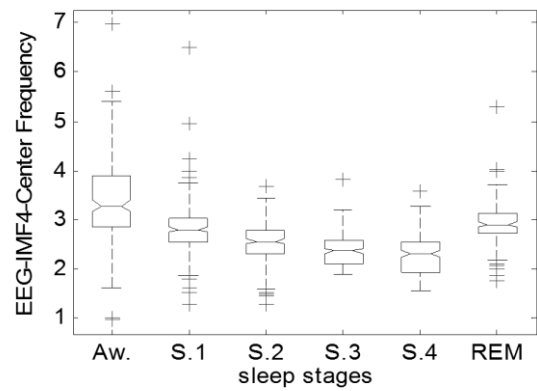
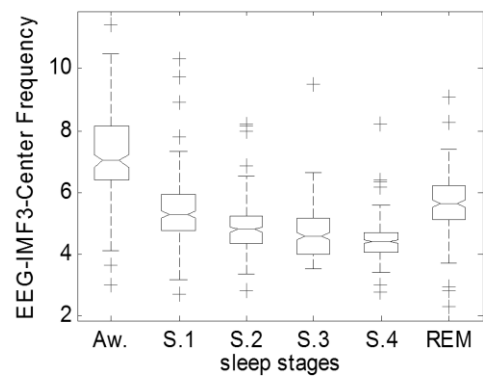
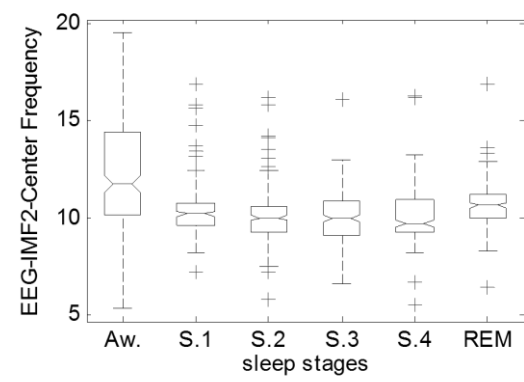
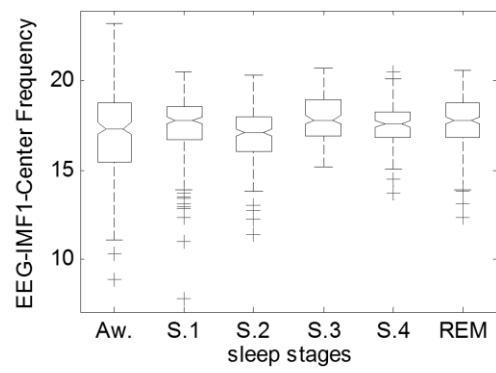
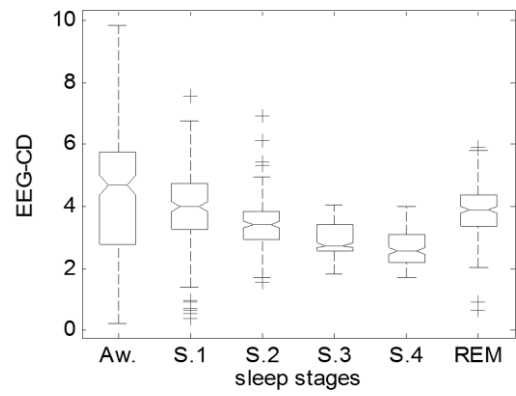
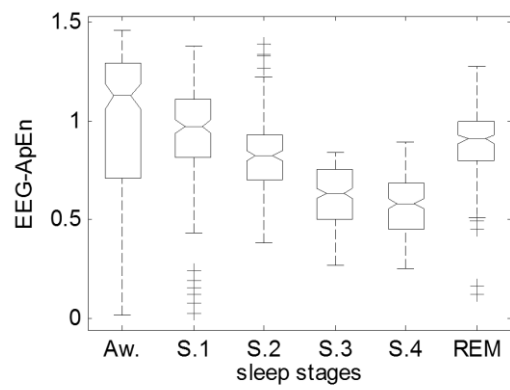


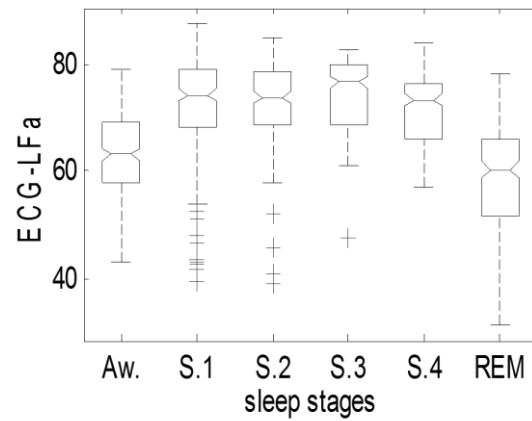
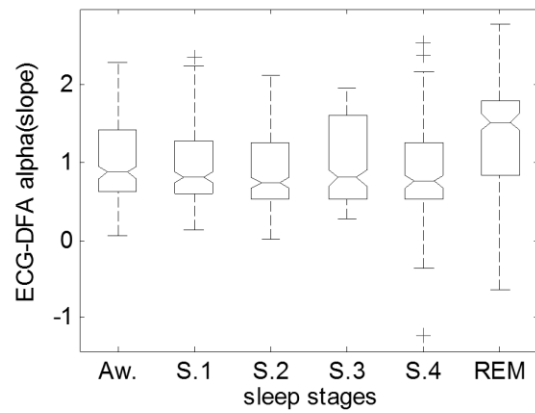
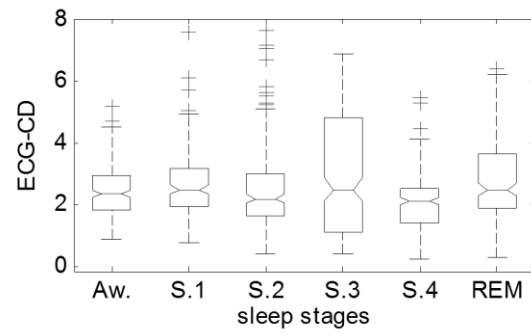
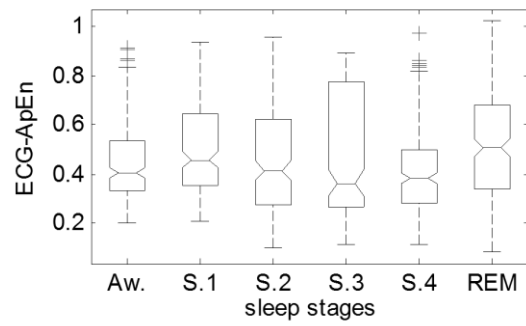
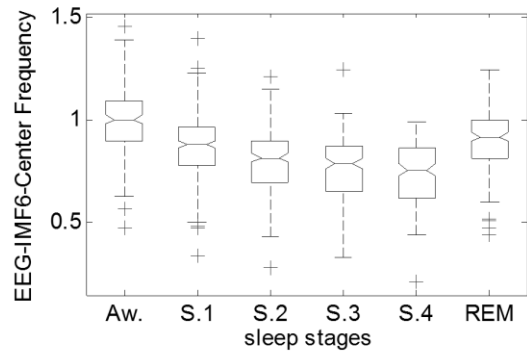
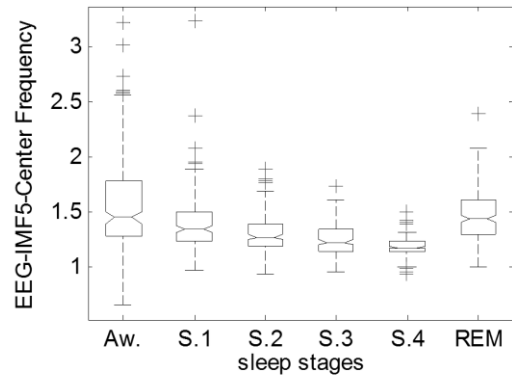


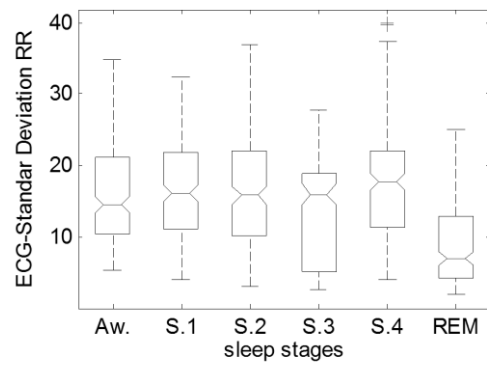
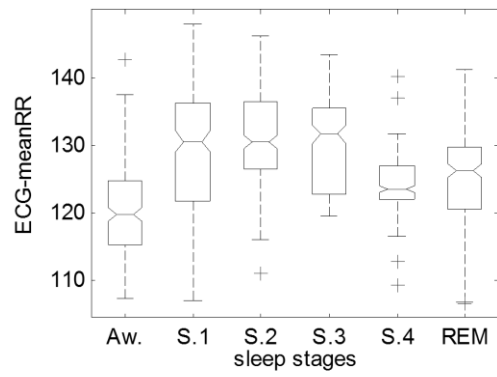
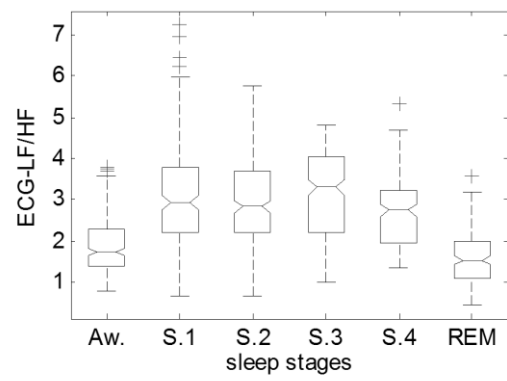
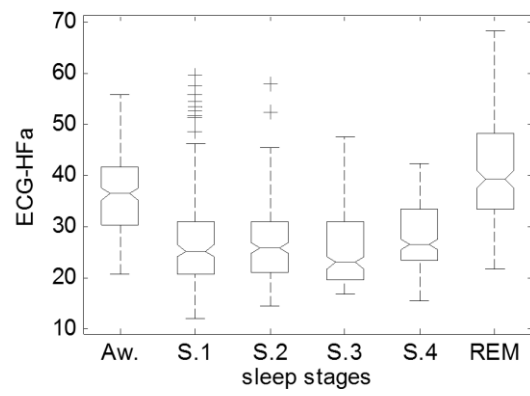






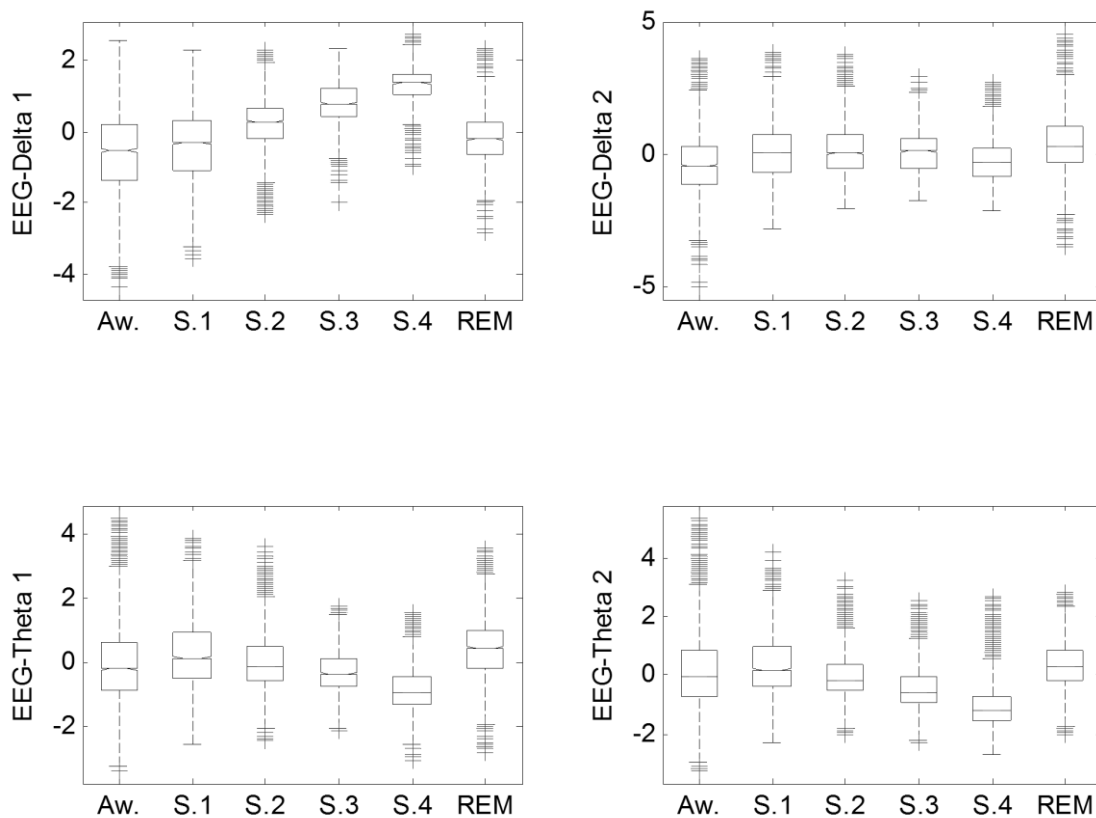


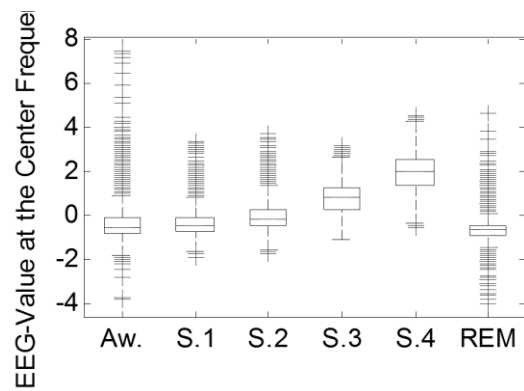
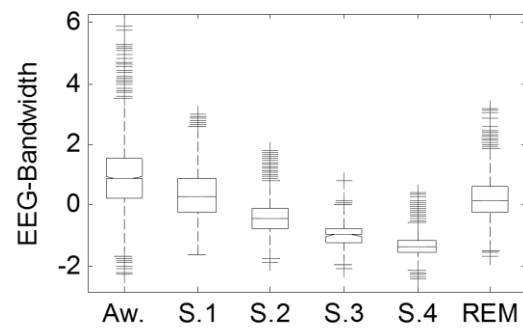
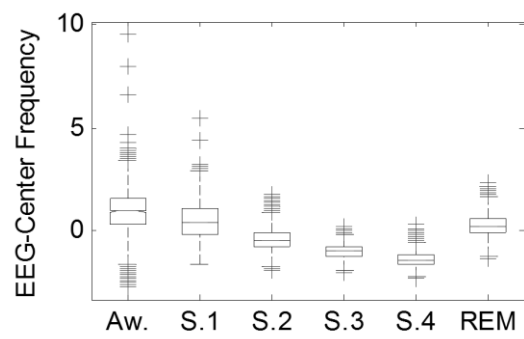
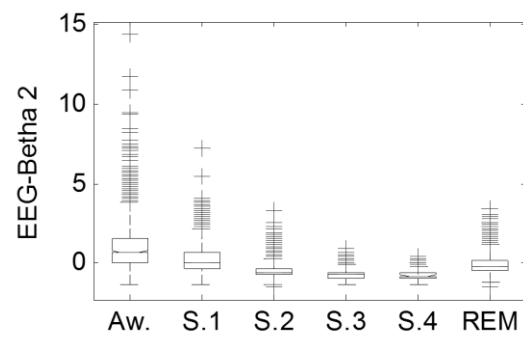
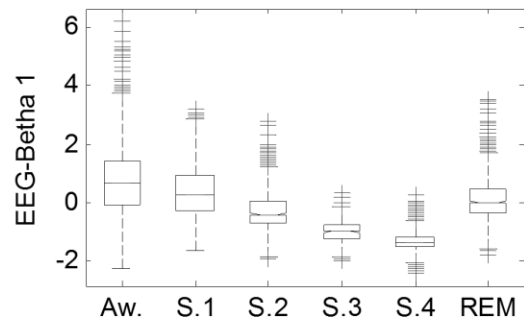
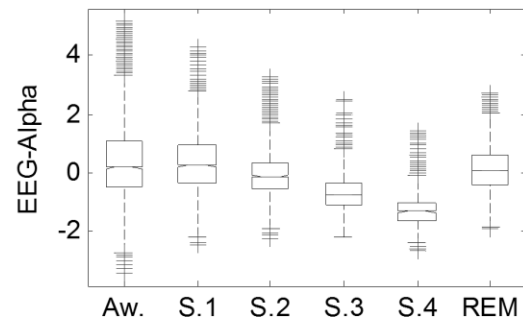


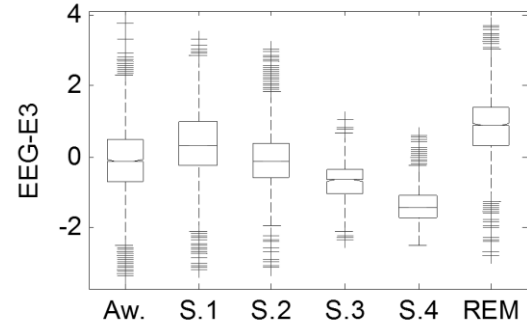
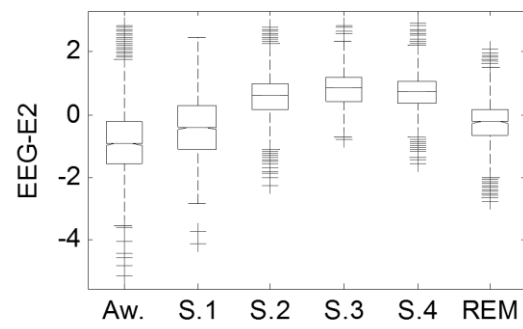
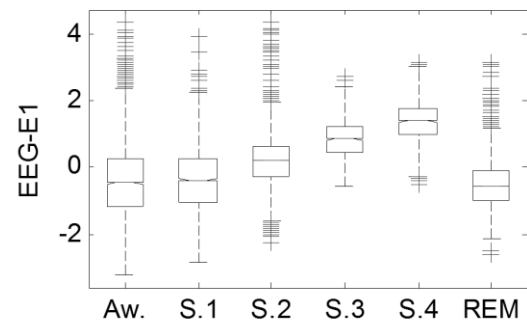
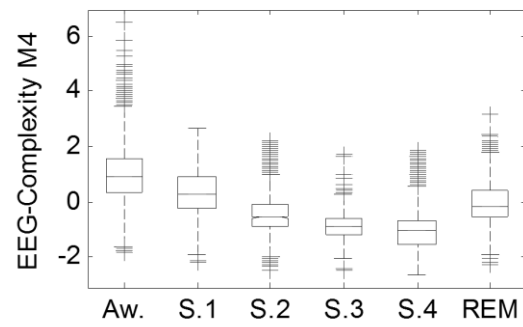
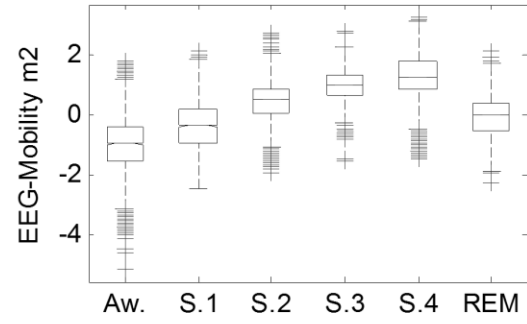
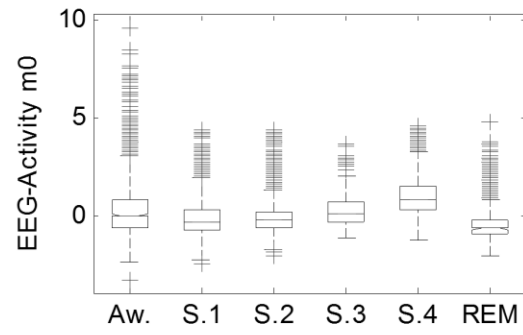


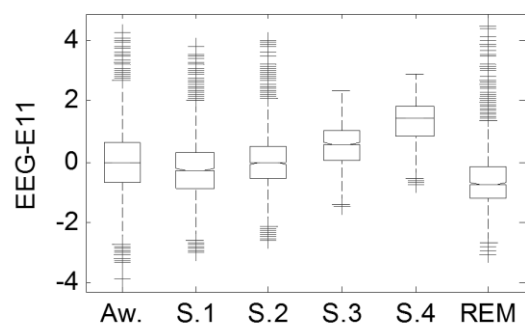
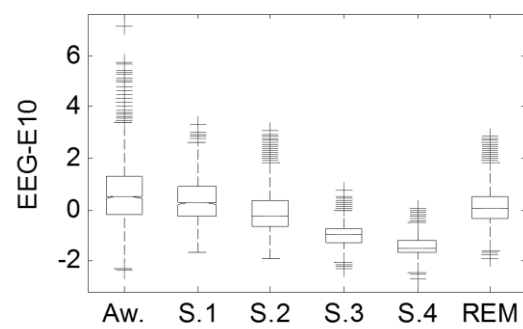
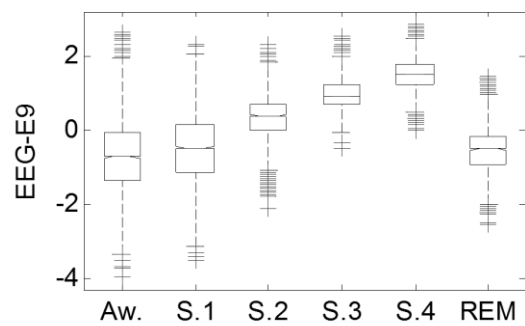
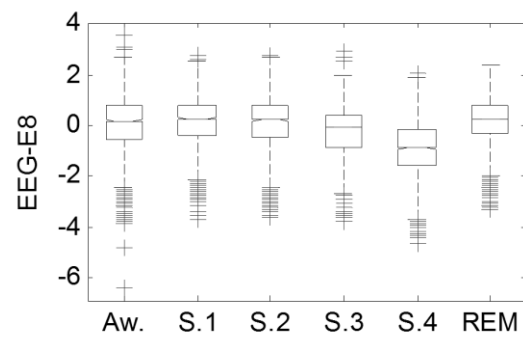
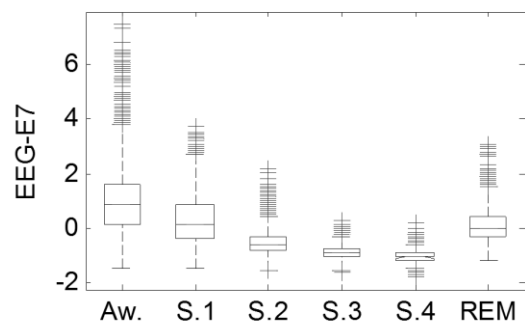
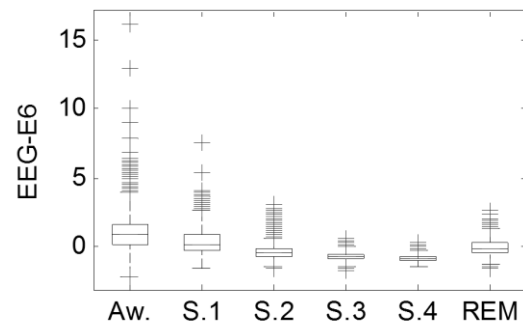
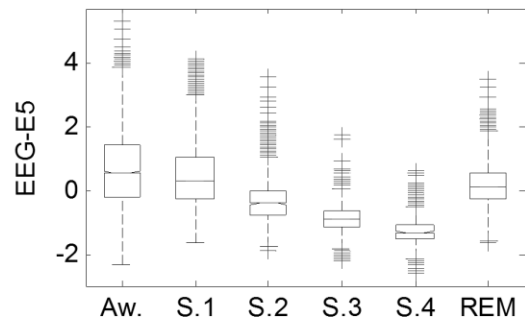
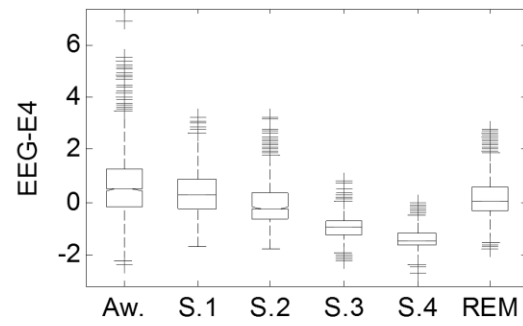
Appendix 4. Proposed 44 features extracted from all subjects (Normalized values)

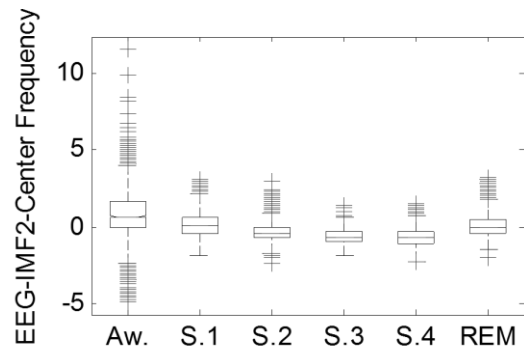
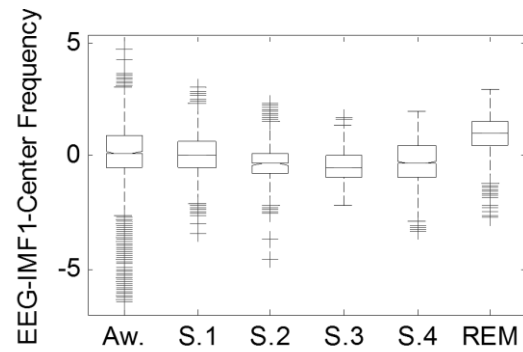
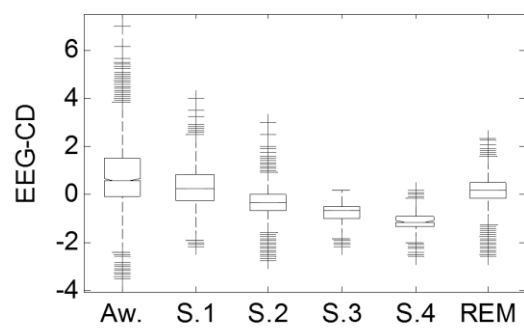
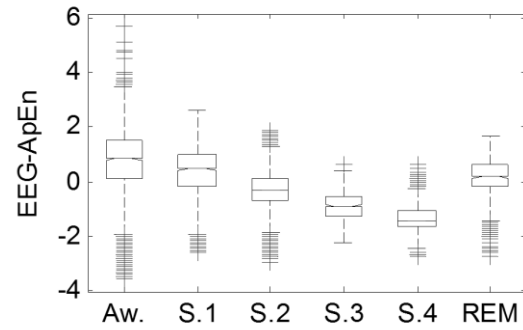
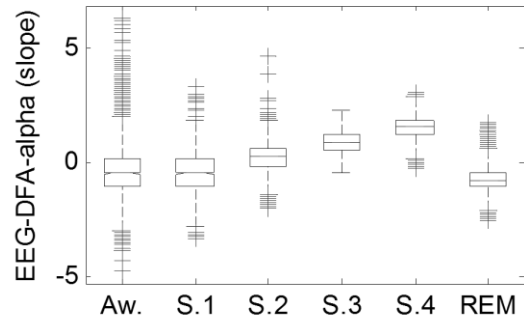
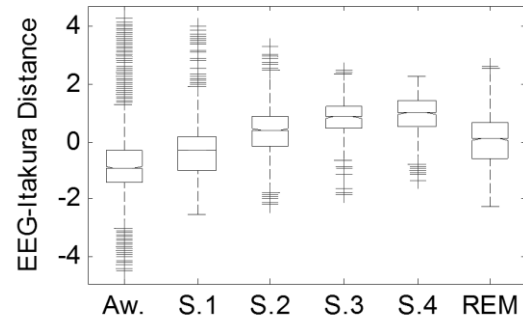
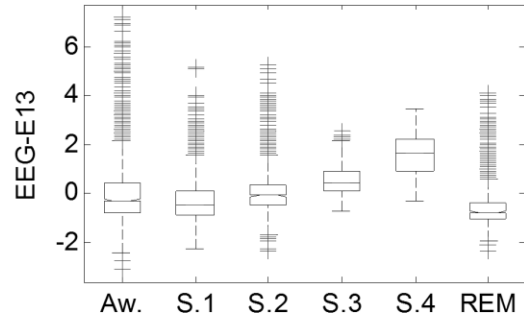
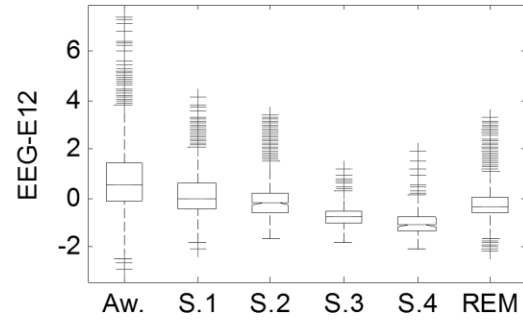
In this appendix all 44 features, computed from all subjects' data, are presented in boxplots. Each boxplot depicts the behavior of one feature for EEG or HRV feature extraction algorithms. The horizontal axis represents the six different sleep stages whereas the vertical axis represents the distribution of the labeled feature across the sleep stages. Features were normalized as described in section 8.1.2.

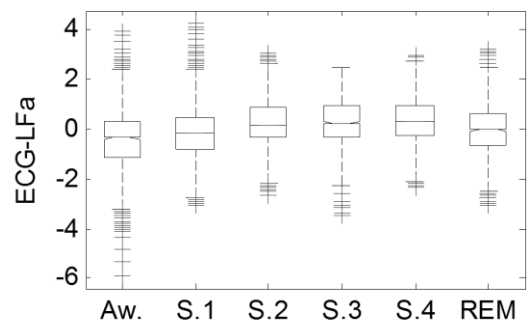
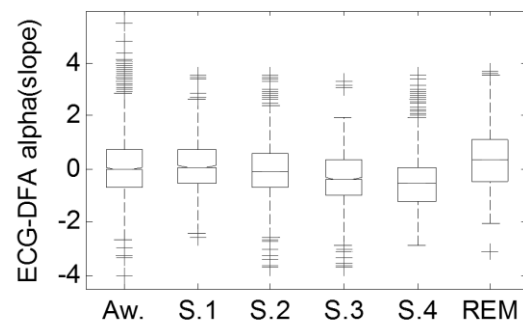
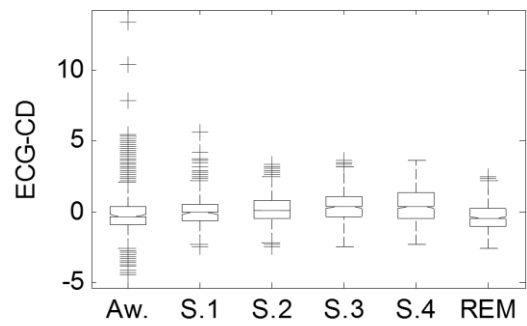
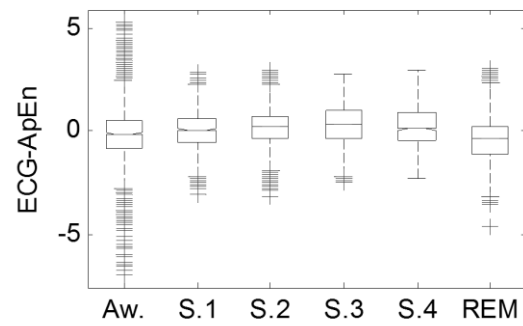
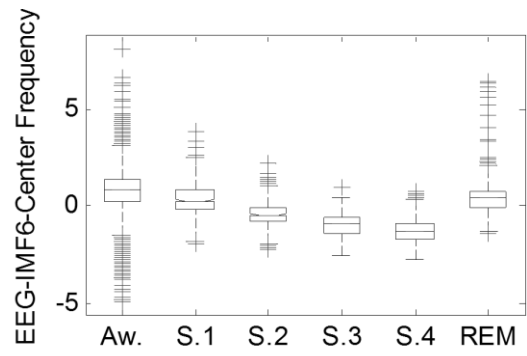
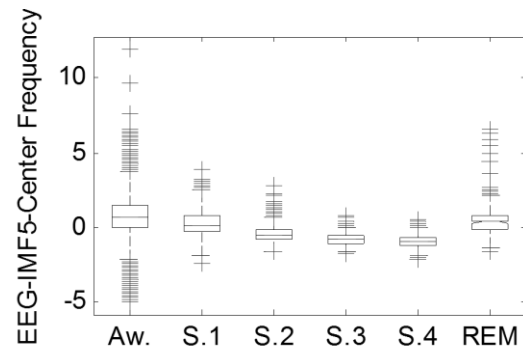
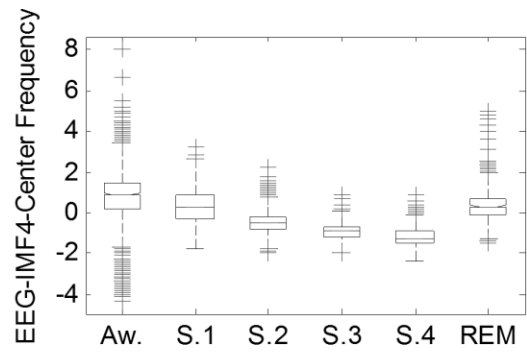
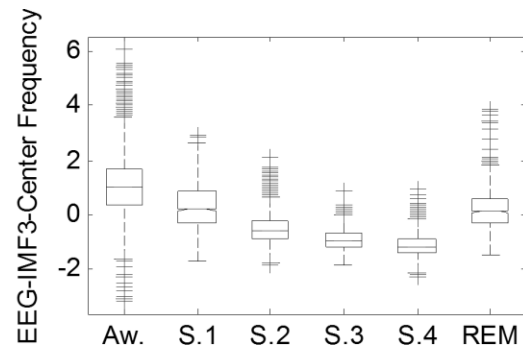


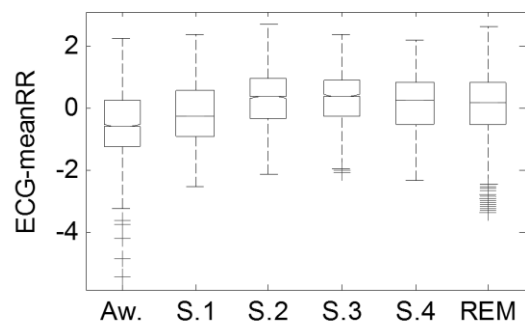
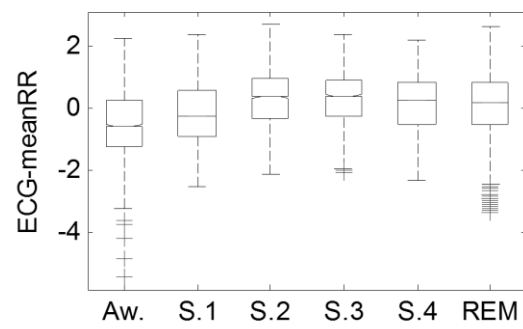
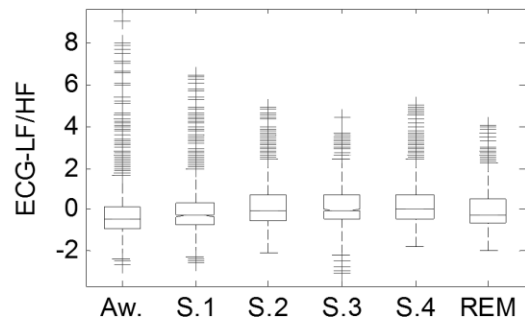
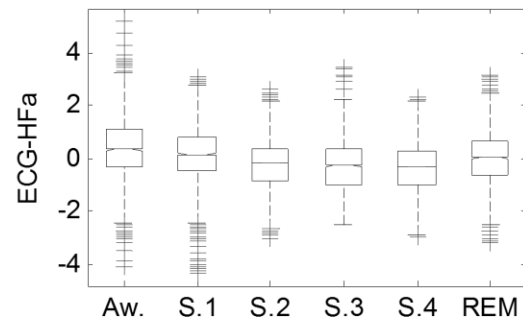












Appendix 5. Correlation between extracted features.

Table A5.1 Correlation matrix part 1 out of 3

	fd1	fd2	ft1	ft2	fal	fb1	fb2	fc	fs	vfc	m0	m2	m4	e1	e2
fd1	1.00 *	-0.31 *	-0.71 *	-0.82 *	-0.85 *	-0.86 *	-0.60 *	-0.83 *	-0.67 *	0.69 *	0.57 *	0.54 *	-0.41 *	0.87 *	0.55
fd2	-0.31 *	1.00 *	0.80 *	0.43 *	0.14	-0.06	-0.25	-0.13	-0.21	-0.15	-0.54 *	0.26	-0.33 *	-0.41 *	0.43
ft1	-0.71 *	0.80 *	1.00 *	0.86 *	0.60 *	0.34 *	0.06	0.30 *	0.13	-0.43 *	-0.60 *	-0.02	-0.11	-0.67 *	0.01
ft2	-0.82 *	0.43 *	0.86 *	1.00 *	0.87 *	0.55 *	0.23	0.54 *	0.31 *	-0.53 *	-0.50 *	-0.21	0.08	-0.68 *	-0.34
fal	-0.85 *	0.14	0.60 *	0.87 *	1.00 *	0.76 *	0.36 *	0.71 *	0.48 *	-0.58 *	-0.41 *	-0.40 *	0.28	-0.66 *	-0.56
fb1	-0.86 *	-0.06	0.34 *	0.55 *	0.76 *	1.00 *	0.77 *	0.93 *	0.84 *	-0.67 *	-0.39 *	-0.73 *	0.63 *	-0.71 *	-0.71
fb2	-0.60 *	-0.25	0.06	0.23	0.36 *	0.77 *	1.00 *	0.82 *	0.93 *	-0.44 *	-0.11	-0.81 *	0.78 *	-0.42 *	-0.64
fc	-0.83 *	-0.13	0.30 *	0.54 *	0.71 *	0.93 *	0.82 *	1.00 *	0.91 *	-0.71 *	-0.35 *	-0.80 *	0.72 *	-0.69 *	-0.81
fs	-0.67 *	-0.21	0.13	0.31 *	0.48 *	0.84 *	0.93 *	0.91 *	1.00 *	-0.66 *	-0.26	-0.89 *	0.85 *	-0.51 *	-0.68
vfc	0.69 *	-0.15	-0.43 *	-0.53 *	-0.58 *	-0.67 *	-0.44 *	-0.71 *	-0.66 *	1.00 *	0.74 *	0.52 *	-0.44 *	0.62 *	0.36
m0	0.57 *	-0.54 *	-0.60 *	-0.50 *	-0.41 *	-0.39 *	-0.11	-0.35 *	-0.26	0.74 *	1.00 *	0.09	0.01	0.65 *	-0.04
m2	0.54 *	0.26	-0.02	-0.21	-0.40 *	-0.73 *	-0.81 *	-0.80 *	-0.89 *	0.52 *	0.09	1.00 *	-0.98 *	0.38 *	0.67
m4	-0.41 *	-0.33 *	-0.11	0.08	0.28	0.63 *	0.78 *	0.72 *	0.85 *	-0.44 *	0.01	-0.98 *	1.00 *	-0.25	-0.63
e1	0.87 *	-0.41 *	-0.67 *	-0.68 *	-0.66 *	-0.71 *	-0.42 *	-0.69 *	-0.51 *	0.62 *	0.65 *	0.38 *	-0.25	1.00 *	0.39
e2	0.55 *	0.43 *	0.01	-0.34 *	-0.56 *	-0.71 *	-0.64 *	-0.81 *	-0.68 *	0.36 *	-0.04	0.67 *	-0.63 *	0.39 *	1.00
e3	-0.63 *	0.59 *	0.77 *	0.71 *	0.55 *	0.36 *	0.02	0.38 *	0.17	-0.58 *	-0.69 *	-0.08	-0.04	-0.74 *	-0.12
e4	-0.82 *	-0.03	0.35 *	0.56 *	0.80 *	0.92 *	0.60 *	0.84 *	0.70 *	-0.68 *	-0.48 *	-0.59 *	0.49 *	-0.72 *	-0.59
e5	0.87 *	-0.02	0.44 *	0.73 *	0.92 *	0.83 *	0.51 *	0.85 *	0.62 *	-0.62 *	-0.36 *	0.67 *	0.47 *	-0.70 *	-0.74
e6	-0.72 *	-0.22	0.15	0.36 *	0.54 *	0.87 *	0.93 *	0.90 *	0.89 *	-0.53 *	-0.21	-0.78 *	0.72 *	-0.57 *	-0.72
e7	-0.74 *	-0.19	0.19	0.39 *	0.55 *	0.91 *	0.92 *	0.92 *	0.91 *	-0.56 *	-0.26	-0.81 *	0.74 *	-0.61 *	-0.74
e8	-0.34 *	0.28	0.39 *	0.34 *	0.34 *	0.24	0.07	0.19	0.15	-0.37 *	-0.37 *	-0.09	0.04	-0.21	0.16
e9	0.92 *	-0.12	-0.54 *	-0.72 *	-0.81 *	-0.87 *	-0.60 *	-0.91 *	-0.71 *	0.73 *	0.54 *	0.61 *	-0.49 *	0.88 *	0.70
e10	-0.82 *	-0.05	0.33 *	0.55 *	0.79 *	0.93 *	0.62 *	0.85 *	0.72 *	-0.69 *	-0.48 *	-0.61 *	0.50 *	-0.72 *	-0.61
e11	0.60 *	-0.65 *	-0.67 *	-0.44 *	-0.28	-0.38 *	-0.20	-0.33 *	-0.26	0.50 *	0.72 *	0.10	0.01	0.81 *	-0.12
e12	-0.59 *	-0.31 *	0.01	0.26	0.58 *	0.83 *	0.70 *	0.76 *	0.75 *	-0.52 *	-0.22	-0.65 *	0.60 *	-0.42 *	-0.59
e13	0.73 *	-0.48 *	-0.68 *	-0.64 *	-0.59 *	-0.54 *	-0.20	-0.54 *	-0.37 *	0.74 *	0.80 *	0.22	-0.09	0.85 *	0.19
Ita	0.42 *	0.24	0.03	-0.17	-0.39 *	-0.61 *	-0.60 *	-0.64 *	-0.69 *	0.37 *	0.01	0.85 *	-0.84 *	0.29 *	0.58
DFA	0.86 *	-0.20	-0.58 *	-0.71 *	-0.75 *	-0.78 *	-0.50 *	-0.84 *	-0.62 *	0.71 *	0.55 *	0.53 *	-0.41 *	0.86 *	0.62
Apen	-0.80 *	0.09	0.39 *	0.50 *	0.62 *	0.86 *	0.69 *	0.81 *	0.80 *	-0.75 *	-0.56 *	-0.76 *	0.68 *	-0.67 *	-0.48
CD	-0.80 *	0.10	0.41 *	0.50 *	0.59 *	0.82 *	0.68 *	0.79 *	0.72 *	-0.67 *	-0.55 *	-0.67 *	0.58 *	-0.72 *	-0.48
IMF1	-0.14	0.04	0.06	0.04	0.03	0.15	0.14	0.28 *	0.25	-0.31 *	-0.21	-0.27	0.24	-0.30 *	-0.23
IMF2	-0.49 *	-0.29 *	-0.05	0.09	0.27	0.72 *	0.91 *	0.75 *	0.90 *	-0.47 *	-0.09	-0.88 *	0.87 *	-0.32 *	-0.57
IMF3	-0.63 *	-0.27	0.08	0.29 *	0.48 *	0.82 *	0.92 *	0.89 *	0.96 *	-0.54 *	-0.11	-0.91 *	0.87 *	-0.44 *	-0.74
IMF4	-0.64 *	-0.20	0.13	0.32 *	0.47 *	0.78 *	0.88 *	0.87 *	0.93 *	-0.56 *	-0.15	-0.88 *	0.83 *	-0.48 *	-0.71
IMF5	-0.53 *	-0.18	0.09	0.21	0.32 *	0.69 *	0.86 *	0.76 *	0.86 *	-0.44 *	-0.08	-0.81 *	0.78 *	-0.40 *	-0.58
IMF6	-0.51 *	-0.22	0.06	0.21	0.35 *	0.68 *	0.80 *	0.77 *	0.86 *	-0.52 *	-0.10	-0.88 *	0.84 *	-0.39 *	-0.59
APEN	-0.18	0.35 *	0.31 *	0.21	0.11	0.06	-0.07	-0.03	-0.11	-0.05	-0.26	0.11	-0.13	-0.21	0.15
CD	-0.06	0.32 *	0.25	0.15	0.08	-0.06	-0.20	-0.14	-0.23	0.07	-0.18	0.28	-0.29 *	-0.05	0.23
DFA	-0.18	-0.01	0.01	-0.02	-0.02	0.22	0.41 *	0.32 *	0.44 *	-0.21	-0.07	-0.40 *	0.41 *	-0.22	-0.16
LFA	0.10	0.03	0.00	-0.05	-0.10	-0.17	-0.08	-0.12	-0.08	0.09	0.13	0.18	-0.16	0.08	0.11
HFA	-0.07	-0.05	-0.03	0.04	0.10	0.14	0.05	0.10	0.05	-0.07	-0.11	-0.16	0.15	-0.05	-0.11
LFHF	0.04	-0.04	-0.02	-0.04	-0.07	-0.06	0.13	0.03	0.14	0.01	0.13	-0.01	0.03	0.05	0.01
MeanRR	0.01	0.32 *	0.24	0.14	0.01	-0.16	-0.31 *	-0.22	-0.25	-0.08	-0.30 *	0.33 *	-0.36 *	-0.03	0.29
SRDRR	0.05	-0.20	-0.15	-0.08	-0.01	0.00	0.11	0.09	0.18	-0.05	0.18	-0.16	0.17	0.11	-0.12

*p<0.01

Table A5.2 Correlation matrix part 2 out of 3

	e3	e4	e5	e6	e7	e8	e9	e10	e11	e12	e13	Ita	DFA	Apen	CD
fd1	* -0.63 *	* -0.82 *	* -0.84 *	* -0.72 *	* -0.74 *	* -0.34 *	* 0.92 *	* -0.82 *	* 0.60 *	* -0.59 *	* 0.73 *	* 0.42 *	* 0.86 *	* -0.80 *	* -0.80
fd2	* 0.59 *	* -0.03	* -0.02	* -0.22	* -0.19	0.28	* -0.12	* -0.05	* -0.65 *	* -0.31 *	* -0.48 *	0.24	* -0.20	0.09	0.10
ft1	* 0.77 *	* 0.35 *	* 0.44 *	* 0.15	* 0.19	* 0.39 *	* -0.54 *	* 0.33 *	* -0.67 *	* 0.01	* -0.68 *	* 0.03	* -0.58 *	* 0.39 *	* 0.41
ft2	* 0.71 *	* 0.56 *	* 0.73 *	* 0.36 *	* 0.39 *	* 0.34 *	* -0.72 *	* 0.55 *	* -0.44 *	* 0.26	* -0.64 *	* -0.17	* -0.71 *	* 0.50 *	* 0.50
fal	* 0.55 *	* 0.80 *	* 0.92 *	* 0.54 *	* 0.55 *	* 0.34 *	* -0.81 *	* 0.79 *	* -0.28	* 0.58 *	* -0.59 *	* -0.39 *	* -0.75 *	* 0.62 *	* 0.59
fb1	* 0.36 *	* 0.92 *	* 0.83 *	* 0.87 *	* 0.91 *	* 0.24	* -0.87 *	* 0.93 *	* -0.38 *	* 0.83 *	* -0.54 *	* -0.61 *	* -0.78 *	* 0.86 *	* 0.82
fb2	* 0.02	* 0.60 *	* 0.51 *	* 0.93 *	* 0.92 *	* 0.07	* -0.60 *	* 0.62 *	* -0.20	* 0.70 *	* -0.20	* -0.60 *	* -0.50 *	* 0.69 *	* 0.68
fc	* 0.38 *	* 0.84 *	* 0.85 *	* 0.90 *	* 0.92 *	* 0.19	* -0.91 *	* 0.85 *	* -0.33 *	* 0.76 *	* -0.54 *	* -0.64 *	* -0.84 *	* 0.81 *	* 0.79
fs	* 0.17	* 0.70 *	* 0.62 *	* 0.89 *	* 0.91 *	* 0.15	* -0.71 *	* 0.72 *	* -0.26	* 0.75 *	* -0.37 *	* -0.69 *	* -0.62 *	* 0.80 *	* 0.72
vfc	* -0.58 *	* -0.68 *	* -0.62 *	* -0.53 *	* -0.56 *	* -0.37 *	* 0.73 *	* -0.69 *	* 0.50 *	* -0.52 *	* 0.74 *	* 0.37 *	* 0.71 *	* -0.75 *	* -0.67
m0	* -0.69 *	* -0.48 *	* -0.36 *	* -0.21	* -0.26	* -0.37 *	* 0.54 *	* -0.48 *	* 0.72 *	* -0.22	* 0.80 *	* 0.01	* 0.55 *	* -0.56 *	* -0.55
m2	* -0.08	* -0.59 *	* -0.57 *	* -0.78 *	* -0.81 *	* -0.09	* 0.61 *	* 0.10	* -0.65 *	* 0.22	* 0.85 *	* 0.53 *	* -0.76 *	* -0.67	
m4	* -0.04	* 0.49 *	* 0.47 *	* 0.72 *	* 0.74 *	* 0.04	* -0.49 *	* 0.50 *	* 0.01	* 0.60 *	* -0.09	* -0.84 *	* -0.41 *	* 0.68 *	* 0.58
e1	* -0.74 *	* -0.72 *	* -0.70 *	* -0.57 *	* -0.61 *	* -0.21	* 0.88 *	* -0.72 *	* 0.81 *	* -0.42 *	* 0.85 *	* 0.29 *	* 0.86 *	* -0.67 *	* -0.72
e2	* -0.12	* -0.59 *	* -0.74 *	* -0.72 *	* -0.74 *	* 0.16	* 0.70 *	* -0.61 *	* -0.12	* -0.59 *	* 0.19	* 0.58 *	* 0.62 *	* -0.48 *	* -0.48
e3	* 1.00 *	* 0.45 *	* 0.50 *	* 0.15	* 0.22	* 0.44 *	* -0.67 *	* 0.42 *	* -0.74 *	* 0.00	* -0.88 *	* 0.00	* -0.74 *	* 0.43 *	* 0.48
e4	* 0.45 *	* 1.00 *	* 0.84 *	* 0.75 *	* 0.78 *	* 0.36 *	* -0.86 *	* 1.00 *	* -0.41 *	* 0.84 *	* -0.61 *	* -0.52 *	* -0.76 *	* 0.81 *	* 0.80
e5	* 0.50 *	* 0.84 *	* 1.00 *	* 0.69 *	* 0.71 *	* 0.32 *	* -0.91 *	* 0.83 *	* -0.27	* 0.65 *	* -0.57 *	* -0.50 *	* -0.83 *	* 0.68 *	* 0.69
e6	* 0.15	* 0.75 *	* 0.69 *	* 1.00 *	* 0.97 *	* 0.16	* -0.76 *	* 0.76 *	* -0.27	* 0.78 *	* -0.35 *	* -0.62 *	* -0.64 *	* 0.75 *	* 0.76
e7	* 0.22	* 0.78 *	* 0.71 *	* 0.97 *	* 1.00 *	* 0.17	* -0.80 *	* 0.79 *	* -0.31 *	* 0.76 *	* -0.40 *	* -0.64 *	* -0.70 *	* 0.81 *	* 0.81
e8	* 0.44 *	* 0.36 *	* 0.32 *	* 0.16	* 0.17	* 1.00 *	* -0.29 *	* 0.30 *	* -0.38 *	* 0.15	* -0.37 *	* -0.02	* -0.29 *	* 0.38 *	* 0.42
e9	* -0.67 *	* -0.86 *	* -0.91 *	* -0.76 *	* -0.80 *	* -0.29 *	* 1.00 *	* -0.86 *	* 0.55 *	* -0.61 *	* 0.76 *	* 0.47 *	* 0.94 *	* -0.78 *	* -0.81
e10	* 0.42 *	* 1.00 *	* 0.83 *	* 0.76 *	* 0.79 *	* 0.30 *	* -0.86 *	* 1.00 *	* -0.40 *	* 0.86 *	* -0.60 *	* -0.53 *	* -0.76 *	* 0.80 *	* 0.80
e11	* -0.74 *	* -0.41 *	* -0.27	* -0.27	* -0.31 *	* -0.38 *	* 0.55 *	* -0.40 *	* 1.00 *	* -0.11	* 0.81 *	* 0.00	* 0.59 *	* -0.51 *	* -0.57
e12	* 0.00	* 0.84 *	* 0.65 *	* 0.78 *	* 0.76 *	* 0.15	* -0.61 *	* 0.86 *	* -0.11	* 1.00 *	* -0.27	* -0.58 *	* -0.47 *	* 0.68 *	* 0.63
e13	* -0.88 *	* -0.61 *	* -0.57 *	* -0.35 *	* -0.40 *	* -0.37 *	* 0.76 *	* -0.60 *	* 0.81 *	* -0.27	* 1.00 *	* 0.13	* 0.80 *	* -0.60 *	* -0.62
Ita	* 0.00	* -0.52 *	* -0.50 *	* -0.62 *	* -0.64 *	* -0.02	* 0.47 *	* -0.53 *	* 0.00	* -0.58 *	* 0.13	* 1.00 *	* 0.38 *	* -0.65 *	* -0.53
DFA	* -0.74 *	* -0.76 *	* -0.83 *	* -0.64 *	* -0.70 *	* -0.29 *	* 0.94 *	* -0.76 *	* 0.59 *	* -0.47 *	* 0.80 *	* 0.38 *	* 1.00 *	* -0.72 *	* -0.77
Apen	* 0.43 *	* 0.81 *	* 0.68 *	* 0.75 *	* 0.81 *	* 0.38 *	* -0.78 *	* 0.80 *	* -0.51 *	* 0.68 *	* -0.60 *	* -0.65 *	* -0.72 *	* 1.00 *	* 0.92
CD	* 0.48 *	* 0.80 *	* 0.69 *	* 0.76 *	* 0.81 *	* 0.42 *	* -0.81 *	* 0.80 *	* -0.57 *	* 0.63 *	* -0.62 *	* -0.53 *	* -0.77 *	* 0.92 *	* 1.00
IMF1	0.24	0.09	0.20	0.14	0.16	* -0.05	* -0.29 *	* 0.10	* -0.23	0.03	* -0.21	* -0.25	* -0.35 *	* 0.19	0.15
IMF2	* -0.02	* 0.56 *	* 0.44 *	* 0.83 *	* 0.84 *	* 0.14	* -0.52 *	* 0.57 *	* -0.15	* 0.67 *	* -0.15	* -0.67 *	* -0.45 *	* 0.71 *	* 0.65
IMF3	* 0.10	* 0.66 *	* 0.64 *	* 0.89 *	* 0.91 *	* 0.13	* -0.68 *	* 0.68 *	* -0.14	* 0.72 *	* -0.25	* -0.73 *	* -0.60 *	* 0.75 *	* 0.69
IMF4	* 0.19	* 0.64 *	* 0.61 *	* 0.83 *	* 0.86 *	* 0.11	* -0.68 *	* 0.65 *	* -0.22	* 0.65 *	* -0.32 *	* -0.70 *	* -0.65 *	* 0.72 *	* 0.69
IMF5	* 0.14	* 0.53 *	* 0.47 *	* 0.77 *	* 0.80 *	* 0.13	* -0.57 *	* 0.54 *	* -0.23	* 0.53 *	* -0.24	* -0.63 *	* -0.54 *	* 0.66 *	* 0.66
IMF6	* 0.16	* 0.55 *	* 0.50 *	* 0.74 *	* 0.78 *	* 0.15	* -0.57 *	* 0.56 *	* -0.21	* 0.56 *	* -0.27	* -0.71 *	* -0.57 *	* 0.70 *	* 0.66
APEN	0.27	0.11	0.05	0.02	0.02	0.20	* -0.12	0.10	* -0.29 *	* -0.05	* -0.22	0.13	* -0.12	0.13	0.25
CD	0.17	0.00	* -0.02	* -0.14	* -0.12	0.16	0.03	* -0.02	* -0.14	* -0.16	* -0.12	0.22	0.00	* -0.04	0.08
DFA	0.08	0.08	0.10	0.31 *	0.31 *	0.01	* -0.21	0.10	* -0.21	0.15	* -0.13	* -0.29 *	* -0.21	0.26	0.25
LFA	* -0.15	* -0.19	* -0.13	* -0.16	* -0.19	* -0.10	0.16	* -0.17	0.05	* -0.05	0.12	0.23	0.11	* -0.23	* -0.23
HFA	0.13	0.18	0.13	0.13	0.16	0.09	* -0.15	0.16	* -0.01	0.05	* -0.10	* -0.22	* -0.09	0.20	0.20
LFHF	* -0.17	* -0.11	* -0.09	* -0.01	* -0.04	* -0.09	0.10	* -0.09	0.04	0.08	0.10	0.04	0.06	* -0.10	* -0.14
MeanRR	* 0.23	* -0.08	* -0.15	* -0.33 *	* -0.29 *	* 0.09	0.08	* -0.07	* -0.16	* -0.12	* -0.25	* 0.36 *	* 0.03	* -0.09	* -0.11
SRDRR	* -0.12	* -0.01	* -0.01	* 0.01	0.00	* -0.04	0.04	0.00	0.13	0.16	0.07	* -0.12	0.03	* -0.06	* -0.17

*p<0.01

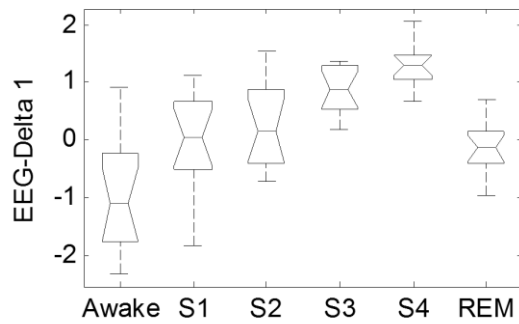
Table A5.3 Correlation matrix part 3 out of 3

	IMF1	IMF2	IMF3	IMF4	IMF5	IMF6	APEN	CD	DFA	LFA	HFA	LFHF	MeanRR	SRDRR
fd1	* -0.14	-0.49 *	* -0.63 *	* -0.64 *	* -0.53 *	* -0.51 *	-0.18	-0.06	-0.18	0.10	-0.07	0.04	0.01	0.05
fd2	0.04	-0.29 *	* -0.27	-0.20	-0.18	-0.22	0.35 *	0.32 *	-0.01	0.03	-0.05	-0.04	0.32 *	-0.20
ft1	* 0.06	-0.05	0.08	0.13	0.09	0.06	0.31 *	0.25	0.01	0.00	-0.03	-0.02	0.24	-0.15
ft2	* 0.04	0.09	0.29 *	0.32 *	0.21	0.21	0.21	0.15	-0.02	-0.05	0.04	-0.04	0.14	-0.08
fal	* 0.03	0.27	0.48 *	0.47 *	0.32 *	0.35 *	0.11	0.08	-0.02	-0.10	0.10	-0.07	0.01	-0.01
fb1	* 0.15	0.72 *	0.82 *	0.78 *	0.69 *	0.68 *	0.06	-0.06	0.22	-0.17	0.14	-0.06	-0.16	0.00
fb2	* 0.14	0.91 *	0.92 *	0.88 *	0.86 *	0.80 *	-0.07	-0.20	0.41 *	-0.08	0.05	0.13	-0.31 *	0.11
fc	* 0.28 *	0.75 *	0.89 *	0.87 *	0.76 *	0.77 *	-0.03	-0.14	0.32 *	-0.12	0.10	0.03	-0.22	0.09
fs	* 0.25	0.90 *	0.96 *	0.93 *	0.86 *	0.86 *	-0.11	-0.23	0.44 *	-0.08	0.05	0.14	-0.25	0.18
vfc	* -0.31 *	-0.47 *	-0.54 *	-0.56 *	-0.44 *	-0.52 *	-0.05	0.07	-0.21	0.09	-0.07	0.01	-0.08	-0.05
m0	* -0.21	-0.09	-0.11	-0.15	-0.08	-0.10	-0.26	-0.18	-0.07	0.13	-0.11	0.13	-0.30 *	0.18
m2	* -0.27	-0.88 *	-0.91 *	-0.88 *	-0.81 *	-0.88 *	0.11	0.28	-0.40 *	0.18	-0.16	-0.01	0.33 *	-0.16
m4	* 0.24	0.87 *	0.87 *	0.83 *	0.78 *	0.84 *	-0.13	-0.29 *	0.41 *	-0.16	0.15	0.03	-0.36 *	0.17
e1	* -0.30 *	-0.32 *	-0.44 *	-0.48 *	-0.40 *	-0.39 *	-0.21	-0.05	-0.22	0.08	-0.05	0.05	-0.03	0.11
e2	* -0.23	-0.57 *	-0.74 *	-0.71 *	-0.58 *	-0.59 *	0.15	0.23	-0.16	0.11	-0.11	0.01	0.29 *	-0.12
e3	* 0.24	-0.02	0.10	0.19	0.14	0.16	0.27	0.17	0.08	-0.15	0.13	-0.17	0.23	-0.12
e4	* 0.09	0.56 *	0.66 *	0.64 *	0.53 *	0.55 *	0.11	0.00	0.08	-0.19	0.18	-0.11	-0.08	-0.01
e5	* 0.20	0.44 *	0.64 *	0.61 *	0.47 *	0.50 *	0.05	-0.02	0.10	-0.13	0.13	-0.09	-0.15	-0.01
e6	* 0.14	0.83 *	0.89 *	0.83 *	0.77 *	0.74 *	0.02	-0.14	0.31 *	-0.16	0.13	-0.01	-0.33 *	0.01
e7	* 0.16	0.84 *	0.91 *	0.86 *	0.80 *	0.78 *	0.02	-0.12	0.31 *	-0.19	0.16	-0.04	-0.29 *	0.00
e8	* -0.05	0.14	0.13	0.11	0.13	0.15	0.20	0.16	0.01	-0.10	0.09	-0.09	0.09	-0.04
e9	* -0.29 *	-0.52 *	-0.68 *	-0.68 *	-0.57 *	-0.57 *	-0.12	0.03	-0.21	0.16	-0.15	0.10	0.08	0.04
e10	* 0.10	0.57 *	0.68 *	0.65 *	0.54 *	0.56 *	0.10	-0.02	0.10	-0.17	0.16	-0.09	-0.07	0.00
e11	* -0.23	-0.15	-0.14	-0.22	-0.23	-0.21	-0.29 *	-0.14	-0.21	0.05	-0.01	0.04	-0.16	0.13
e12	* 0.03	0.67 *	0.72 *	0.65 *	0.53 *	0.56 *	-0.05	-0.16	0.15	-0.05	0.05	0.08	-0.12	0.16
e13	* -0.21	-0.15	-0.25	-0.32 *	-0.24	-0.27	-0.22	-0.12	-0.13	0.12	-0.10	0.10	-0.25	0.07
Ita	* -0.25	-0.67 *	-0.73 *	-0.70 *	-0.63 *	-0.71 *	0.13	0.22	-0.29 *	0.23	-0.22	0.04	0.36 *	-0.12
DFA	* -0.35 *	-0.45 *	-0.60 *	-0.65 *	-0.54 *	-0.57 *	-0.12	0.00	-0.21	0.11	-0.09	0.06	0.03	0.03
Apen	* 0.19	0.71 *	0.75 *	0.72 *	0.66 *	0.70 *	0.13	-0.04	0.26	-0.23	0.20	-0.10	-0.09	-0.06
CD	* 0.15	0.65 *	0.69 *	0.69 *	0.66 *	0.66 *	0.25	0.08	0.25	-0.23	0.20	-0.14	-0.11	-0.17
IMF1	1.00 *	0.19	0.25	0.33 *	0.25	0.30 *	-0.11	-0.22	0.45 *	0.06	-0.06	0.15	-0.15	0.13
IMF2	* 0.19	1.00 *	0.93 *	0.89 *	0.88 *	0.85 *	-0.06	-0.19	0.37 *	-0.16	0.13	0.06	-0.32 *	0.13
IMF3	* 0.25	0.93 *	1.00 *	0.96 *	0.89 *	0.89 *	-0.12	-0.22	0.36 *	-0.11	0.09	0.12	-0.32 *	0.19
IMF4	* 0.33 *	0.89 *	0.96 *	1.00 *	0.93 *	0.92 *	-0.15	-0.23	0.41 *	-0.08	0.06	0.17	-0.31 *	0.26
IMF5	* 0.25	0.88 *	0.89 *	0.93 *	1.00 *	0.92 *	-0.12	-0.17	0.41 *	-0.14	0.10	0.11	-0.32 *	0.20
IMF6	* 0.30 *	0.85 *	0.89 *	0.92 *	0.92 *	1.00 *	-0.17	-0.25	0.42 *	-0.12	0.10	0.10	-0.31 *	0.22
APEN	-0.11	-0.06	-0.12	-0.15	-0.12	-0.17	1.00 *	0.79 *	-0.02	-0.21	0.19	-0.35 *	0.16	-0.63
CD	-0.22	-0.19	-0.22	-0.23	-0.17	-0.25	0.79 *	1.00 *	-0.15	-0.25	0.24	-0.32 *	0.13	-0.58
DFA	0.45 *	0.37 *	0.36 *	0.41 *	0.41 *	0.42 *	-0.02	-0.15	1.00 *	0.21	-0.22	0.31 *	-0.26	0.01
LFA	0.06	-0.16	-0.11	-0.08	-0.14	-0.12	-0.21	-0.25	0.21	1.00 *	-1.00 *	0.88 *	0.29 *	0.47
HFA	-0.06	0.13	0.09	0.06	0.10	0.10	0.19	0.24	-0.22	-1.00 *	1.00 *	-0.88 *	-0.29 *	-0.46
LFHF	0.15	0.06	0.12	0.17	0.11	0.10	-0.35 *	-0.32 *	0.31 *	0.88 *	-0.88 *	1.00 *	0.19	0.63
MeanRR	-0.15	-0.32 *	-0.32 *	-0.31 *	-0.32 *	-0.31 *	0.16	0.13	-0.26	0.29 *	-0.29 *	0.19	1.00 *	0.21
SRDRR	0.13	0.13	0.19	0.26	0.20	0.22	-0.63 *	-0.58 *	0.01	0.47 *	-0.46 *	0.63 *	0.21	1.00

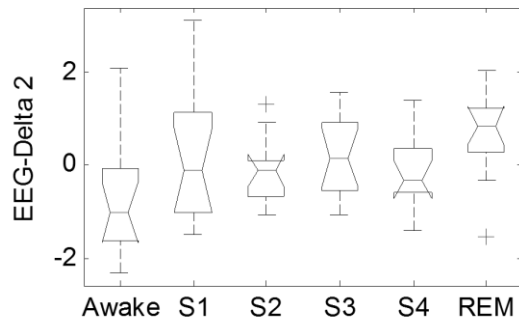
*p<0.01

Appendix 6. EEG and HRV ANOVA-one way analysis from Power Analysis

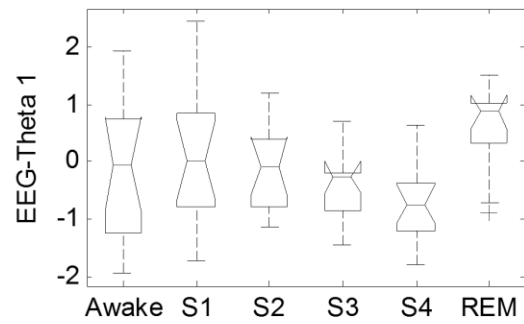
The power analysis and statistical differences for EEG and HRV features are presented in this section. Each boxplot (left side) displays the samples taken from the total population and the feature under analysis is labeled on the vertical axis, the one-way ANOVA table (right side) exhibits statistical differences among sleep stages for each feature ($p < 0.01$).



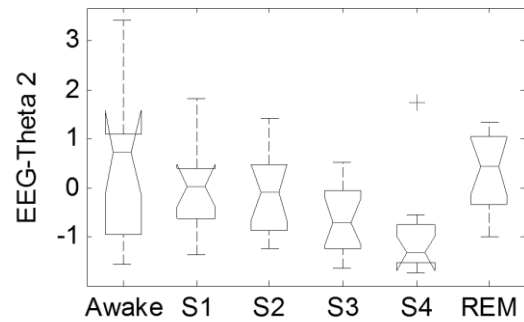
ANOVA Table					
Source	SS	df	MS	F	Prob>F
Groups	42.173	5	8.4346	16.94	2.63037e-011
Error	38.8338	78	0.49787		
Total	81.0068	83			



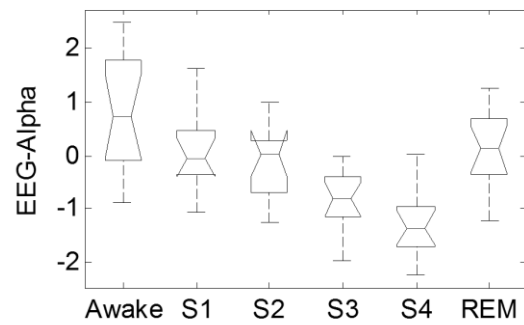
ANOVA Table					
Source	SS	df	MS	F	Prob>F
Groups	14.1676	5	2.83352	2.78	0.0231
Error	79.4842	78	1.01903		
Total	93.6518	83			



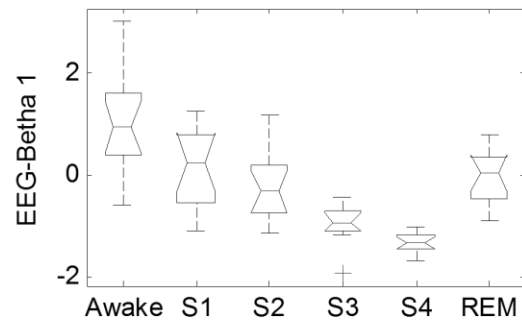
ANOVA Table					
Source	SS	df	MS	F	Prob>F
Groups	15.1659	5	3.03318	3.52	0.0064
Error	67.2451	78	0.86212		
Total	82.411	83			



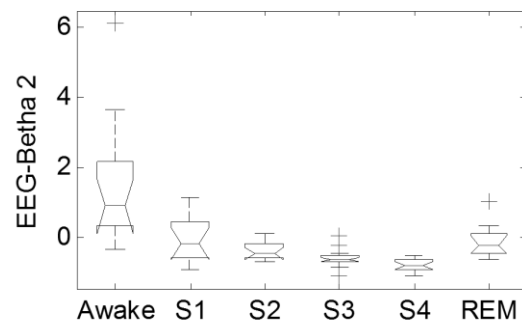
ANOVA Table					
Source	SS	df	MS	F	Prob>F
Groups	22.0837	5	4.41674	4.82	0.0007
Error	71.4337	78	0.91582		
Total	93.5174	83			



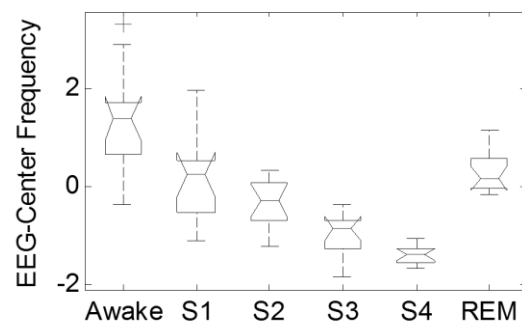
ANOVA Table					
Source	SS	df	MS	F	Prob>F
Groups	36.8021	5	7.36042	12.53	6.15505e-009
Error	45.8077	78	0.58728		
Total	82.6098	83			



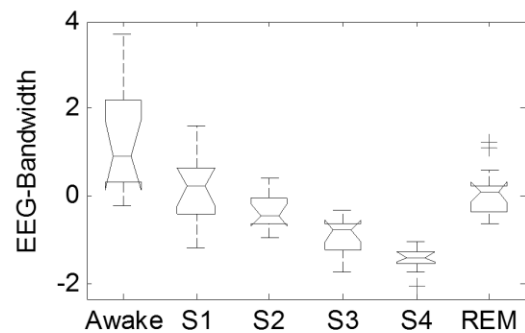
ANOVA Table					
Source	SS	df	MS	F	Prob>F
Groups	50.8014	5	10.1603	25.91	2.55351e-015
Error	30.5869	78	0.3921		
Total	81.3883	83			



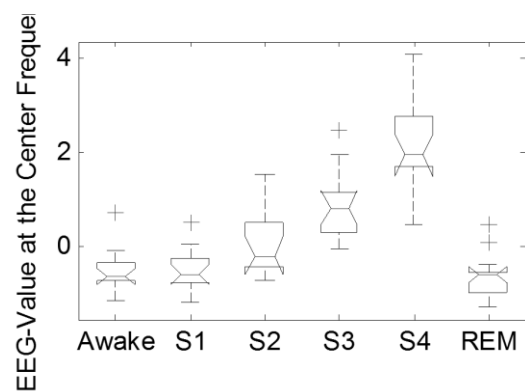
ANOVA Table					
Source	SS	df	MS	F	Prob>F
Groups	44.4317	5	8.88635	13.66	1.41657e-009
Error	50.731	78	0.6504		
Total	95.1627	83			



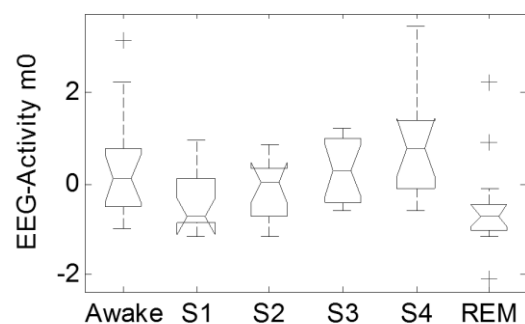
ANOVA Table					
Source	SS	df	MS	F	Prob>F
Groups	65.3295	5	13.0659	32.5	0
Error	31.3566	78	0.402		
Total	96.6861	83			



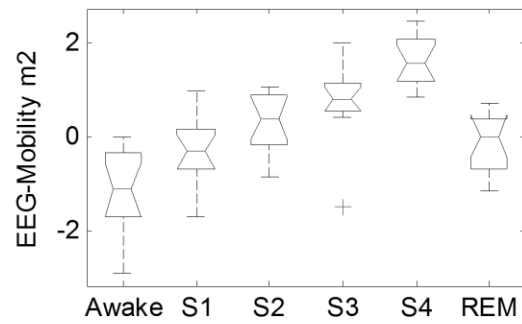
ANOVA Table					
Source	SS	df	MS	F	Prob>F
Groups	61.2298	5	12.246	29.06	1.11022e-016
Error	32.8667	78	0.4214		
Total	94.0965	83			



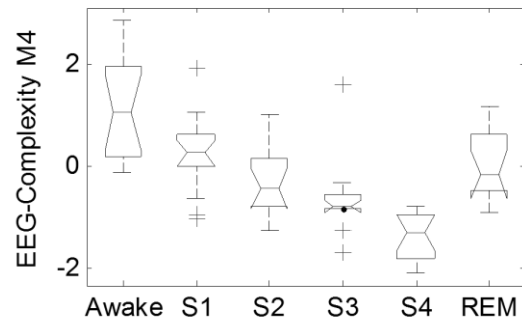
ANOVA Table					
Source	SS	df	MS	F	Prob>F
Groups	83.301	5	16.6601	37.13	0
Error	35.002	78	0.4487		
Total	118.302	83			



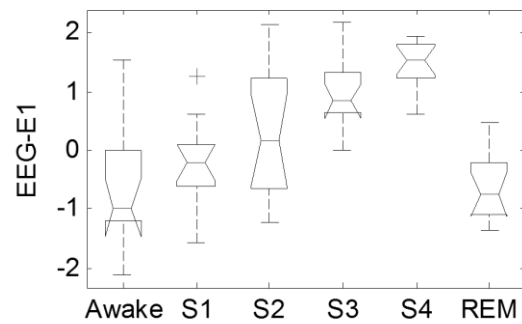
ANOVA Table					
Source	SS	df	MS	F	Prob>F
Groups	21.3494	5	4.26988	4.83	0.0007
Error	68.9652	78	0.88417		
Total	90.3146	83			



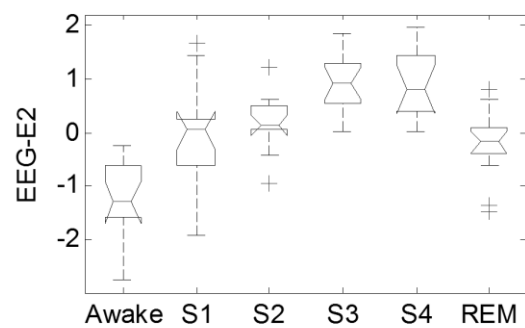
ANOVA Table					
Source	SS	df	MS	F	Prob>F
Groups	61.3364	5	12.2673	25.15	5.21805e-015
Error	38.0485	78	0.4878		
Total	99.385	83			



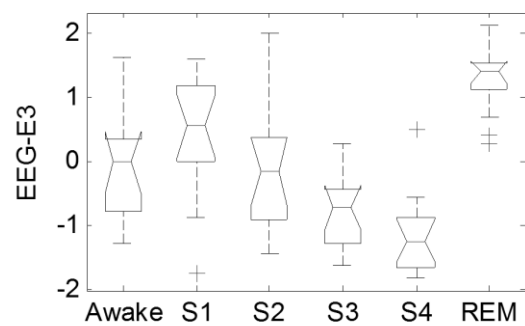
ANOVA Table					
Source	SS	df	MS	F	Prob>F
Groups	49.0558	5	9.81115	18.32	5.47684e-012
Error	41.7651	78	0.53545		
Total	90.8209	83			



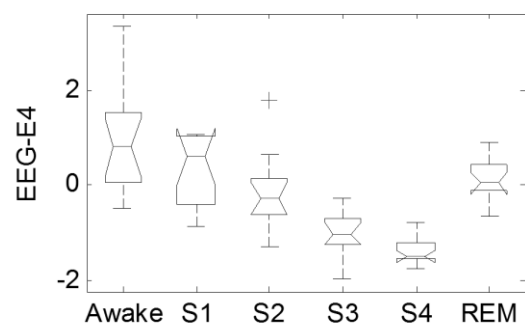
ANOVA Table					
Source	SS	df	MS	F	Prob>F
Groups	53.082	5	10.6164	17.98	8.03813e-012
Error	46.0547	78	0.5904		
Total	99.1366	83			



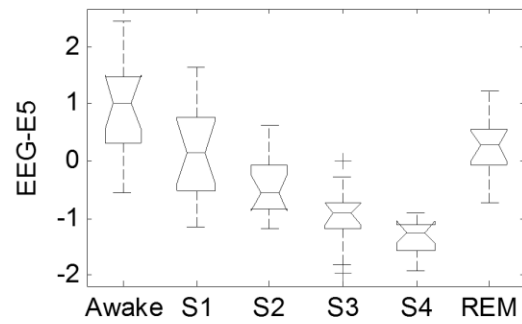
ANOVA Table					
Source	SS	df	MS	F	Prob>F
Groups	46.5452	5	9.30904	19.71	1.20703e-012
Error	36.8449	78	0.47237		
Total	83.3901	83			



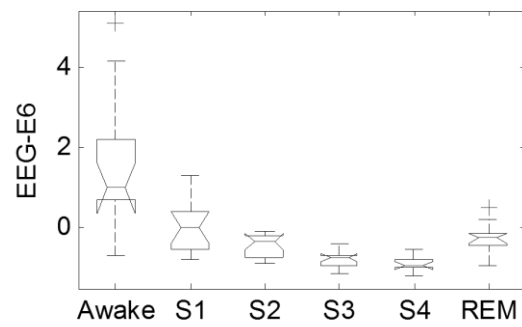
ANOVA Table					
Source	SS	df	MS	F	Prob>F
Groups	54.393	5	10.8786	16.67	3.62722e-011
Error	50.917	78	0.6528		
Total	105.309	83			



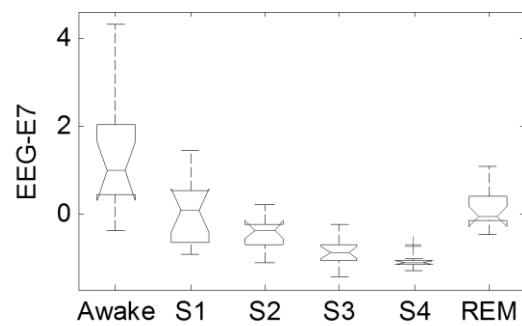
ANOVA Table					
Source	SS	df	MS	F	Prob>F
Groups	52.771	5	10.5542	24.14	1.35447e-014
Error	34.1088	78	0.4373		
Total	86.8798	83			



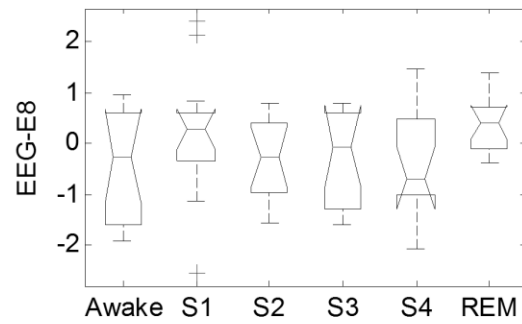
ANOVA Table					
Source	SS	df	MS	F	Prob>F
Groups	50.0354	5	10.0071	24.45	1.0103e-014
Error	31.928	78	0.4093		
Total	81.9634	83			



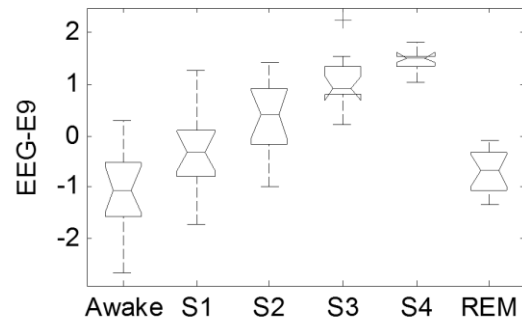
ANOVA Table					
Source	SS	df	MS	F	Prob>F
Groups	48.0657	5	9.61314	17.22	1.9046e-011
Error	43.5406	78	0.55821		
Total	91.6063	83			



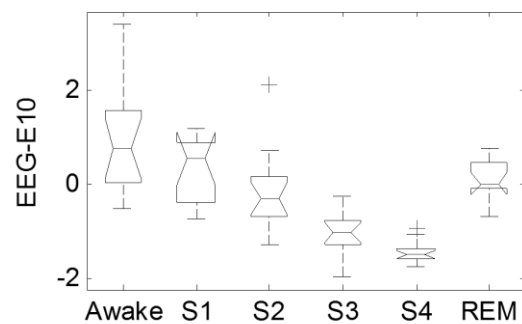
ANOVA Table					
Source	SS	df	MS	F	Prob>F
Groups	50.2757	5	10.0551	20.65	4.442e-013
Error	37.9788	78	0.4869		
Total	88.2545	83			



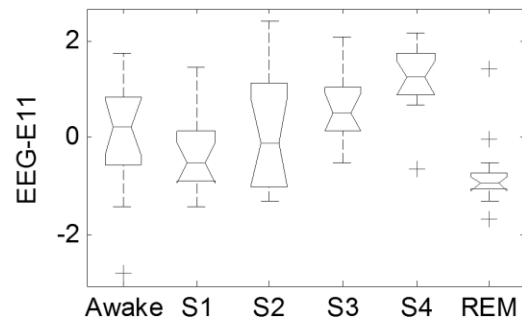
ANOVA Table					
Source	SS	df	MS	F	Prob>F
Groups	7.137	5	1.42739	1.52	0.1932
Error	73.243	78	0.93901		
Total	80.3799	83			



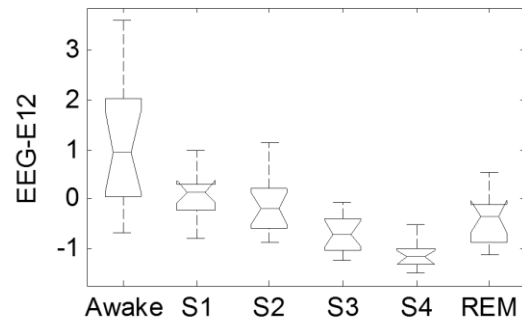
ANOVA Table					
Source	SS	df	MS	F	Prob>F
Groups	67.841	5	13.5682	32.17	0
Error	32.901	78	0.4218		
Total	100.742	83			



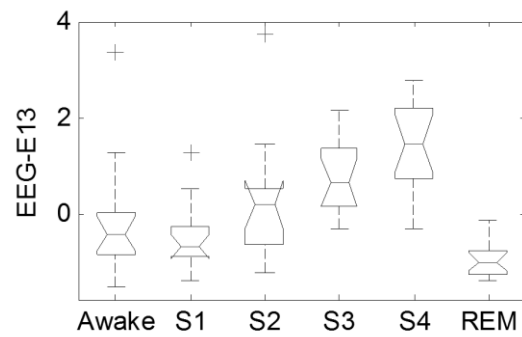
ANOVA Table					
Source	SS	df	MS	F	Prob>F
Groups	55.339	5	11.0678	23.98	1.57652e-014
Error	35.9947	78	0.4615		
Total	91.3338	83			



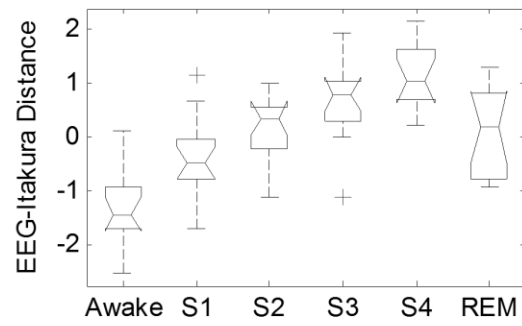
ANOVA Table					
Source	SS	df	MS	F	Prob>F
Groups	35.1205	5	7.0241	8.45	2.00364e-006
Error	64.8571	78	0.8315		
Total	99.9776	83			



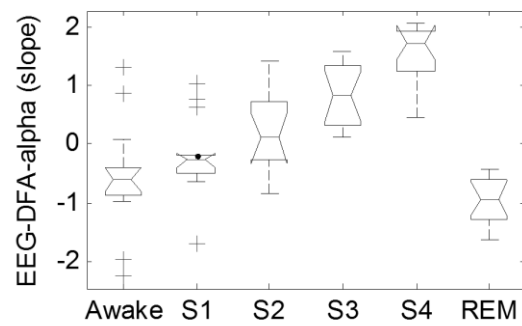
ANOVA Table					
Source	SS	df	MS	F	Prob>F
Groups	42.3985	5	8.4797	17.67	1.14302e-011
Error	37.4346	78	0.47993		
Total	79.833	83			



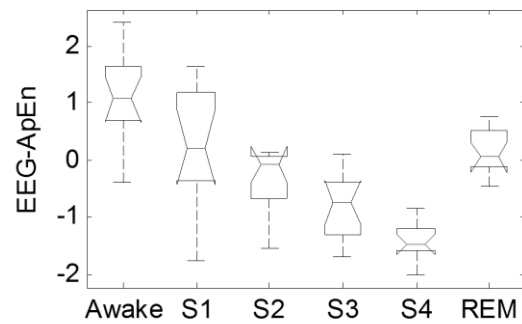
ANOVA Table					
Source	SS	df	MS	F	Prob>F
Groups	52.769	5	10.5538	12.41	7.29354e-009
Error	66.359	78	0.8508		
Total	119.128	83			



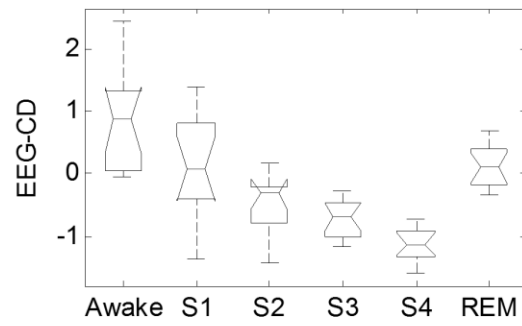
ANOVA Table					
Source	SS	df	MS	F	Prob>F
Groups	51.7741	5	10.3548	20.51	5.14366e-013
Error	39.3778	78	0.5048		
Total	91.152	83			



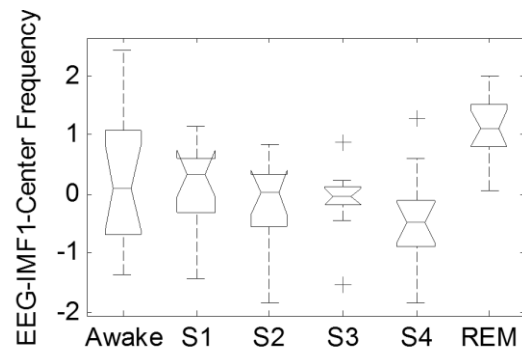
ANOVA Table					
Source	SS	df	MS	F	Prob>F
Groups	63.5459	5	12.7092	29.02	1.11022e-016
Error	34.1639	78	0.438		
Total	97.7098	83			



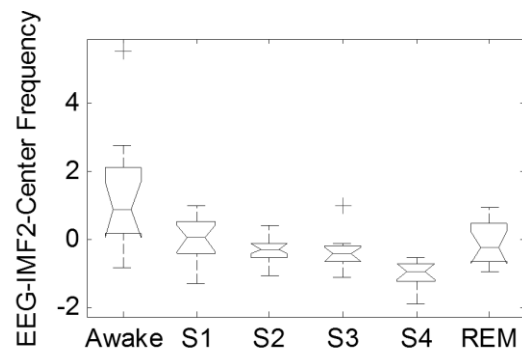
ANOVA Table					
Source	SS	df	MS	F	Prob>F
Groups	57.1601	5	11.432	27.66	5.55112e-016
Error	32.2321	78	0.4132		
Total	89.3922	83			



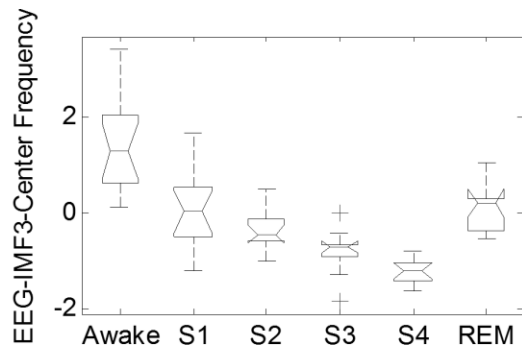
ANOVA Table					
Source	SS	df	MS	F	Prob>F
Groups	39.1057	5	7.82114	24.07	1.44329e-014
Error	25.3447	78	0.32493		
Total	64.4504	83			



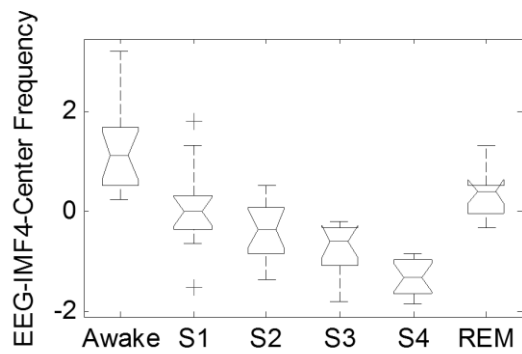
ANOVA Table					
Source	SS	df	MS	F	Prob>F
Groups	21.0265	5	4.2053	7.14	1.50815e-005
Error	45.9169	78	0.58868		
Total	66.9434	83			



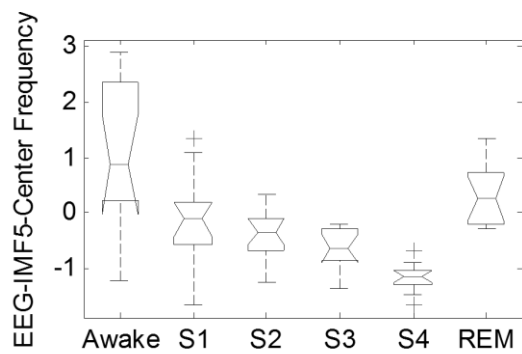
ANOVA Table					
Source	SS	df	MS	F	Prob>F
Groups	40.0299	5	8.00599	11.59	2.1781e-008
Error	53.8677	78	0.69061		
Total	93.8976	83			



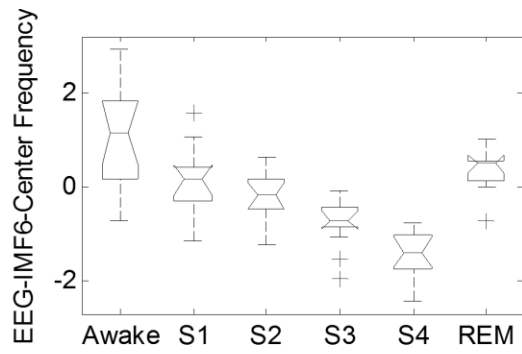
ANOVA Table					
Source	SS	df	MS	F	Prob>F
Groups	59.5866	5	11.9173	31.57	0
Error	29.4414	78	0.3775		
Total	89.028	83			



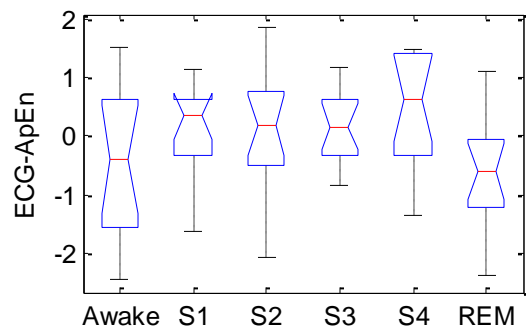
ANOVA Table					
Source	SS	df	MS	F	Prob>F
Groups	59.4792	5	11.8958	29.59	1.11022e-016
Error	31.3586	78	0.402		
Total	90.8377	83			



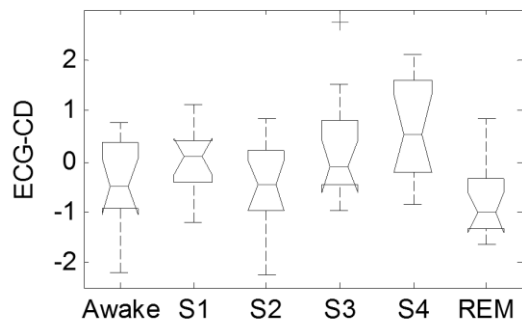
ANOVA Table					
Source	SS	df	MS	F	Prob>F
Groups	41.4947	5	8.29893	16.24	5.96625e-011
Error	39.8562	78	0.51098		
Total	81.3509	83			



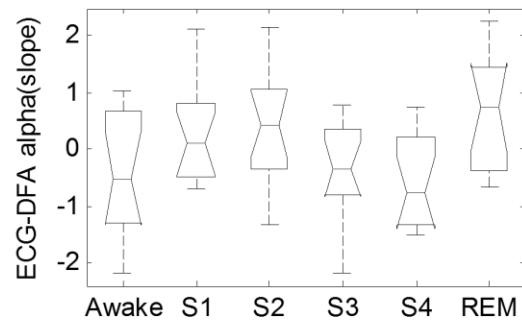
ANOVA Table					
Source	SS	df	MS	F	Prob>F
Groups	51.3667	5	10.2733	23.25	3.20854e-014
Error	34.4707	78	0.4419		
Total	85.8374	83			



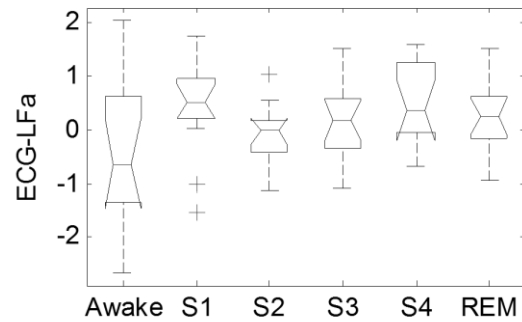
ANOVA Table					
Source	SS	df	MS	F	Prob>F
Groups	11.4095	5	2.28191	2.42	0.0426
Error	73.4069	78	0.94111		
Total	84.8164	83			



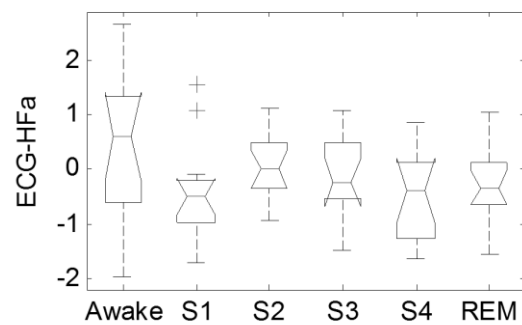
ANOVA Table					
Source	SS	df	MS	F	Prob>F
Groups	18.8577	5	3.77153	5.01	0.0005
Error	58.7335	78	0.75299		
Total	77.5912	83			



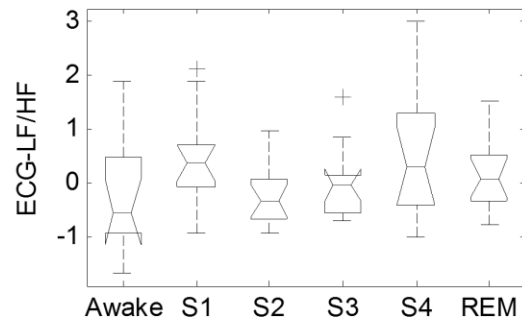
ANOVA Table					
Source	SS	df	MS	F	Prob>F
Groups	17.2288	5	3.44576	3.85	0.0036
Error	69.7239	78	0.8939		
Total	86.9527	83			



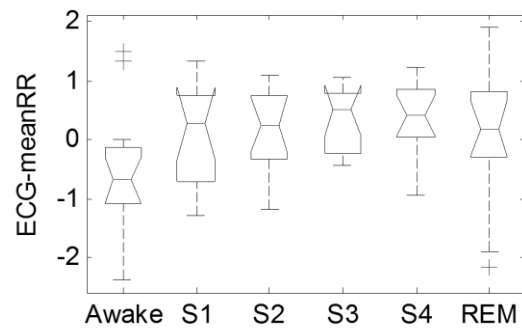
ANOVA Table					
Source	SS	df	MS	F	Prob>F
Groups	9.4138	5	1.88276	2.66	0.0285
Error	55.2273	78	0.70804		
Total	64.6411	83			



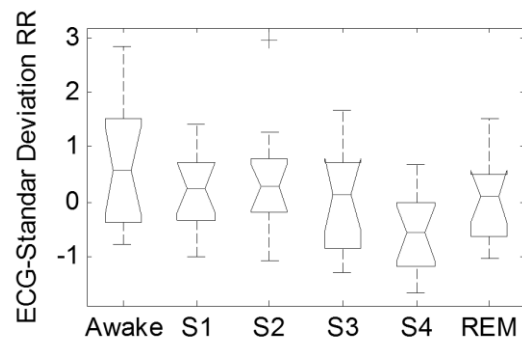
ANOVA Table					
Source	SS	df	MS	F	Prob>F
Groups	9.003	5	1.80061	2.49	0.0378
Error	56.2923	78	0.7217		
Total	65.2954	83			



ANOVA Table					
Source	SS	df	MS	F	Prob>F
Groups	7.3472	5	1.46944	2.08	0.0764
Error	55.0265	78	0.70547		
Total	62.3737	83			



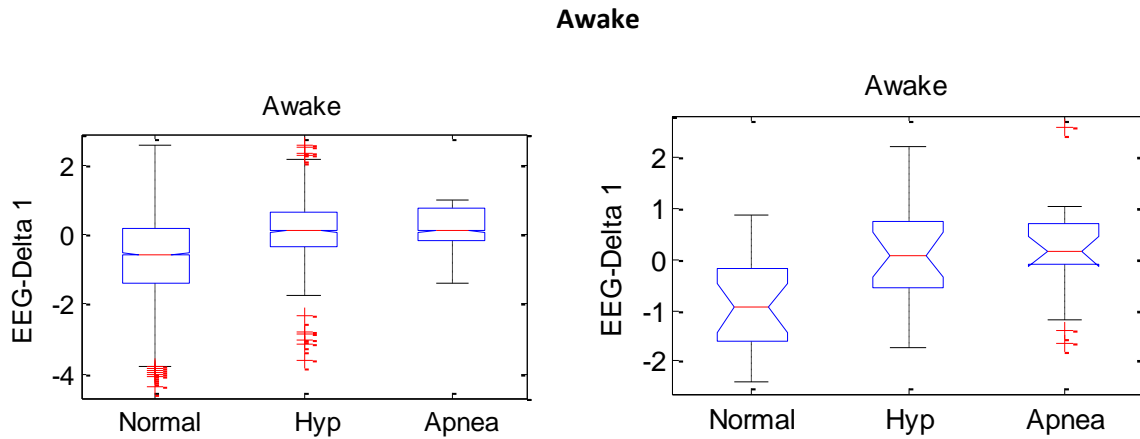
ANOVA Table					
Source	SS	df	MS	F	Prob>F
Groups	7.2498	5	1.44997	2.07	0.0785
Error	54.7203	78	0.70154		
Total	61.9701	83			



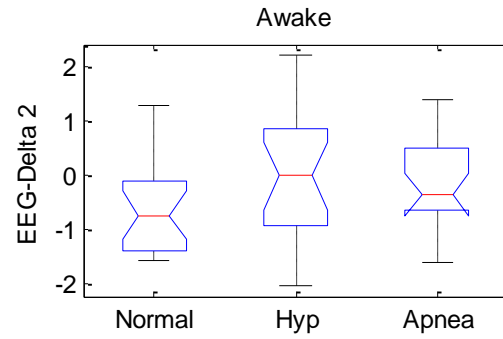
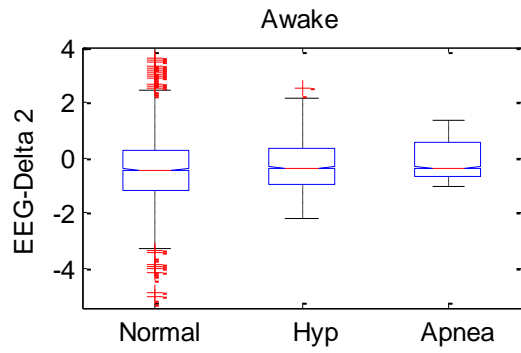
ANOVA Table					
Source	SS	df	MS	F	Prob>F
Groups	13.4375	5	2.6875	3.29	0.0094
Error	63.6361	78	0.81585		
Total	77.0736	83			

Appendix 7. Features Vs. Respiratory Events

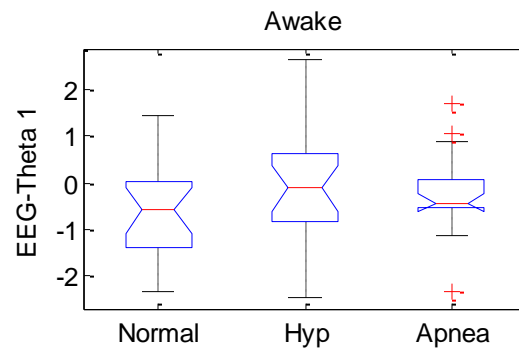
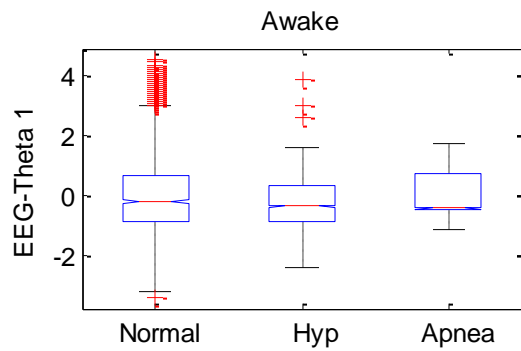
The power analysis and statistical differences for EEG and HRV features with different breathing conditions are presented in this section. Two boxplots are employed in this examination, the first boxplot (left side) displays the total population whereas the second boxplot shows the samples taken from the total population. Again, the feature under analysis is labeled on the vertical axis of each boxplot and the corresponding one-way ANOVA table is presented underneath both plots.



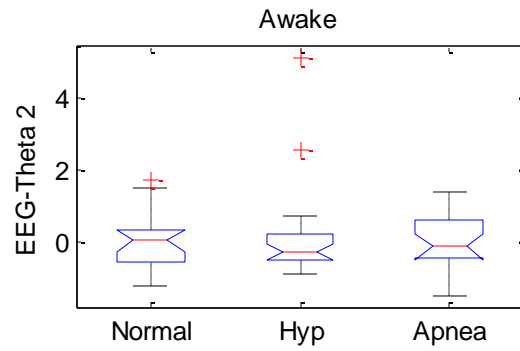
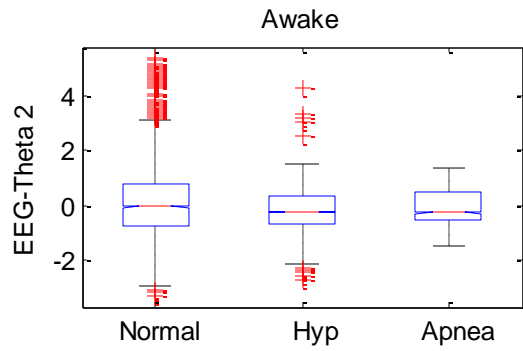
ANOVA Table					
Source	SS	df	MS	F	Prob>F
Groups	11.7549	2	5.87747	6.35	0.0033
Error	50.8811	55	0.92511		
Total	62.636	57			



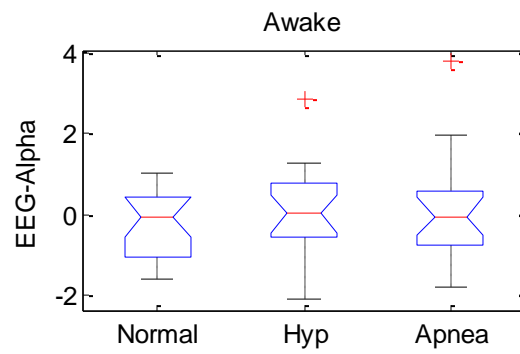
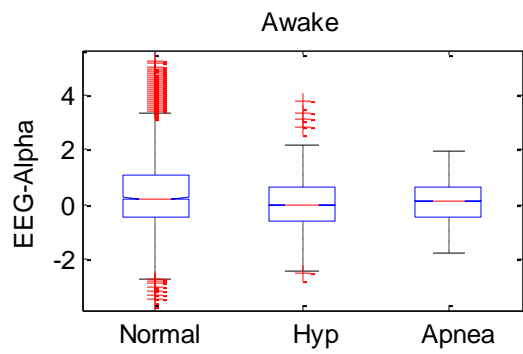
ANOVA Table					
Source	SS	df	MS	F	Prob>F
Groups	2.6367	2	1.31836	1.51	0.2299
Error	48.0132	55	0.87297		
Total	50.6499	57			



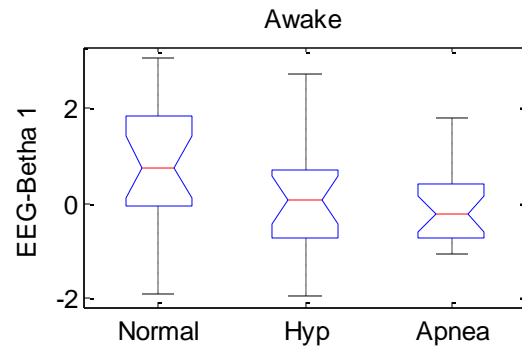
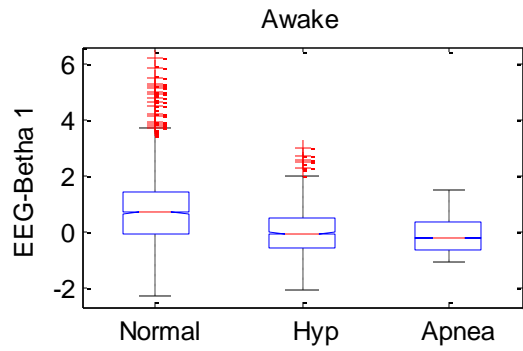
ANOVA Table					
Source	SS	df	MS	F	Prob>F
Groups	3.7777	2	1.88886	1.6	0.2103
Error	64.7495	55	1.17726		
Total	68.5273	57			



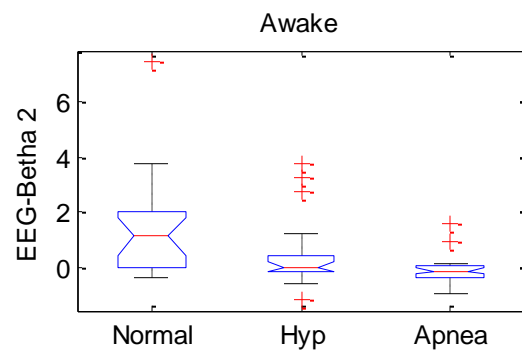
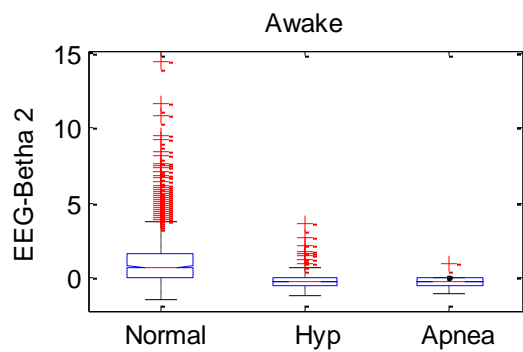
ANOVA Table					
Source	SS	df	MS	F	Prob>F
Groups	0.224	2	0.11199	0.11	0.9003
Error	58.5399	55	1.06436		
Total	58.7639	57			



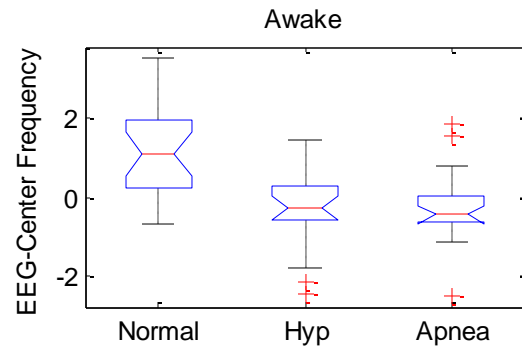
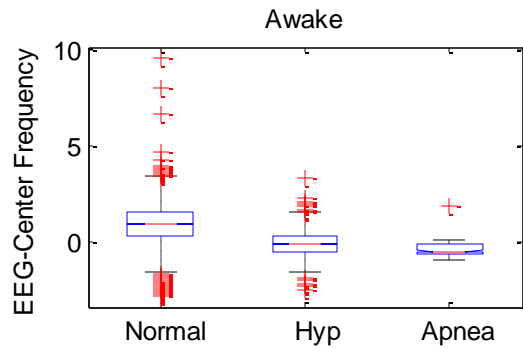
ANOVA Table					
Source	SS	df	MS	F	Prob>F
Groups	1.5463	2	0.77317	0.64	0.5288
Error	65.9683	55	1.19942		
Total	67.5146	57			



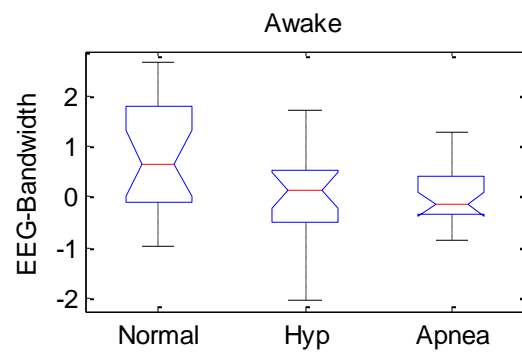
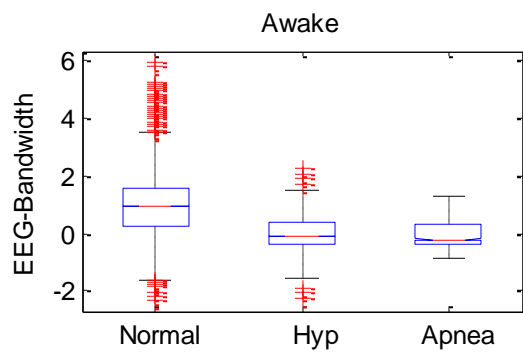
ANOVA Table					
Source	SS	df	MS	F	Prob>F
Groups	6.9279	2	3.46395	2.59	0.0843
Error	73.6216	55	1.33858		
Total	80.5496	57			



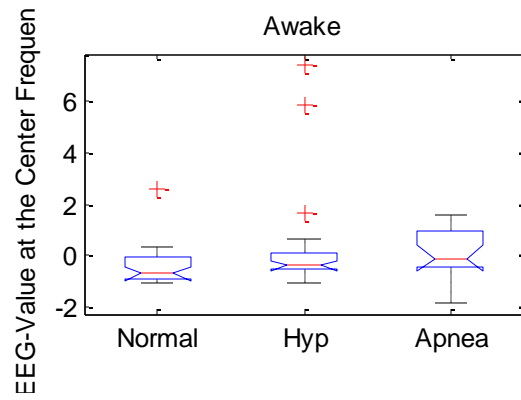
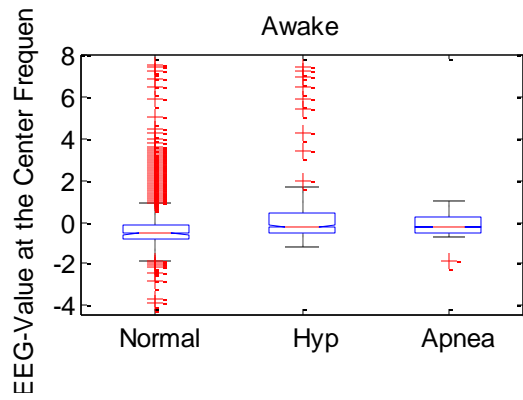
ANOVA Table					
Source	SS	df	MS	F	Prob>F
Groups	22.024	2	11.0118	6.19	0.0038
Error	97.912	55	1.7802		
Total	119.936	57			



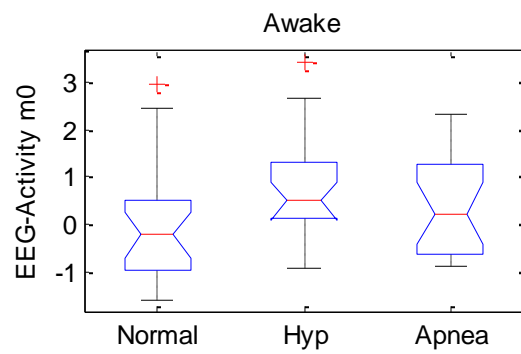
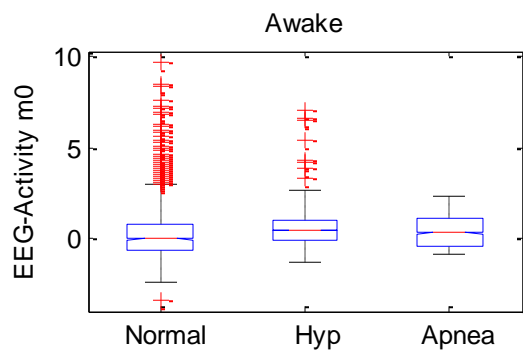
ANOVA Table					
Source	SS	df	MS	F	Prob>F
Groups	22.3349	2	11.1675	10.36	0.0002
Error	59.3141	55	1.0784		
Total	81.649	57			



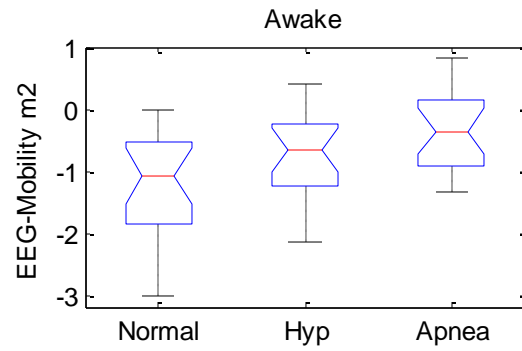
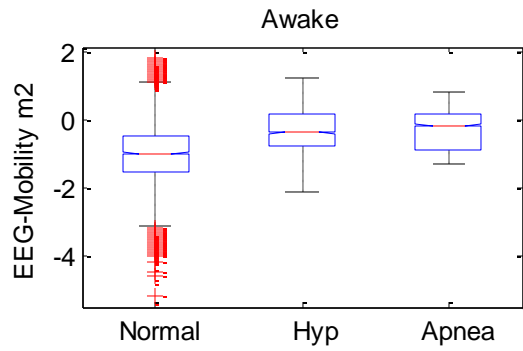
ANOVA Table					
Source	SS	df	MS	F	Prob>F
Groups	6.0098	2	3.00492	4.43	0.0165
Error	37.3244	55	0.67863		
Total	43.3343	57			



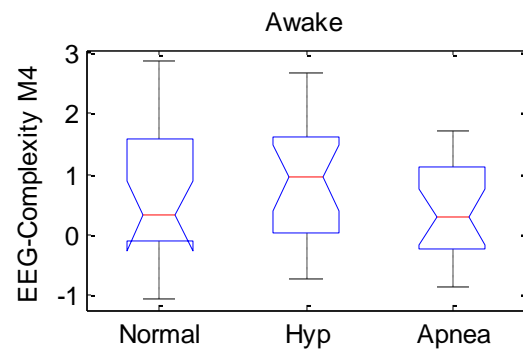
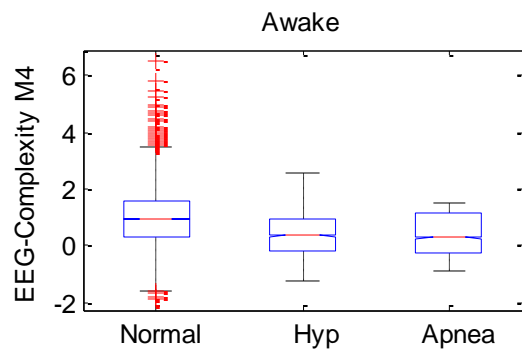
ANOVA Table					
Source	SS	df	MS	F	Prob>F
Groups	5.733	2	2.86656	1.3	0.2801
Error	121.04	55	2.20073		
Total	126.773	57			



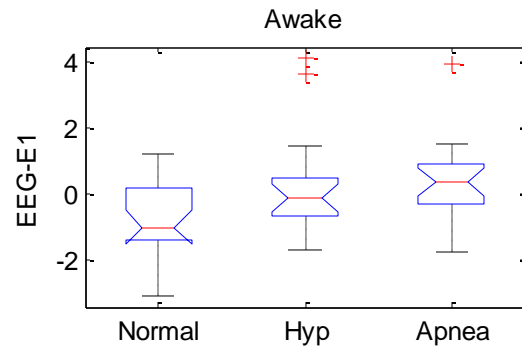
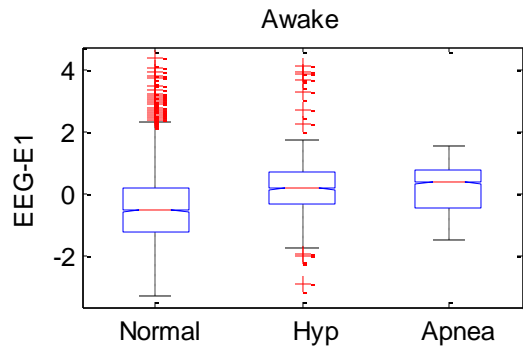
ANOVA Table					
Source	SS	df	MS	F	Prob>F
Groups	5.4603	2	2.73015	2.02	0.1421
Error	74.2481	55	1.34997		
Total	79.7084	57			



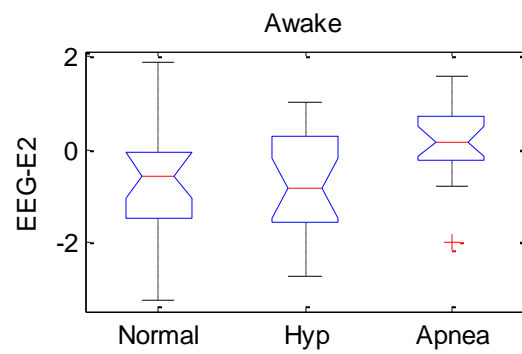
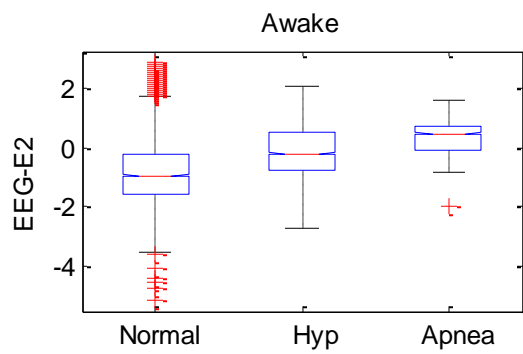
ANOVA Table					
Source	SS	df	MS	F	Prob>F
Groups	7.4538	2	3.72691	6.65	0.0026
Error	30.8349	55	0.56063		
Total	38.2887	57			



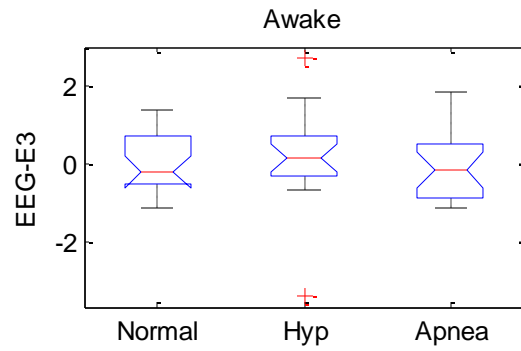
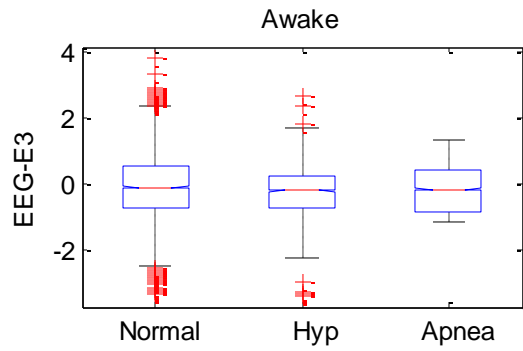
ANOVA Table					
Source	SS	df	MS	F	Prob>F
Groups	2.5184	2	1.25921	1.48	0.2375
Error	46.9297	55	0.85327		
Total	49.4481	57			



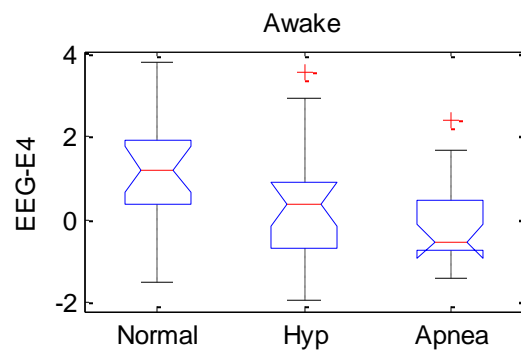
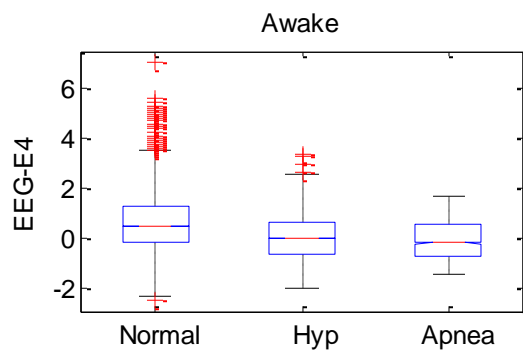
ANOVA Table					
Source	SS	df	MS	F	Prob>F
Groups	11.186	2	5.59314	3.39	0.0408
Error	90.705	55	1.64919		
Total	101.892	57			



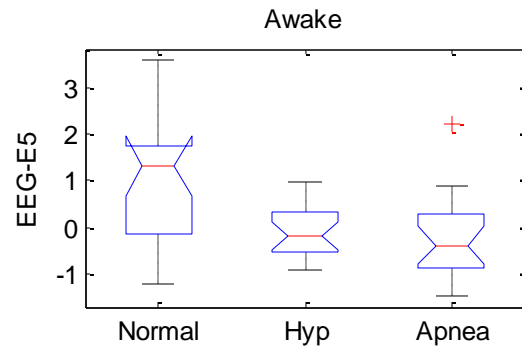
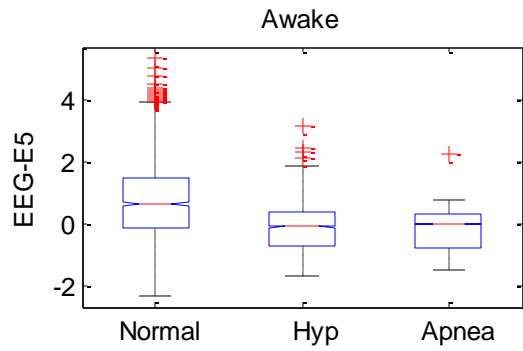
ANOVA Table					
Source	SS	df	MS	F	Prob>F
Groups	11.4485	2	5.72423	5.34	0.0076
Error	58.9566	55	1.07194		
Total	70.4051	57			



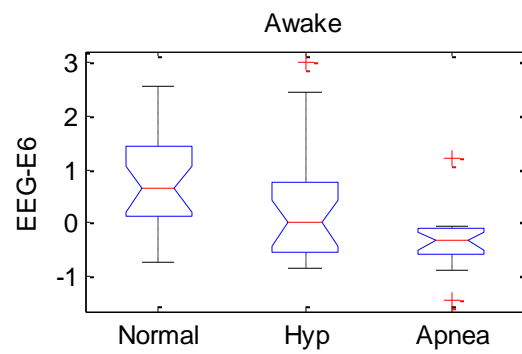
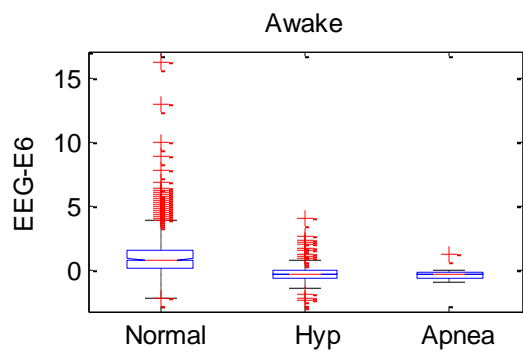
ANOVA Table					
Source	SS	df	MS	F	Prob>F
Groups	0.5418	2	0.27091	0.29	0.746
Error	50.5763	55	0.91957		
Total	51.1181	57			



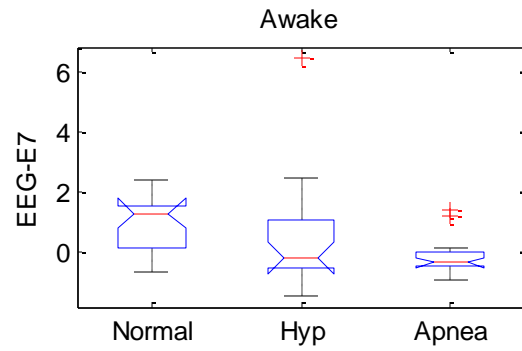
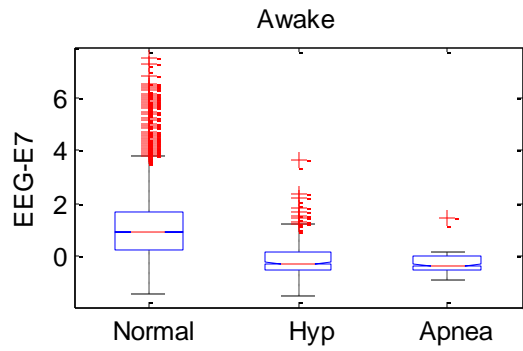
ANOVA Table					
Source	SS	df	MS	F	Prob>F
Groups	11.9364	2	5.96819	3.97	0.0245
Error	82.6474	55	1.50268		
Total	94.5838	57			



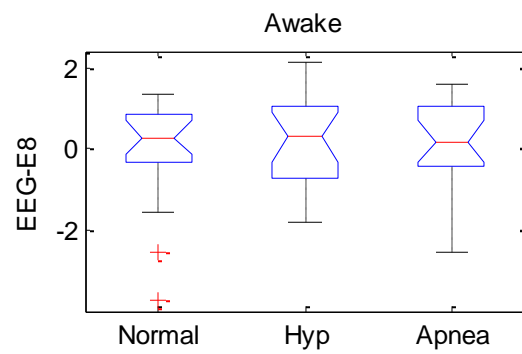
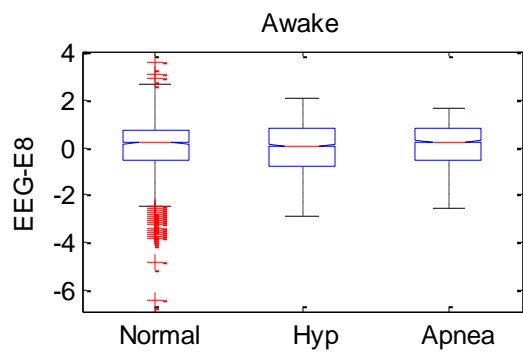
ANOVA Table					
Source	SS	df	MS	F	Prob>F
Groups	16.3724	2	8.18622	8.77	0.0005
Error	51.3119	55	0.93294		
Total	67.6843	57			



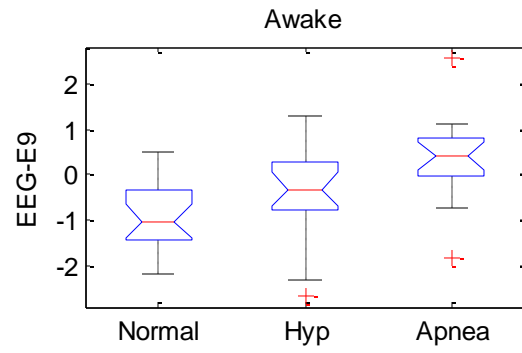
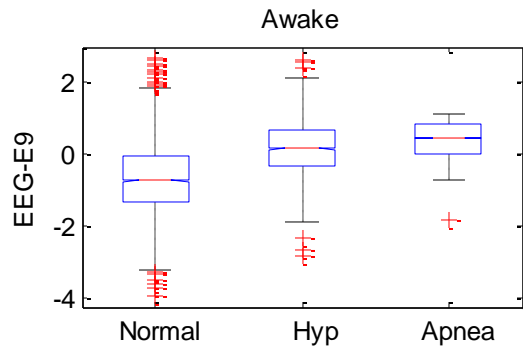
ANOVA Table					
Source	SS	df	MS	F	Prob>F
Groups	11.7728	2	5.88639	8.24	0.0007
Error	39.2819	55	0.71422		
Total	51.0547	57			



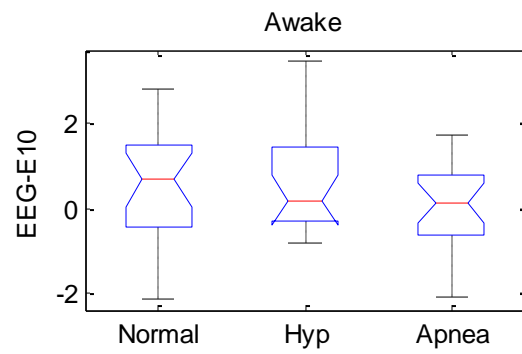
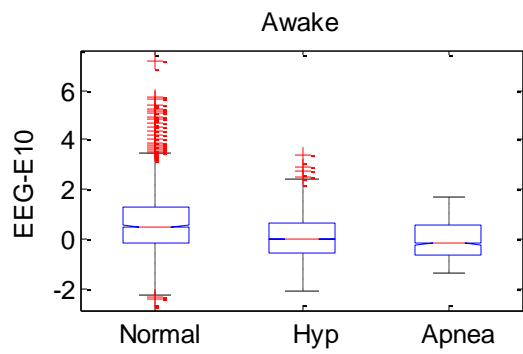
ANOVA Table					
Source	SS	df	MS	F	Prob>F
Groups	10.6283	2	5.31417	3.73	0.0303
Error	78.3545	55	1.42463		
Total	88.9828	57			



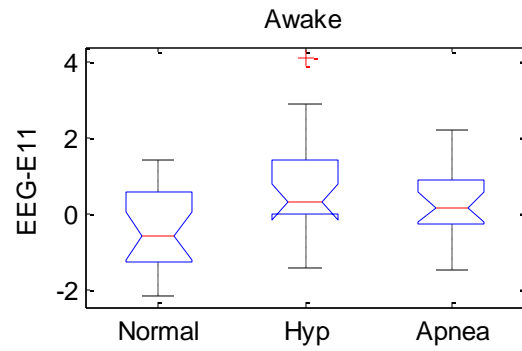
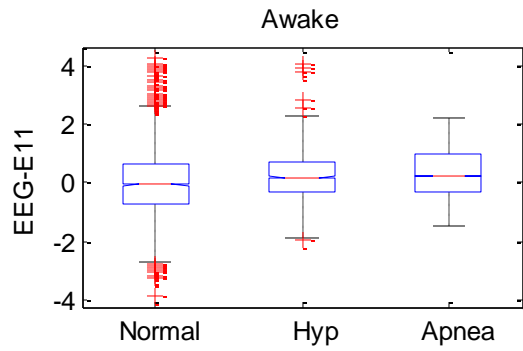
ANOVA Table					
Source	SS	df	MS	F	Prob>F
Groups	1.0204	2	0.51018	0.39	0.6814
Error	72.6523	55	1.32095		
Total	73.6727	57			



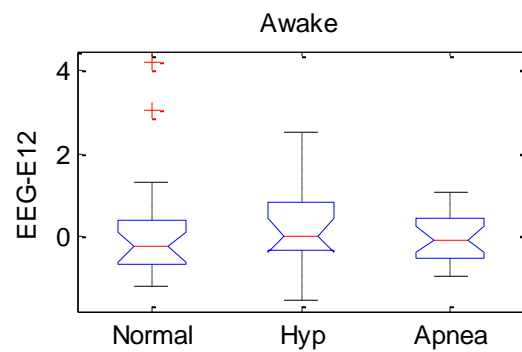
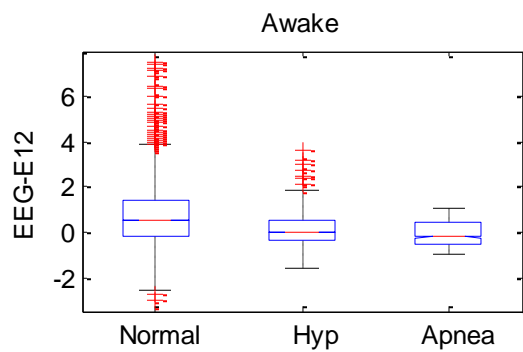
ANOVA Table					
Source	SS	df	MS	F	Prob>F
Groups	14.1605	2	7.08025	8.76	0.0005
Error	44.4547	55	0.80827		
Total	58.6152	57			



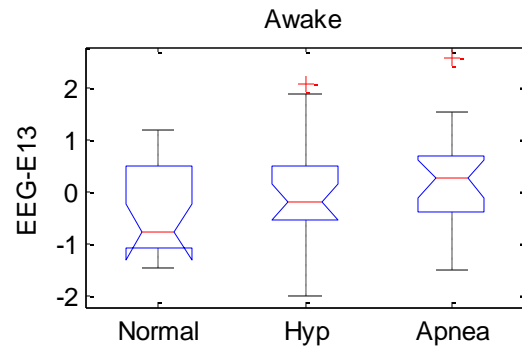
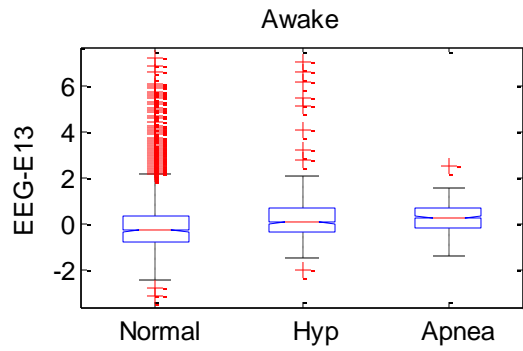
ANOVA Table					
Source	SS	df	MS	F	Prob>F
Groups	3.8734	2	1.93669	1.41	0.2537
Error	75.739	55	1.37707		
Total	79.6124	57			



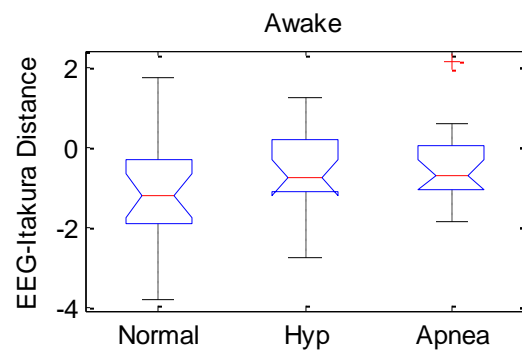
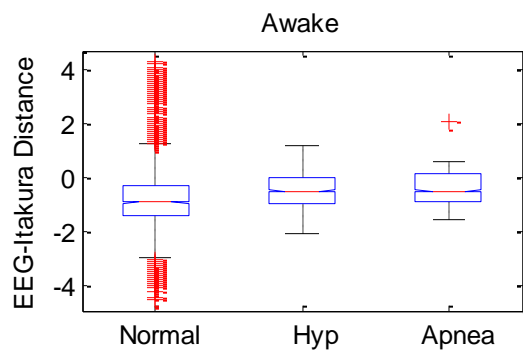
ANOVA Table					
Source	SS	df	MS	F	Prob>F
Groups	11.2276	2	5.61381	4.77	0.0123
Error	64.7599	55	1.17745		
Total	75.9875	57			



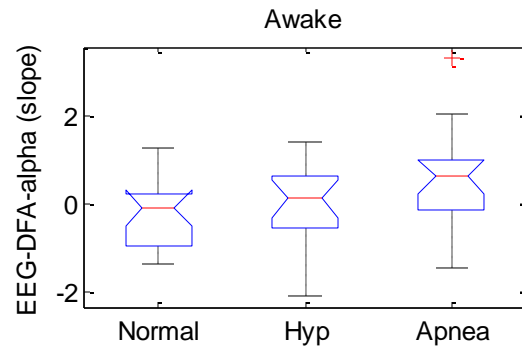
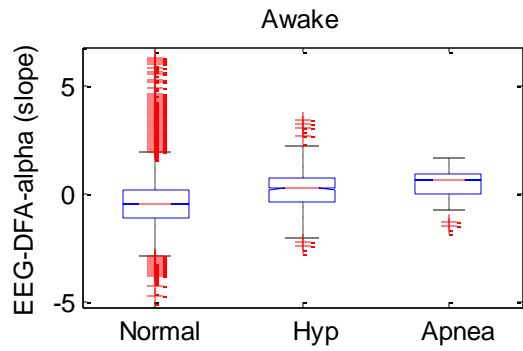
ANOVA Table					
Source	SS	df	MS	F	Prob>F
Groups	0.9185	2	0.45926	0.43	0.6527
Error	58.7525	55	1.06823		
Total	59.671	57			



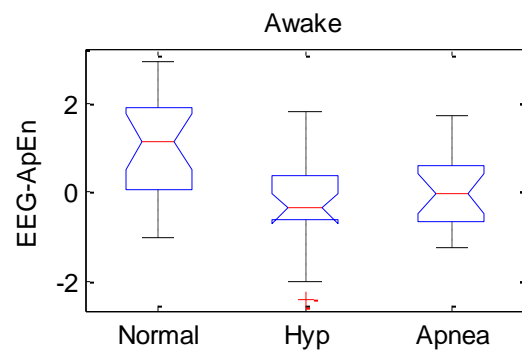
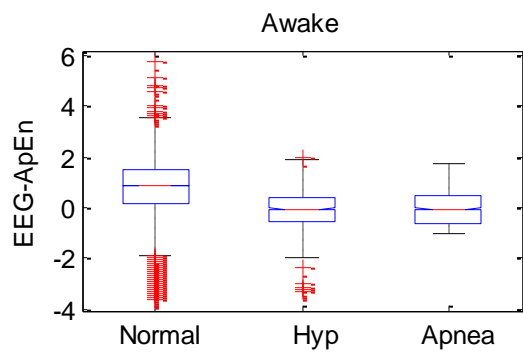
ANOVA Table					
Source	SS	df	MS	F	Prob>F
Groups	2.3356	2	1.16781	1.16	0.3217
Error	55.4733	55	1.00861		
Total	57.8089	57			



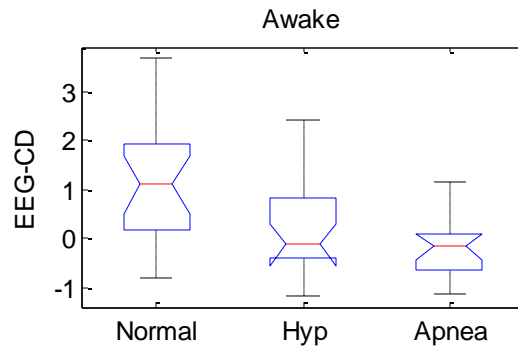
ANOVA Table					
Source	SS	df	MS	F	Prob>F
Groups	4.904	2	2.45201	1.98	0.1477
Error	68.0931	55	1.23806		
Total	72.9971	57			



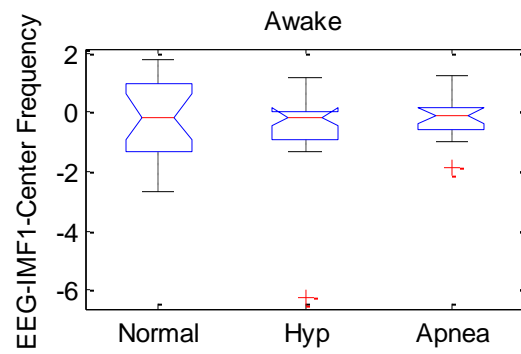
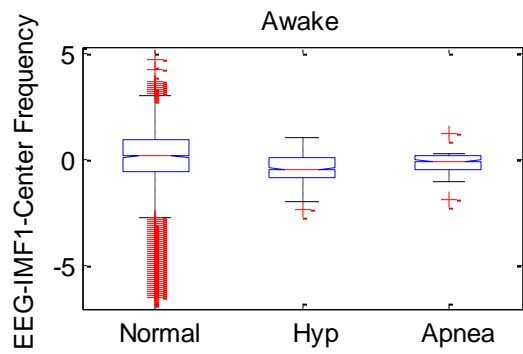
ANOVA Table					
Source	SS	df	MS	F	Prob>F
Groups	4.8263	2	2.41314	2.54	0.0878
Error	52.1743	55	0.94862		
Total	57.0006	57			



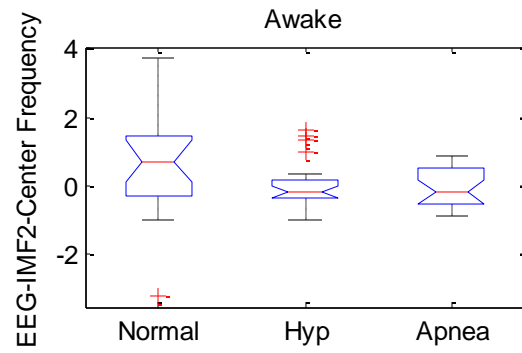
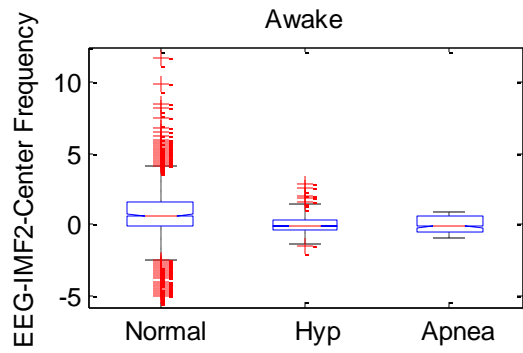
ANOVA Table					
Source	SS	df	MS	F	Prob>F
Groups	14.2336	2	7.11678	6.94	0.0021
Error	56.3905	55	1.02528		
Total	70.6241	57			



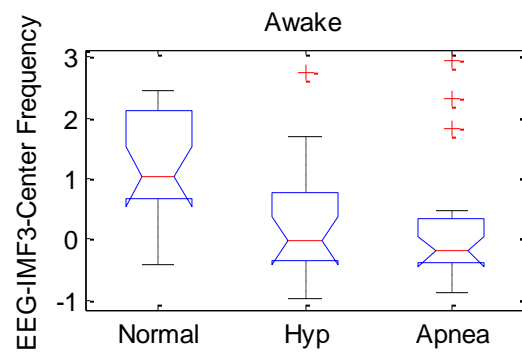
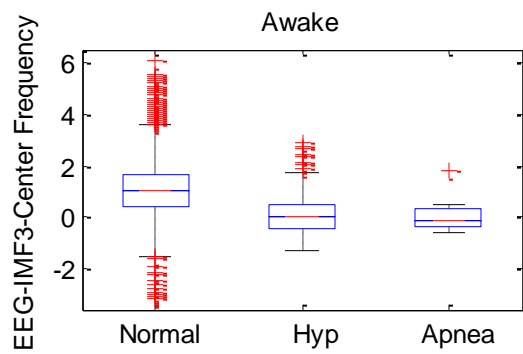
ANOVA Table					
Source	SS	df	MS	F	Prob>F
Groups	16.734	2	8.367	10.57	0.0001
Error	43.5366	55	0.79157		
Total	60.2706	57			



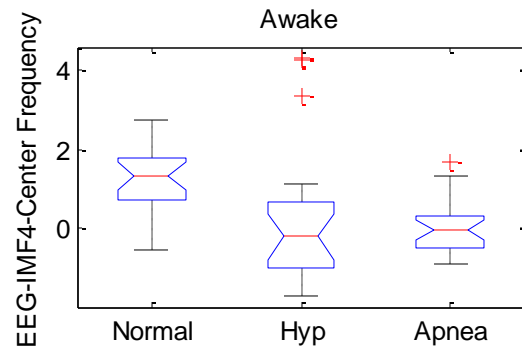
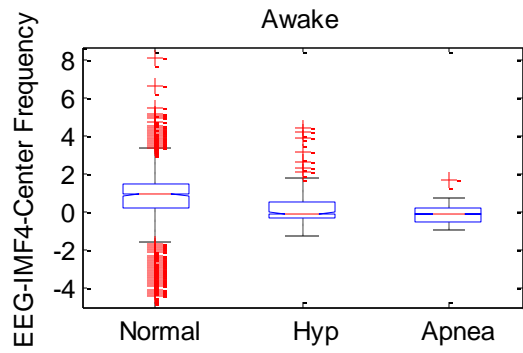
ANOVA Table					
Source	SS	df	MS	F	Prob>F
Groups	1.5554	2	0.77771	0.54	0.5846
Error	78.9087	55	1.4347		
Total	80.4642	57			



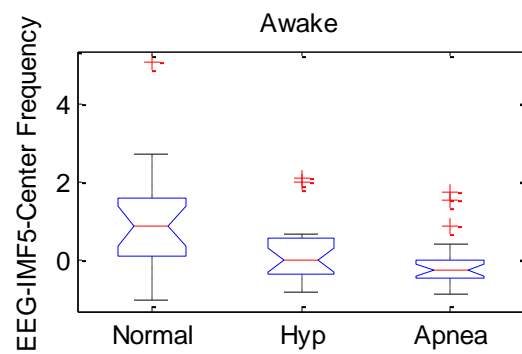
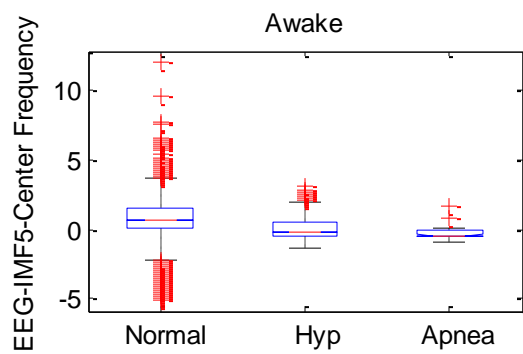
ANOVA Table					
Source	SS	df	MS	F	Prob>F
Groups	5.5083	2	2.75415	2.52	0.0899
Error	60.1568	55	1.09376		
Total	65.6651	57			



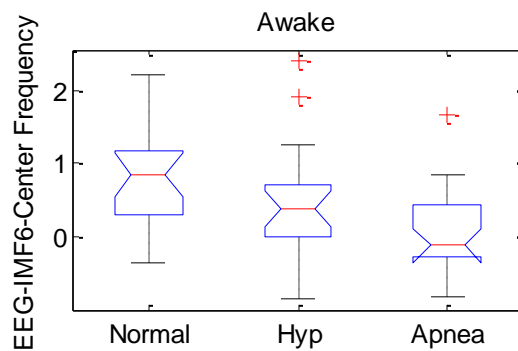
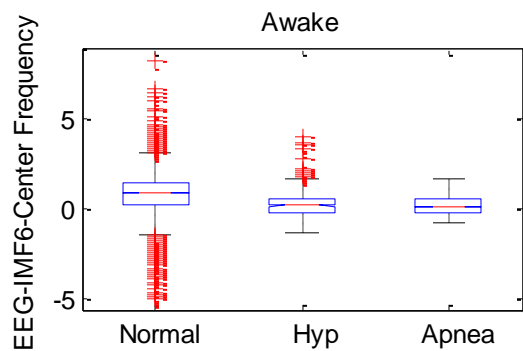
ANOVA Table					
Source	SS	df	MS	F	Prob>F
Groups	10.5435	2	5.27173	5.75	0.0054
Error	50.449	55	0.91725		
Total	60.9925	57			



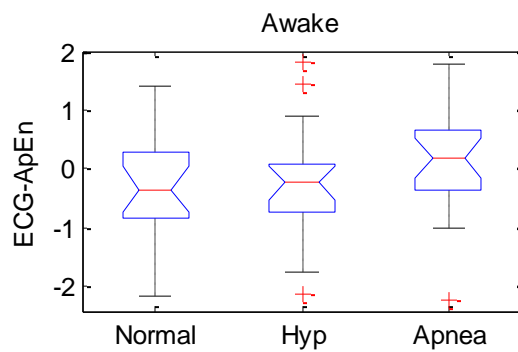
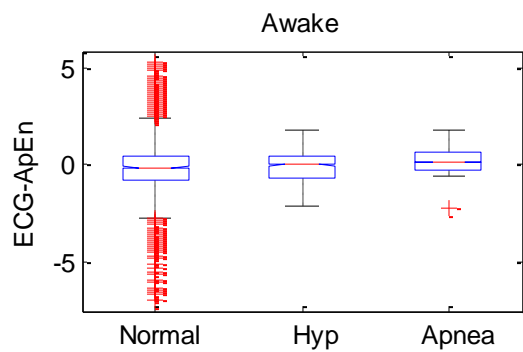
ANOVA Table					
Source	SS	df	MS	F	Prob>F
Groups	14.0914	2	7.04569	4.88	0.0112
Error	79.4298	55	1.44418		
Total	93.5212	57			



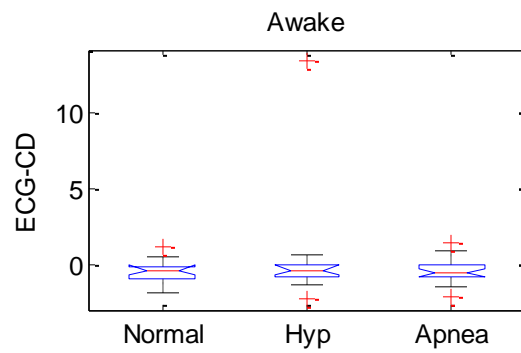
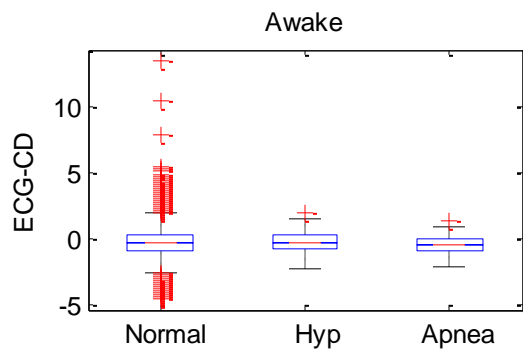
ANOVA Table					
Source	SS	df	MS	F	Prob>F
Groups	11.6631	2	5.83155	5.76	0.0053
Error	55.6557	55	1.01192		
Total	67.3188	57			



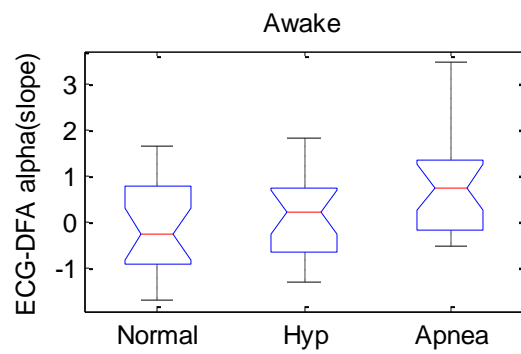
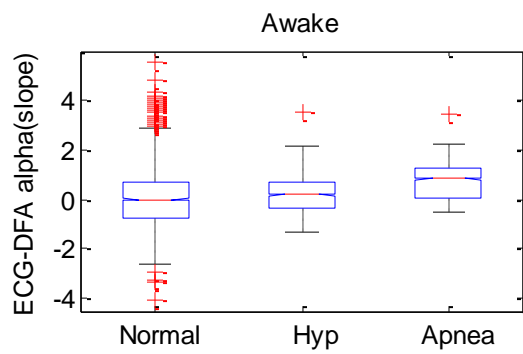
ANOVA Table					
Source	SS	df	MS	F	Prob>F
Groups	5.763	2	2.88152	5.69	0.0057
Error	27.8337	55	0.50607		
Total	33.5968	57			



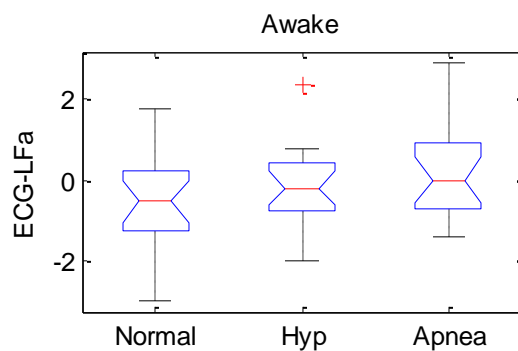
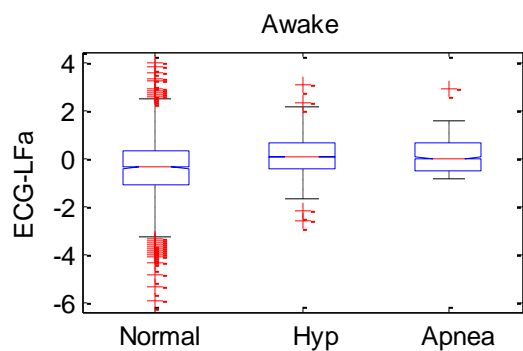
ANOVA Table					
Source	SS	df	MS	F	Prob>F
Groups	1.9857	2	0.99283	1.21	0.306
Error	45.125	55	0.82045		
Total	47.1107	57			



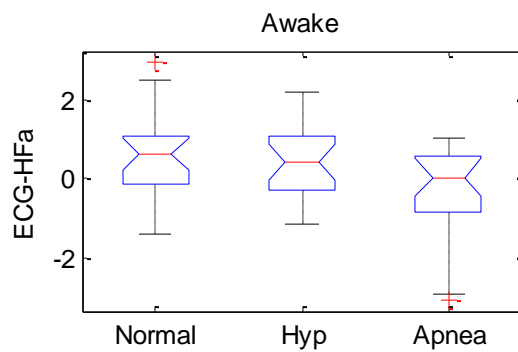
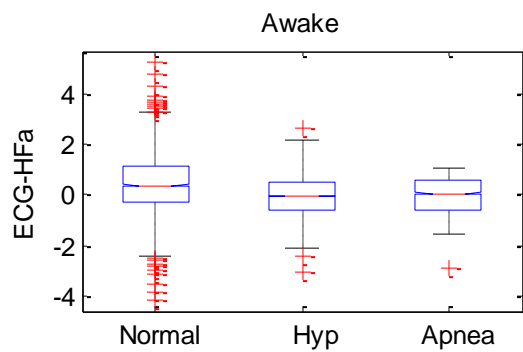
ANOVA Table					
Source	SS	df	MS	F	Prob>F
Groups	4.953	2	2.47671	0.64	0.5314
Error	213.011	55	3.87293		
Total	217.965	57			



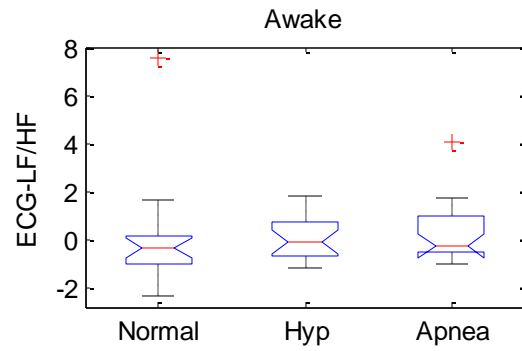
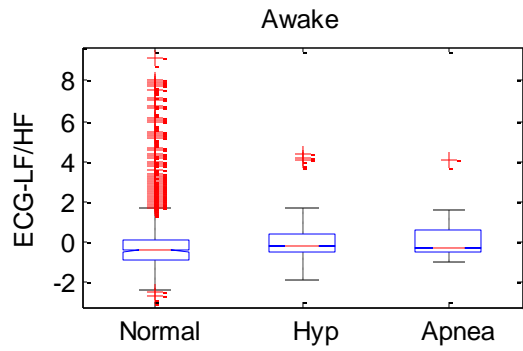
ANOVA Table					
Source	SS	df	MS	F	Prob>F
Groups	7.4013	2	3.70067	3.82	0.0279
Error	53.2654	55	0.96846		
Total	60.6667	57			



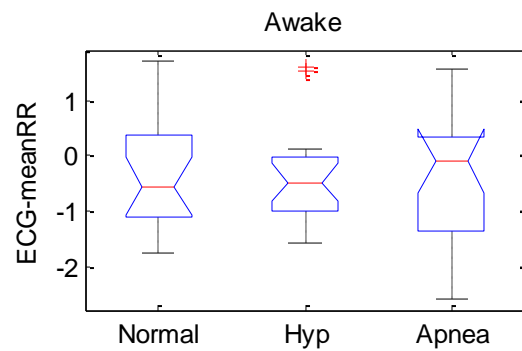
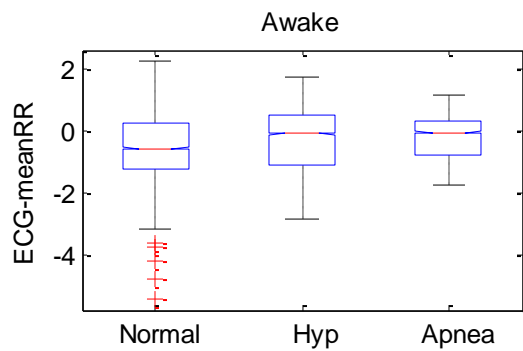
ANOVA Table					
Source	SS	df	MS	F	Prob>F
Groups	3.6645	2	1.83226	1.75	0.1826
Error	57.4584	55	1.0447		
Total	61.123	57			



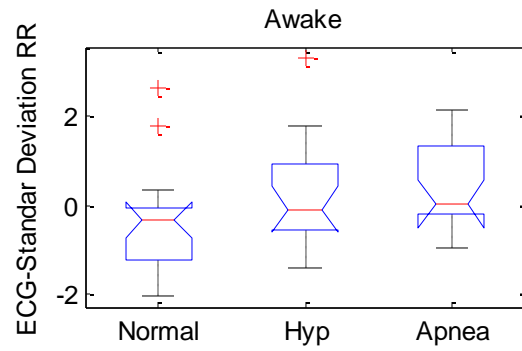
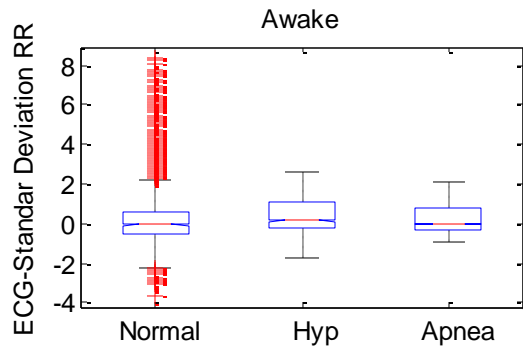
ANOVA Table					
Source	SS	df	MS	F	Prob>F
Groups	7.4016	2	3.70079	3.34	0.0427
Error	60.8931	55	1.10715		
Total	68.2947	57			



ANOVA Table					
Source	SS	df	MS	F	Prob>F
Groups	0.663	2	0.33148	0.16	0.8554
Error	116.421	55	2.11675		
Total	117.084	57			

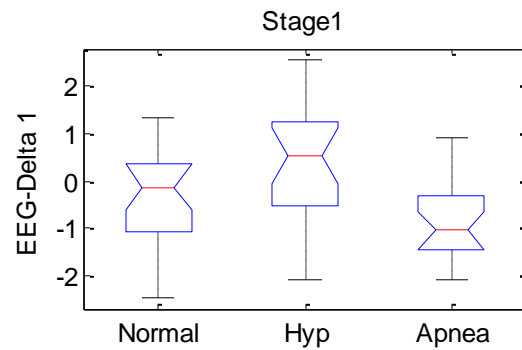
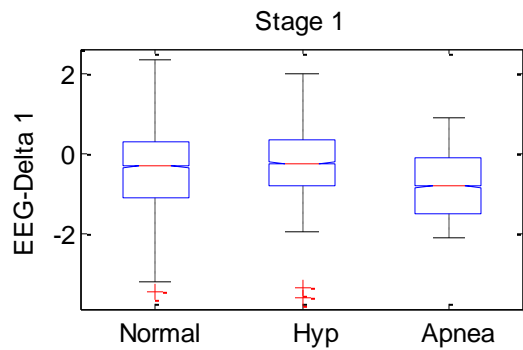


ANOVA Table					
Source	SS	df	MS	F	Prob>F
Groups	0.1259	2	0.06297	0.06	0.9389
Error	54.8364	55	0.99703		
Total	54.9623	57			

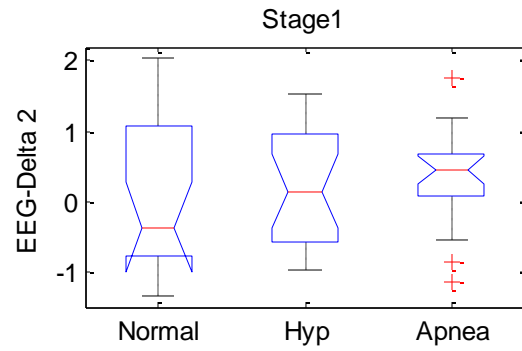
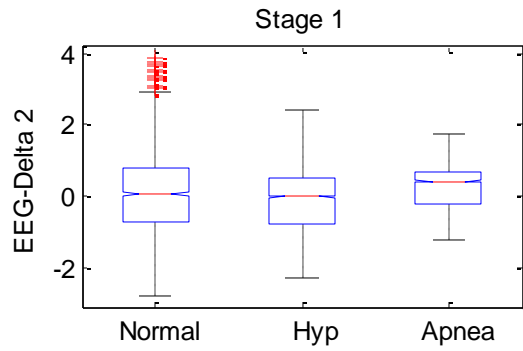


ANOVA Table					
Source	SS	df	MS	F	Prob>F
Groups	6.3583	2	3.17915	2.66	0.0789
Error	65.7219	55	1.19494		
Total	72.0802	57			

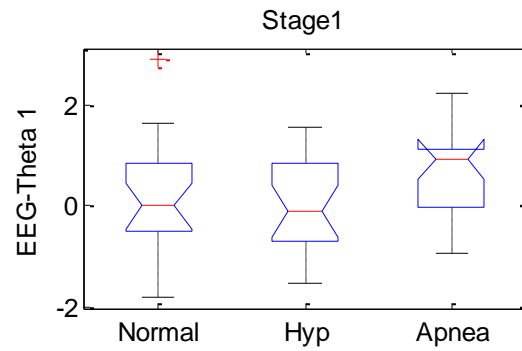
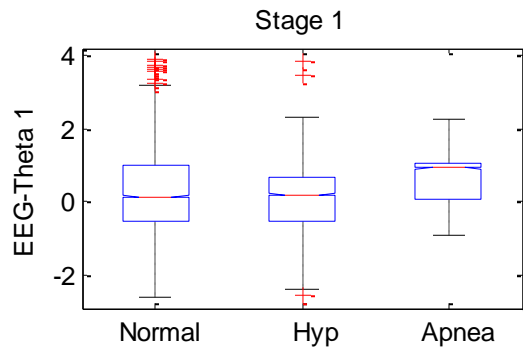
Stage 1



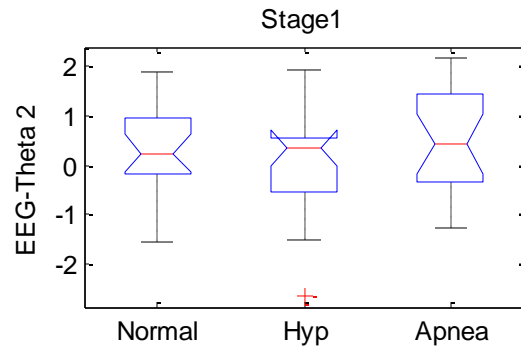
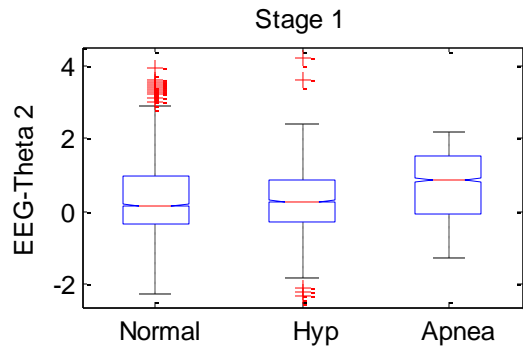
ANOVA Table					
Source	SS	df	MS	F	Prob>F
Groups	16.0951	2	8.04755	7.36	0.0014
Error	65.5809	60	1.09301		
Total	81.676	62			



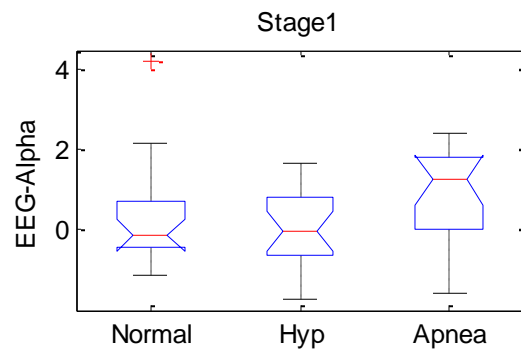
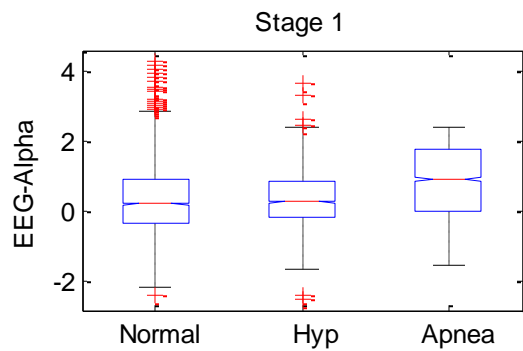
ANOVA Table					
Source	SS	df	MS	F	Prob>F
Groups	0.5344	2	0.26718	0.36	0.7001
Error	44.6934	60	0.74489		
Total	45.2277	62			



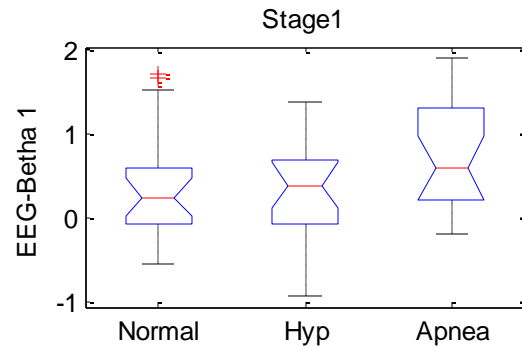
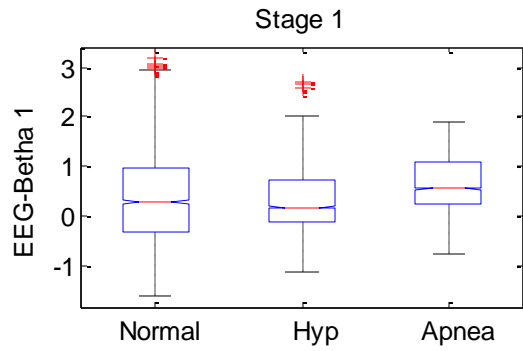
ANOVA Table					
Source	SS	df	MS	F	Prob>F
Groups	4.6513	2	2.32563	2.44	0.0954
Error	57.0941	60	0.95157		
Total	61.7454	62			



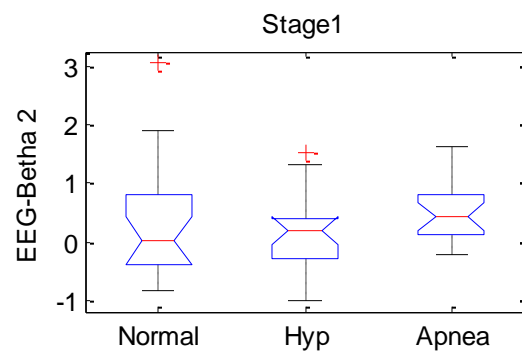
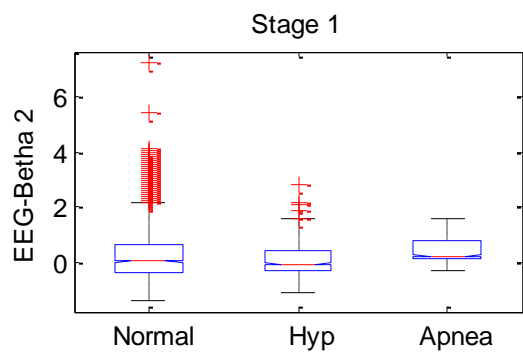
ANOVA Table					
Source	SS	df	MS	F	Prob>F
Groups	2.946	2	1.47302	1.48	0.2368
Error	59.8848	60	0.99808		
Total	62.8308	62			



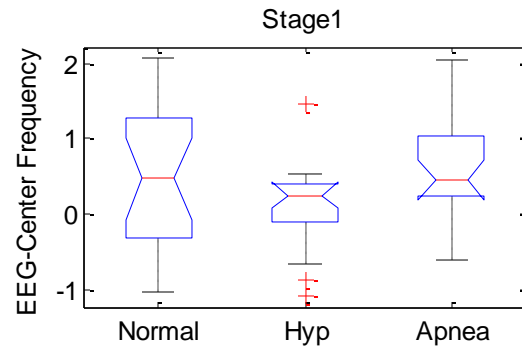
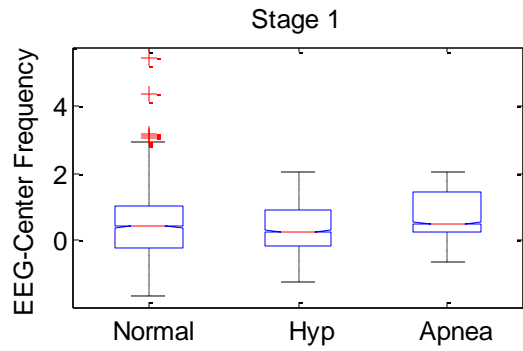
ANOVA Table					
Source	SS	df	MS	F	Prob>F
Groups	8.6839	2	4.34194	3.9	0.0256
Error	66.8161	60	1.1136		
Total	75.5	62			



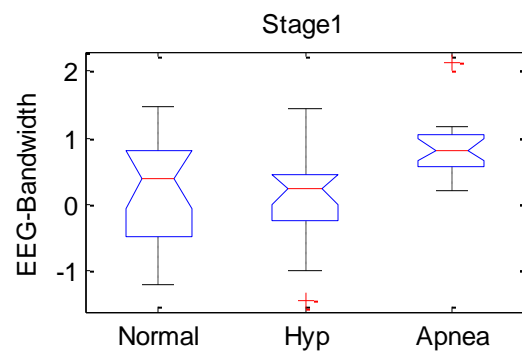
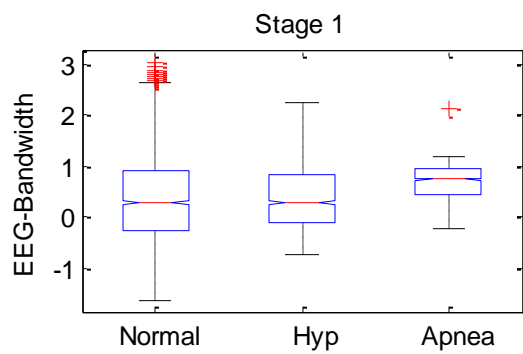
ANOVA Table					
Source	SS	df	MS	F	Prob>F
Groups	2.2231	2	1.11154	2.77	0.0704
Error	24.0362	60	0.4006		
Total	26.2593	62			



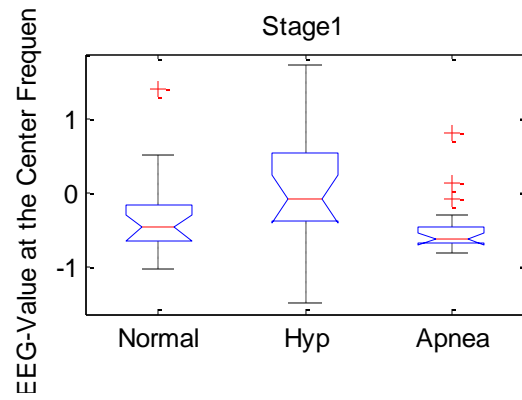
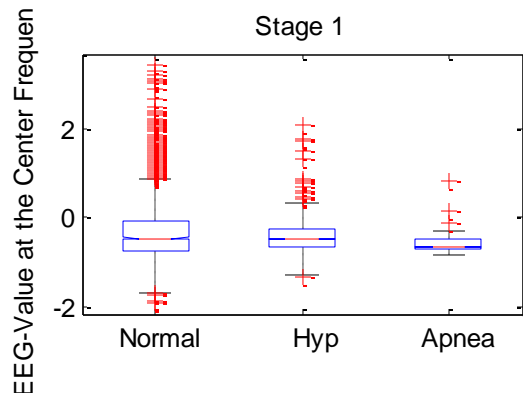
ANOVA Table					
Source	SS	df	MS	F	Prob>F
Groups	1.3454	2	0.67271	1.29	0.2842
Error	31.4106	60	0.52351		
Total	32.756	62			



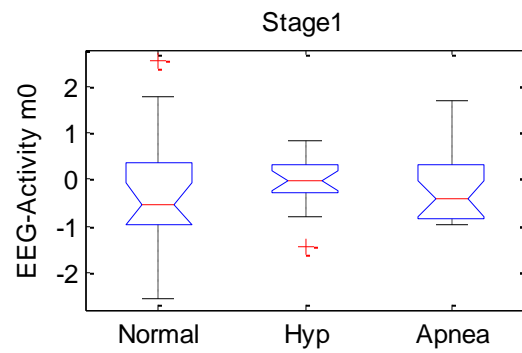
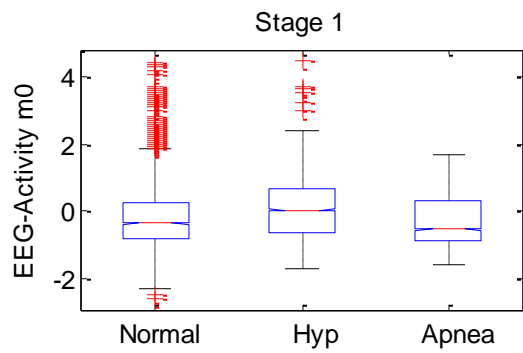
ANOVA Table					
Source	SS	df	MS	F	Prob>F
Groups	3.0011	2	1.50054	2.98	0.0586
Error	30.2582	60	0.5043		
Total	33.2593	62			



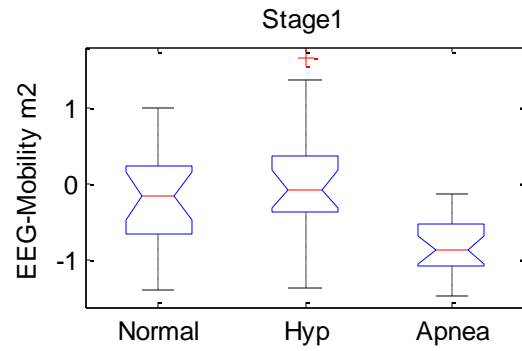
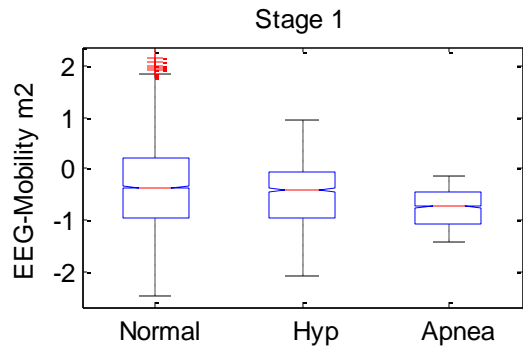
ANOVA Table					
Source	SS	df	MS	F	Prob>F
Groups	6.3147	2	3.15737	8.18	0.0007
Error	23.1502	60	0.38584		
Total	29.465	62			



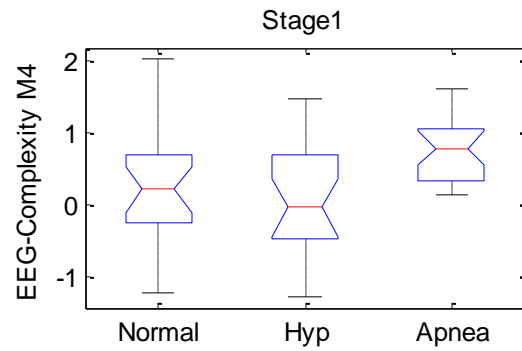
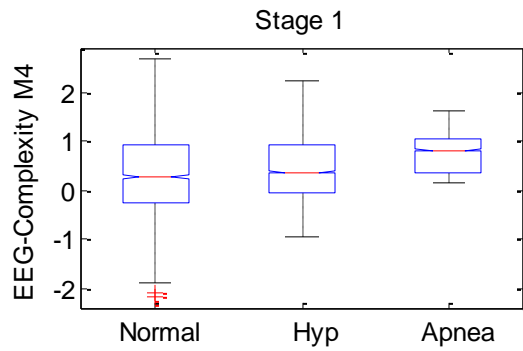
ANOVA Table					
Source	SS	df	MS	F	Prob>F
Groups	3.1852	2	1.59258	4.79	0.0117
Error	19.9383	60	0.33231		
Total	23.1235	62			



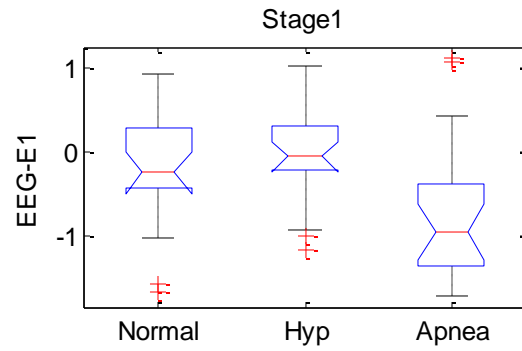
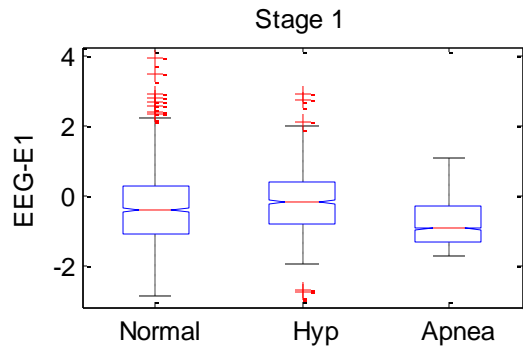
ANOVA Table					
Source	SS	df	MS	F	Prob>F
Groups	0.4083	2	0.20416	0.25	0.7793
Error	48.9131	60	0.81522		
Total	49.3214	62			



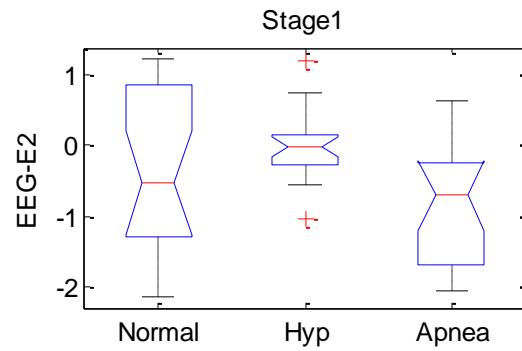
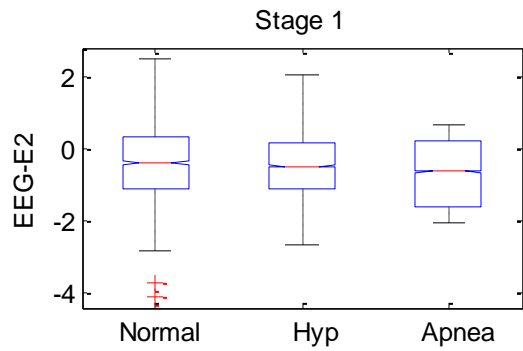
ANOVA Table					
Source	SS	df	MS	F	Prob>F
Groups	7.9279	2	3.96395	10.69	0.0001
Error	22.2499	60	0.37083		
Total	30.1778	62			



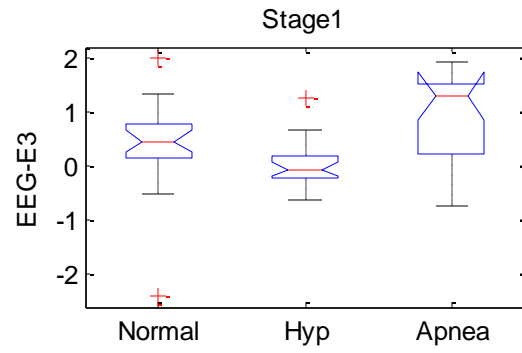
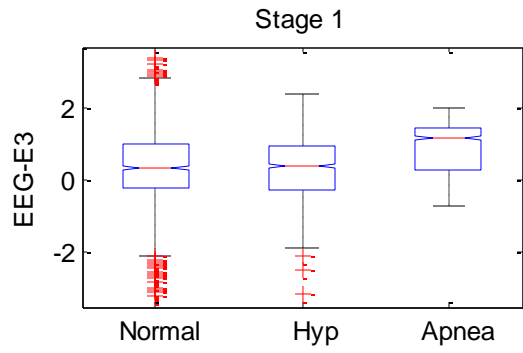
ANOVA Table					
Source	SS	df	MS	F	Prob>F
Groups	5.88	2	2.93999	6.87	0.0021
Error	25.6655	60	0.42776		
Total	31.5455	62			



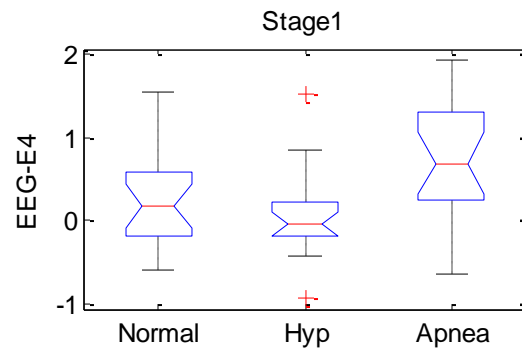
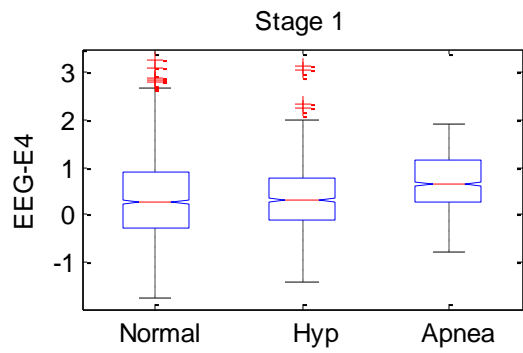
ANOVA Table					
Source	SS	df	MS	F	Prob>F
Groups	5.016	2	2.50802	5.39	0.0071
Error	27.9407	60	0.46568		
Total	32.9567	62			



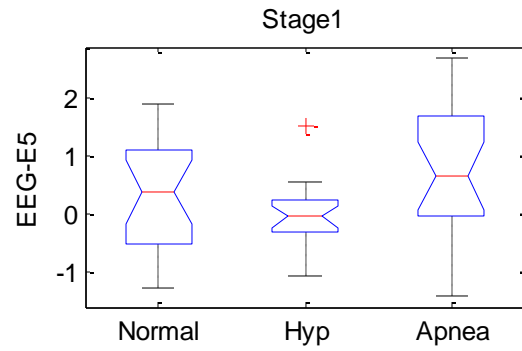
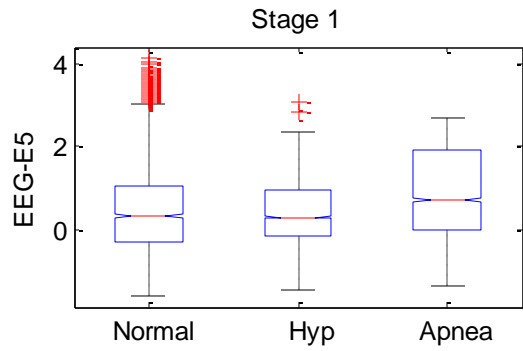
ANOVA Table					
Source	SS	df	MS	F	Prob>F
Groups	7.7095	2	3.85476	5.35	0.0073
Error	43.2124	60	0.72021		
Total	50.9219	62			



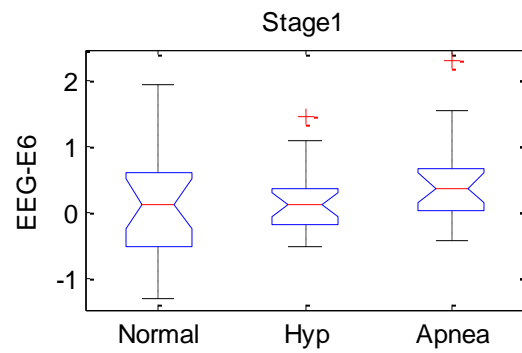
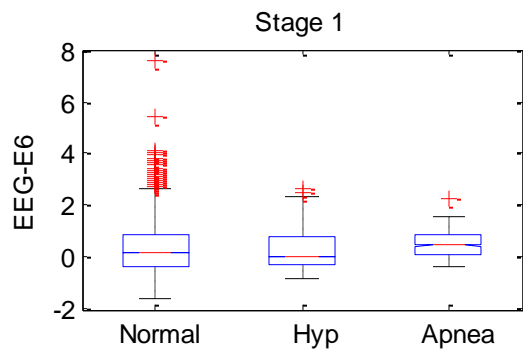
ANOVA Table					
Source	SS	df	MS	F	Prob>F
Groups	9.3292	2	4.66462	9.26	0.0003
Error	30.2229	60	0.50372		
Total	39.5522	62			



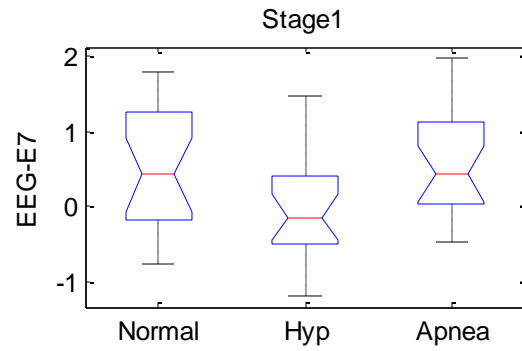
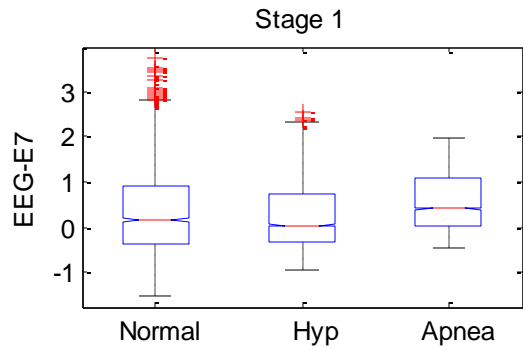
ANOVA Table					
Source	SS	df	MS	F	Prob>F
Groups	5.2094	2	2.60471	6.86	0.0021
Error	22.7691	60	0.37949		
Total	27.9786	62			



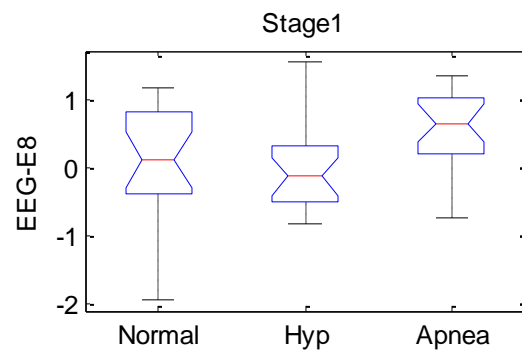
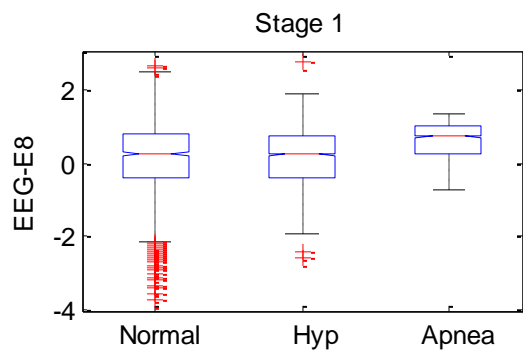
ANOVA Table					
Source	SS	df	MS	F	Prob>F
Groups	6.6757	2	3.33783	4.45	0.0157
Error	44.9855	60	0.74976		
Total	51.6611	62			



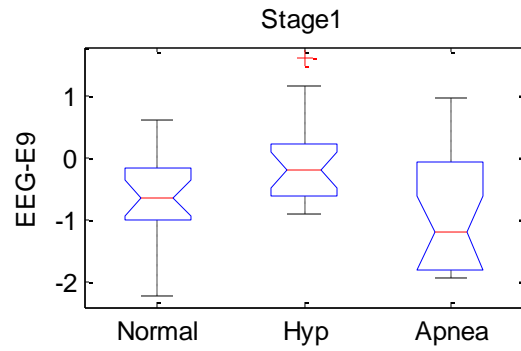
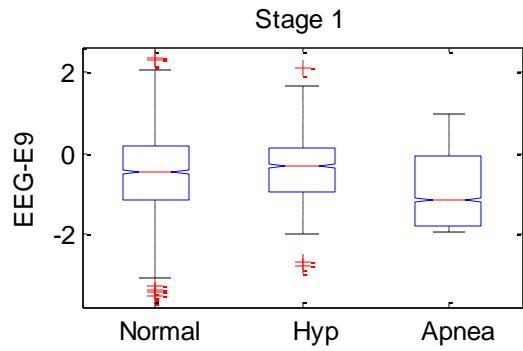
ANOVA Table					
Source	SS	df	MS	F	Prob>F
Groups	1.3365	2	0.66824	1.61	0.2076
Error	24.8443	60	0.41407		
Total	26.1808	62			



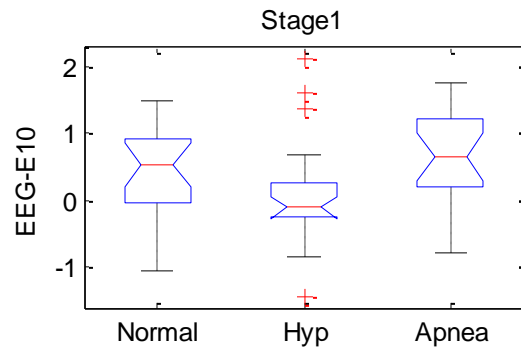
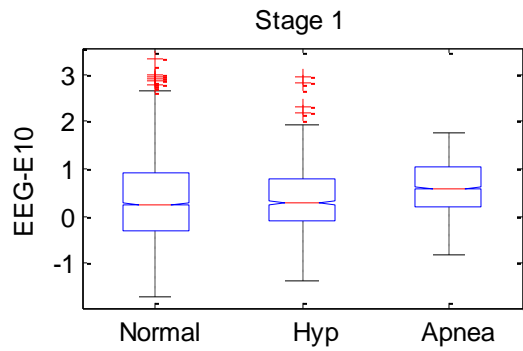
ANOVA Table					
Source	SS	df	MS	F	Prob>F
Groups	5.9801	2	2.99006	6.26	0.0034
Error	28.6621	60	0.4777		
Total	34.6422	62			



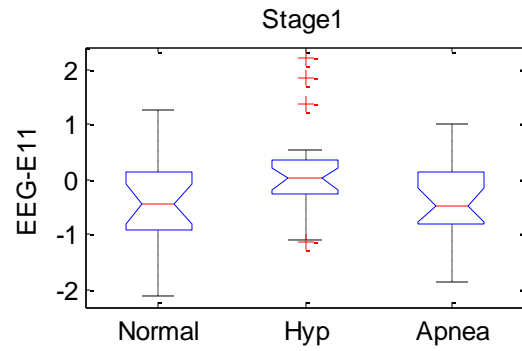
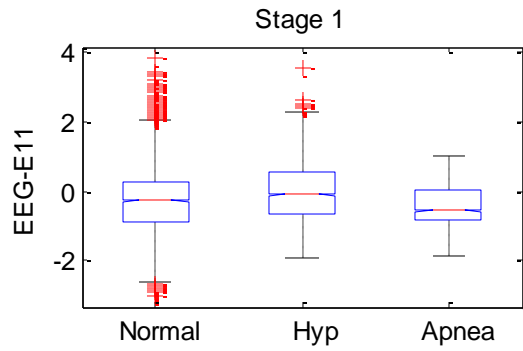
ANOVA Table					
Source	SS	df	MS	F	Prob>F
Groups	4.8294	2	2.41469	5.33	0.0074
Error	27.1991	60	0.45332		
Total	32.0285	62			



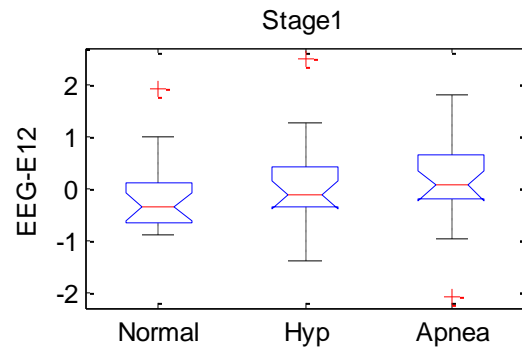
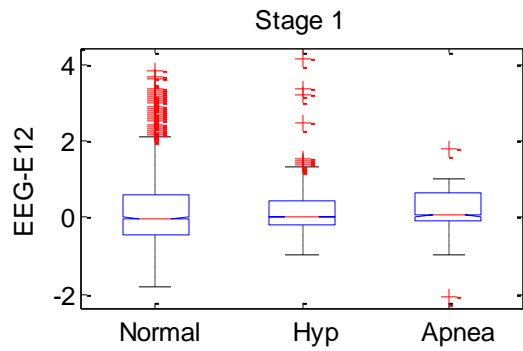
ANOVA Table					
Source	SS	df	MS	F	Prob>F
Groups	7.0399	2	3.51994	6.11	0.0039
Error	34.5845	60	0.57641		
Total	41.6244	62			



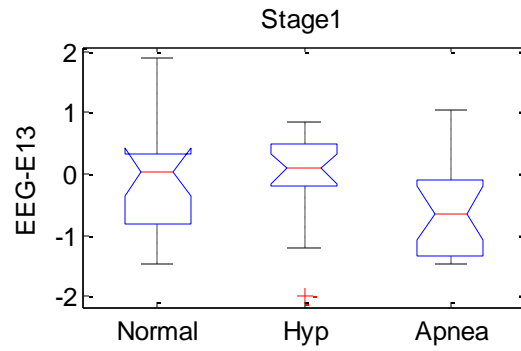
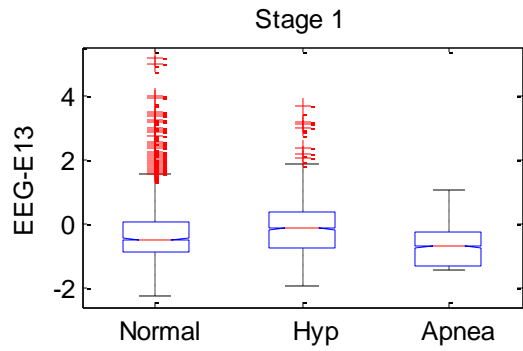
ANOVA Table					
Source	SS	df	MS	F	Prob>F
Groups	4.4133	2	2.20664	3.72	0.0301
Error	35.6129	60	0.59355		
Total	40.0262	62			



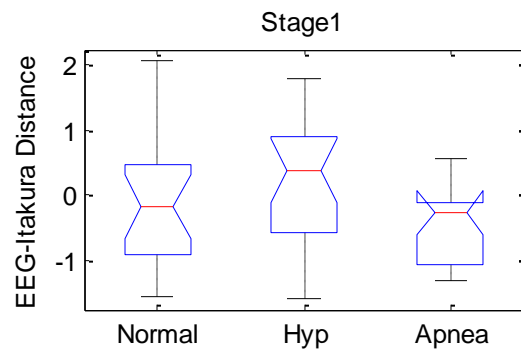
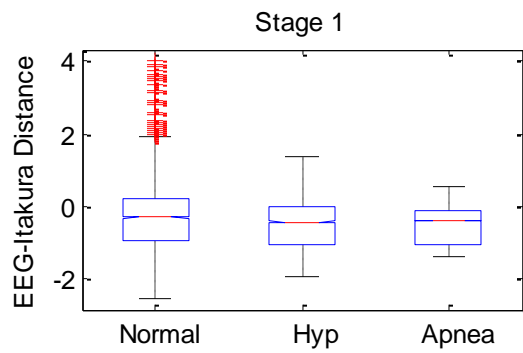
ANOVA Table					
Source	SS	df	MS	F	Prob>F
Groups	3.2227	2	1.61136	2.3	0.1089
Error	42.0076	60	0.70013		
Total	45.2304	62			



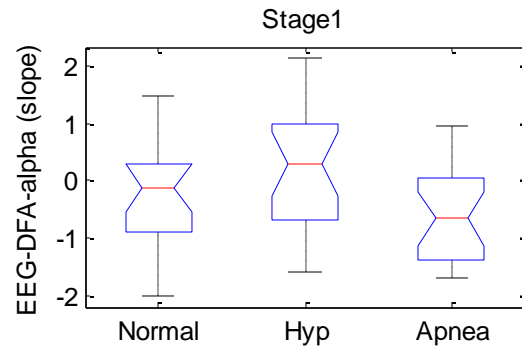
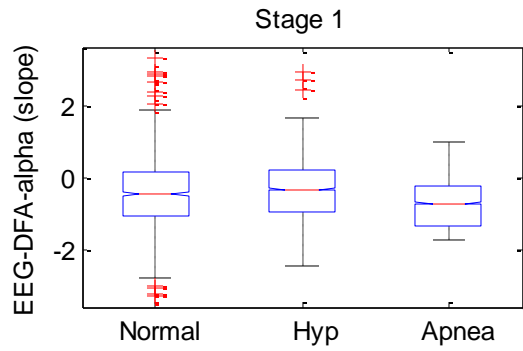
ANOVA Table					
Source	SS	df	MS	F	Prob>F
Groups	0.7143	2	0.35716	0.57	0.5679
Error	37.5239	60	0.6254		
Total	38.2382	62			



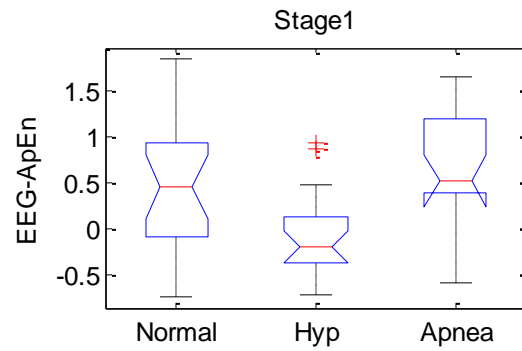
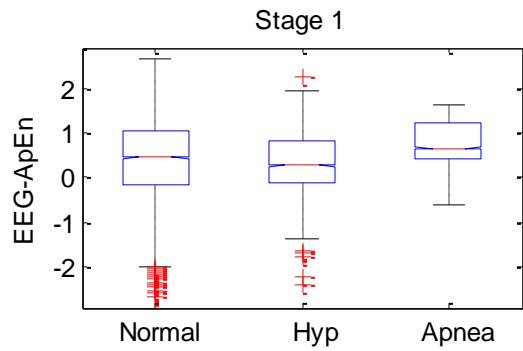
ANOVA Table					
Source	SS	df	MS	F	Prob>F
Groups	3.1077	2	1.55383	2.62	0.0809
Error	35.5359	60	0.59226		
Total	38.6435	62			



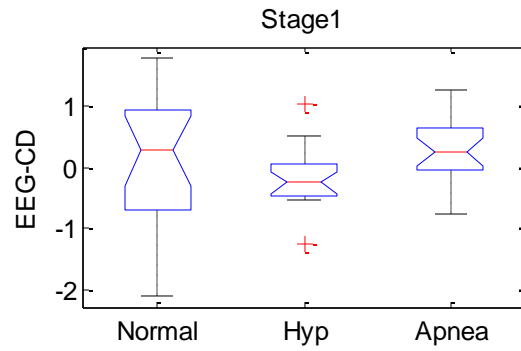
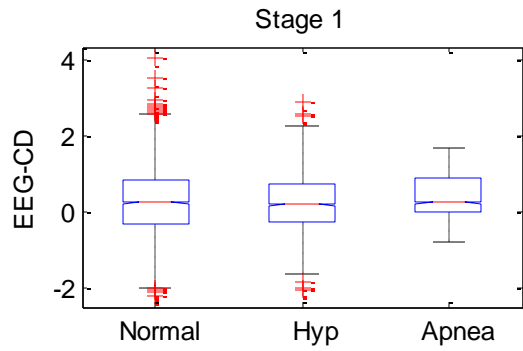
ANOVA Table					
Source	SS	df	MS	F	Prob>F
Groups	4.7984	2	2.39919	3.24	0.0462
Error	44.4541	60	0.7409		
Total	49.2524	62			



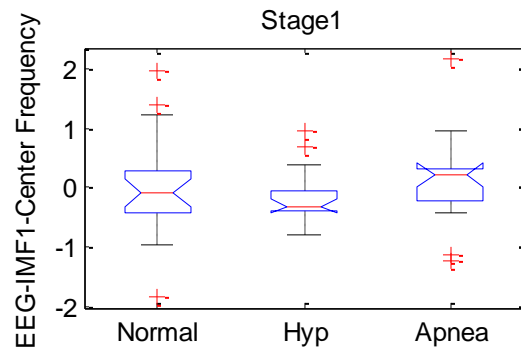
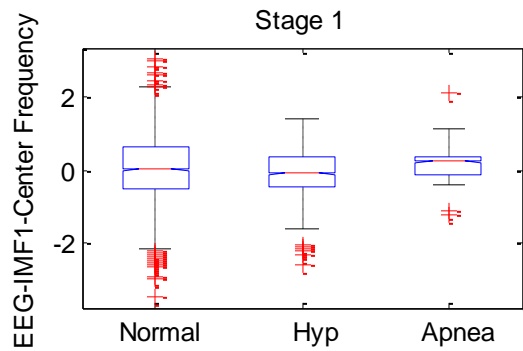
ANOVA Table					
Source	SS	df	MS	F	Prob>F
Groups	8.4218	2	4.2109	4.68	0.0129
Error	53.9428	60	0.89905		
Total	62.3646	62			



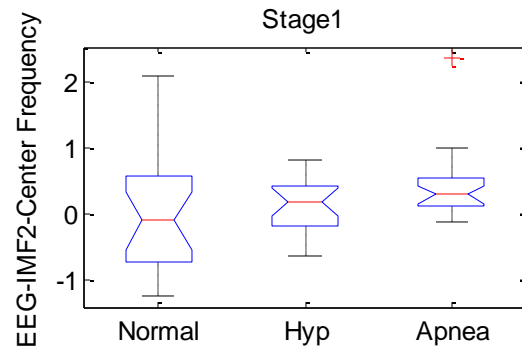
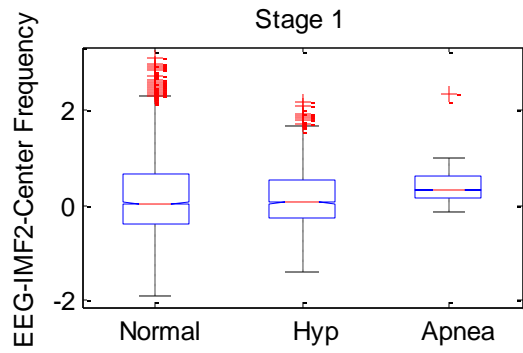
ANOVA Table					
Source	SS	df	MS	F	Prob>F
Groups	5.661	2	2.83052	7.68	0.0011
Error	22.1188	60	0.36865		
Total	27.7798	62			



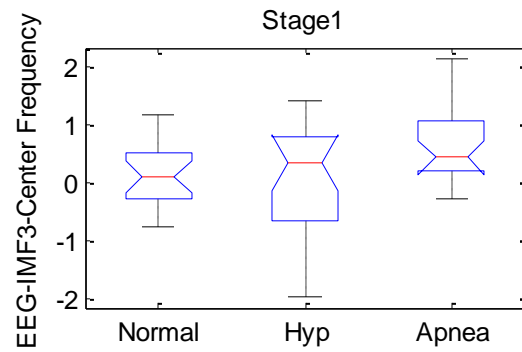
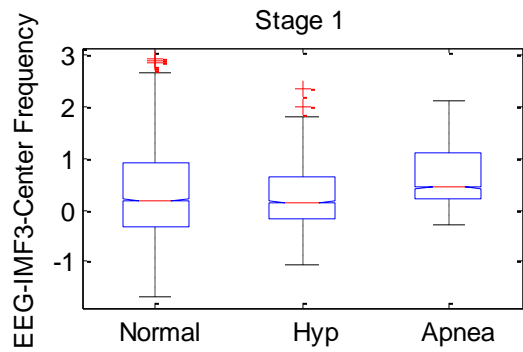
ANOVA Table					
Source	SS	df	MS	F	Prob>F
Groups	2.2322	2	1.11611	2.35	0.1039
Error	28.4724	60	0.47454		
Total	30.7047	62			



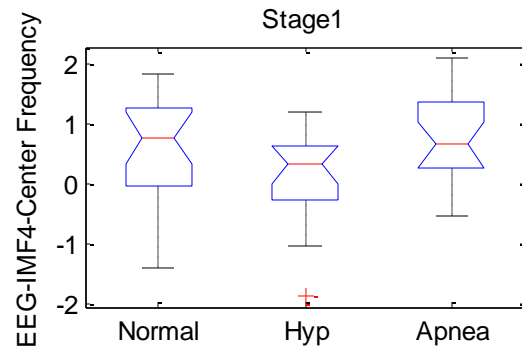
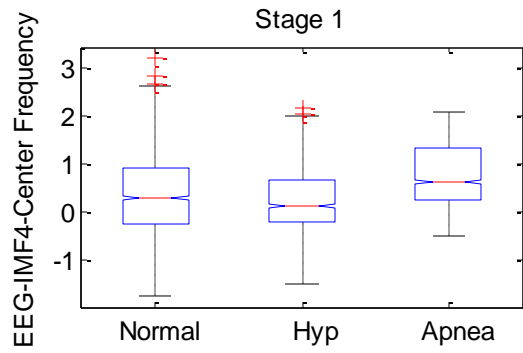
ANOVA Table					
Source	SS	df	MS	F	Prob>F
Groups	0.988	2	0.49402	1.08	0.3465
Error	27.4719	60	0.45786		
Total	28.4599	62			



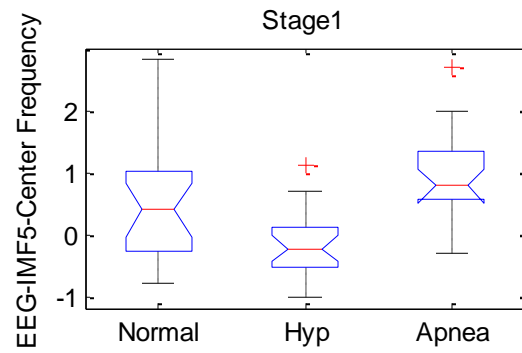
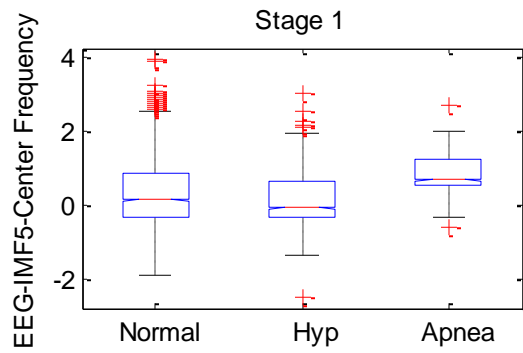
ANOVA Table					
Source	SS	df	MS	F	Prob>F
Groups	2.0649	2	1.03243	2.66	0.0783
Error	23.2986	60	0.38831		
Total	25.3635	62			



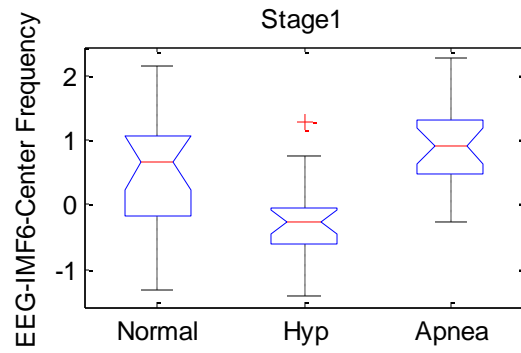
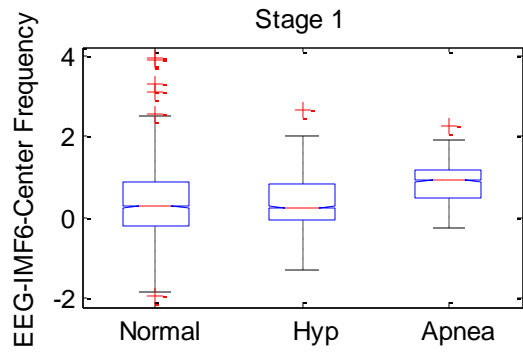
ANOVA Table					
Source	SS	df	MS	F	Prob>F
Groups	3.5115	2	1.75577	3.38	0.0406
Error	31.1465	60	0.51911		
Total	34.658	62			



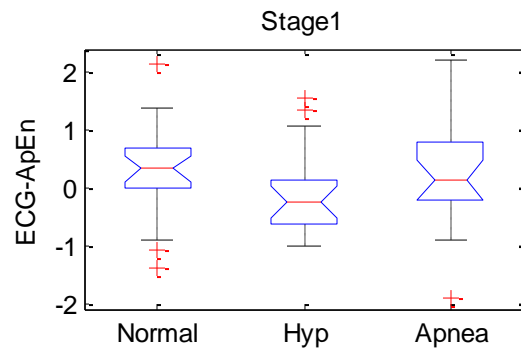
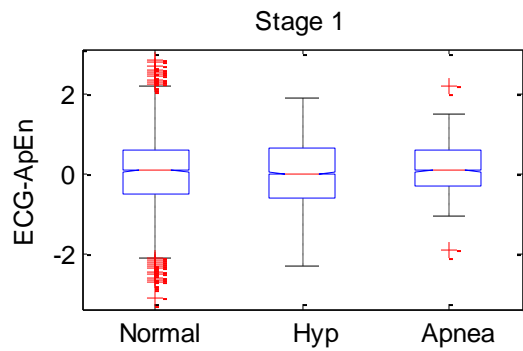
ANOVA Table					
Source	SS	df	MS	F	Prob>F
Groups	3.4989	2	1.74947	2.91	0.0622
Error	36.0741	60	0.60124		
Total	39.5731	62			



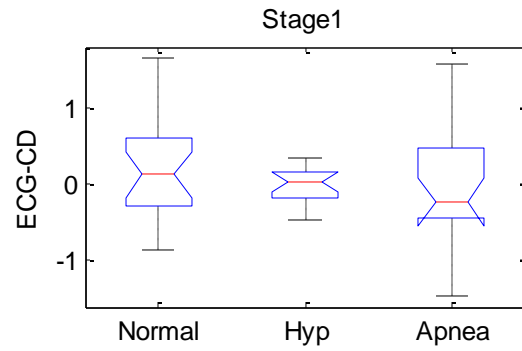
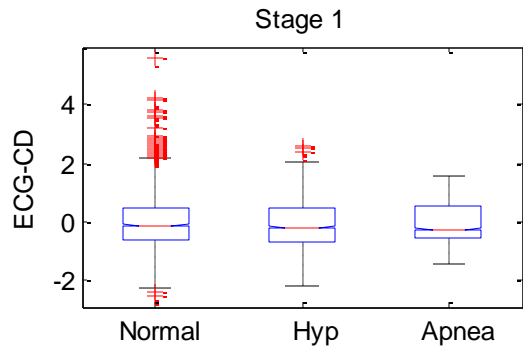
ANOVA Table					
Source	SS	df	MS	F	Prob>F
Groups	14.3836	2	7.19182	11.49	5.97528e-005
Error	37.5658	60	0.6261		
Total	51.9495	62			



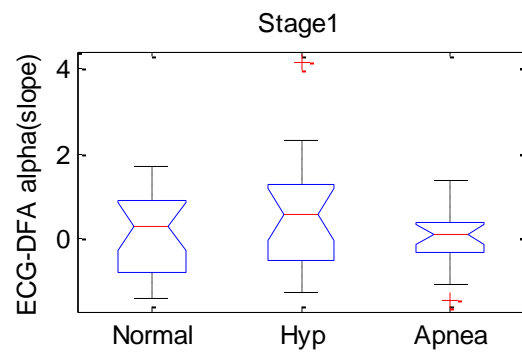
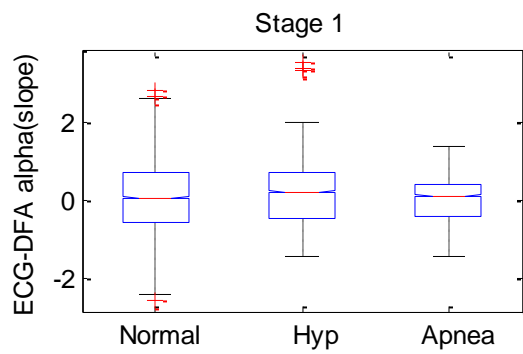
ANOVA Table					
Source	SS	df	MS	F	Prob>F
Groups	14.3444	2	7.17218	14.02	1.01085e-005
Error	30.6981	60	0.51164		
Total	45.0425	62			



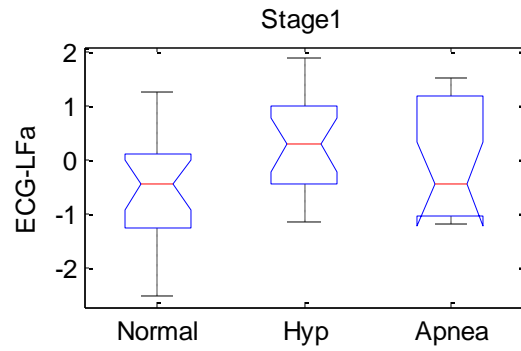
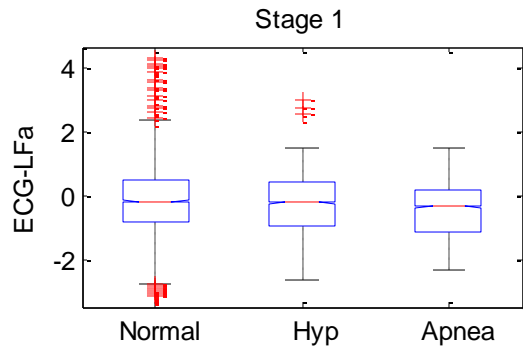
ANOVA Table					
Source	SS	df	MS	F	Prob>F
Groups	1.7887	2	0.89433	1.32	0.2752
Error	40.7009	60	0.67835		
Total	42.4896	62			



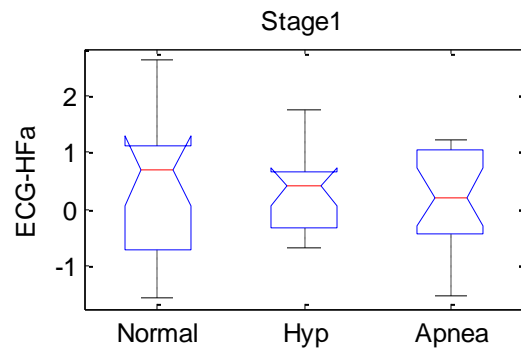
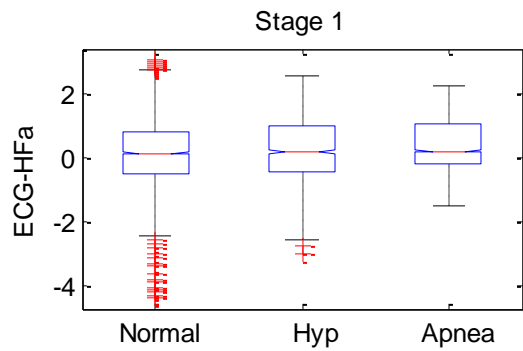
ANOVA Table					
Source	SS	df	MS	F	Prob>F
Groups	1.0742	2	0.53712	1.46	0.2402
Error	22.0627	60	0.36771		
Total	23.137	62			



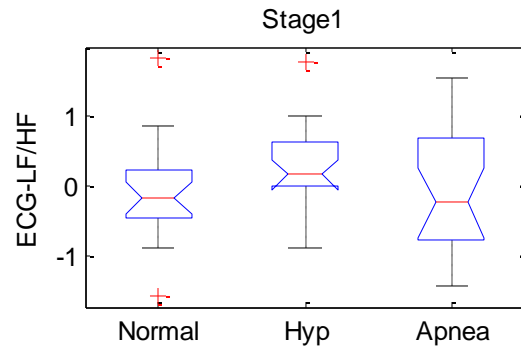
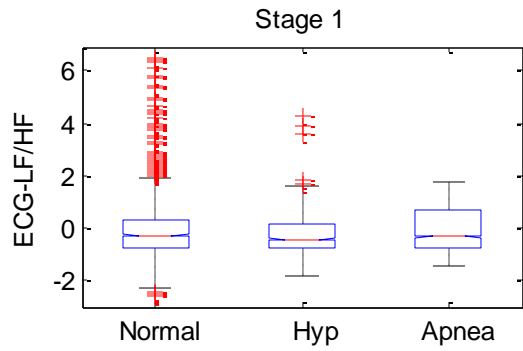
ANOVA Table					
Source	SS	df	MS	F	Prob>F
Groups	4.6642	2	2.33208	2.24	0.1154
Error	62.5008	60	1.04168		
Total	67.1649	62			



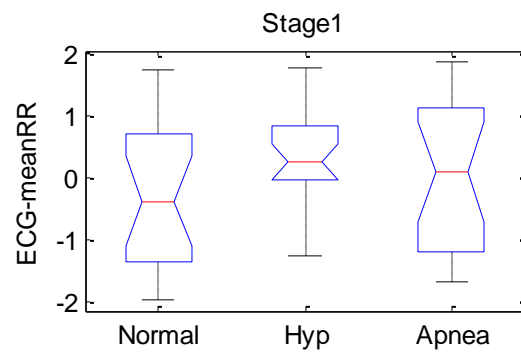
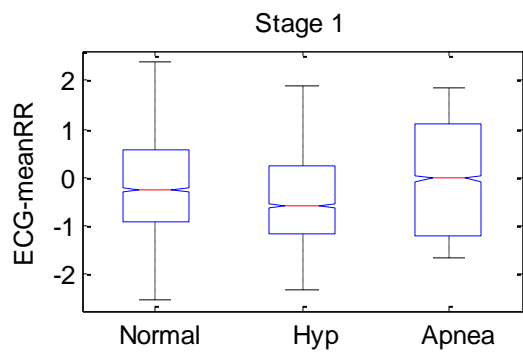
ANOVA Table					
Source	SS	df	MS	F	Prob>F
Groups	7.3725	2	3.68624	3.84	0.0269
Error	57.5608	60	0.95935		
Total	64.9333	62			



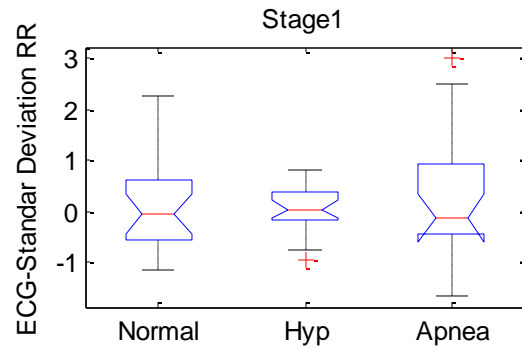
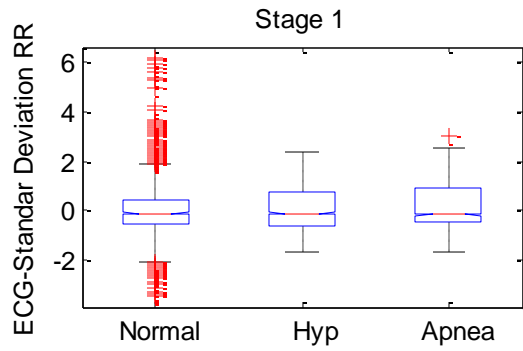
ANOVA Table					
Source	SS	df	MS	F	Prob>F
Groups	0.58	2	0.29183	0.3	0.7378
Error	3262.61	3400	0.95959		
Total	3263.19	3402			



ANOVA Table					
Source	SS	df	MS	F	Prob>F
Groups	1.6332	2	0.81662	1.65	0.2002
Error	29.6505	60	0.49418		
Total	31.2838	62			

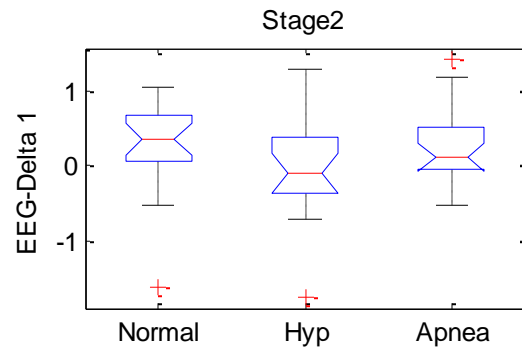
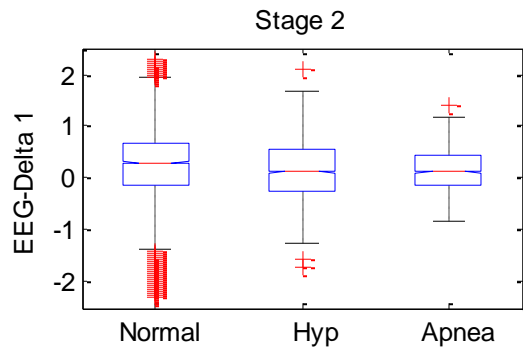


ANOVA Table					
Source	SS	df	MS	F	Prob>F
Groups	3.8219	2	1.91094	1.64	0.202
Error	69.7835	60	1.16306		
Total	73.6054	62			

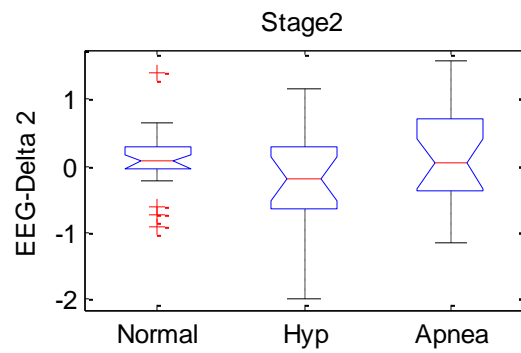
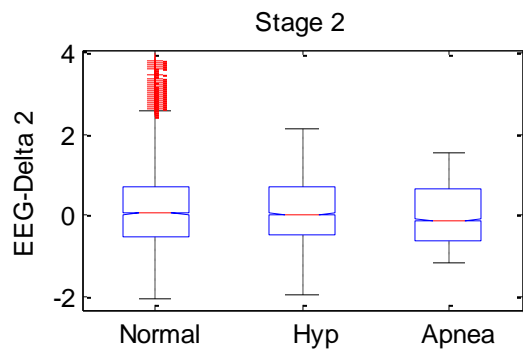


ANOVA Table					
Source	SS	df	MS	F	Prob>F
Groups	0.3412	2	0.17062	0.24	0.785
Error	42.1241	60	0.70207		
Total	42.4654	62			

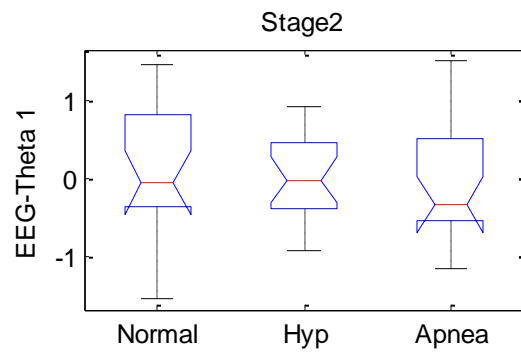
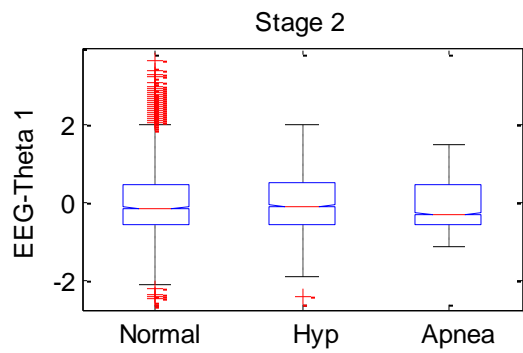
Stage 2



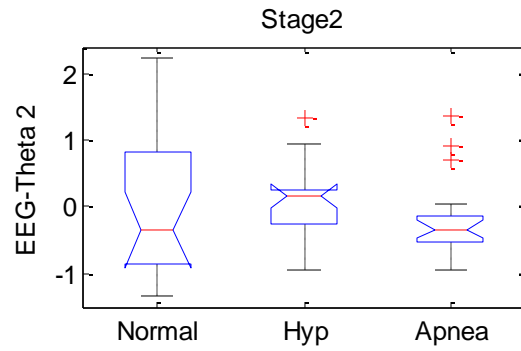
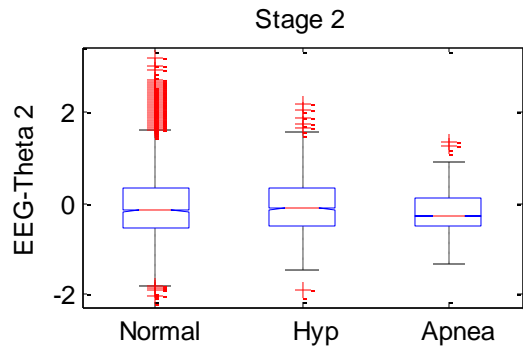
ANOVA Table					
Source	SS	df	MS	F	Prob>F
Groups	1.4021	2	0.70105	2.03	0.1407
Error	20.7528	60	0.34588		
Total	22.1549	62			



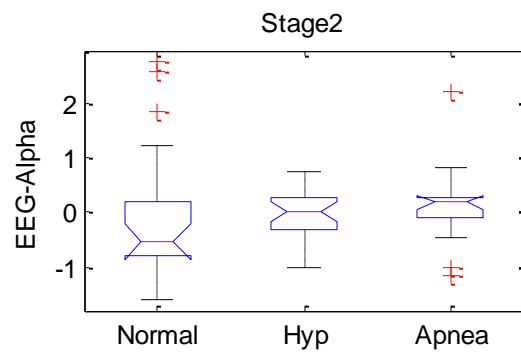
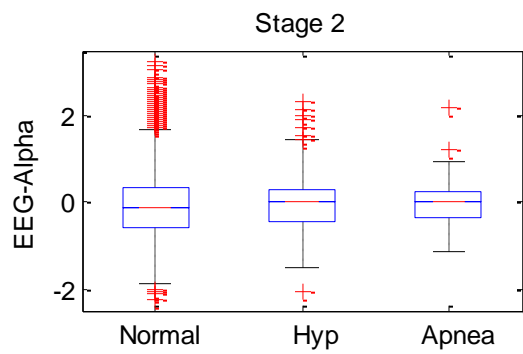
ANOVA Table					
Source	SS	df	MS	F	Prob>F
Groups	1.0718	2	0.5359	1.13	0.3306
Error	28.5208	60	0.47535		
Total	29.5926	62			



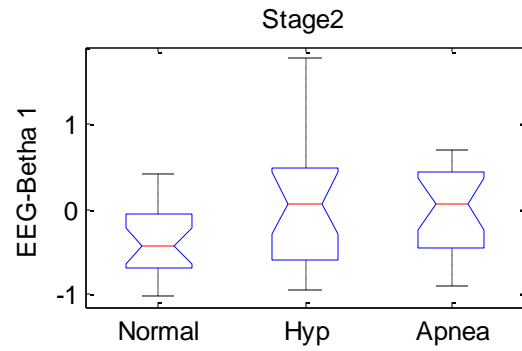
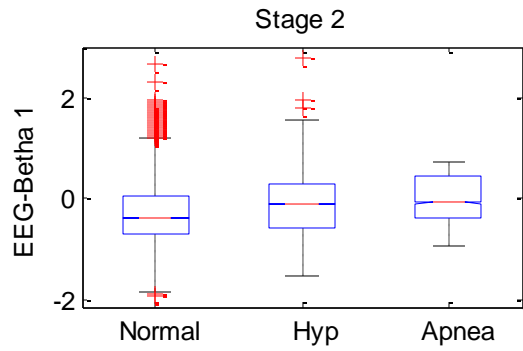
ANOVA Table					
Source	SS	df	MS	F	Prob>F
Groups	0.4458	2	0.2229	0.45	0.6411
Error	29.857	60	0.49762		
Total	30.3028	62			



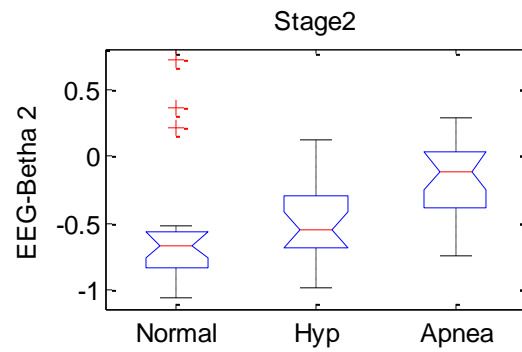
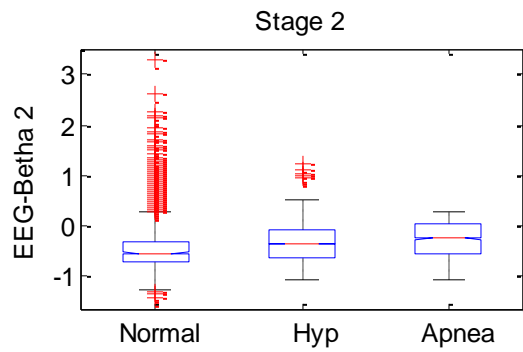
ANOVA Table					
Source	SS	df	MS	F	Prob>F
Groups	0.7324	2	0.36621	0.68	0.5098
Error	32.2496	60	0.53749		
Total	32.982	62			



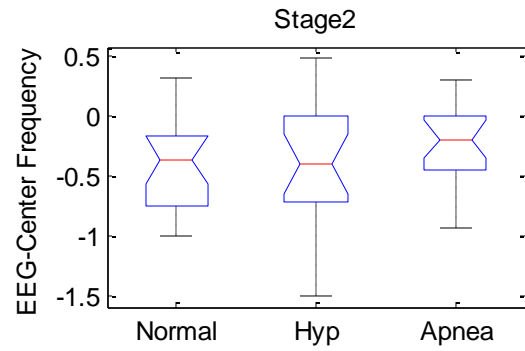
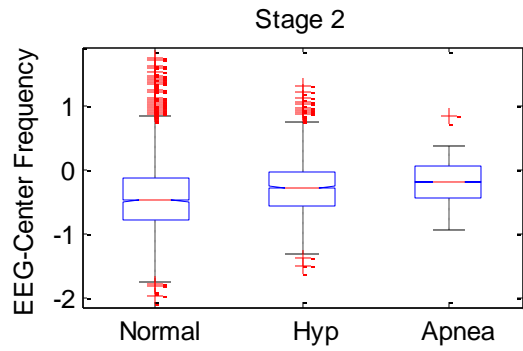
ANOVA Table					
Source	SS	df	MS	F	Prob>F
Groups	0.5382	2	0.26912	0.38	0.6886
Error	43.0124	60	0.71687		
Total	43.5507	62			



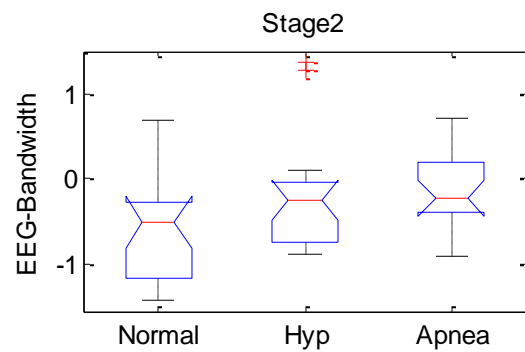
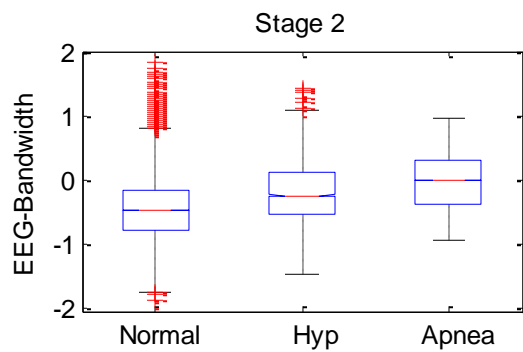
ANOVA Table					
Source	SS	df	MS	F	Prob>F
Groups	1.9429	2	0.97145	2.83	0.067
Error	20.6046	60	0.34341		
Total	22.5475	62			



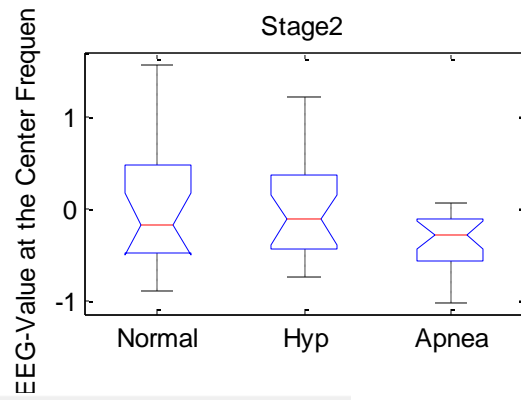
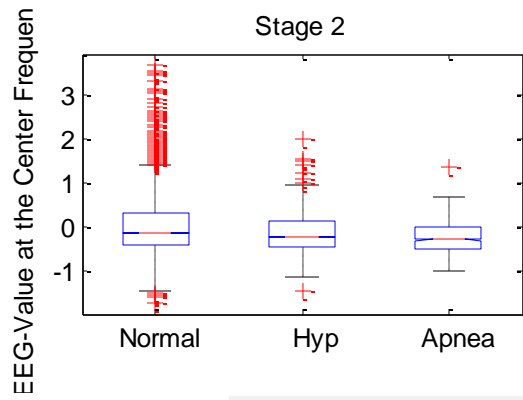
ANOVA Table					
Source	SS	df	MS	F	Prob>F
Groups	1.58753	2	0.79376	6.18	0.0036
Error	7.70655	60	0.12844		
Total	9.29408	62			



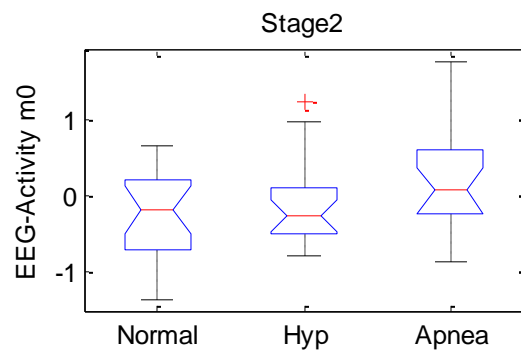
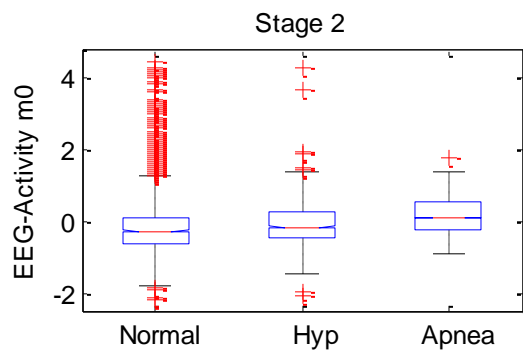
ANOVA Table					
Source	SS	df	MS	F	Prob>F
Groups	0.3107	2	0.15533	0.84	0.4353
Error	11.0516	60	0.18419		
Total	11.3623	62			



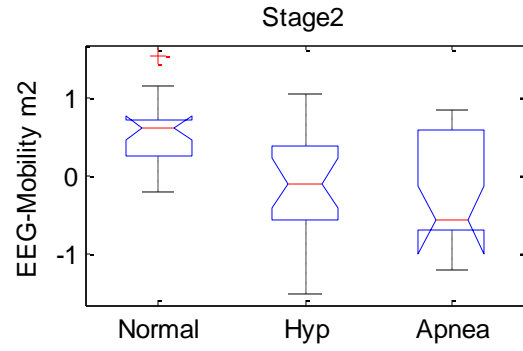
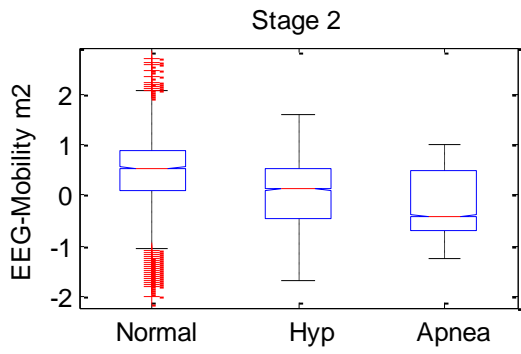
ANOVA Table					
Source	SS	df	MS	F	Prob>F
Groups	2.748	2	1.37401	4.33	0.0176
Error	19.0521	60	0.31754		
Total	21.8001	62			



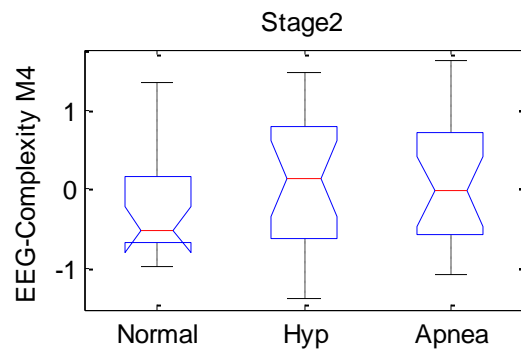
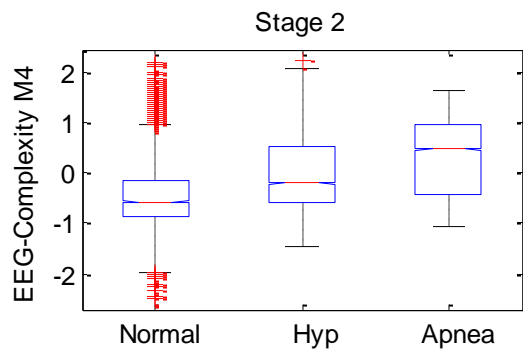
ANOVA Table					
Source	SS	df	MS	F	Prob>F
Groups	1.8512	2	0.92559	3.29	0.0443
Error	16.9042	60	0.28174		
Total	18.7554	62			



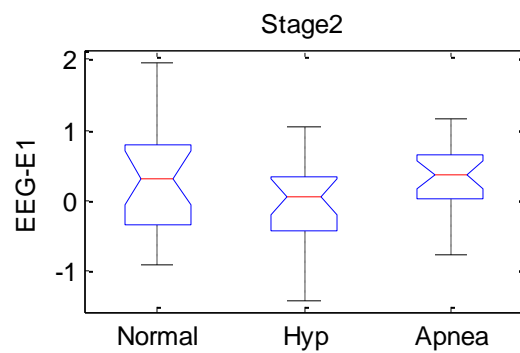
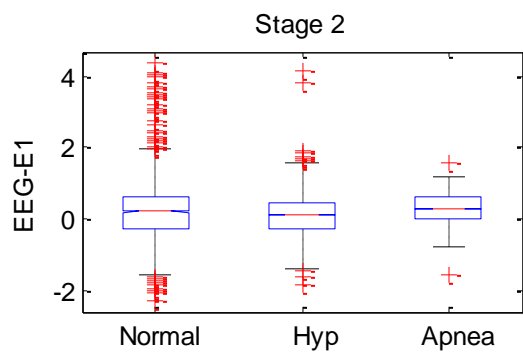
ANOVA Table					
Source	SS	df	MS	F	Prob>F
Groups	2.4061	2	1.20303	3.19	0.0483
Error	22.6362	60	0.37727		
Total	25.0423	62			



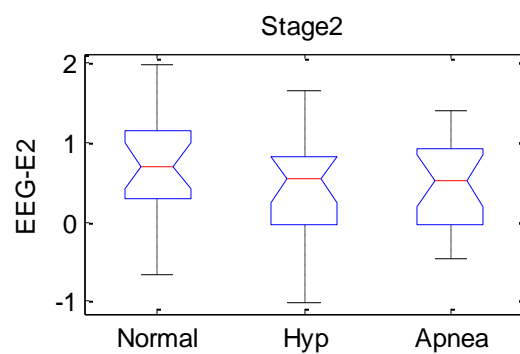
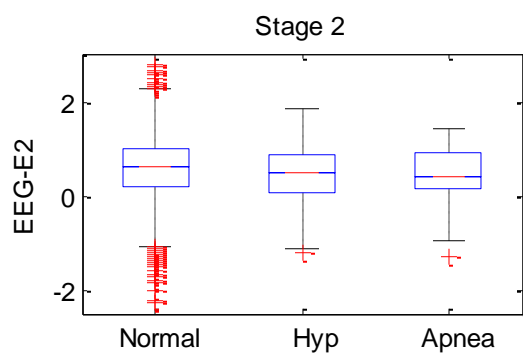
ANOVA Table					
Source	SS	df	MS	F	Prob>F
Groups	7.8061	2	3.90303	10.28	0.0001
Error	22.7763	60	0.3796		
Total	30.5824	62			



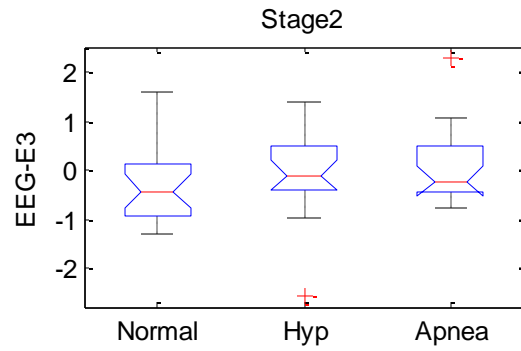
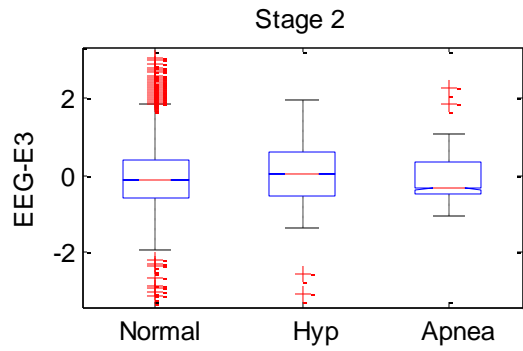
ANOVA Table					
Source	SS	df	MS	F	Prob>F
Groups	2.239	2	1.11952	1.72	0.1872
Error	38.9753	60	0.64959		
Total	41.2144	62			



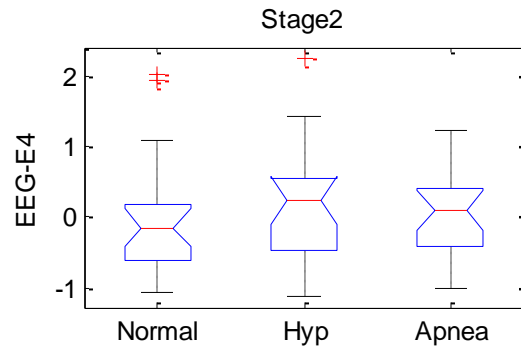
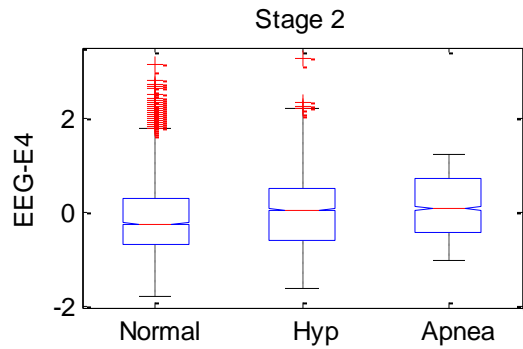
ANOVA Table					
Source	SS	df	MS	F	Prob>F
Groups	1.1291	2	0.56454	1.39	0.2578
Error	24.4281	60	0.40714		
Total	25.5572	62			



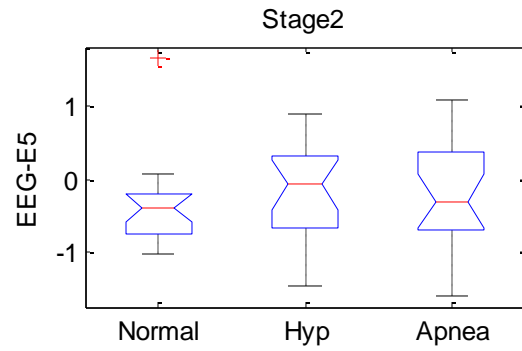
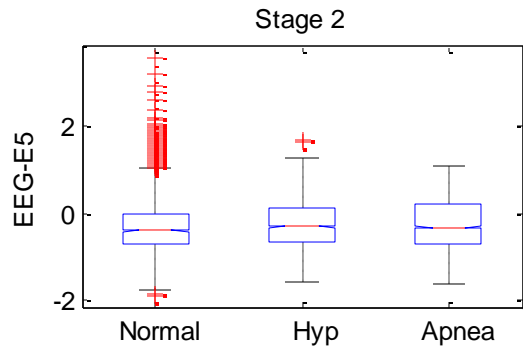
ANOVA Table					
Source	SS	df	MS	F	Prob>F
Groups	0.5448	2	0.27238	0.7	0.5028
Error	23.4999	60	0.39167		
Total	24.0447	62			



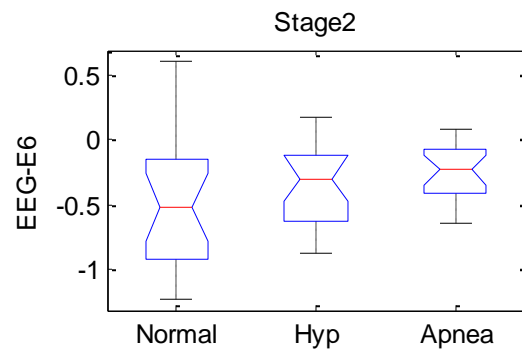
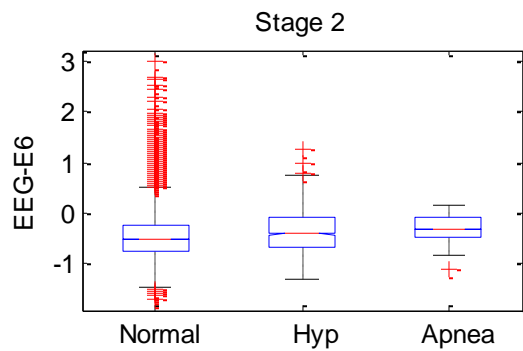
ANOVA Table					
Source	SS	df	MS	F	Prob>F
Groups	1.7706	2	0.88529	1.5	0.2304
Error	35.307	60	0.58845		
Total	37.0776	62			



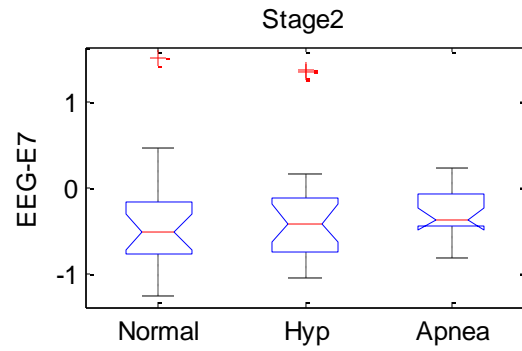
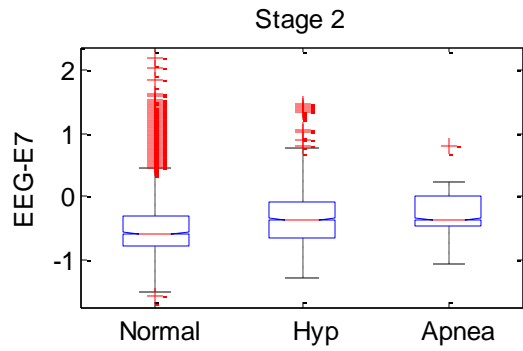
ANOVA Table					
Source	SS	df	MS	F	Prob>F
Groups	0.545	2	0.27248	0.44	0.6463
Error	37.1866	60	0.61978		
Total	37.7316	62			



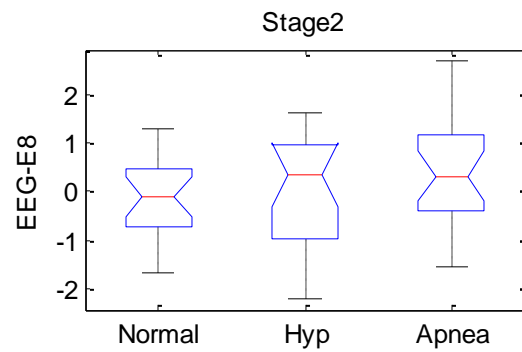
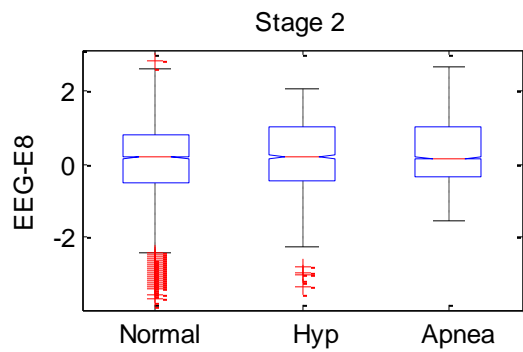
ANOVA Table					
Source	SS	df	MS	F	Prob>F
Groups	0.5859	2	0.29297	0.77	0.4687
Error	22.9072	60	0.38179		
Total	23.4932	62			



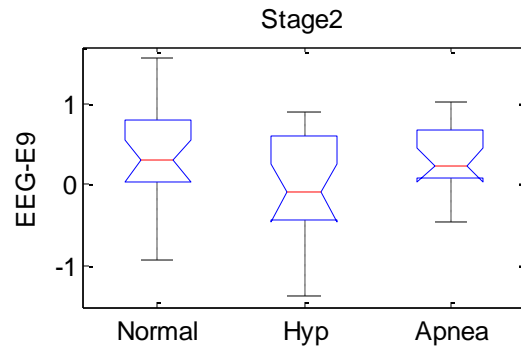
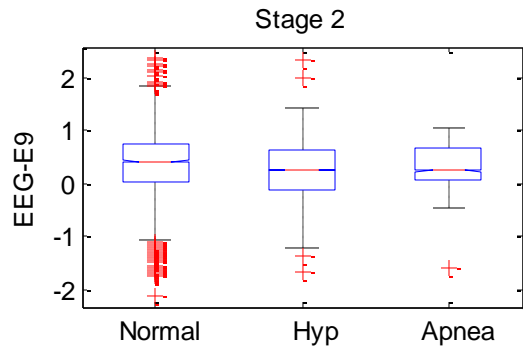
ANOVA Table					
Source	SS	df	MS	F	Prob>F
Groups	0.56815	2	0.28408	2.2	0.1202
Error	7.76369	60	0.12939		
Total	8.33184	62			



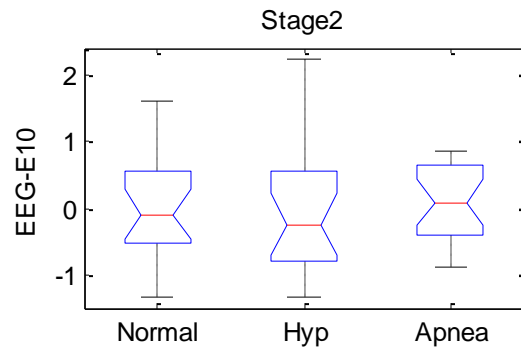
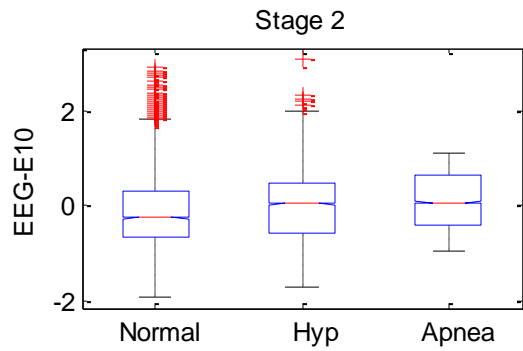
ANOVA Table					
Source	SS	df	MS	F	Prob>F
Groups	0.0948	2	0.04741	0.17	0.8448
Error	16.8222	60	0.28037		
Total	16.917	62			



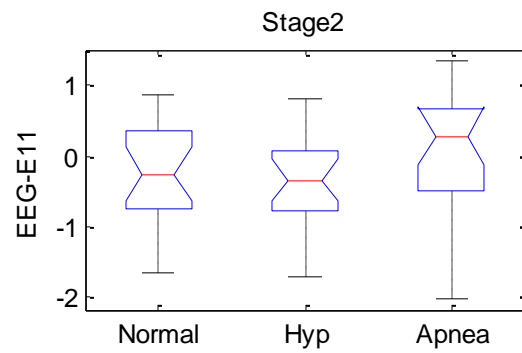
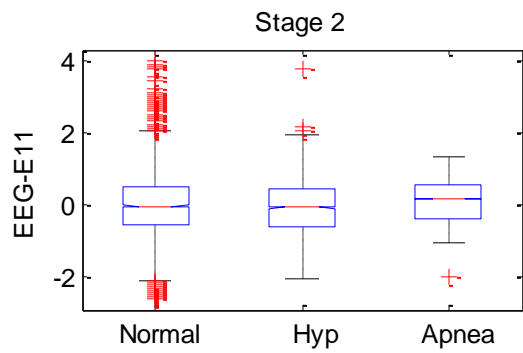
ANOVA Table					
Source	SS	df	MS	F	Prob>F
Groups	2.5504	2	1.27521	1.29	0.2838
Error	59.476	60	0.99127		
Total	62.0264	62			



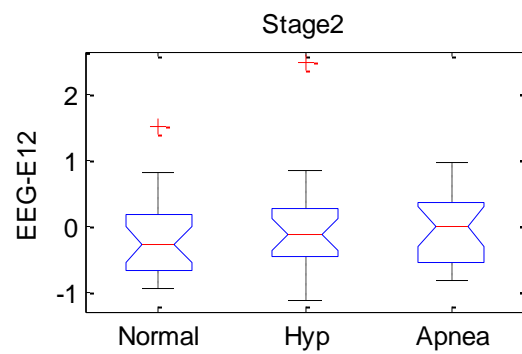
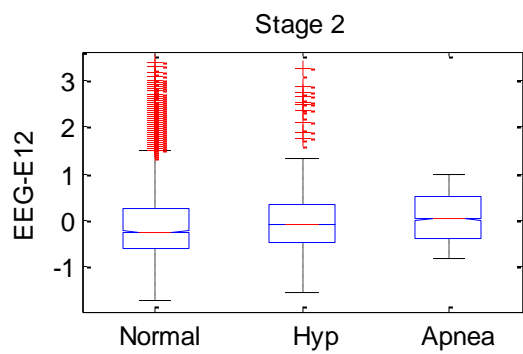
ANOVA Table					
Source	SS	df	MS	F	Prob>F
Groups	1.8316	2	0.91581	2.96	0.0595
Error	18.5747	60	0.30958		
Total	20.4063	62			



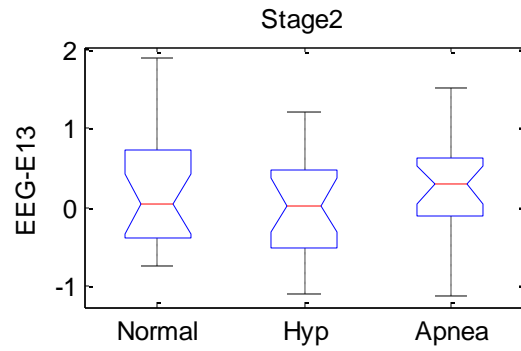
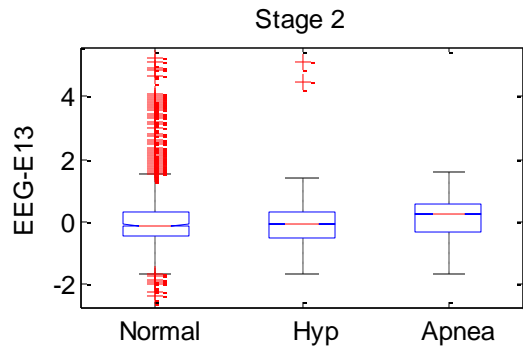
ANOVA Table					
Source	SS	df	MS	F	Prob>F
Groups	0.3108	2	0.15539	0.25	0.7799
Error	37.3496	60	0.62249		
Total	37.6604	62			



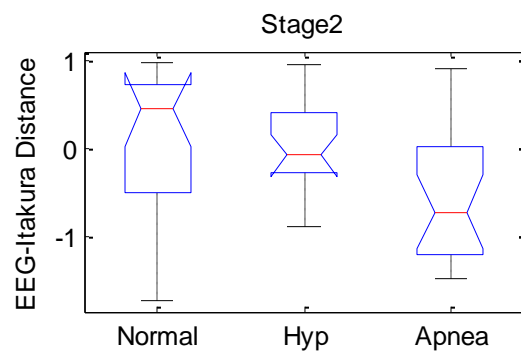
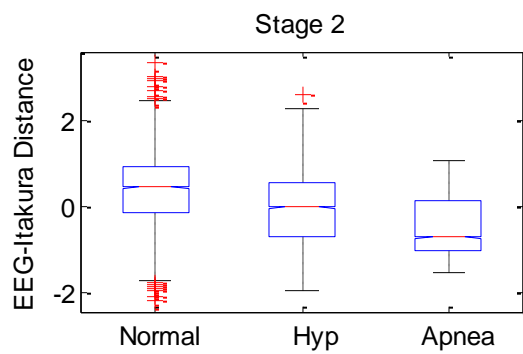
ANOVA Table					
Source	SS	df	MS	F	Prob>F
Groups	2.4551	2	1.22756	2.2	0.1201
Error	33.5442	60	0.55907		
Total	35.9994	62			



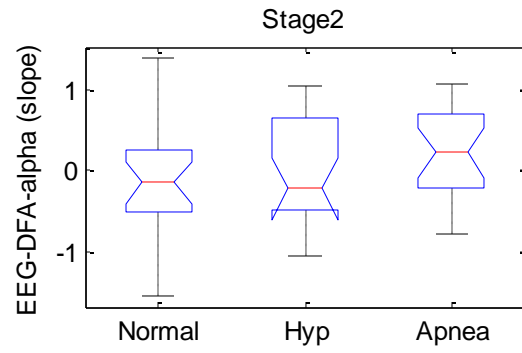
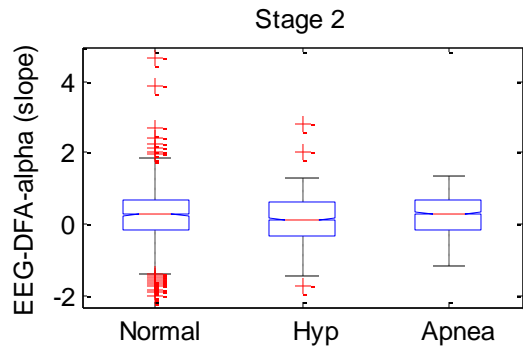
ANOVA Table					
Source	SS	df	MS	F	Prob>F
Groups	0.2536	2	0.1268	0.29	0.7476
Error	26.0259	60	0.43376		
Total	26.2795	62			



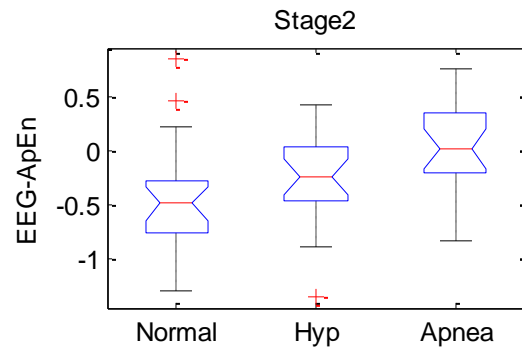
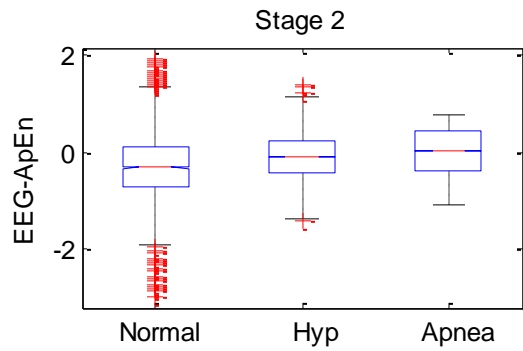
ANOVA Table					
Source	SS	df	MS	F	Prob>F
Groups	0.5179	2	0.25895	0.57	0.5689
Error	27.2859	60	0.45477		
Total	27.8038	62			



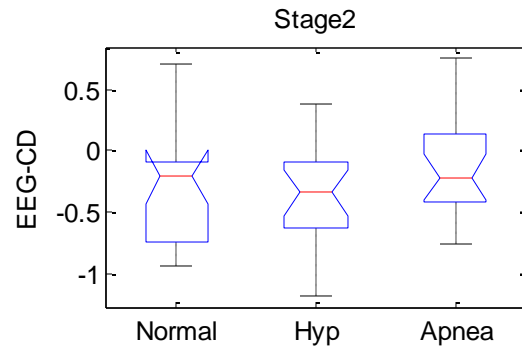
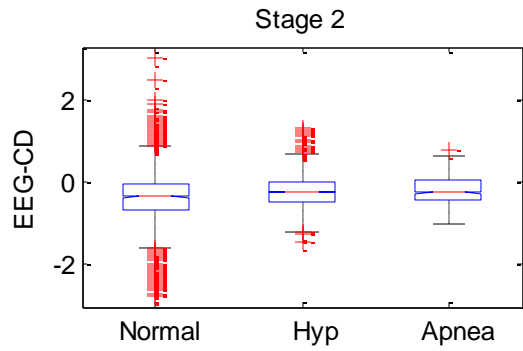
ANOVA Table					
Source	SS	df	MS	F	Prob>F
Groups	5.5875	2	2.79373	5.93	0.0045
Error	28.2661	60	0.4711		
Total	33.8536	62			



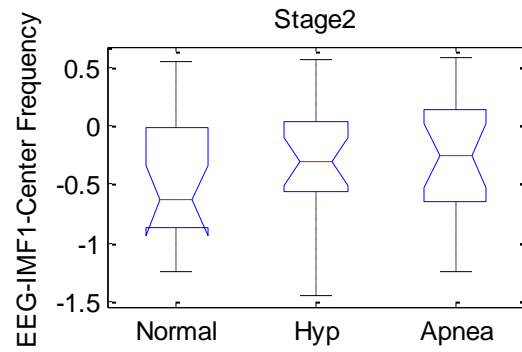
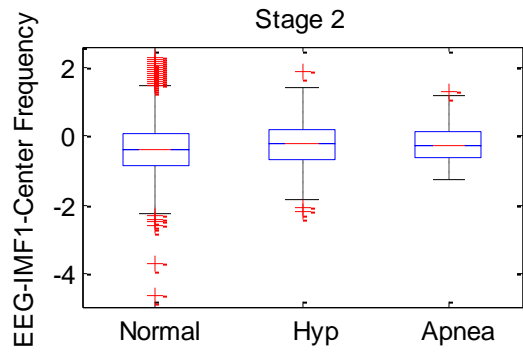
ANOVA Table					
Source	SS	df	MS	F	Prob>F
Groups	0.7841	2	0.39204	0.96	0.3885
Error	24.492	60	0.4082		
Total	25.2761	62			



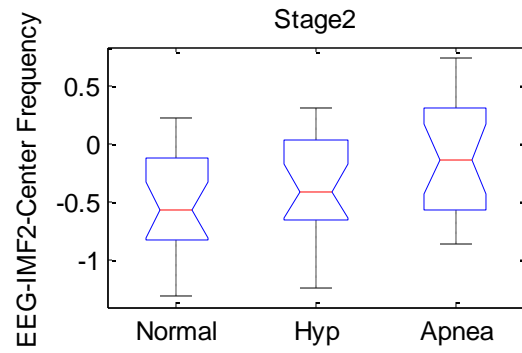
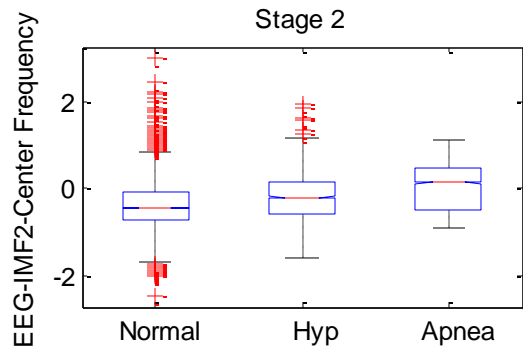
ANOVA Table					
Source	SS	df	MS	F	Prob>F
Groups	2.5631	2	1.28155	6.22	0.0035
Error	12.3576	60	0.20596		
Total	14.9207	62			



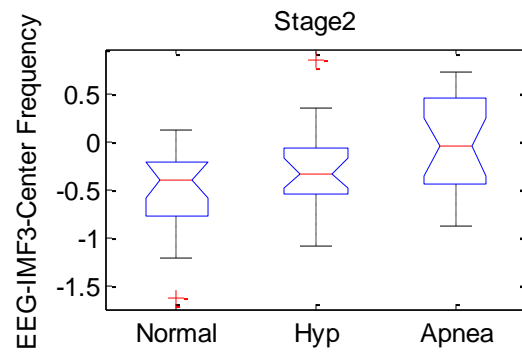
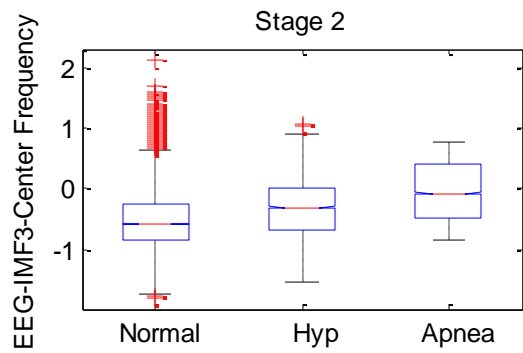
ANOVA Table					
Source	SS	df	MS	F	Prob>F
Groups	0.622	2	0.31099	1.84	0.1679
Error	10.1481	60	0.16914		
Total	10.7701	62			



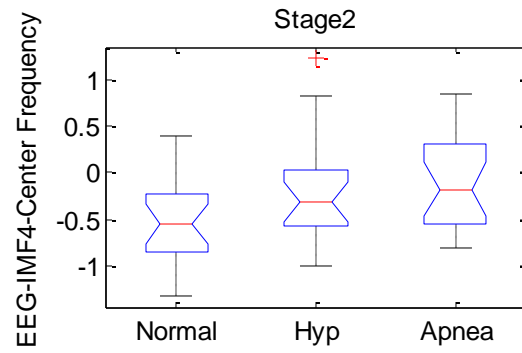
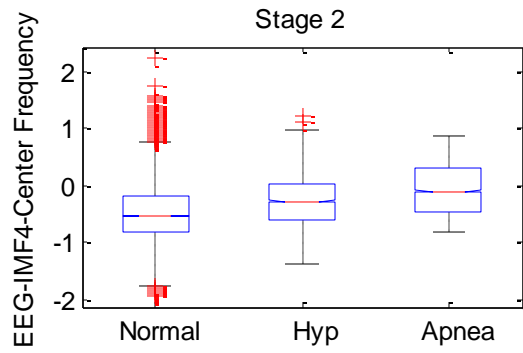
ANOVA Table					
Source	SS	df	MS	F	Prob>F
Groups	0.3637	2	0.18184	0.68	0.5122
Error	16.1281	60	0.2688		
Total	16.4918	62			



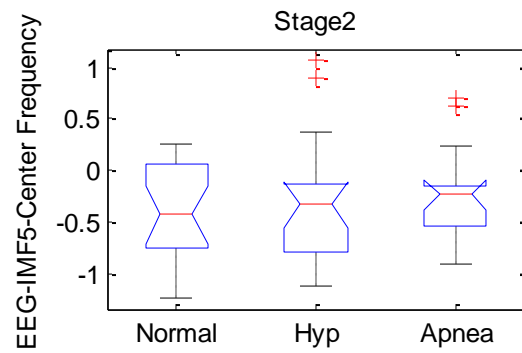
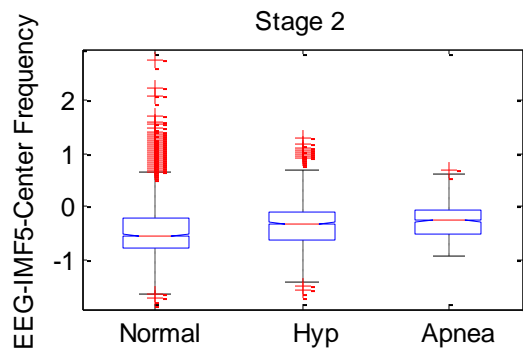
ANOVA Table					
Source	SS	df	MS	F	Prob>F
Groups	1.7311	2	0.86555	3.98	0.0238
Error	13.0403	60	0.21734		
Total	14.7714	62			



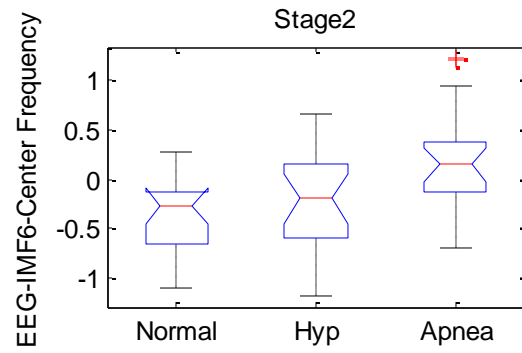
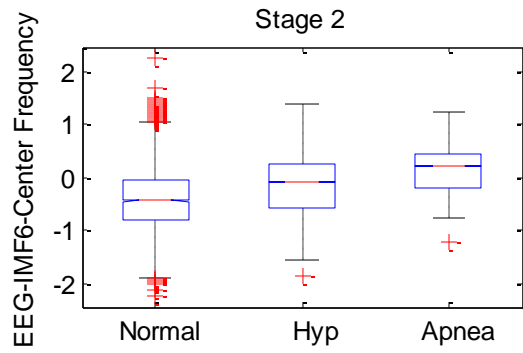
ANOVA Table					
Source	SS	df	MS	F	Prob>F
Groups	2.2195	2	1.10976	5.6	0.0059
Error	11.8922	60	0.1982		
Total	14.1117	62			



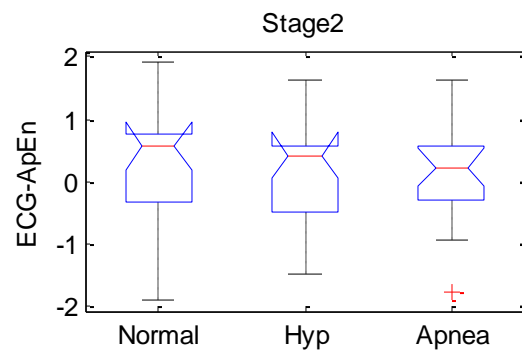
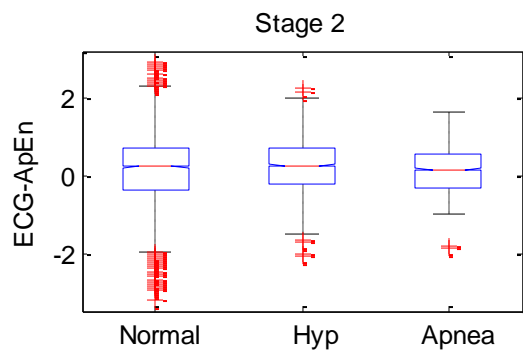
ANOVA Table					
Source	SS	df	MS	F	Prob>F
Groups	2.2081	2	1.10403	4.32	0.0177
Error	15.3458	60	0.25576		
Total	17.5538	62			



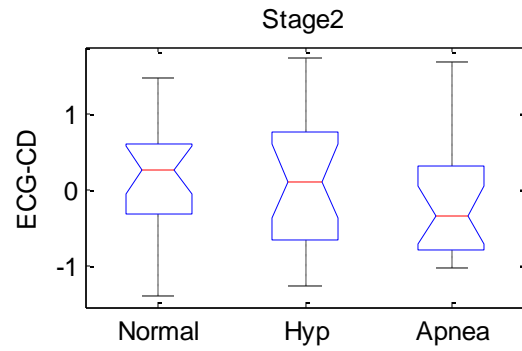
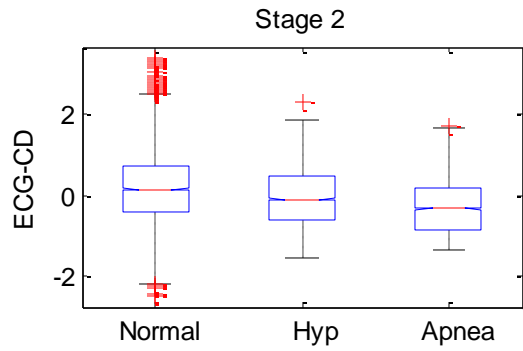
ANOVA Table					
Source	SS	df	MS	F	Prob>F
Groups	0.1825	2	0.09126	0.38	0.686
Error	14.4353	60	0.24059		
Total	14.6178	62			



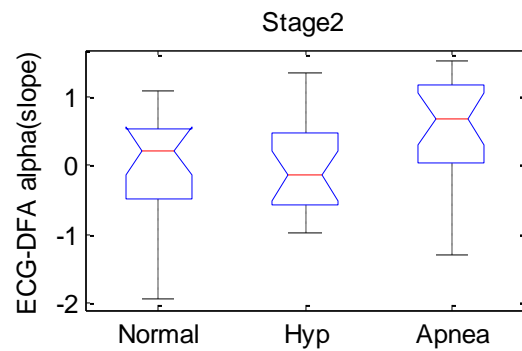
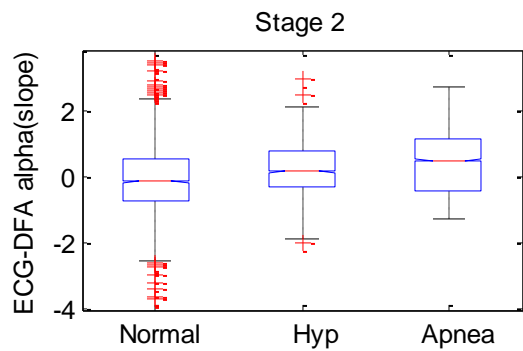
ANOVA Table					
Source	SS	df	MS	F	Prob>F
Groups	3.7824	2	1.89118	6.31	0.0032
Error	17.9731	60	0.29955		
Total	21.7554	62			



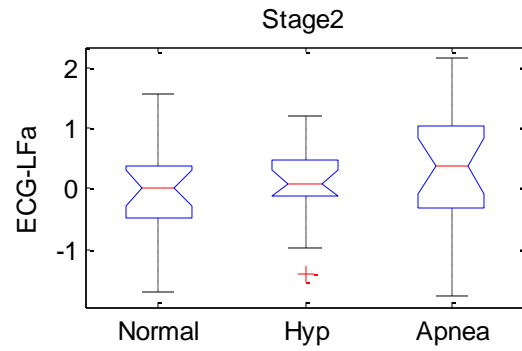
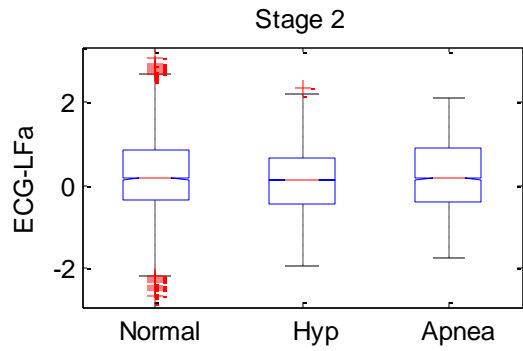
ANOVA Table					
Source	SS	df	MS	F	Prob>F
Groups	0.8199	2	0.40997	0.68	0.5104
Error	36.165	60	0.60275		
Total	36.985	62			



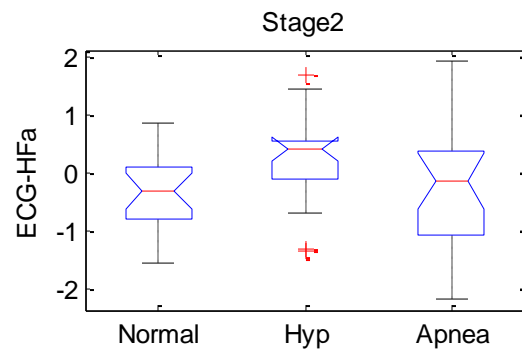
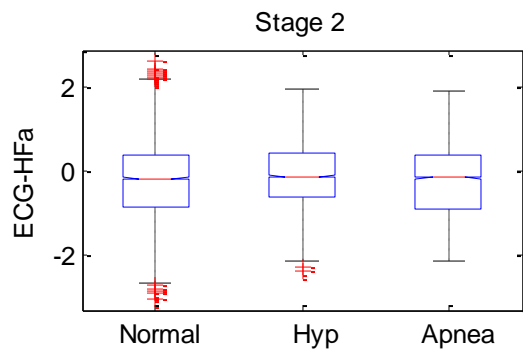
ANOVA Table					
Source	SS	df	MS	F	Prob>F
Groups	1.5419	2	0.77093	1.25	0.2937
Error	36.988	60	0.61647		
Total	38.5299	62			



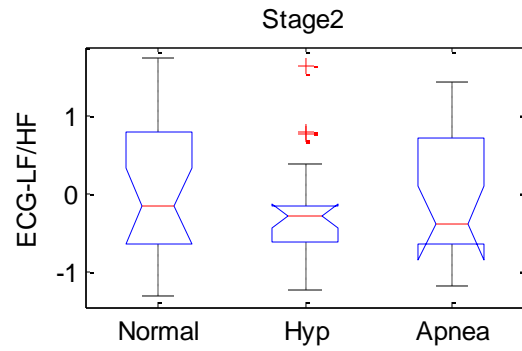
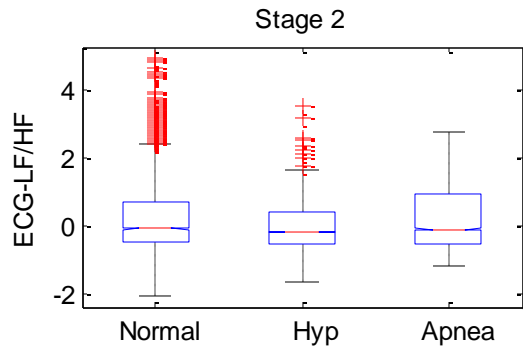
ANOVA Table					
Source	SS	df	MS	F	Prob>F
Groups	4.5112	2	2.25558	3.62	0.0329
Error	37.4098	60	0.6235		
Total	41.921	62			



ANOVA Table					
Source	SS	df	MS	F	Prob>F
Groups	1.0532	2	0.5266	0.83	0.4389
Error	37.8468	60	0.63078		
Total	38.9001	62			

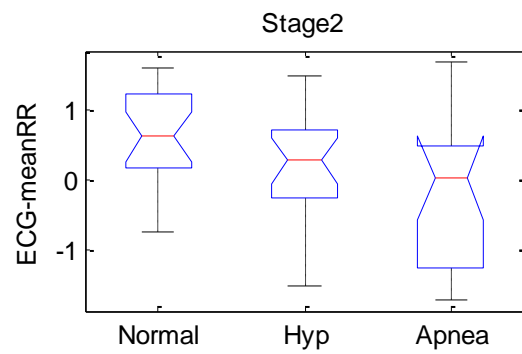
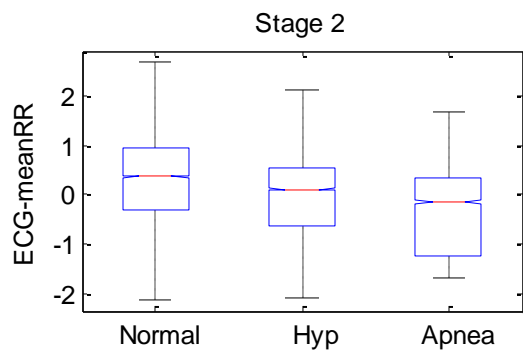


ANOVA Table					
Source	SS	df	MS	F	Prob>F
Groups	4.0072	2	2.00358	3	0.0572
Error	40.036	60	0.66727		
Total	44.0432	62			

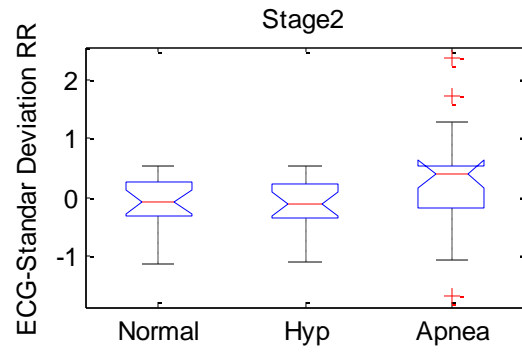
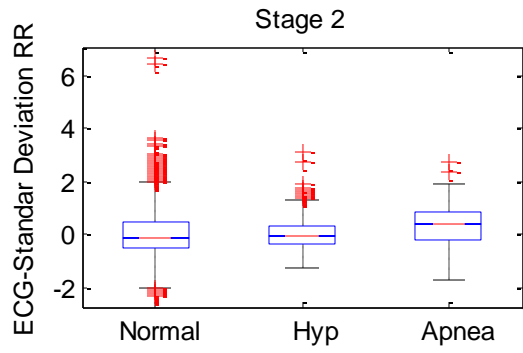


ANOVA Table					
Source	SS	df	MS	F	Prob>F
Groups	0.8341	2	0.41703	0.69	0.5042
Error	36.1204	60	0.60201		
Total	36.9545	62			

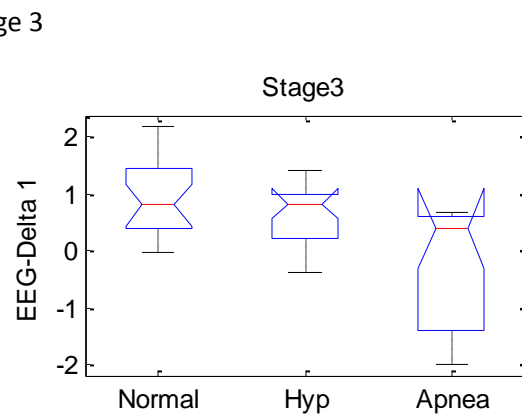
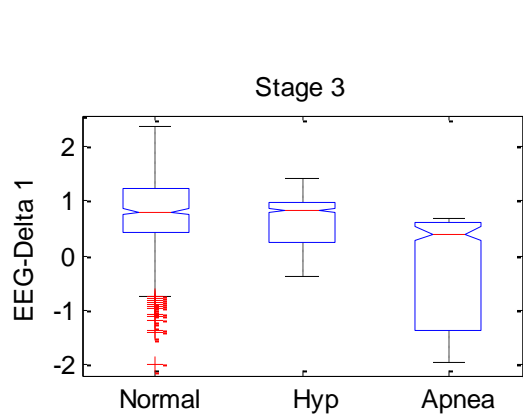
}



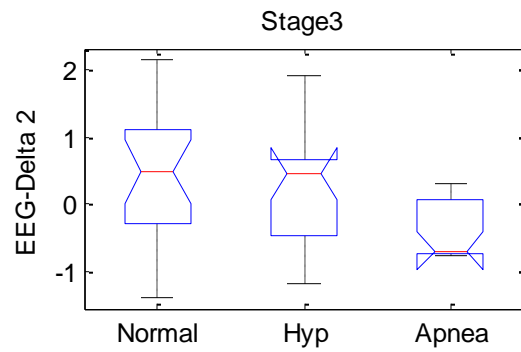
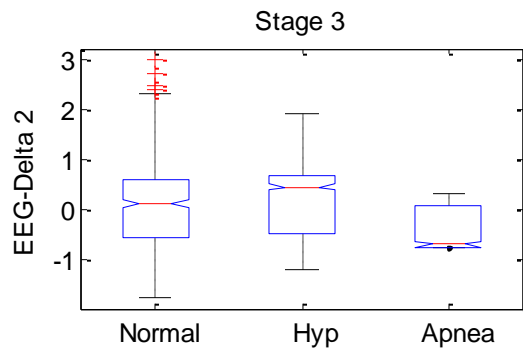
ANOVA Table					
Source	SS	df	MS	F	Prob>F
Groups	6.4836	2	3.24179	4.98	0.01
Error	39.0522	60	0.65087		
Total	45.5358	62			



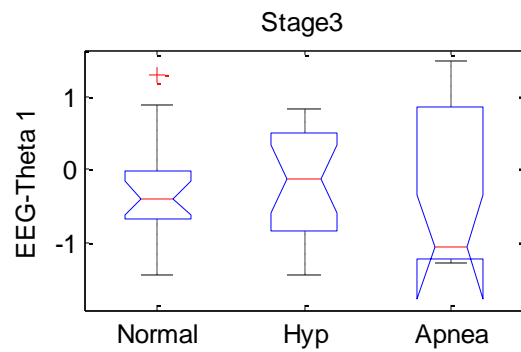
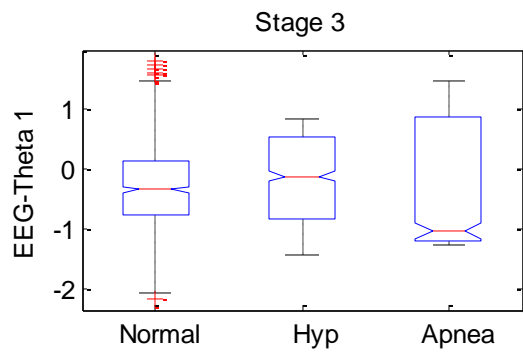
ANOVA Table					
Source	SS	df	MS	F	Prob>F
Groups	1.8136	2	0.90681	2.3	0.1087
Error	23.6208	60	0.39368		
Total	25.4344	62			



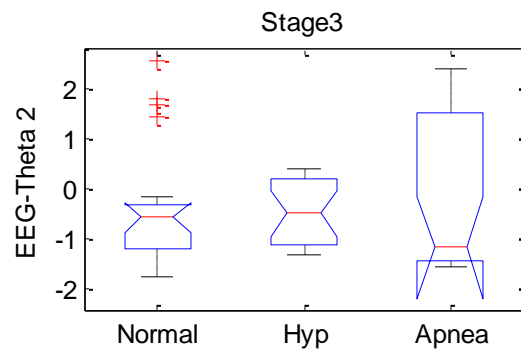
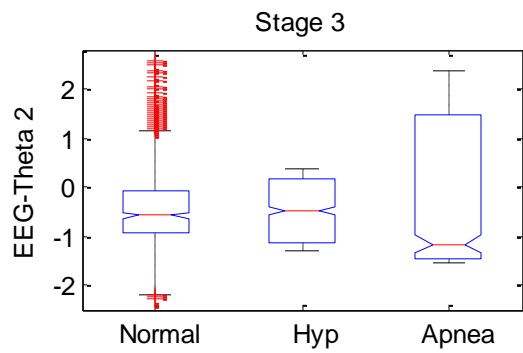
ANOVA Table					
Source	SS	df	MS	F	Prob>F
Groups	4.4245	2	2.21227	4.58	0.0173
Error	16.4117	34	0.4827		
Total	20.8363	36			



ANOVA Table					
Source	SS	df	MS	F	Prob>F
Groups	2.205	2	1.10252	1.16	0.3258
Error	32.3364	34	0.95107		
Total	34.5415	36			

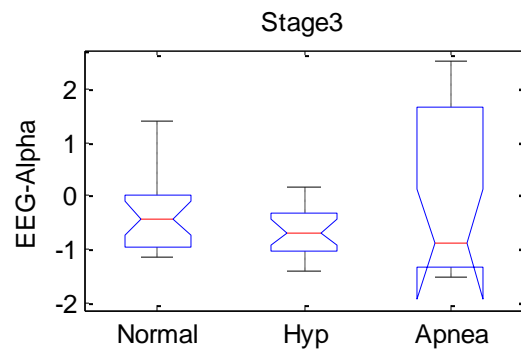
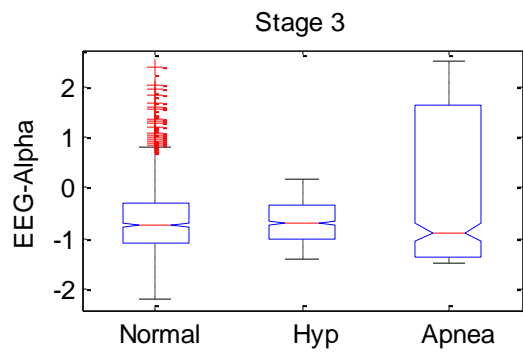


ANOVA Table					
Source	SS	df	MS	F	Prob>F
Groups	0.0194	2	0.0097	0.02	0.9842
Error	20.6882	34	0.60848		
Total	20.7076	36			



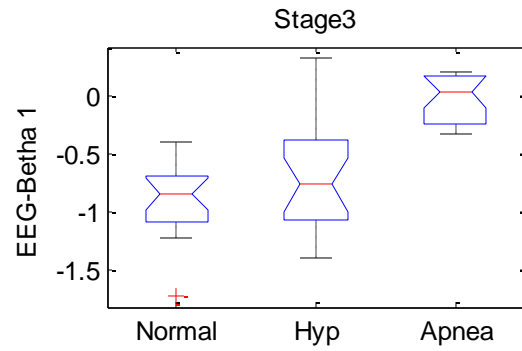
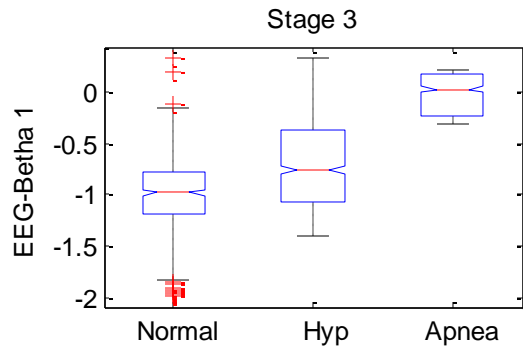
ANOVA Table

Source	SS	df	MS	F	Prob>F
Groups	0.2687	2	0.13436	0.1	0.901
Error	43.6877	34	1.28493		
Total	43.9564	36			

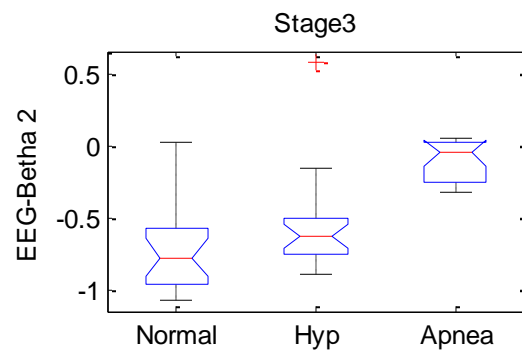
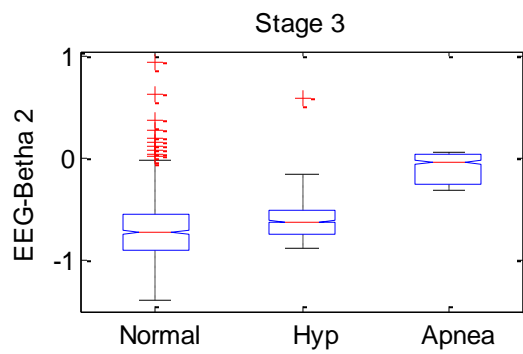


ANOVA Table

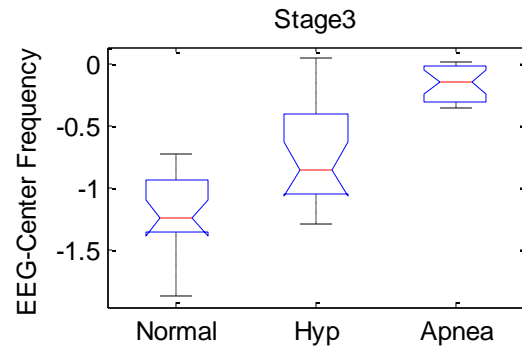
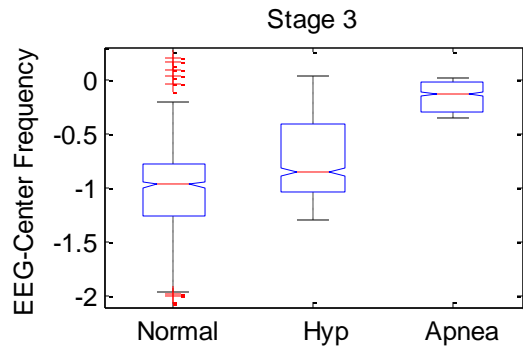
Source	SS	df	MS	F	Prob>F
Groups	1.2327	2	0.61635	1.06	0.3586
Error	19.8221	34	0.583		
Total	21.0548	36			



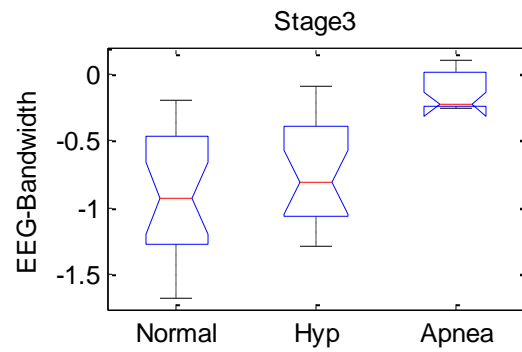
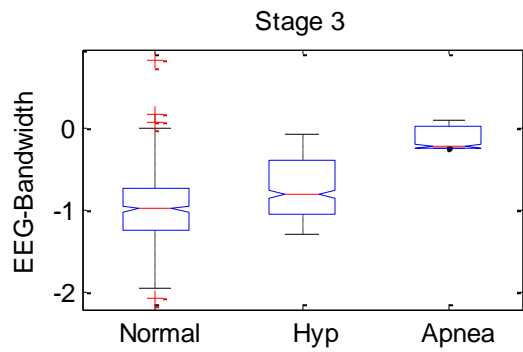
ANOVA Table					
Source	SS	df	MS	F	Prob>F
Groups	1.88087	2	0.94044	6.25	0.0049
Error	5.11861	34	0.15055		
Total	6.99948	36			



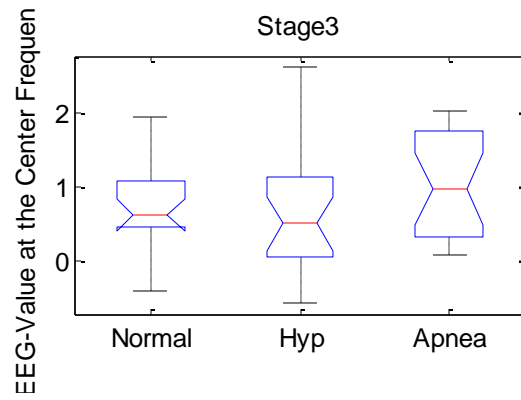
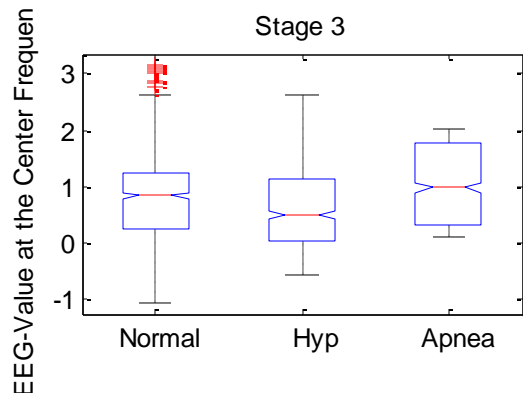
ANOVA Table					
Source	SS	df	MS	F	Prob>F
Groups	1.24031	2	0.62015	6.51	0.004
Error	3.23665	34	0.0952		
Total	4.47696	36			



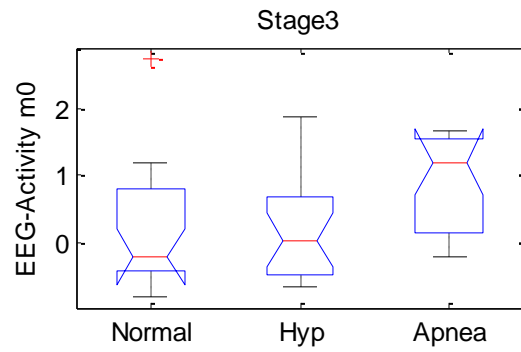
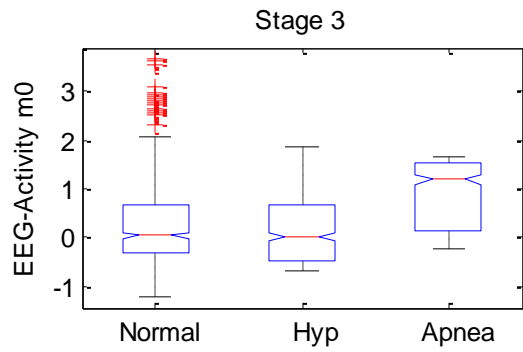
ANOVA Table					
Source	SS	df	MS	F	Prob>F
Groups	3.7181	2	1.85905	16.07	1.22126e-005
Error	3.93279	34	0.11567		
Total	7.65089	36			



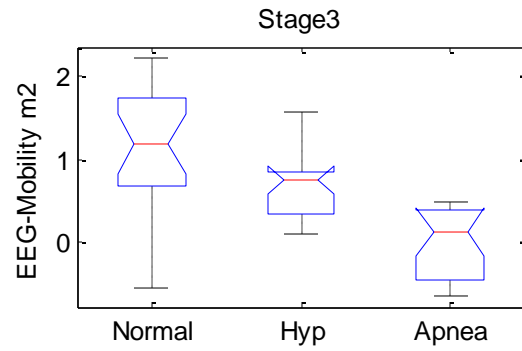
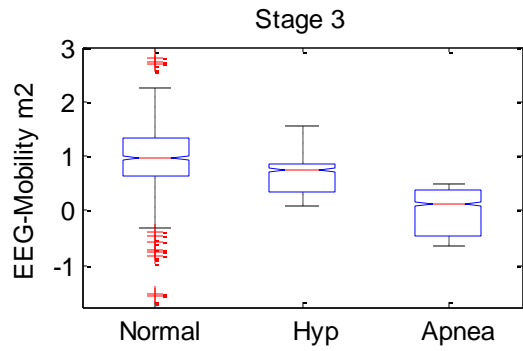
ANOVA Table					
Source	SS	df	MS	F	Prob>F
Groups	1.77639	2	0.8882	4.78	0.0148
Error	6.31195	34	0.18565		
Total	8.08835	36			



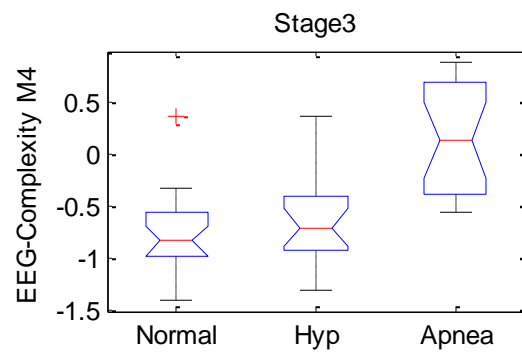
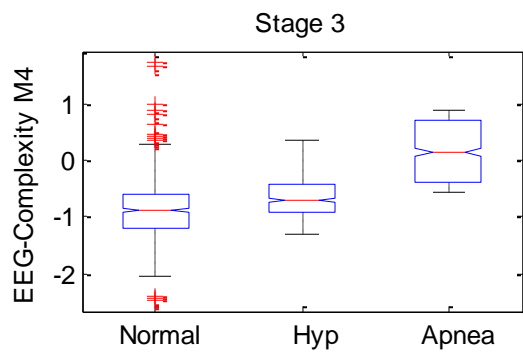
ANOVA Table					
Source	SS	df	MS	F	Prob>F
Groups	0.3365	2	0.16826	0.29	0.753
Error	19.9951	34	0.58809		
Total	20.3316	36			



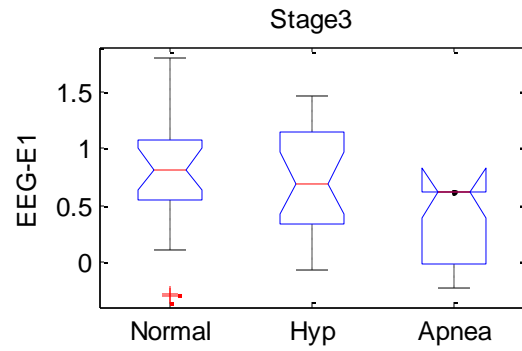
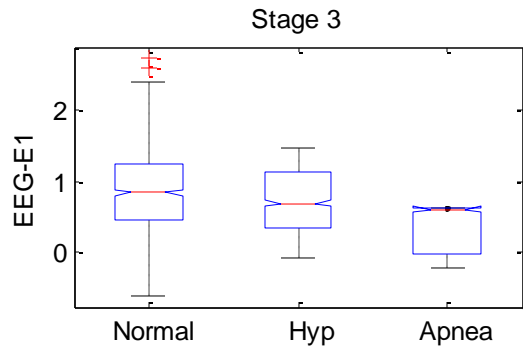
ANOVA Table					
Source	SS	df	MS	F	Prob>F
Groups	1.3095	2	0.65477	0.87	0.4271
Error	25.5195	34	0.75057		
Total	26.829	36			



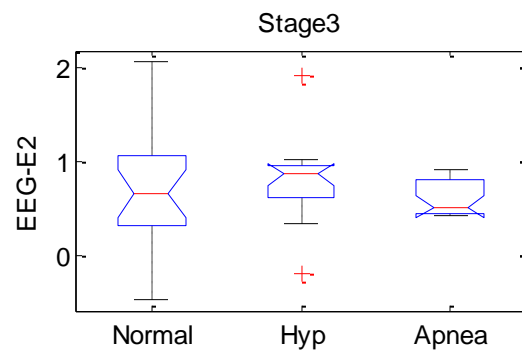
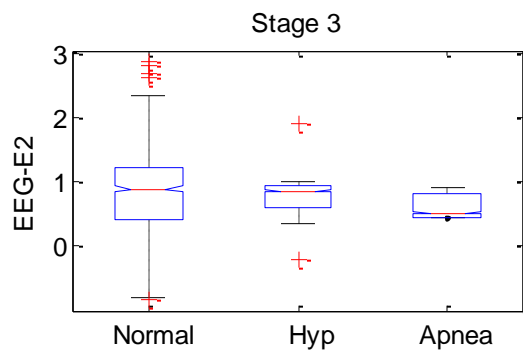
ANOVA Table					
Source	SS	df	MS	F	Prob>F
Groups	4.1522	2	2.07609	4.9	0.0135
Error	14.4095	34	0.42381		
Total	18.5617	36			



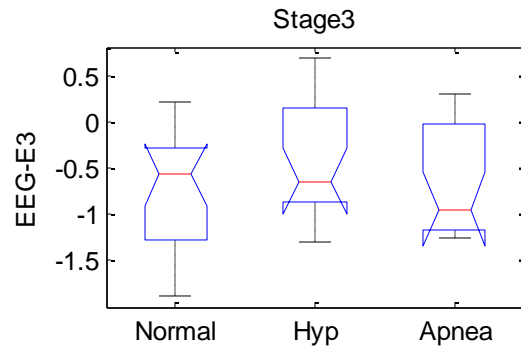
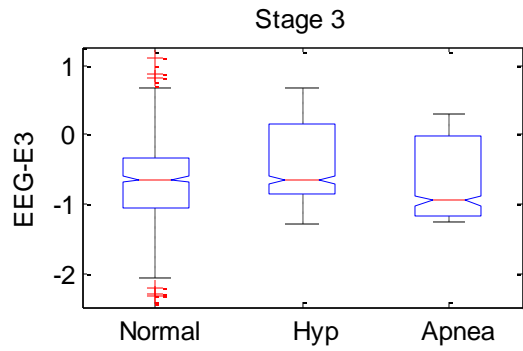
ANOVA Table					
Source	SS	df	MS	F	Prob>F
Groups	2.38078	2	1.19039	5.95	0.0061
Error	6.80741	34	0.20022		
Total	9.18819	36			



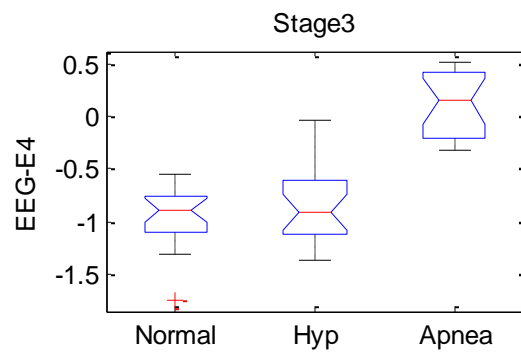
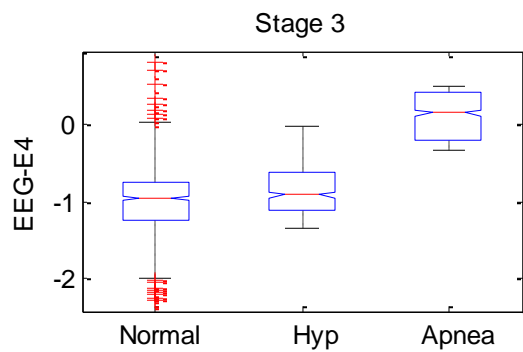
ANOVA Table					
Source	SS	df	MS	F	Prob>F
Groups	0.44521	2	0.2226	0.87	0.4271
Error	8.67631	34	0.25519		
Total	9.12152	36			



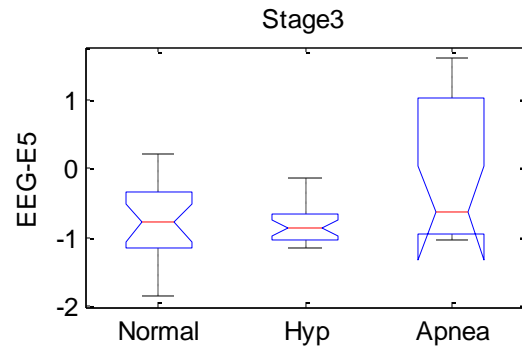
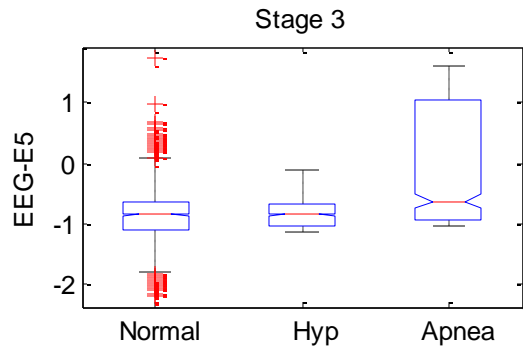
ANOVA Table					
Source	SS	df	MS	F	Prob>F
Groups	0.07189	2	0.03594	0.13	0.8769
Error	9.26719	34	0.27256		
Total	9.33908	36			



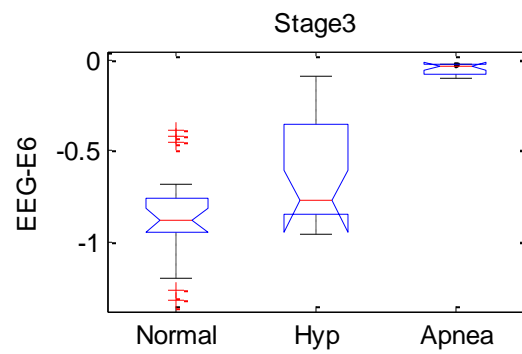
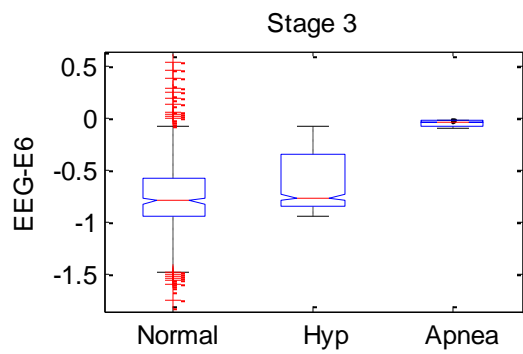
ANOVA Table					
Source	SS	df	MS	F	Prob>F
Groups	0.5828	2	0.29138	0.76	0.4746
Error	13.0034	34	0.38245		
Total	13.5861	36			



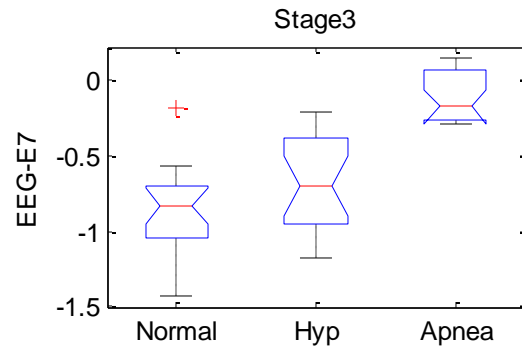
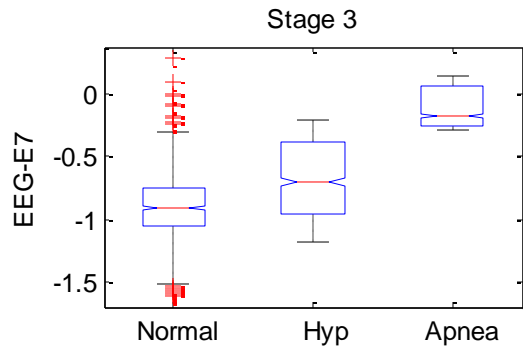
ANOVA Table					
Source	SS	df	MS	F	Prob>F
Groups	2.87369	2	1.43685	12.99	6.44951e-005
Error	3.76138	34	0.11063		
Total	6.63507	36			



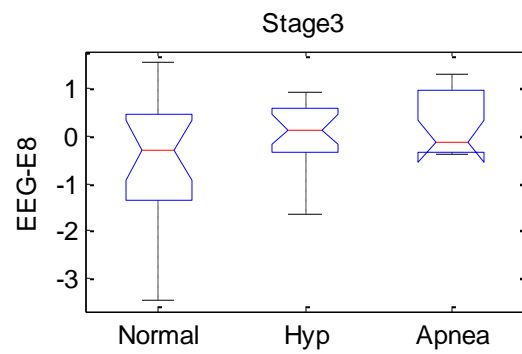
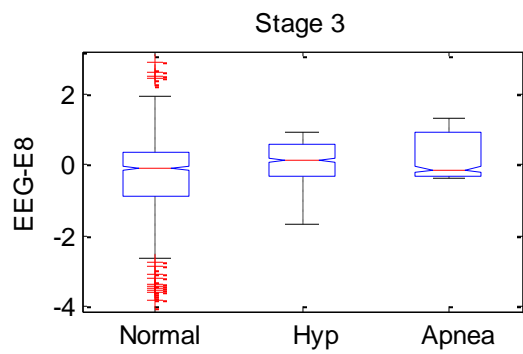
ANOVA Table					
Source	SS	df	MS	F	Prob>F
Groups	1.5292	2	0.76461	2.31	0.1145
Error	11.2452	34	0.33074		
Total	12.7745	36			



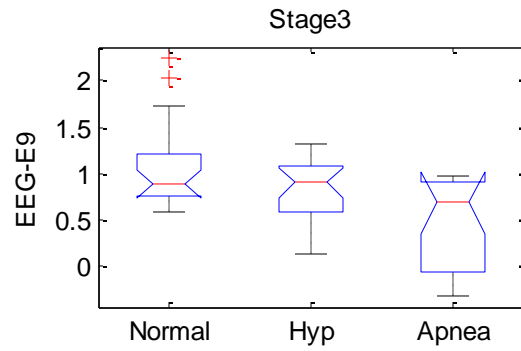
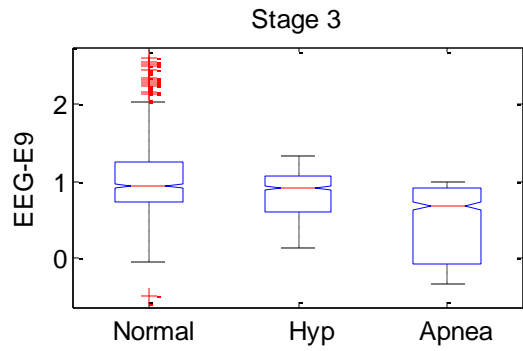
ANOVA Table					
Source	SS	df	MS	F	Prob>F
Groups	1.85837	2	0.92918	13.02	6.33756e-005
Error	2.42665	34	0.07137		
Total	4.28502	36			



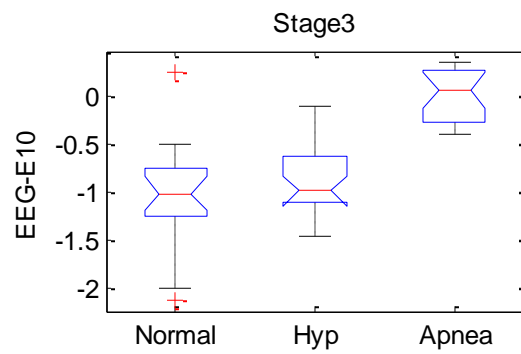
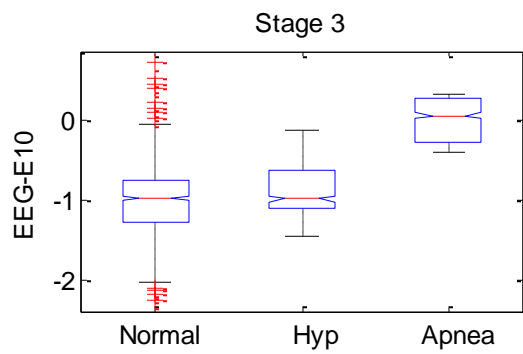
ANOVA Table					
Source	SS	df	MS	F	Prob>F
Groups	1.56006	2	0.78003	9.67	0.0005
Error	2.74334	34	0.08069		
Total	4.3034	36			



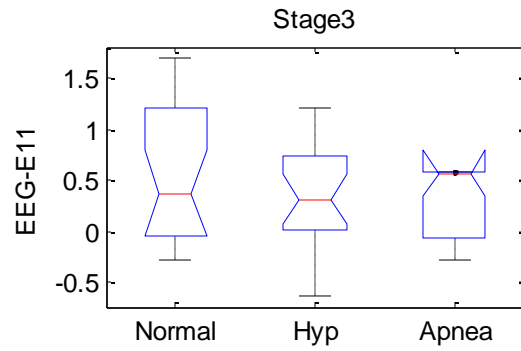
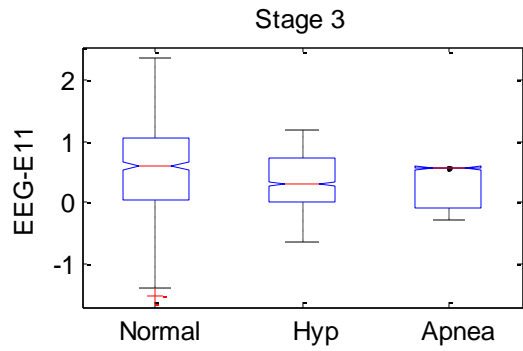
ANOVA Table					
Source	SS	df	MS	F	Prob>F
Groups	3.3234	2	1.66171	1.32	0.281
Error	42.8651	34	1.26074		
Total	46.1885	36			



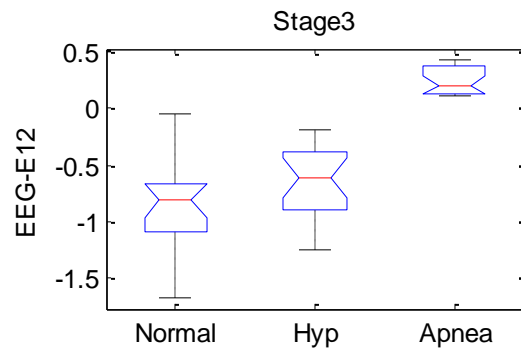
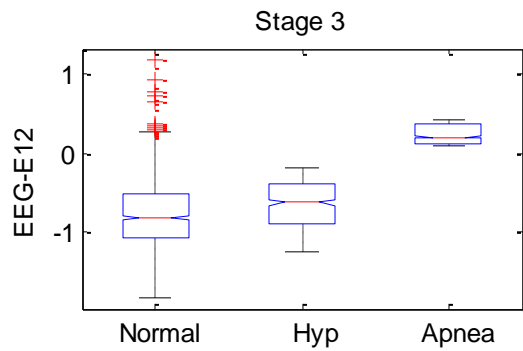
ANOVA Table					
Source	SS	df	MS	F	Prob>F
Groups	1.09852	2	0.54926	2.74	0.0787
Error	6.80972	34	0.20029		
Total	7.90824	36			



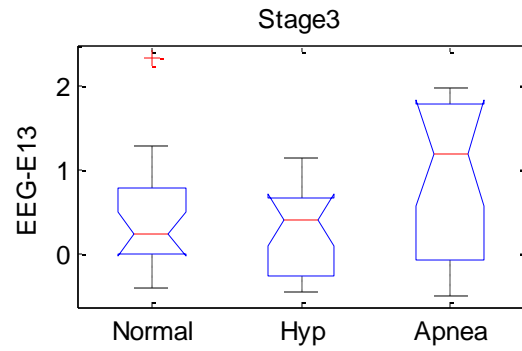
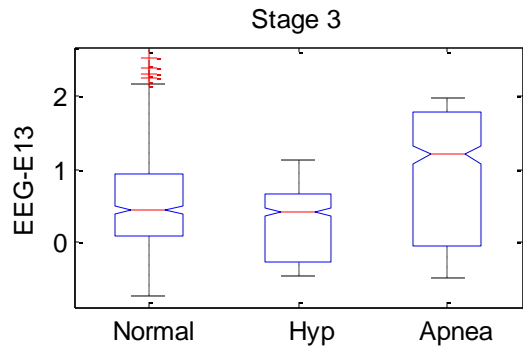
ANOVA Table					
Source	SS	df	MS	F	Prob>F
Groups	2.9098	2	1.45488	6.31	0.0047
Error	7.8397	34	0.23058		
Total	10.7495	36			



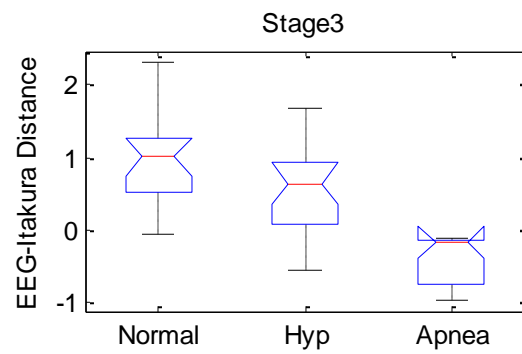
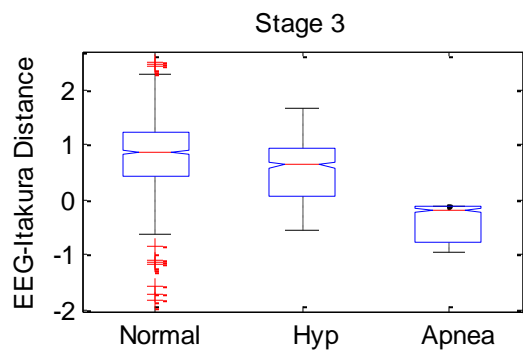
ANOVA Table					
Source	SS	df	MS	F	Prob>F
Groups	0.4691	2	0.23456	0.6	0.5535
Error	13.2483	34	0.38966		
Total	13.7174	36			



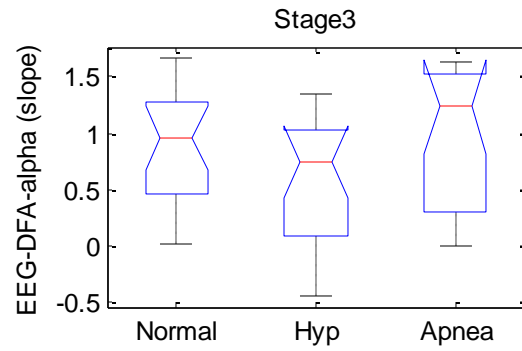
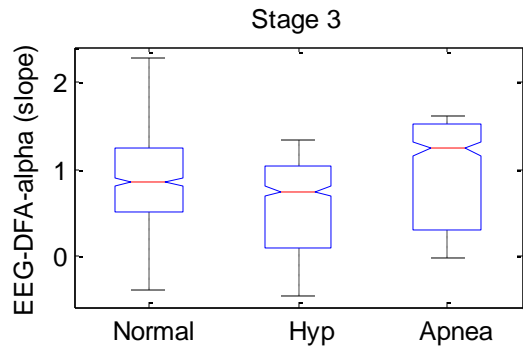
ANOVA Table					
Source	SS	df	MS	F	Prob>F
Groups	3.30337	2	1.65169	14.67	2.54642e-005
Error	3.82727	34	0.11257		
Total	7.13065	36			



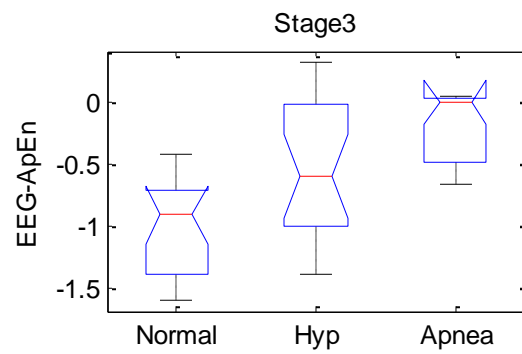
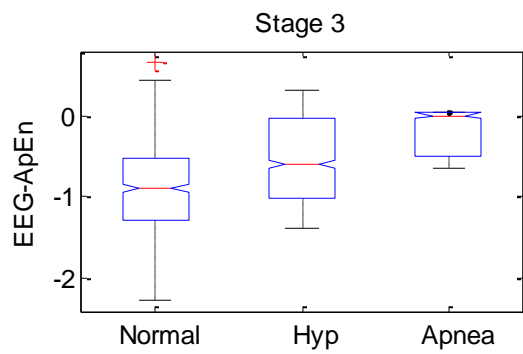
ANOVA Table					
Source	SS	df	MS	F	Prob>F
Groups	0.9665	2	0.48323	1.09	0.3464
Error	15.0173	34	0.44168		
Total	15.9837	36			



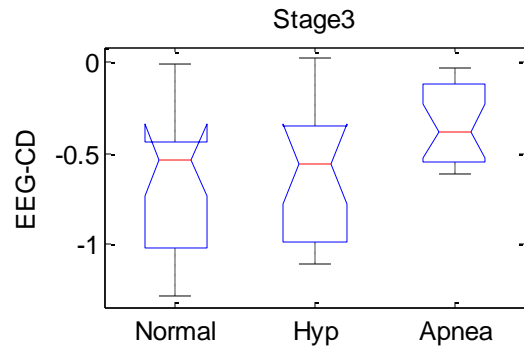
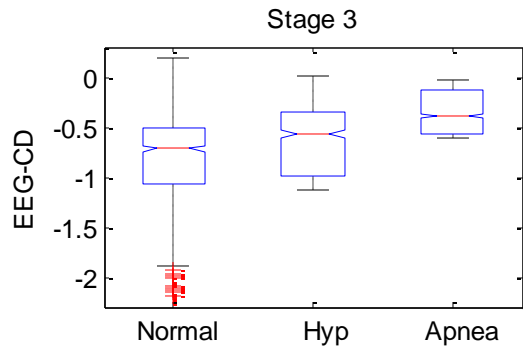
ANOVA Table					
Source	SS	df	MS	F	Prob>F
Groups	5.2881	2	2.64403	8.39	0.0011
Error	10.714	34	0.31512		
Total	16.0021	36			



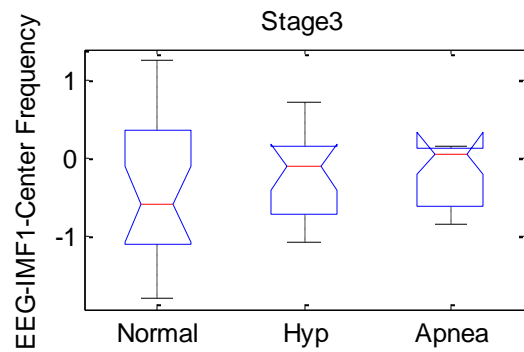
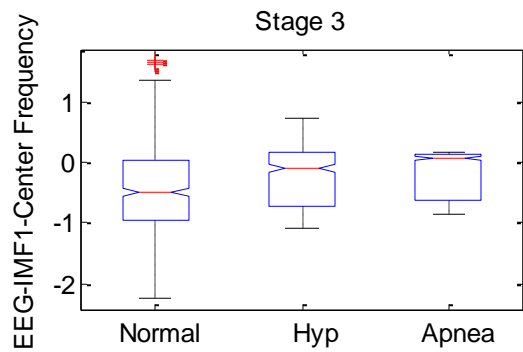
ANOVA Table					
Source	SS	df	MS	F	Prob>F
Groups	1.0319	2	0.51597	1.6	0.2163
Error	10.9507	34	0.32208		
Total	11.9827	36			



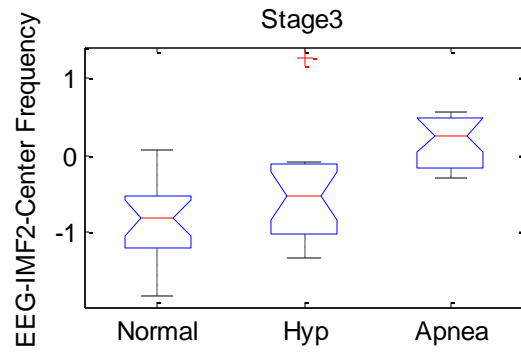
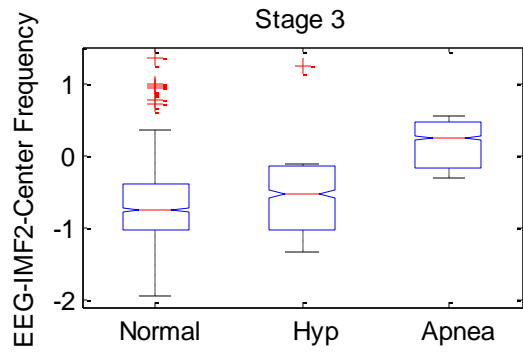
ANOVA Table					
Source	SS	df	MS	F	Prob>F
Groups	2.70536	2	1.35268	6.78	0.0033
Error	6.78785	34	0.19964		
Total	9.49321	36			



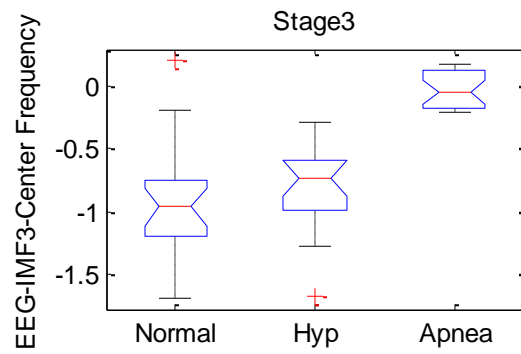
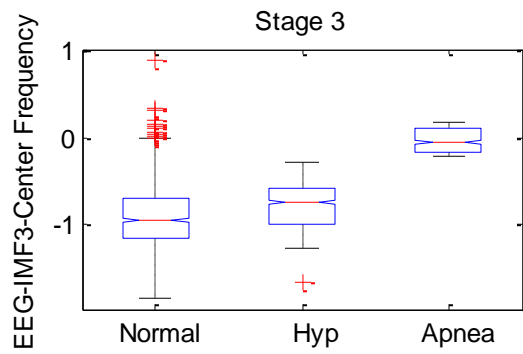
ANOVA Table					
Source	SS	df	MS	F	Prob>F
Groups	0.27399	2	0.13699	1.16	0.3251
Error	4.00996	34	0.11794		
Total	4.28395	36			



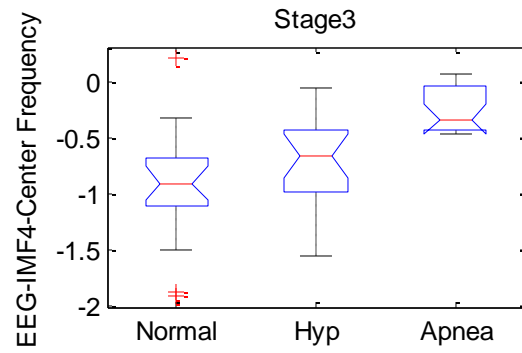
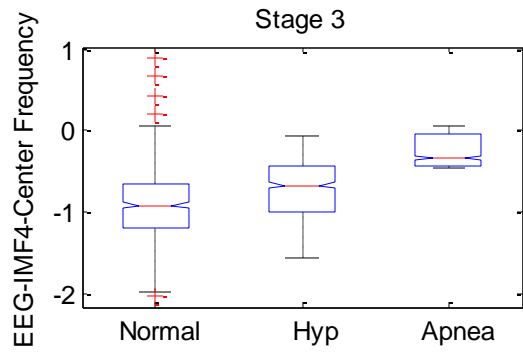
ANOVA Table					
Source	SS	df	MS	F	Prob>F
Groups	0.309	2	0.15448	0.3	0.7428
Error	17.51	34	0.515		
Total	17.819	36			



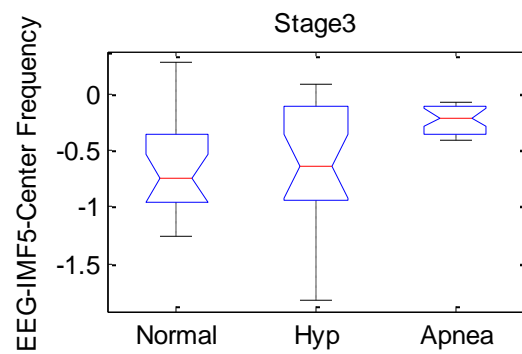
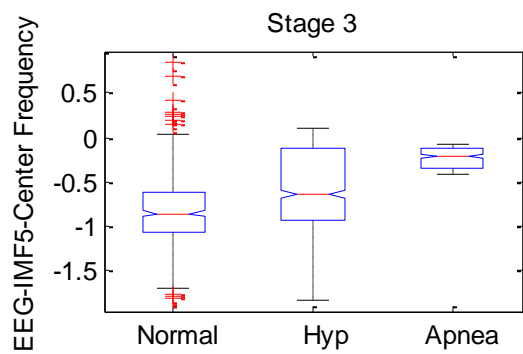
ANOVA Table					
Source	SS	df	MS	F	Prob>F
Groups	3.1676	2	1.58382	5.15	0.0111
Error	10.4494	34	0.30733		
Total	13.617	36			



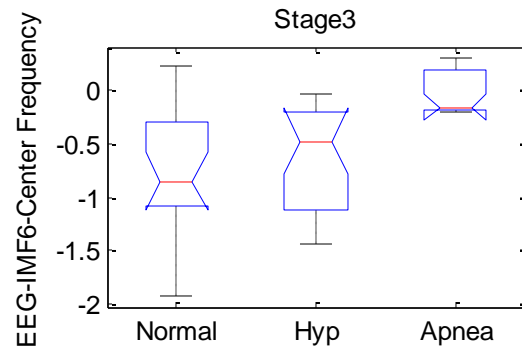
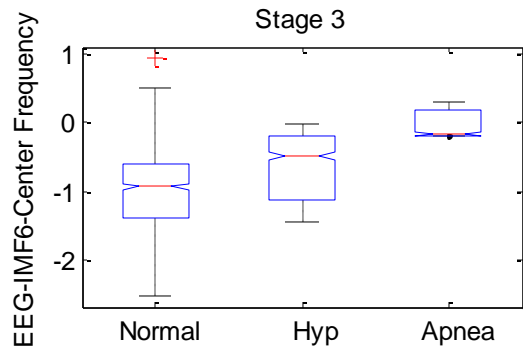
ANOVA Table					
Source	SS	df	MS	F	Prob>F
Groups	1.97076	2	0.98538	7.9	0.0015
Error	4.24272	34	0.12479		
Total	6.21349	36			



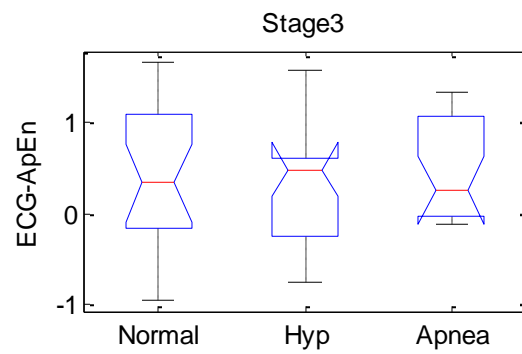
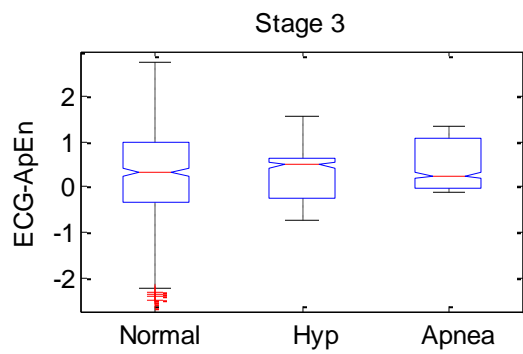
ANOVA Table					
Source	SS	df	MS	F	Prob>F
Groups	1.38337	2	0.69169	3.39	0.0456
Error	6.94307	34	0.20421		
Total	8.32644	36			



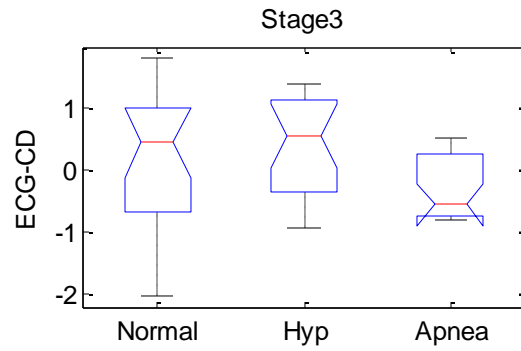
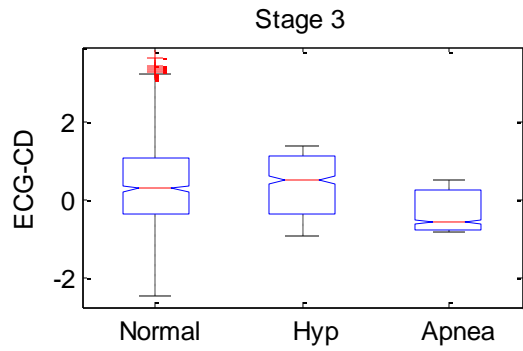
ANOVA Table					
Source	SS	df	MS	F	Prob>F
Groups	0.53107	2	0.26553	1.3	0.2869
Error	6.9686	34	0.20496		
Total	7.49967	36			



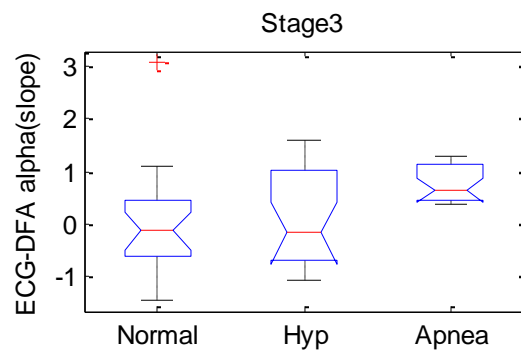
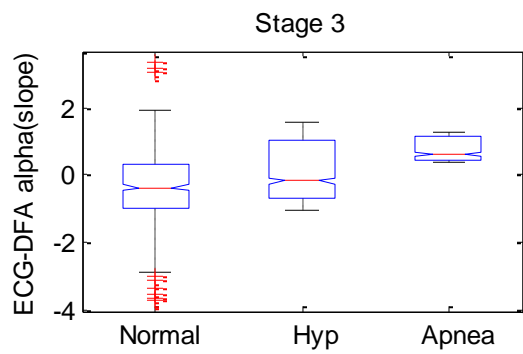
ANOVA Table					
Source	SS	df	MS	F	Prob>F
Groups	1.4656	2	0.73279	2.71	0.0807
Error	9.1826	34	0.27008		
Total	10.6482	36			



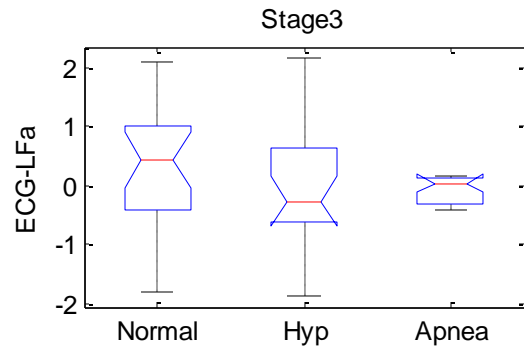
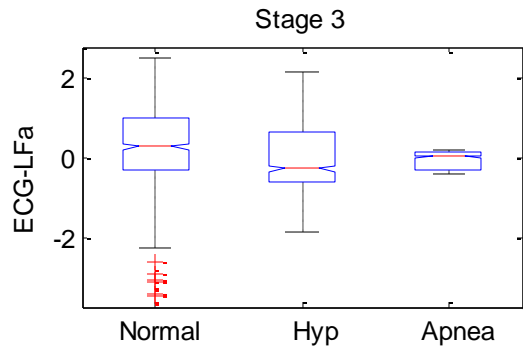
ANOVA Table					
Source	SS	df	MS	F	Prob>F
Groups	0.0585	2	0.02925	0.06	0.9458
Error	17.8289	34	0.52438		
Total	17.8874	36			



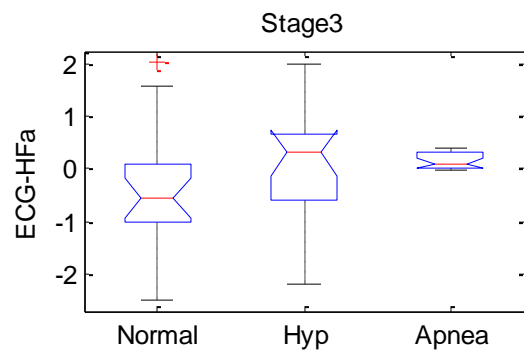
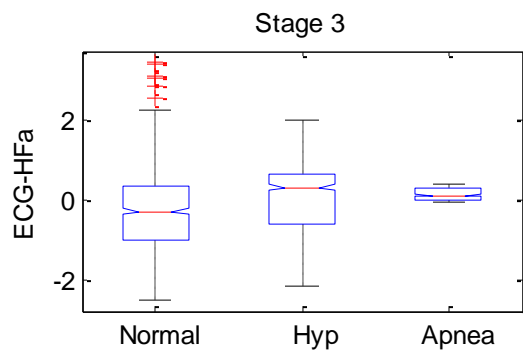
ANOVA Table					
Source	SS	df	MS	F	Prob>F
Groups	1.5747	2	0.78735	0.78	0.4648
Error	34.1598	34	1.0047		
Total	35.7345	36			



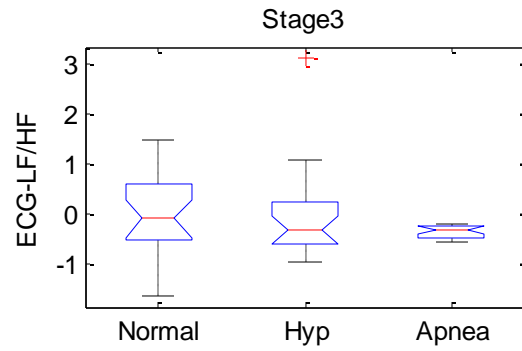
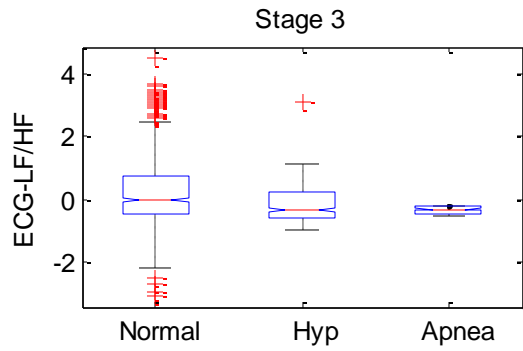
ANOVA Table					
Source	SS	df	MS	F	Prob>F
Groups	1.5679	2	0.78396	0.83	0.4465
Error	32.2825	34	0.94948		
Total	33.8504	36			



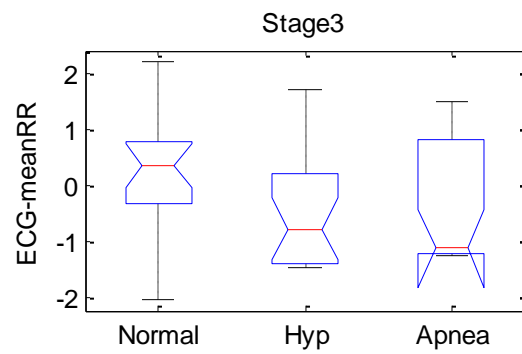
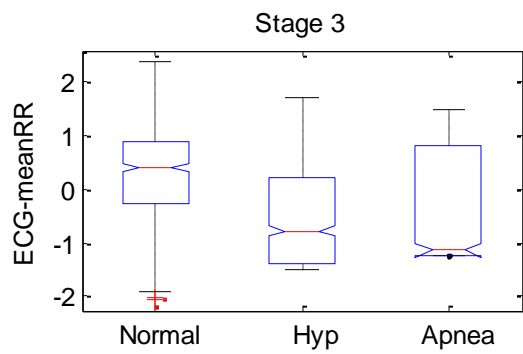
ANOVA Table					
Source	SS	df	MS	F	Prob>F
Groups	0.5242	2	0.26208	0.2	0.8164
Error	43.663	34	1.28421		
Total	44.1872	36			



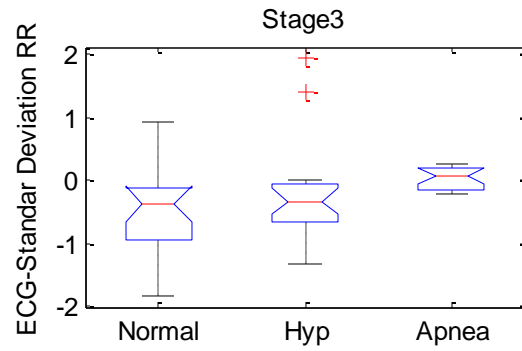
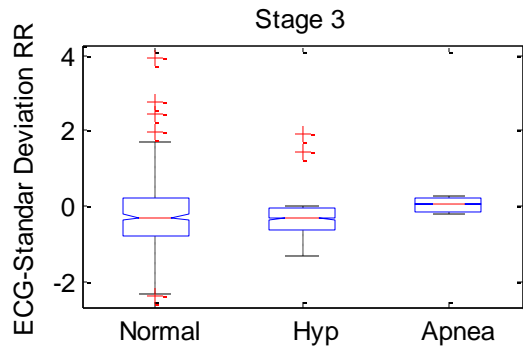
ANOVA Table					
Source	SS	df	MS	F	Prob>F
Groups	2.6587	2	1.32934	1.27	0.2938
Error	35.5829	34	1.04656		
Total	38.2416	36			



ANOVA Table					
Source	SS	df	MS	F	Prob>F
Groups	0.4109	2	0.20546	0.24	0.786
Error	28.8024	34	0.84713		
Total	29.2133	36			

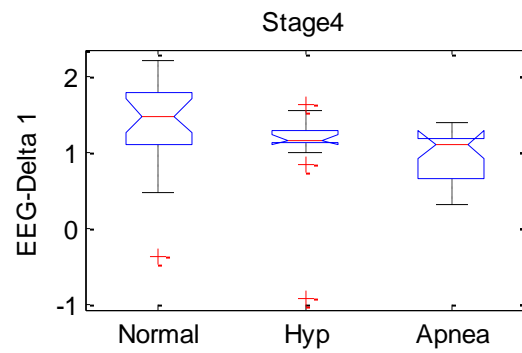
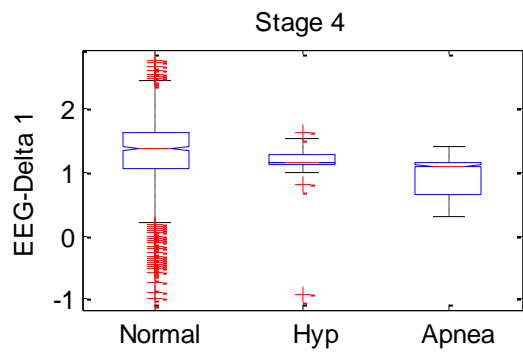


ANOVA Table					
Source	SS	df	MS	F	Prob>F
Groups	3.595	2	1.79752	1.78	0.1847
Error	34.4139	34	1.01217		
Total	38.0089	36			

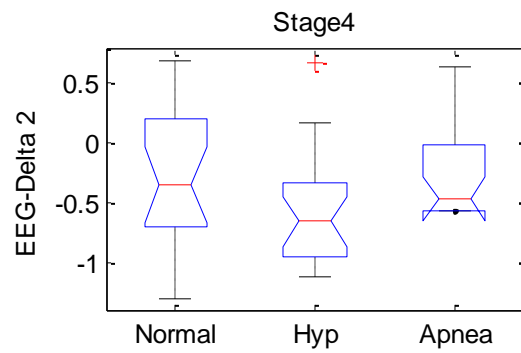
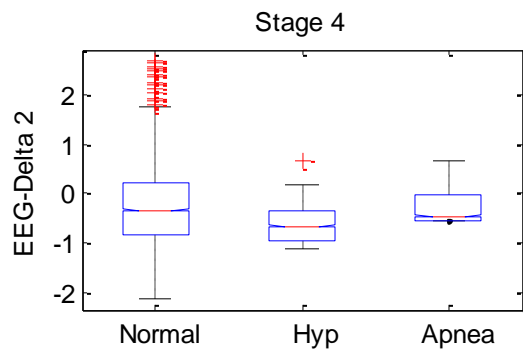


ANOVA Table					
Source	SS	df	MS	F	Prob>F
Groups	0.6655	2	0.33274	0.55	0.5801
Error	20.4456	34	0.60134		
Total	21.1111	36			

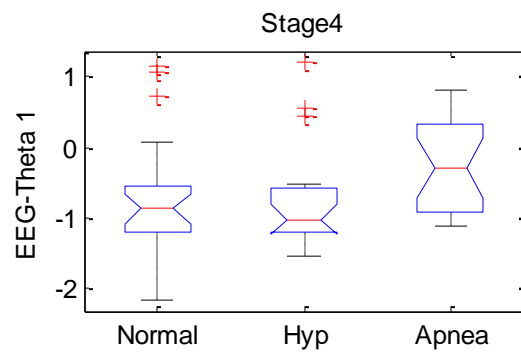
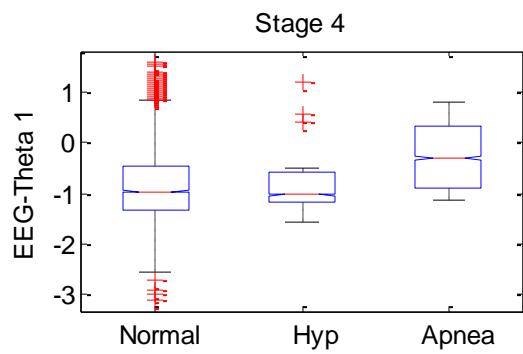
Stage 4



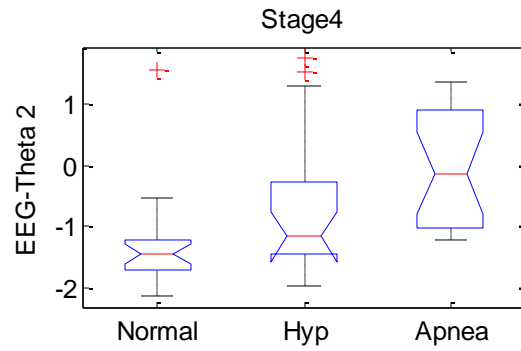
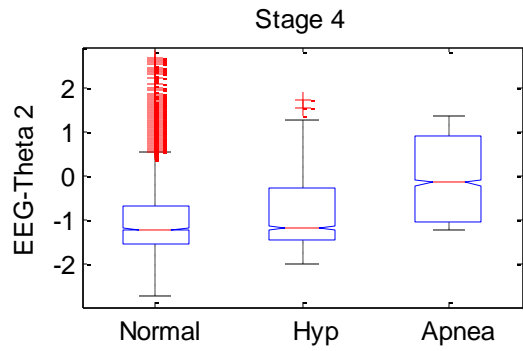
ANOVA Table					
Source	SS	df	MS	F	Prob>F
Groups	1.6203	2	0.81017	2.56	0.0893
Error	13.2938	42	0.31652		
Total	14.9142	44			



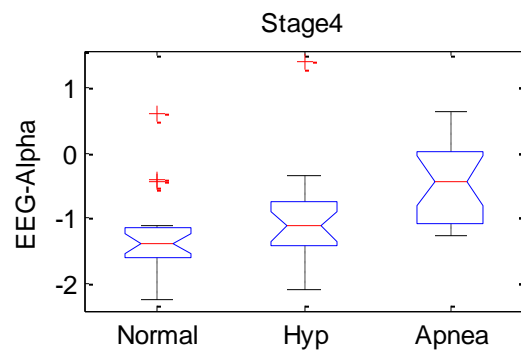
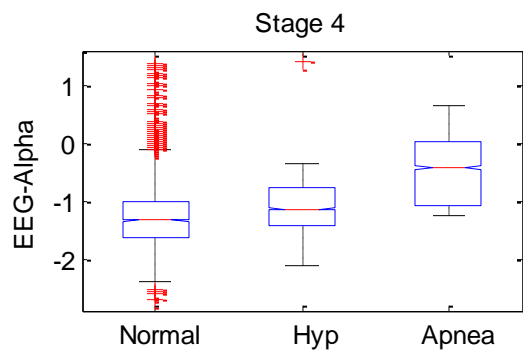
ANOVA Table					
Source	SS	df	MS	F	Prob>F
Groups	0.6202	2	0.31008	1.08	0.3499
Error	12.0938	42	0.28795		
Total	12.7139	44			



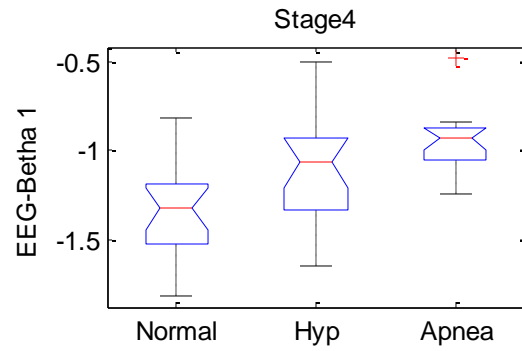
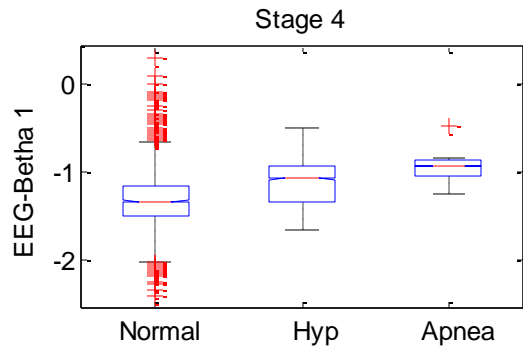
ANOVA Table					
Source	SS	df	MS	F	Prob>F
Groups	1.3662	2	0.68308	1.05	0.3599
Error	27.3975	42	0.65232		
Total	28.7637	44			



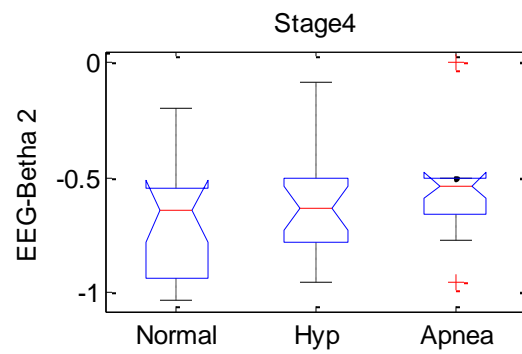
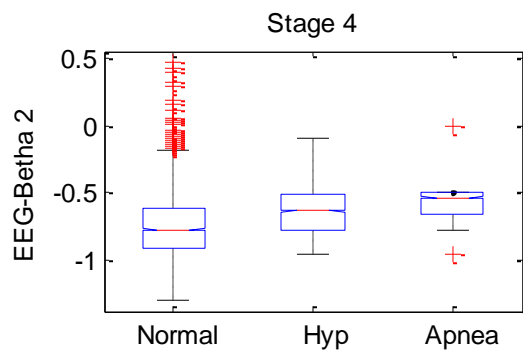
ANOVA Table					
Source	SS	df	MS	F	Prob>F
Groups	10.2781	2	5.13905	5.44	0.0079
Error	39.6573	42	0.94422		
Total	49.9354	44			



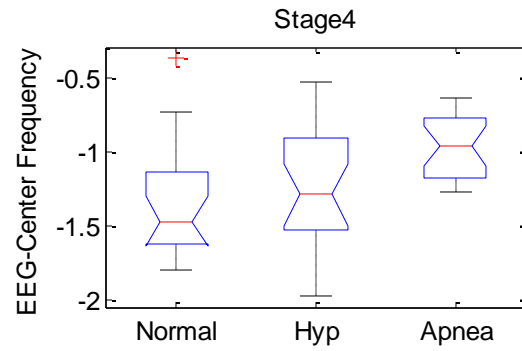
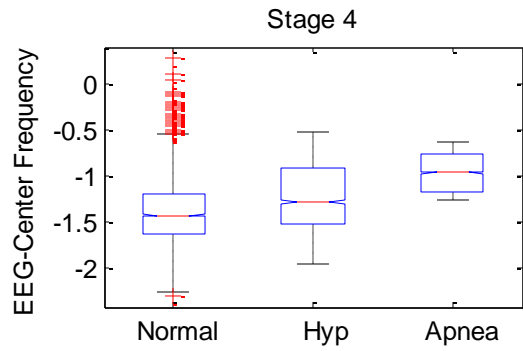
ANOVA Table					
Source	SS	df	MS	F	Prob>F
Groups	4.1752	2	2.08762	4.25	0.0209
Error	20.647	42	0.4916		
Total	24.8223	44			



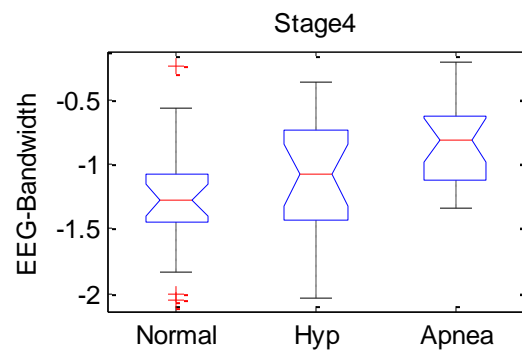
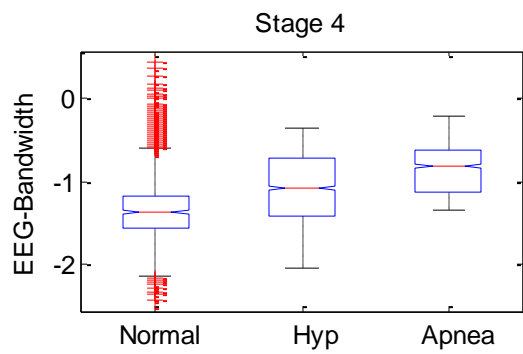
ANOVA Table					
Source	SS	df	MS	F	Prob>F
Groups	1.32914	2	0.66457	9.55	0.0004
Error	2.9218	42	0.06957		
Total	4.25095	44			



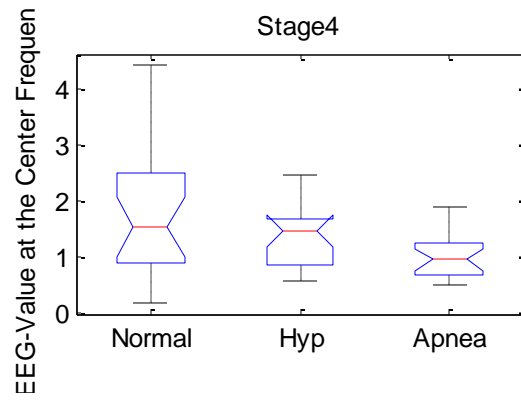
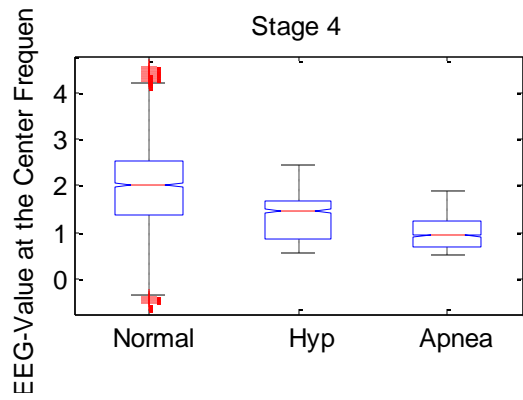
ANOVA Table					
Source	SS	df	MS	F	Prob>F
Groups	0.14499	2	0.0725	1.3	0.2827
Error	2.33853	42	0.05568		
Total	2.48352	44			



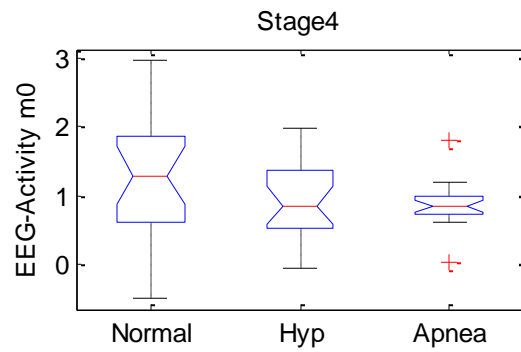
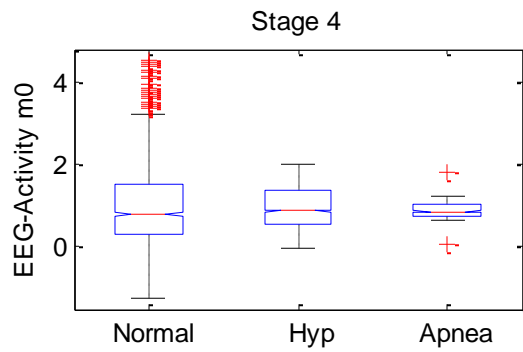
ANOVA Table					
Source	SS	df	MS	F	Prob>F
Groups	1.11623	2	0.55811	4.29	0.0202
Error	5.46397	42	0.13009		
Total	6.5802	44			



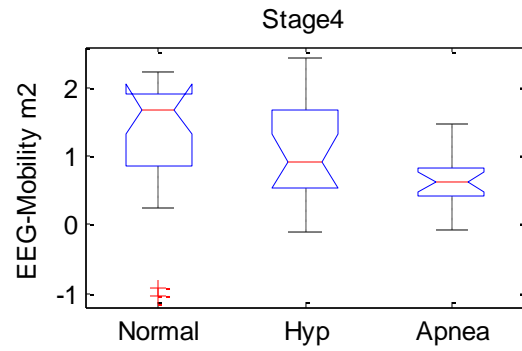
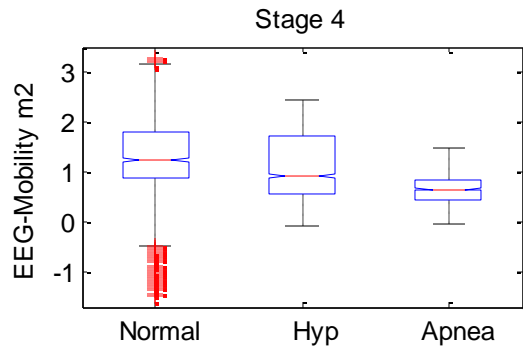
ANOVA Table					
Source	SS	df	MS	F	Prob>F
Groups	1.12916	2	0.56458	2.84	0.0699
Error	8.36036	42	0.19906		
Total	9.48952	44			



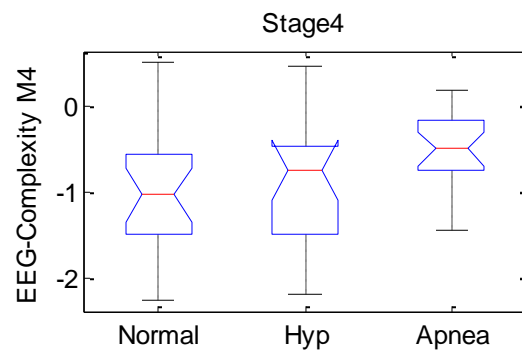
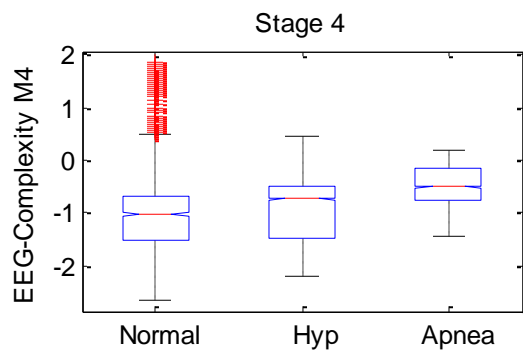
ANOVA Table					
Source	SS	df	MS	F	Prob>F
Groups	3.6732	2	1.83662	2.43	0.1007
Error	31.8044	42	0.75725		
Total	35.4776	44			



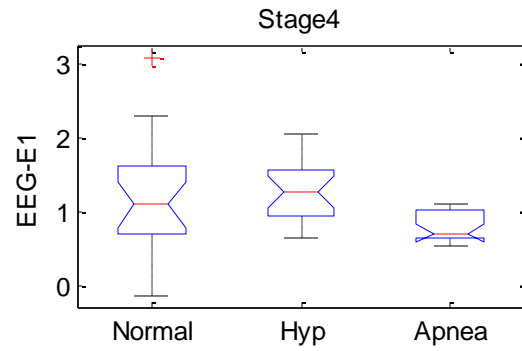
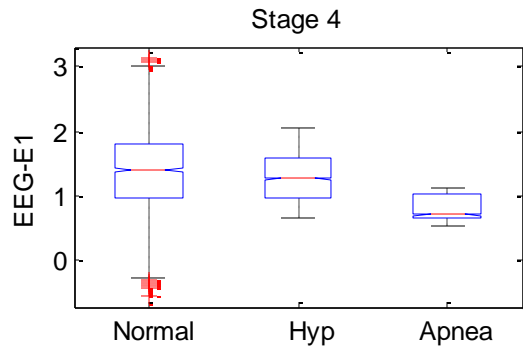
ANOVA Table					
Source	SS	df	MS	F	Prob>F
Groups	1.2154	2	0.60772	1.14	0.3302
Error	22.4305	42	0.53406		
Total	23.6459	44			



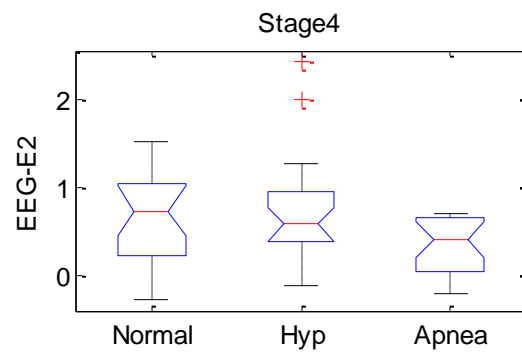
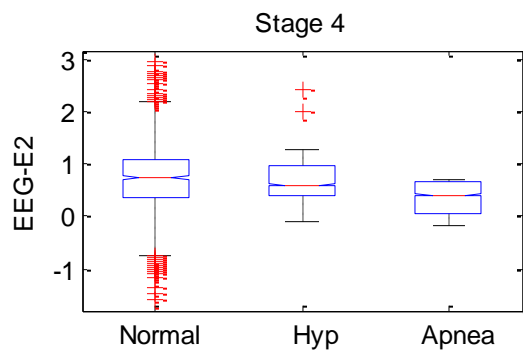
ANOVA Table					
Source	SS	df	MS	F	Prob>F
Groups	2.839	2	1.41952	2.11	0.1345
Error	28.322	42	0.67433		
Total	31.161	44			



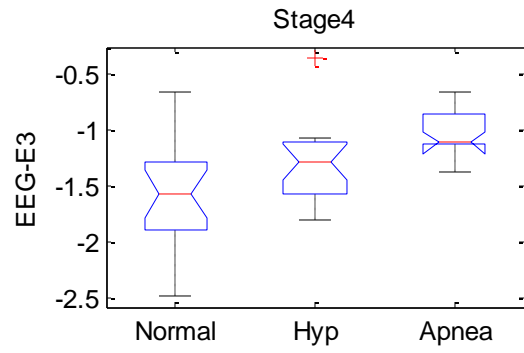
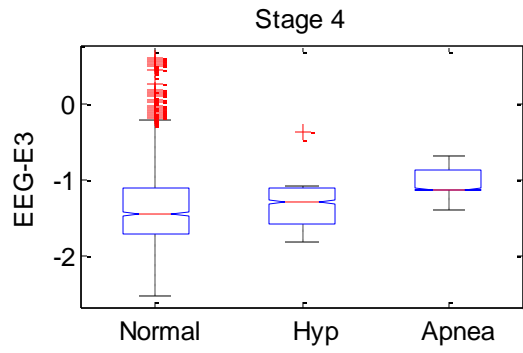
ANOVA Table					
Source	SS	df	MS	F	Prob>F
Groups	1.8355	2	0.91775	2	0.1481
Error	19.2797	42	0.45904		
Total	21.1152	44			



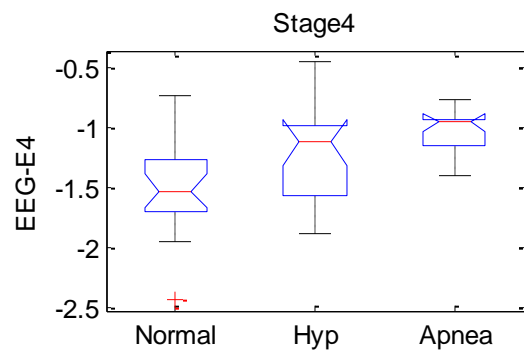
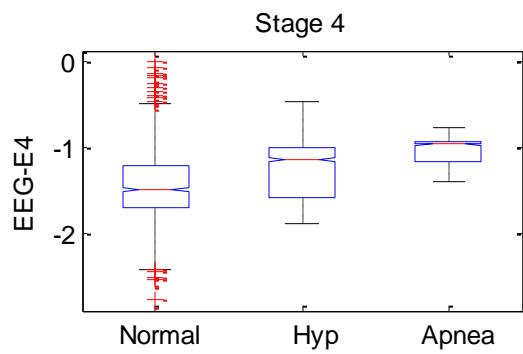
ANOVA Table					
Source	SS	df	MS	F	Prob>F
Groups	1.2929	2	0.64647	1.9	0.1617
Error	14.263	42	0.3396		
Total	15.5559	44			



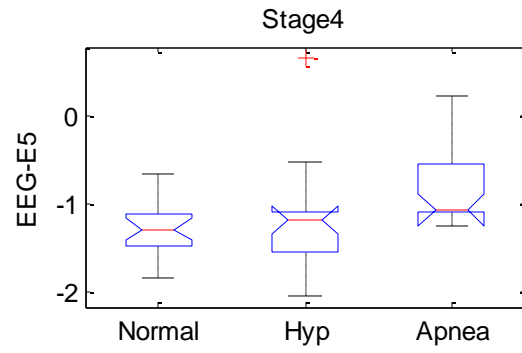
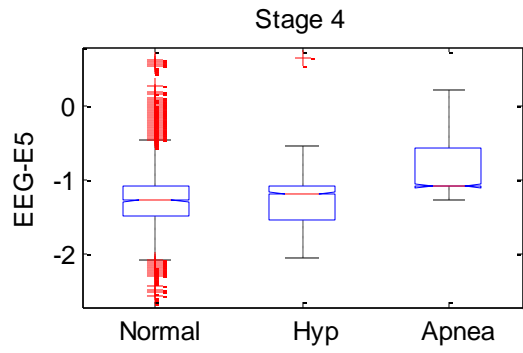
ANOVA Table					
Source	SS	df	MS	F	Prob>F
Groups	1.2128	2	0.60638	2.03	0.1442
Error	12.5552	42	0.29893		
Total	13.768	44			



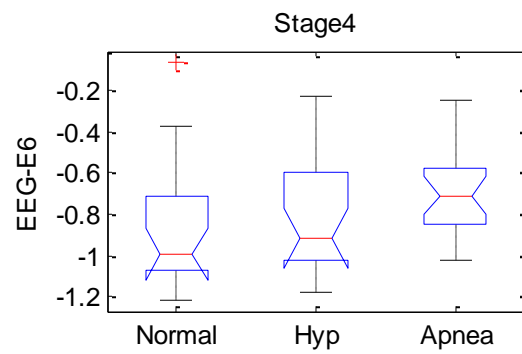
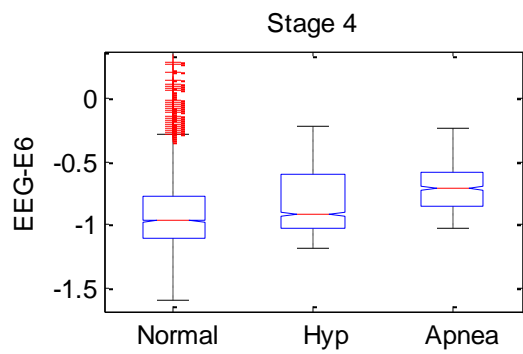
ANOVA Table					
Source	SS	df	MS	F	Prob>F
Groups	2.06622	2	1.03311	7.05	0.0023
Error	6.15753	42	0.14661		
Total	8.22375	44			



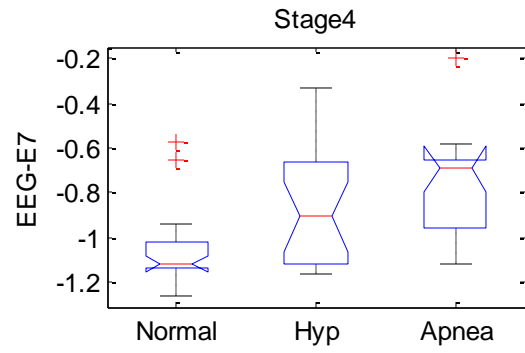
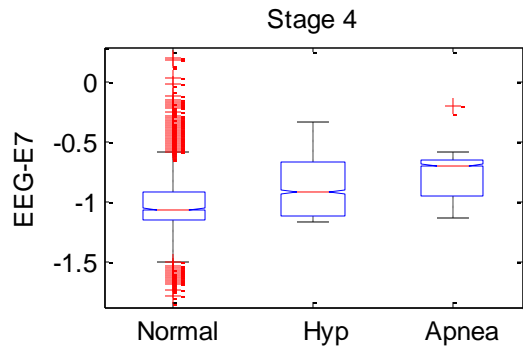
ANOVA Table					
Source	SS	df	MS	F	Prob>F
Groups	1.38476	2	0.69238	5.55	0.0073
Error	5.23998	42	0.12476		
Total	6.62474	44			



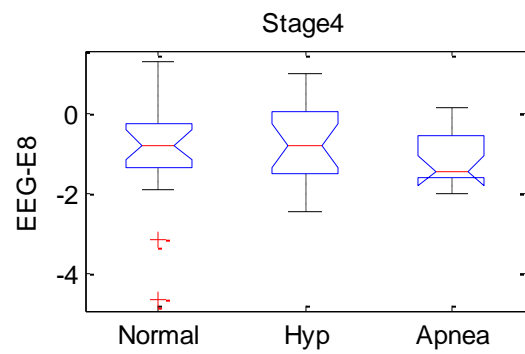
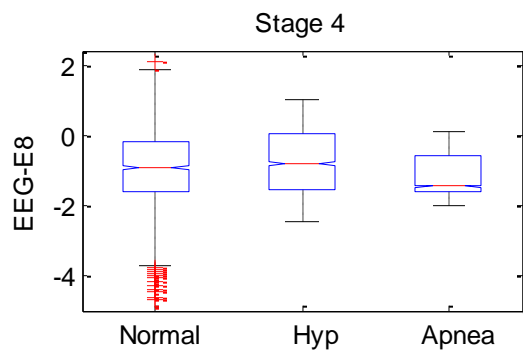
ANOVA Table					
Source	SS	df	MS	F	Prob>F
Groups	1.5268	2	0.76341	3.55	0.0377
Error	9.0375	42	0.21518		
Total	10.5643	44			



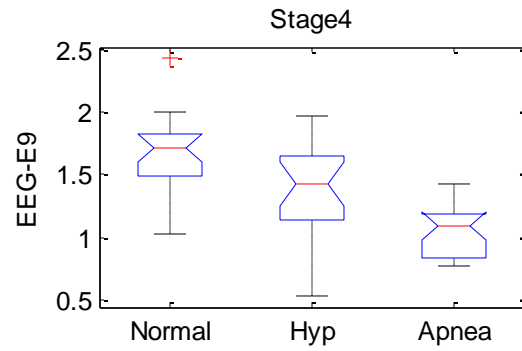
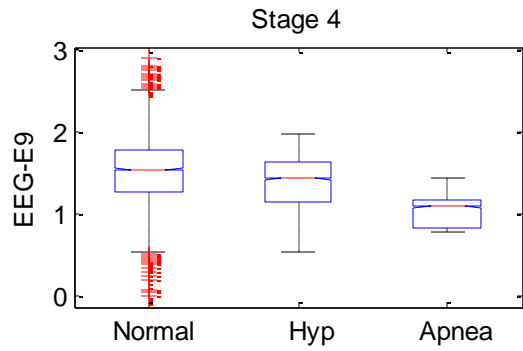
ANOVA Table					
Source	SS	df	MS	F	Prob>F
Groups	0.17491	2	0.08746	1.07	0.3513
Error	3.42432	42	0.08153		
Total	3.59923	44			



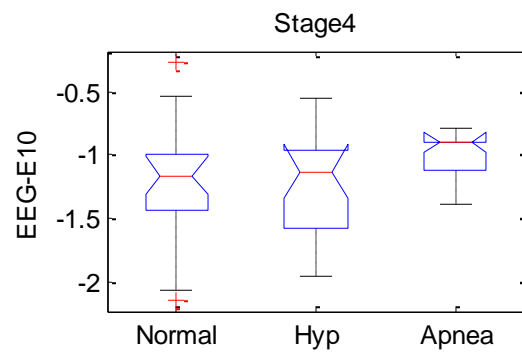
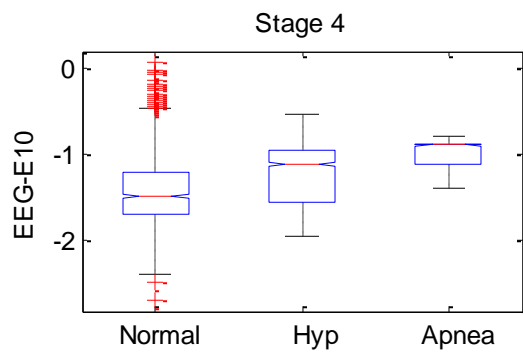
ANOVA Table					
Source	SS	df	MS	F	Prob>F
Groups	0.71901	2	0.35951	7	0.0024
Error	2.15741	42	0.05137		
Total	2.87642	44			



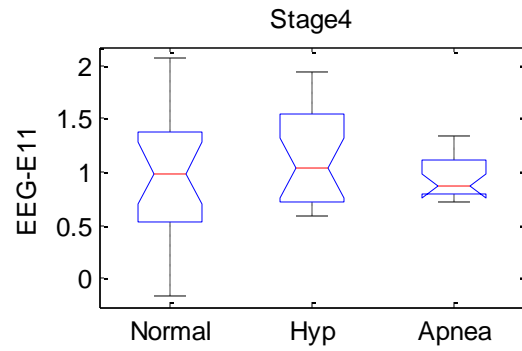
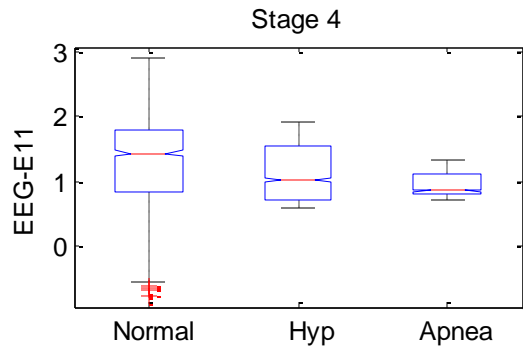
ANOVA Table					
Source	SS	df	MS	F	Prob>F
Groups	0.9783	2	0.48917	0.37	0.6936
Error	55.6612	42	1.32527		
Total	56.6395	44			



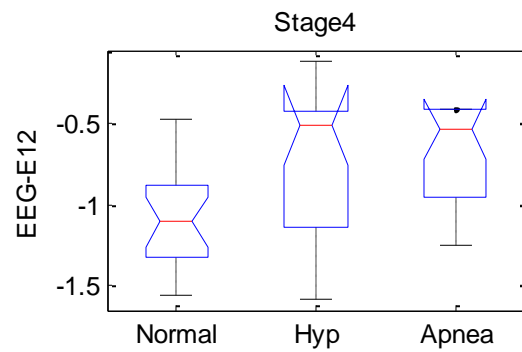
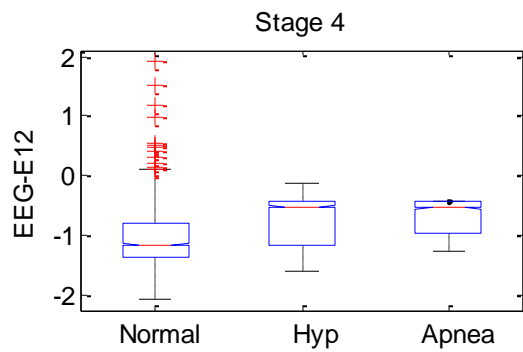
ANOVA Table					
Source	SS	df	MS	F	Prob>F
Groups	2.2573	2	1.12865	11.06	0.0001
Error	4.28635	42	0.10206		
Total	6.54364	44			



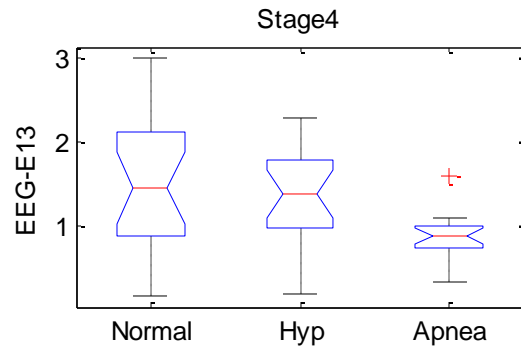
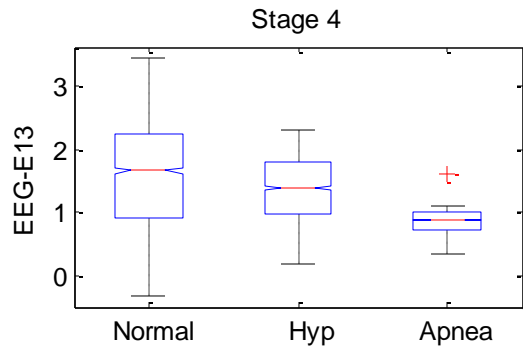
ANOVA Table					
Source	SS	df	MS	F	Prob>F
Groups	0.27413	2	0.13706	0.91	0.4088
Error	6.29891	42	0.14997		
Total	6.57304	44			



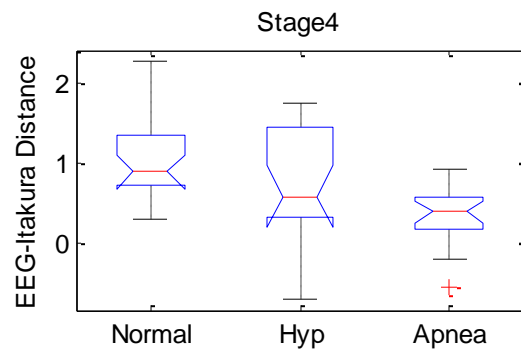
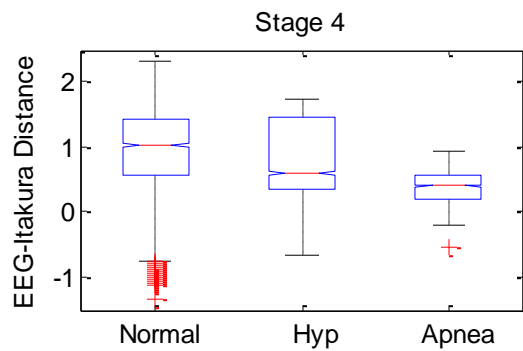
ANOVA Table					
Source	SS	df	MS	F	Prob>F
Groups	0.2075	2	0.10374	0.37	0.693
Error	11.7771	42	0.28041		
Total	11.9846	44			



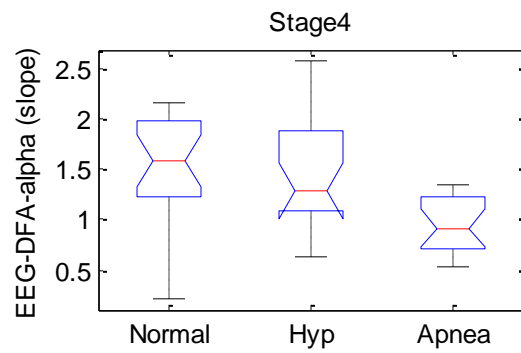
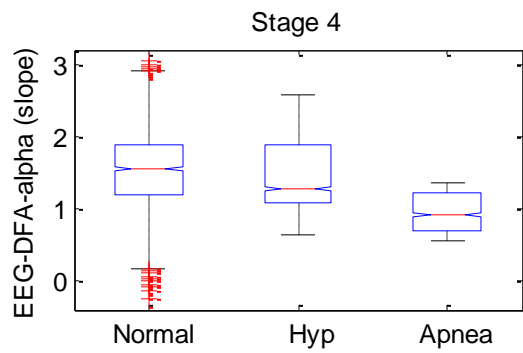
ANOVA Table					
Source	SS	df	MS	F	Prob>F
Groups	1.39837	2	0.69919	4.54	0.0164
Error	6.47073	42	0.15407		
Total	7.86911	44			



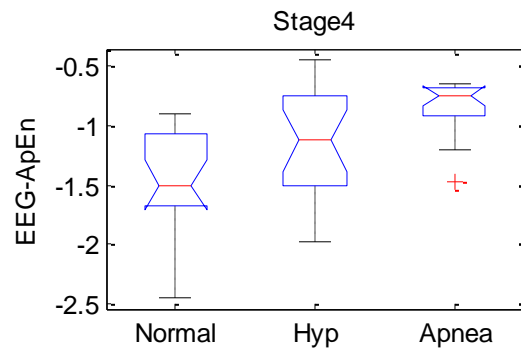
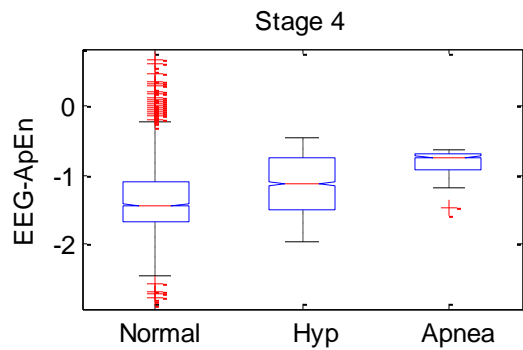
ANOVA Table					
Source	SS	df	MS	F	Prob>F
Groups	1.9947	2	0.99736	2.54	0.0912
Error	16.5128	42	0.39316		
Total	18.5076	44			



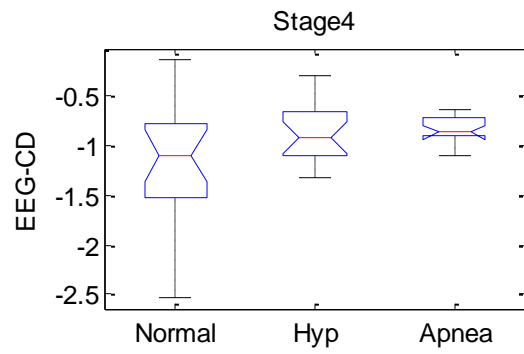
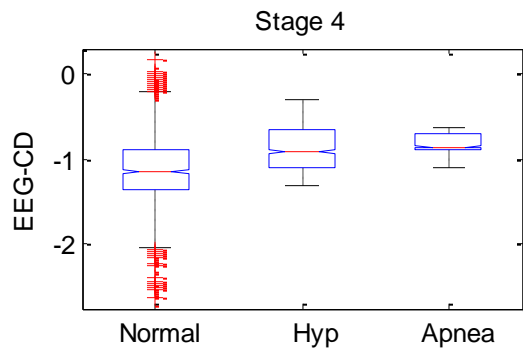
ANOVA Table					
Source	SS	df	MS	F	Prob>F
Groups	3.97	2	1.985	5.46	0.0078
Error	15.2762	42	0.36372		
Total	19.2462	44			



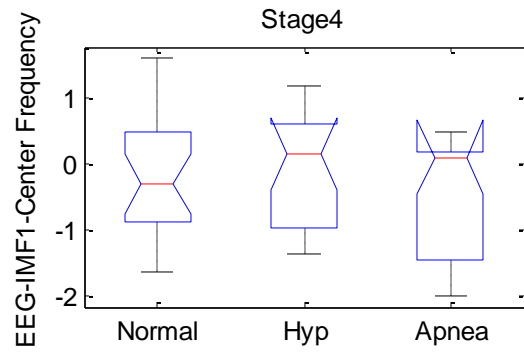
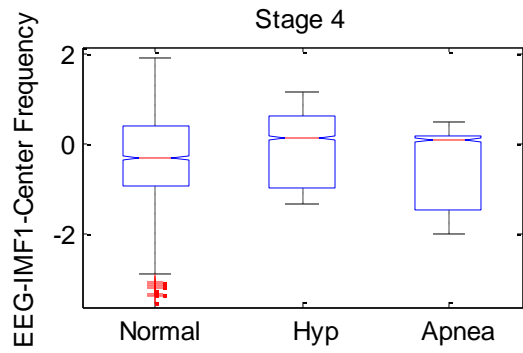
ANOVA Table					
Source	SS	df	MS	F	Prob>F
Groups	2.0281	2	1.01404	3.96	0.0265
Error	10.7421	42	0.25577		
Total	12.7702	44			



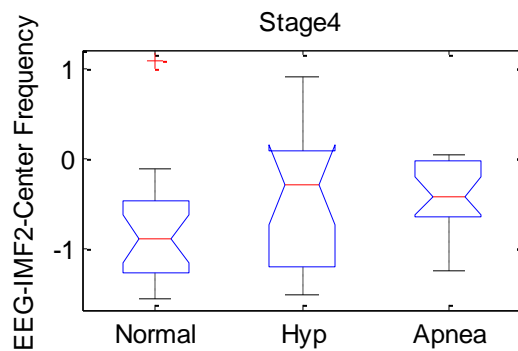
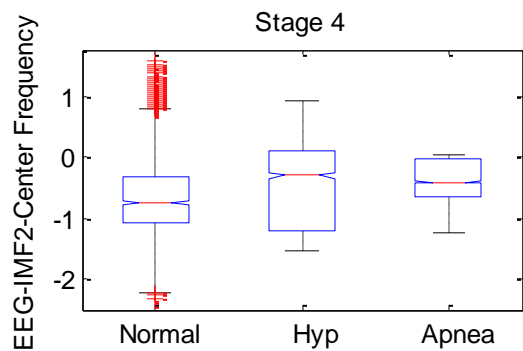
ANOVA Table					
Source	SS	df	MS	F	Prob>F
Groups	2.41924	2	1.20962	6.93	0.0025
Error	7.33212	42	0.17457		
Total	9.75136	44			



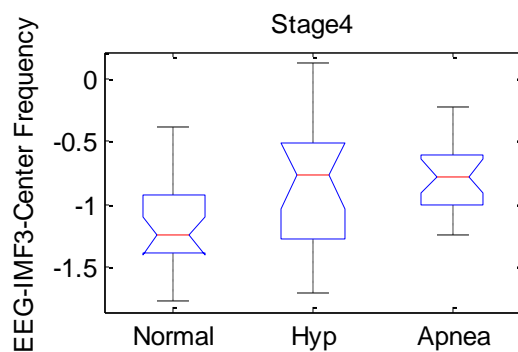
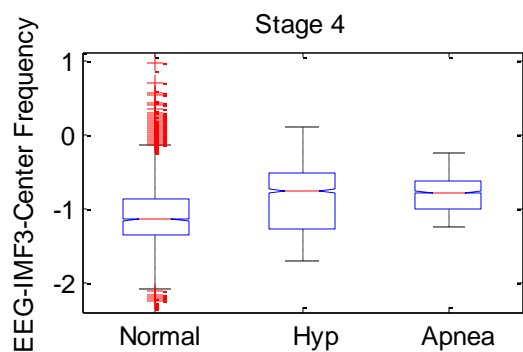
ANOVA Table					
Source	SS	df	MS	F	Prob>F
Groups	1.2187	2	0.60935	6.79	0.0028
Error	3.76838	42	0.08972		
Total	4.98708	44			



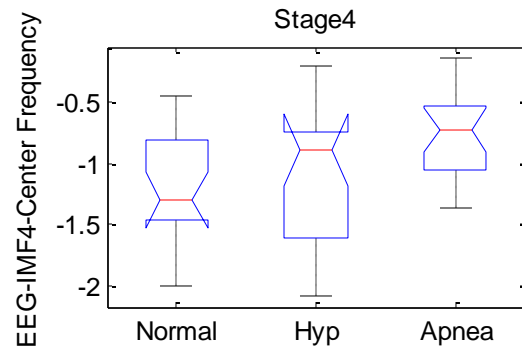
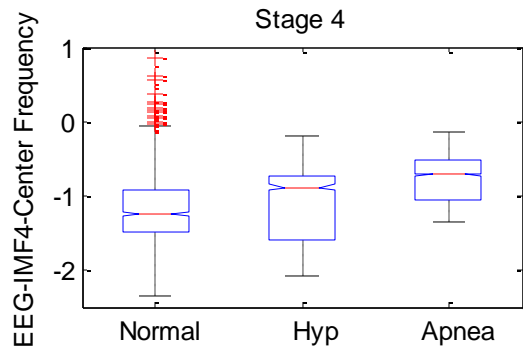
ANOVA Table					
Source	SS	df	MS	F	Prob>F
Groups	1.1413	2	0.57067	0.7	0.5024
Error	34.2556	42	0.81561		
Total	35.3969	44			



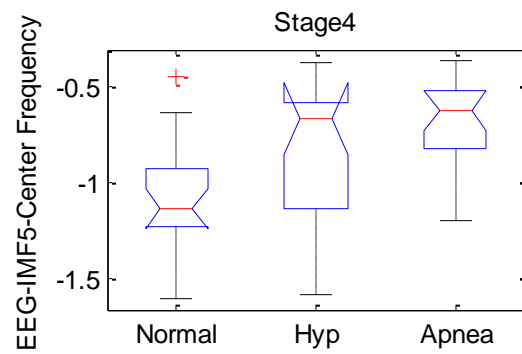
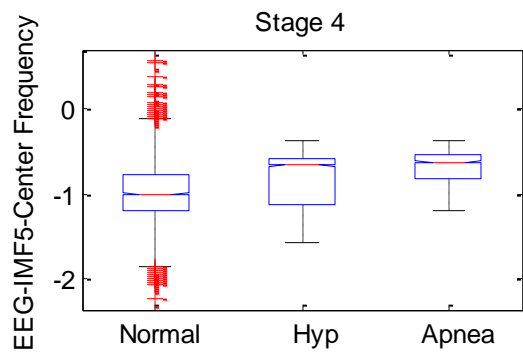
ANOVA Table					
Source	SS	df	MS	F	Prob>F
Groups	1.4685	2	0.73426	1.84	0.1708
Error	16.7256	42	0.39823		
Total	18.1942	44			



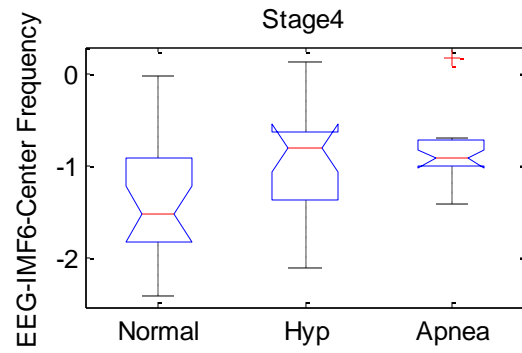
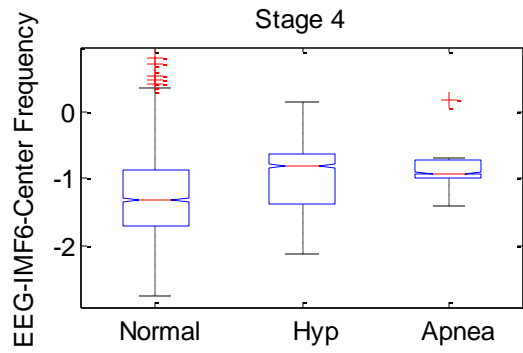
ANOVA Table					
Source	SS	df	MS	F	Prob>F
Groups	1.32532	2	0.66266	4.25	0.0208
Error	6.54359	42	0.1558		
Total	7.86891	44			



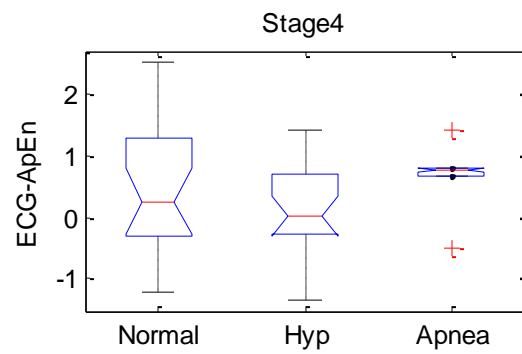
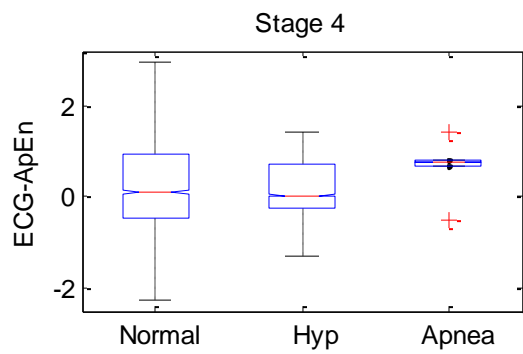
ANOVA Table					
Source	SS	df	MS	F	Prob>F
Groups	1.1408	2	0.57042	2.56	0.0893
Error	9.3573	42	0.22279		
Total	10.4981	44			



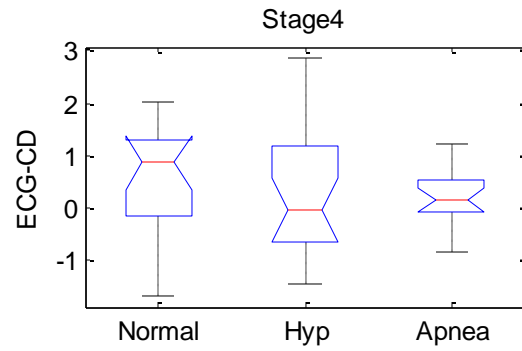
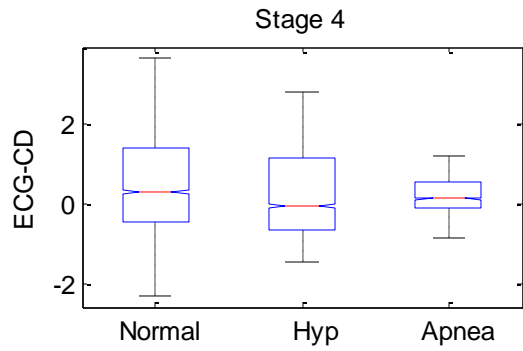
ANOVA Table					
Source	SS	df	MS	F	Prob>F
Groups	1.08928	2	0.54464	5.56	0.0072
Error	4.11049	42	0.09787		
Total	5.19977	44			



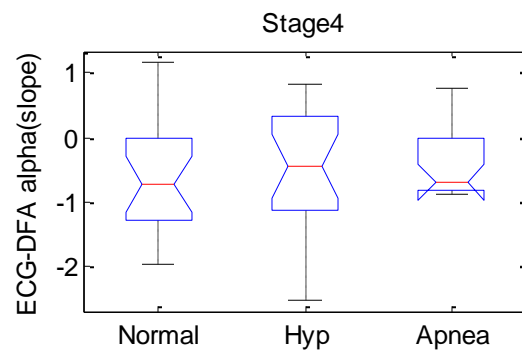
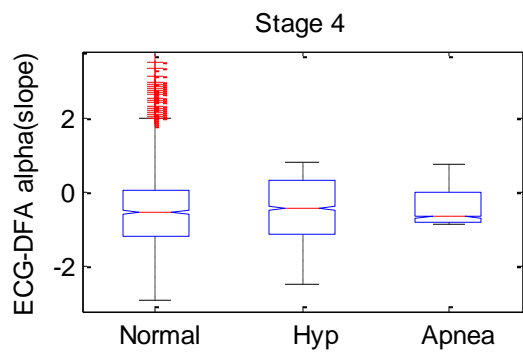
ANOVA Table					
Source	SS	df	MS	F	Prob>F
Groups	2.6841	2	1.34206	3.93	0.0272
Error	14.3362	42	0.34134		
Total	17.0203	44			



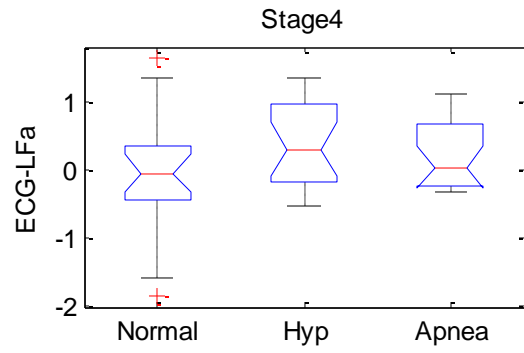
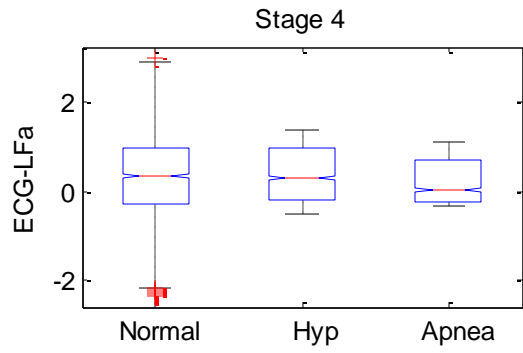
ANOVA Table					
Source	SS	df	MS	F	Prob>F
Groups	1.4693	2	0.73463	1.01	0.3721
Error	30.4773	42	0.72565		
Total	31.9466	44			



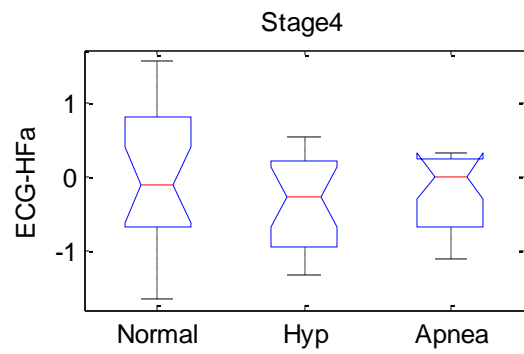
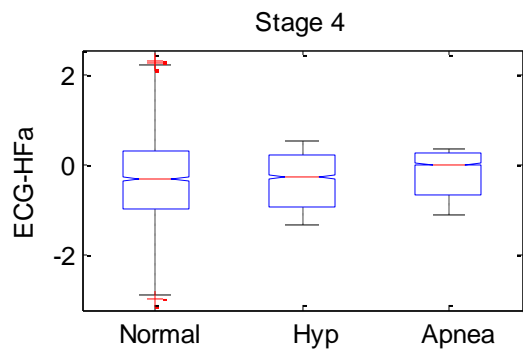
ANOVA Table					
Source	SS	df	MS	F	Prob>F
Groups	1.0965	2	0.54827	0.54	0.5869
Error	42.6684	42	1.01591		
Total	43.7649	44			



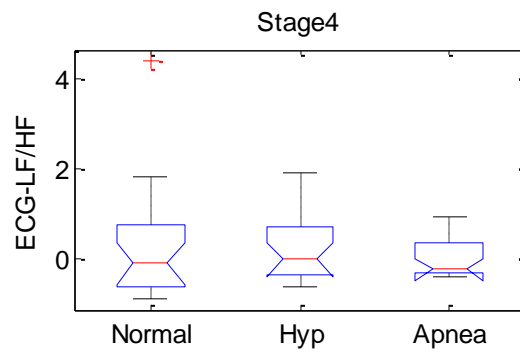
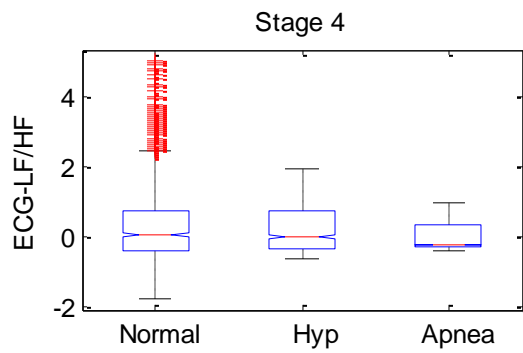
ANOVA Table					
Source	SS	df	MS	F	Prob>F
Groups	2.2321	2	1.11607	0.81	0.4538
Error	58.2265	42	1.38635		
Total	60.4587	44			



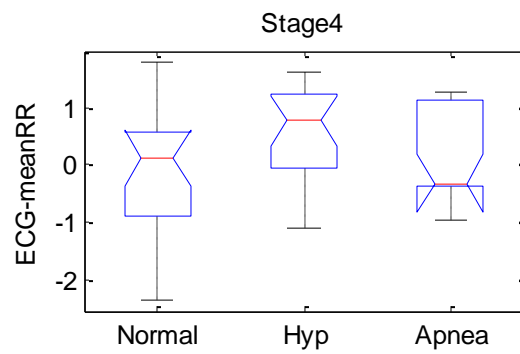
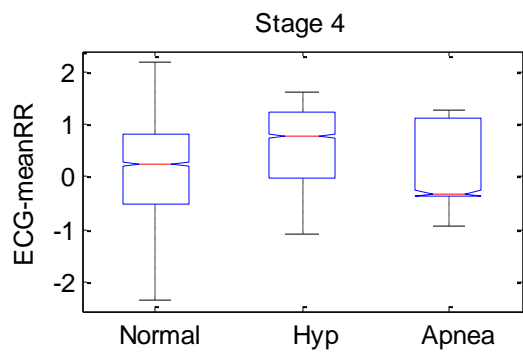
ANOVA Table					
Source	SS	df	MS	F	Prob>F
Groups	0.3719	2	0.18596	0.23	0.7984
Error	34.5085	42	0.82163		
Total	34.8804	44			



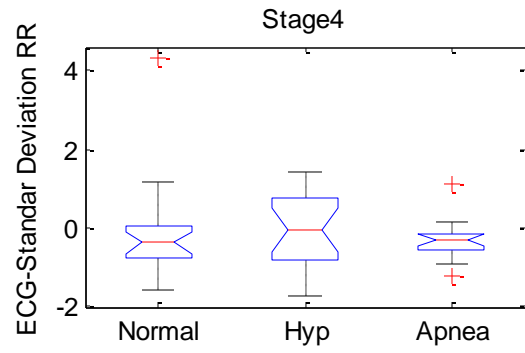
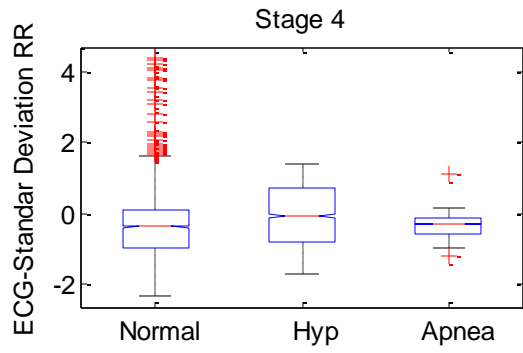
ANOVA Table					
Source	SS	df	MS	F	Prob>F
Groups	1.0185	2	0.50924	0.85	0.4344
Error	25.1484	42	0.59877		
Total	26.1669	44			



ANOVA Table					
Source	SS	df	MS	F	Prob>F
Groups	0.3875	2	0.19373	0.21	0.814
Error	39.354	42	0.937		
Total	39.7414	44			

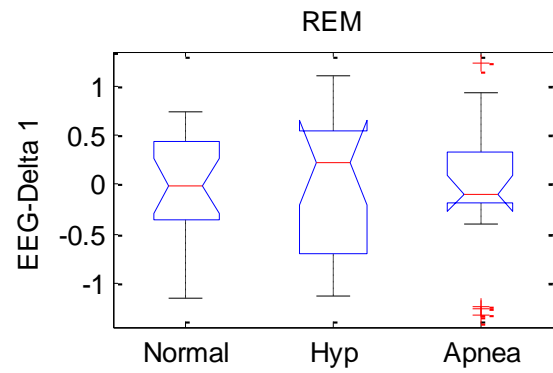
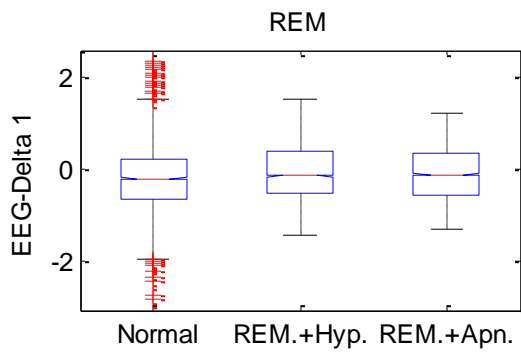


ANOVA Table					
Source	SS	df	MS	F	Prob>F
Groups	3.3311	2	1.66555	1.9	0.1622
Error	36.8122	42	0.87648		
Total	40.1433	44			

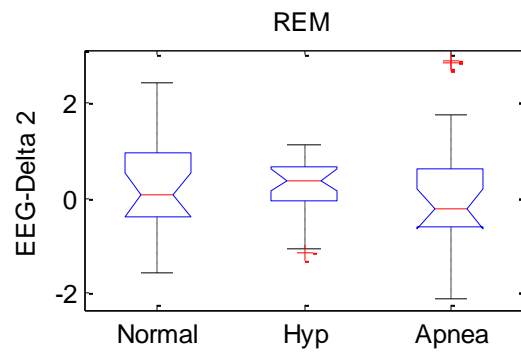
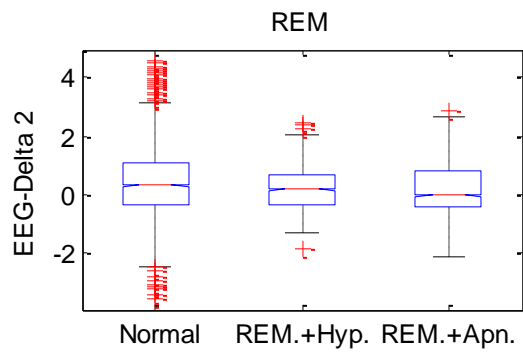


ANOVA Table					
Source	SS	df	MS	F	Prob>F
Groups	0.2657	2	0.13285	0.11	0.8942
Error	49.7524	42	1.18458		
Total	50.0181	44			

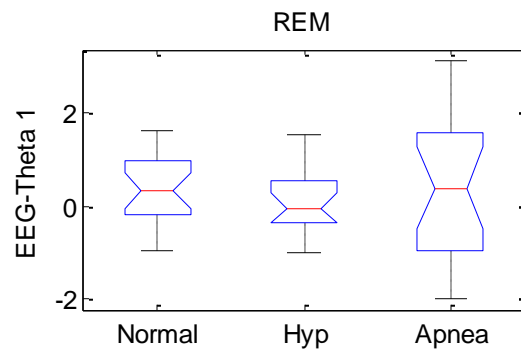
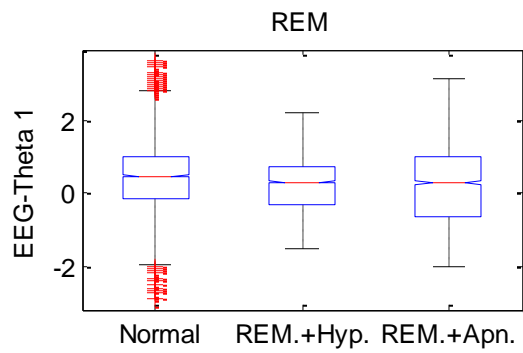
REM



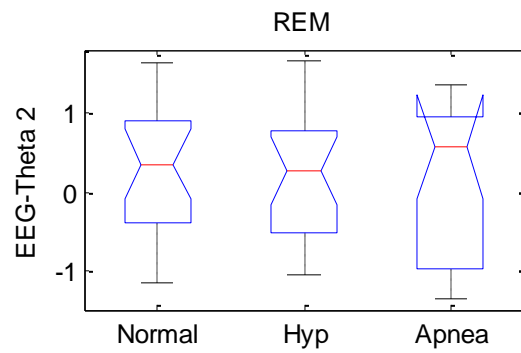
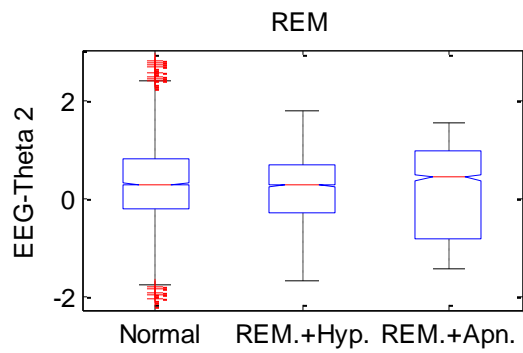
ANOVA Table					
Source	SS	df	MS	F	Prob>F
Groups	0.0003	2	0.00017	0	0.9996
Error	24.0669	60	0.40111		
Total	24.0672	62			



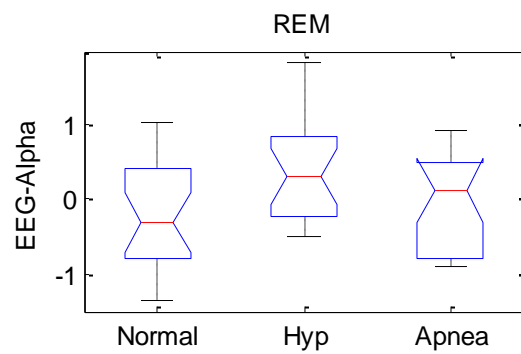
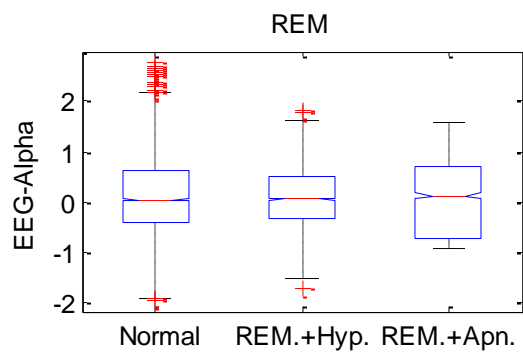
ANOVA Table					
Source	SS	df	MS	F	Prob>F
Groups	0.8986	2	0.44931	0.41	0.6659
Error	65.8631	60	1.09772		
Total	66.7617	62			



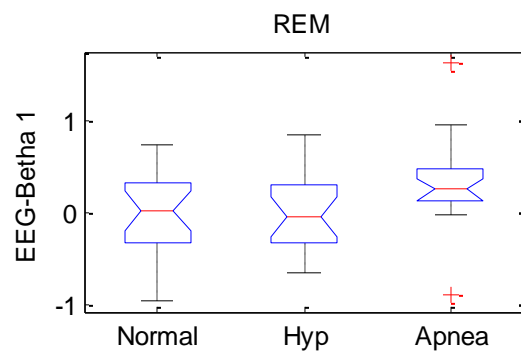
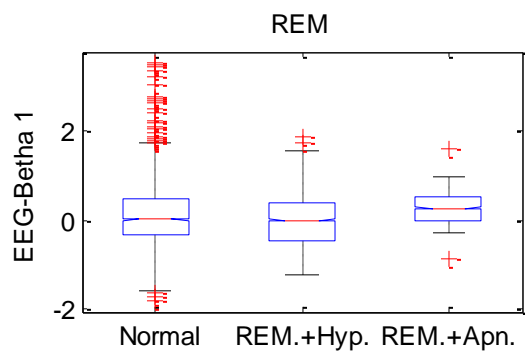
ANOVA Table					
Source	SS	df	MS	F	Prob>F
Groups	1.0173	2	0.50866	0.4	0.6724
Error	76.3782	60	1.27297		
Total	77.3956	62			



ANOVA Table					
Source	SS	df	MS	F	Prob>F
Groups	1.3941	2	0.69703	1.01	0.3717
Error	41.5619	60	0.6927		
Total	42.956	62			

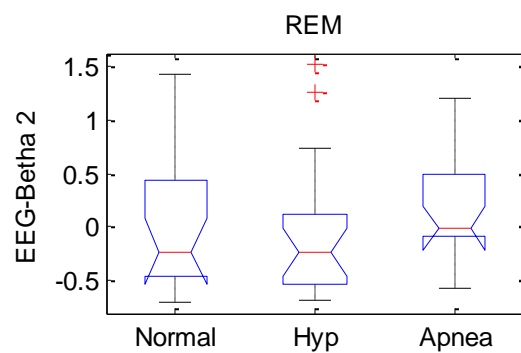
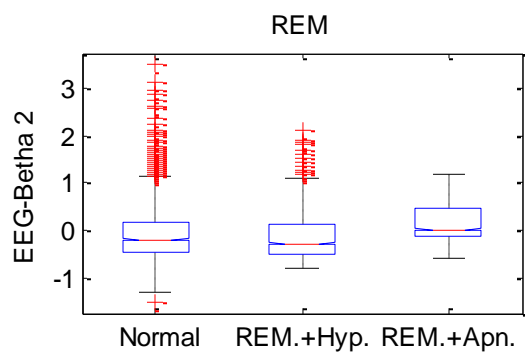


ANOVA Table					
Source	SS	df	MS	F	Prob>F
Groups	3.0789	2	1.53946	3.51	0.0362
Error	26.3146	60	0.43858		
Total	29.3935	62			



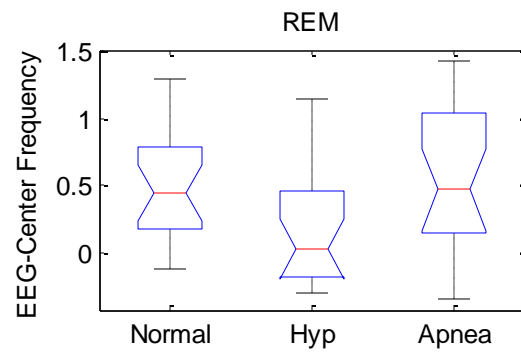
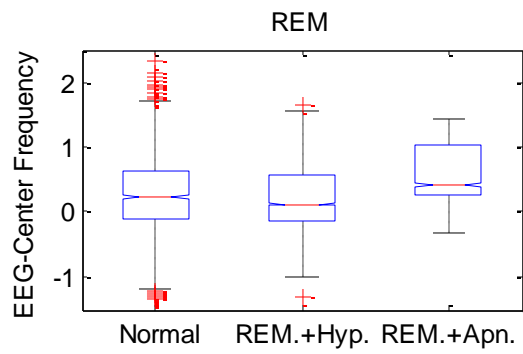
ANOVA Table

Source	SS	df	MS	F	Prob>F
Groups	1.6237	2	0.81183	3.95	0.0244
Error	12.3275	60	0.20546		
Total	13.9511	62			

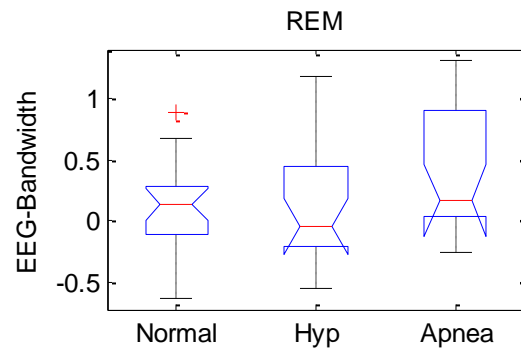
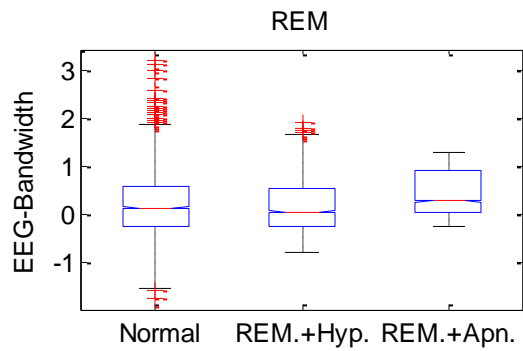


ANOVA Table

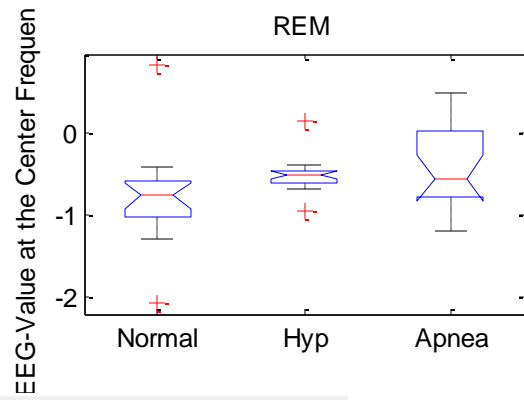
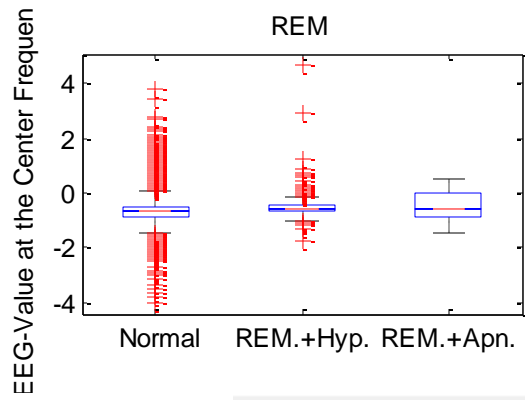
Source	SS	df	MS	F	Prob>F
Groups	0.8185	2	0.40925	1.27	0.2884
Error	19.3437	60	0.32239		
Total	20.1622	62			



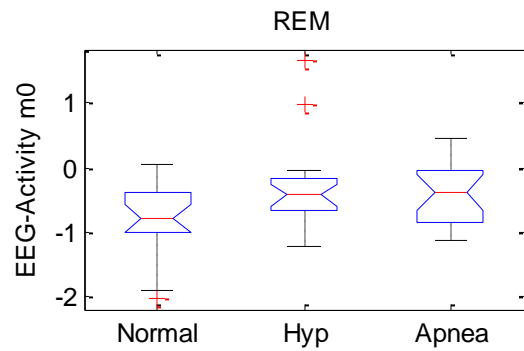
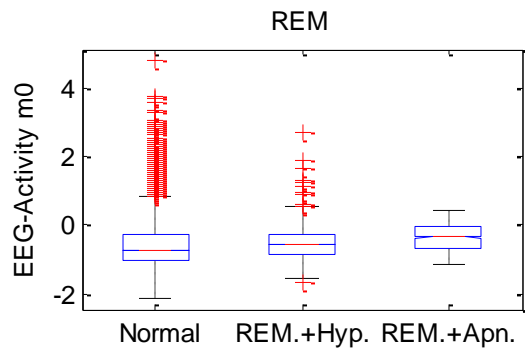
ANOVA Table					
Source	SS	df	MS	F	Prob>F
Groups	1.8852	2	0.94259	4.94	0.0103
Error	11.4448	60	0.19075		
Total	13.33	62			



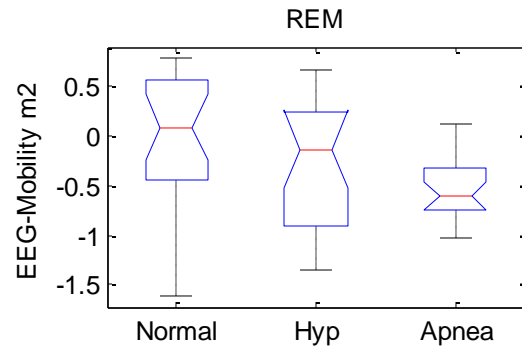
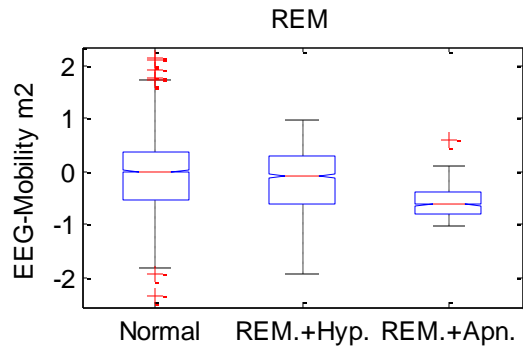
ANOVA Table					
Source	SS	df	MS	F	Prob>F
Groups	1.7697	2	0.88486	4.07	0.022
Error	13.0383	60	0.2173		
Total	14.808	62			



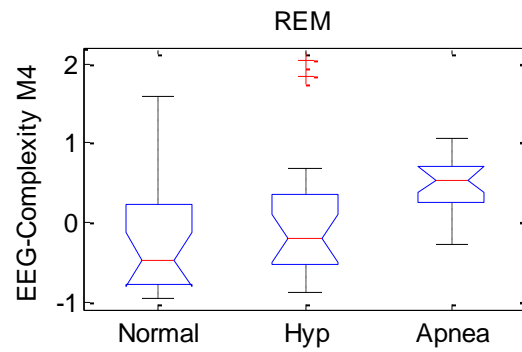
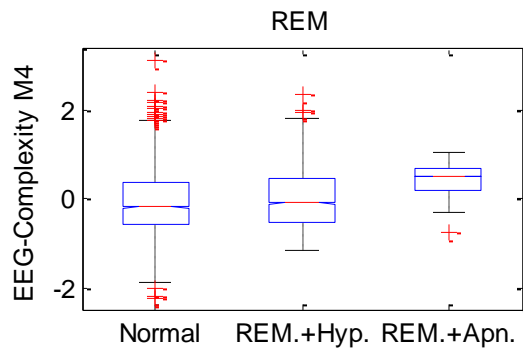
ANOVA Table					
Source	SS	df	MS	F	Prob>F
Groups	1.4537	2	0.72686	3.91	0.0252
Error	11.1399	60	0.18567		
Total	12.5937	62			



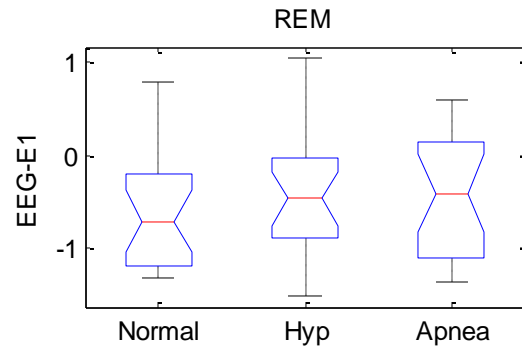
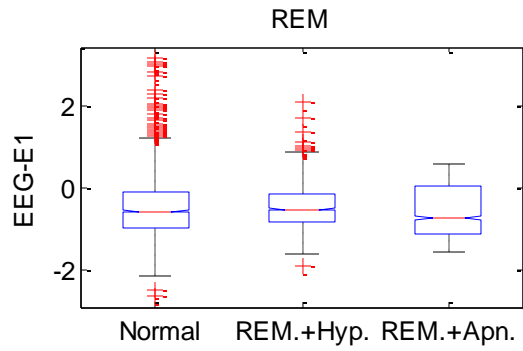
ANOVA Table					
Source	SS	df	MS	F	Prob>F
Groups	2.5293	2	1.26466	4.03	0.0228
Error	18.8198	60	0.31366		
Total	21.3491	62			



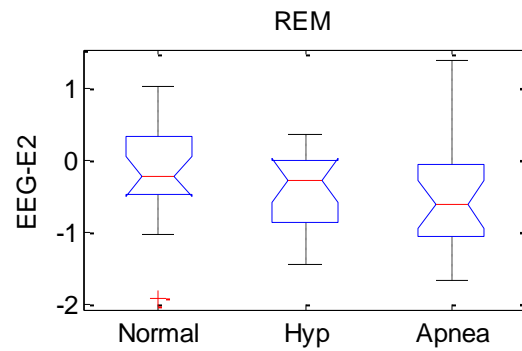
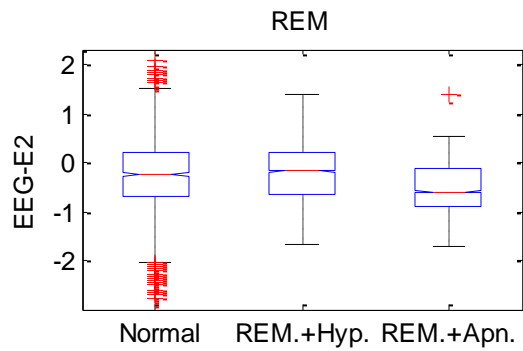
ANOVA Table					
Source	SS	df	MS	F	Prob>F
Groups	2.3629	2	1.18146	3.84	0.0269
Error	18.4394	60	0.30732		
Total	20.8023	62			



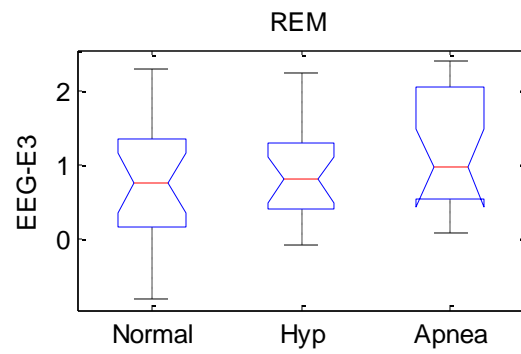
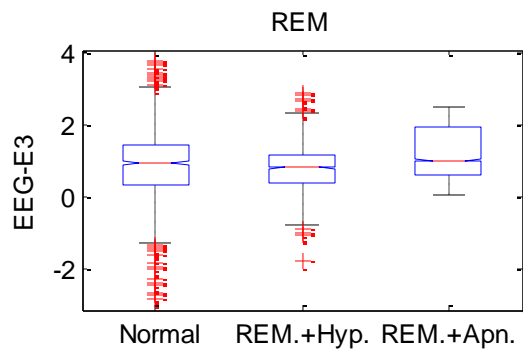
ANOVA Table					
Source	SS	df	MS	F	Prob>F
Groups	4.1171	2	2.05857	4.3	0.018
Error	28.7402	60	0.479		
Total	32.8573	62			



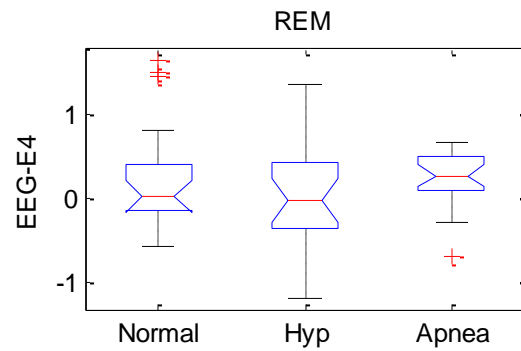
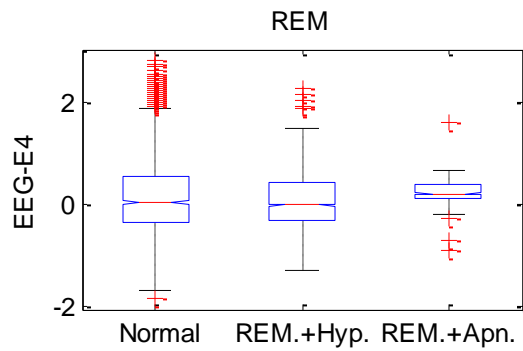
ANOVA Table					
Source	SS	df	MS	F	Prob>F
Groups	0.3683	2	0.18416	0.43	0.6516
Error	25.6136	60	0.42689		
Total	25.982	62			



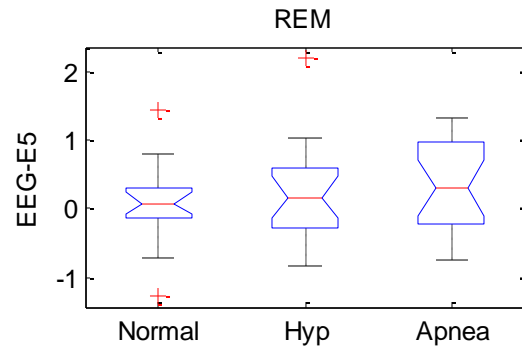
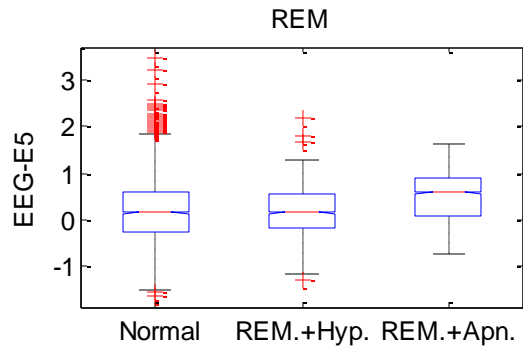
ANOVA Table					
Source	SS	df	MS	F	Prob>F
Groups	1.3529	2	0.67644	1.51	0.2288
Error	26.8469	60	0.44745		
Total	28.1997	62			



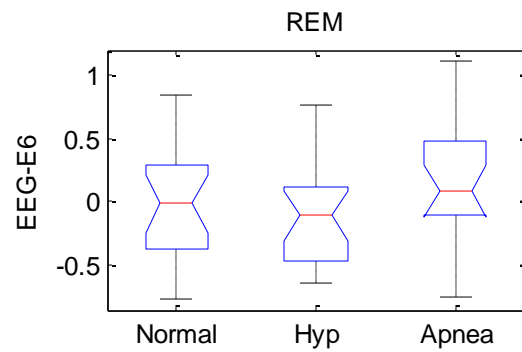
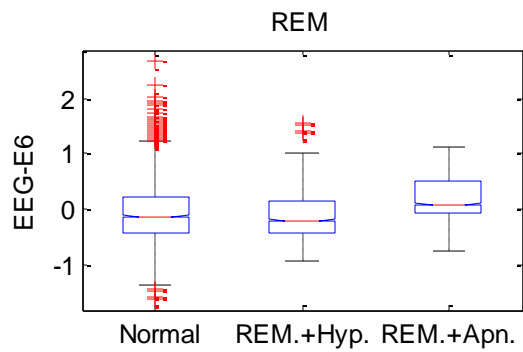
ANOVA Table					
Source	SS	df	MS	F	Prob>F
Groups	2.2616	2	1.13079	1.9	0.1586
Error	35.7288	60	0.59548		
Total	37.9903	62			



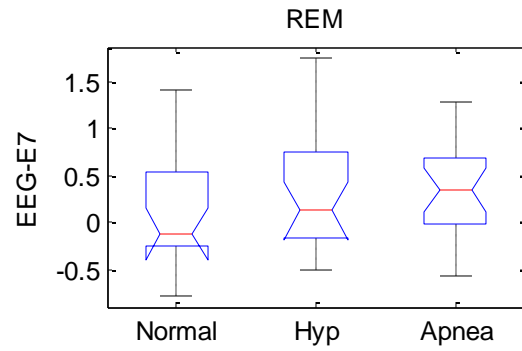
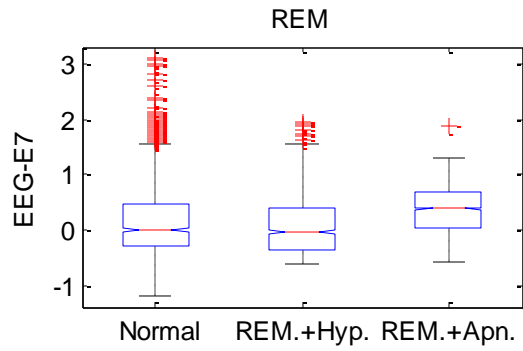
ANOVA Table					
Source	SS	df	MS	F	Prob>F
Groups	0.4125	2	0.20626	0.69	0.5039
Error	17.8519	60	0.29753		
Total	18.2644	62			



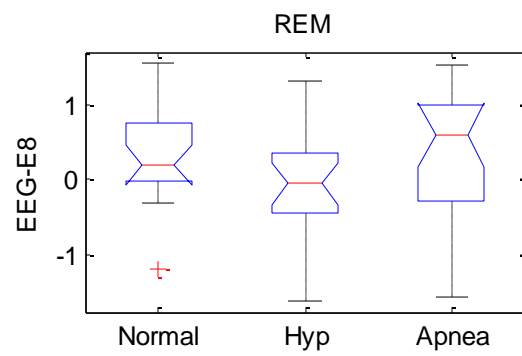
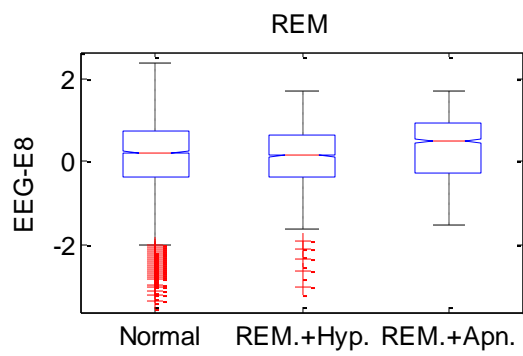
ANOVA Table					
Source	SS	df	MS	F	Prob>F
Groups	0.8623	2	0.43115	1.12	0.332
Error	23.0319	60	0.38387		
Total	23.8942	62			



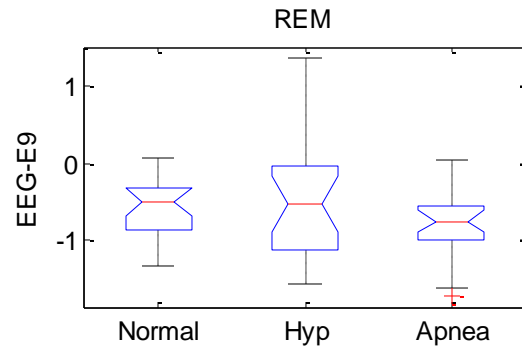
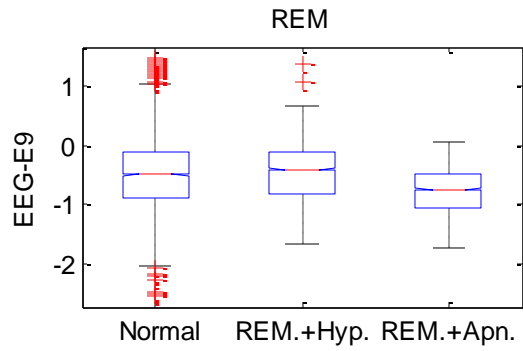
ANOVA Table					
Source	SS	df	MS	F	Prob>F
Groups	1.0881	2	0.54407	2.97	0.0587
Error	10.9769	60	0.18295		
Total	12.0651	62			



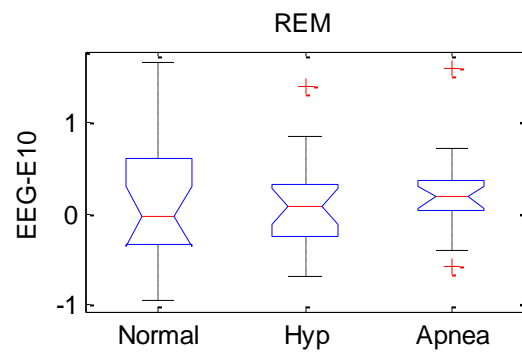
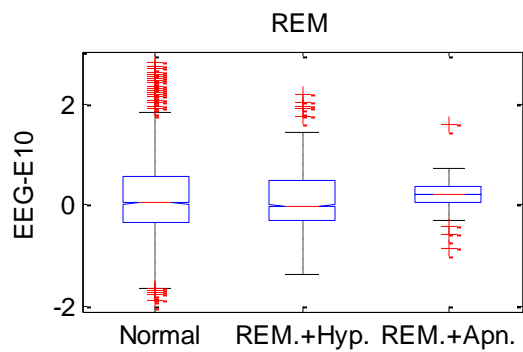
ANOVA Table					
Source	SS	df	MS	F	Prob>F
Groups	0.828	2	0.414	1.37	0.2631
Error	18.1932	60	0.30322		
Total	19.0212	62			



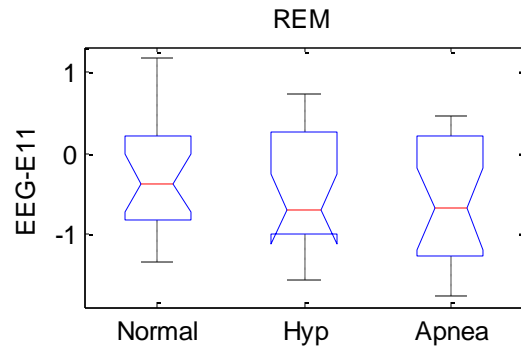
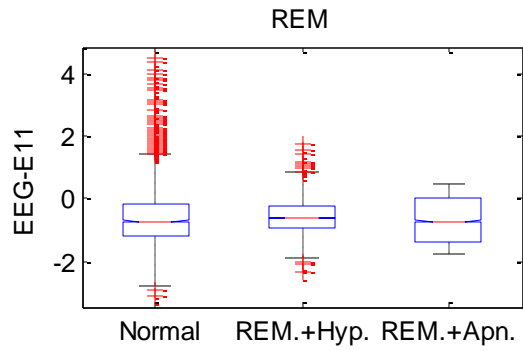
ANOVA Table					
Source	SS	df	MS	F	Prob>F
Groups	1.7089	2	0.85446	1.76	0.181
Error	29.1518	60	0.48586		
Total	30.8607	62			



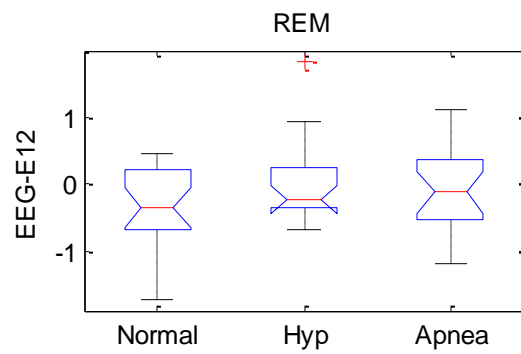
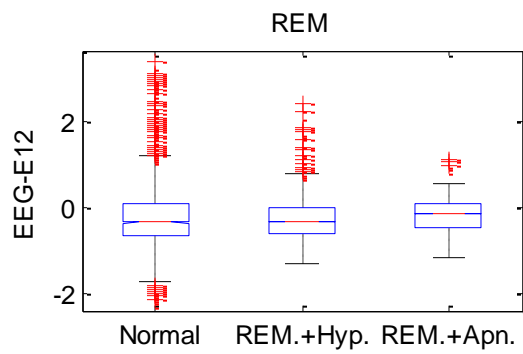
ANOVA Table					
Source	SS	df	MS	F	Prob>F
Groups	0.7846	2	0.39231	1.3	0.2792
Error	18.0596	60	0.30099		
Total	18.8442	62			



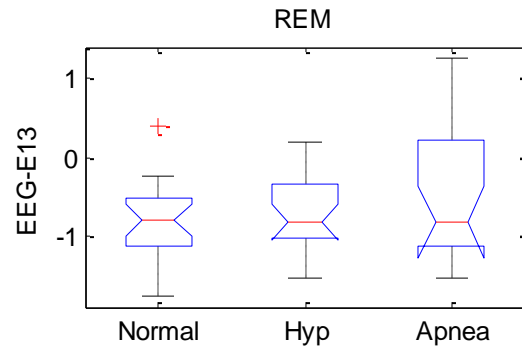
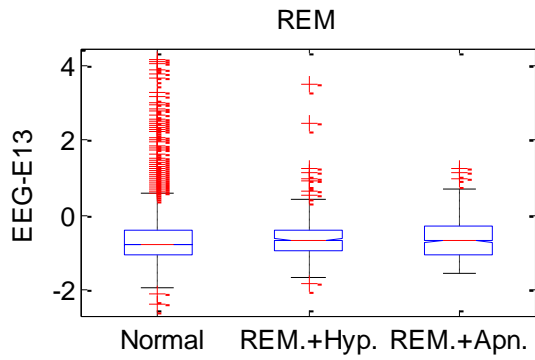
ANOVA Table					
Source	SS	df	MS	F	Prob>F
Groups	0.1842	2	0.09208	0.3	0.7388
Error	18.1614	60	0.30269		
Total	18.3456	62			



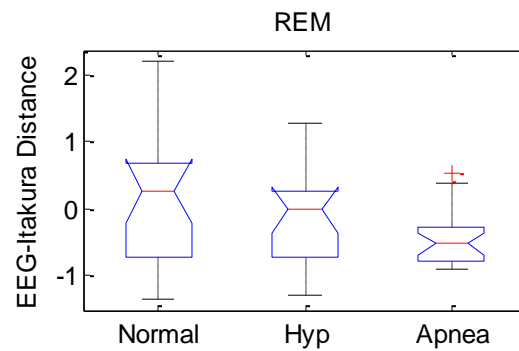
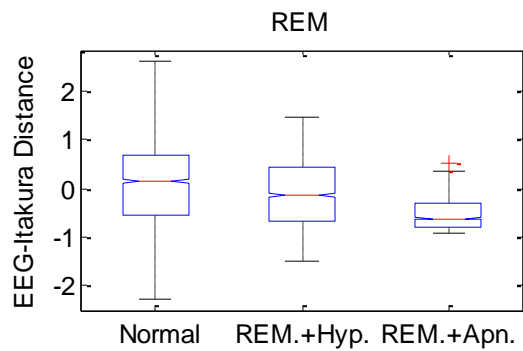
ANOVA Table					
Source	SS	df	MS	F	Prob>F
Groups	0.696	2	0.34798	0.67	0.5133
Error	30.9622	60	0.51604		
Total	31.6581	62			



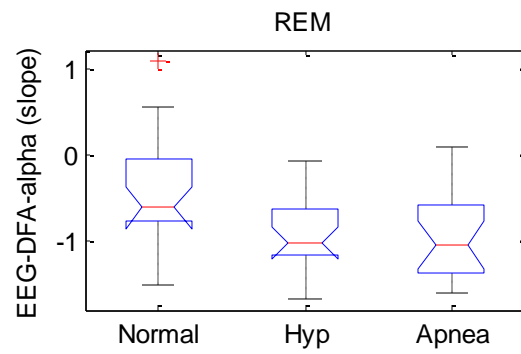
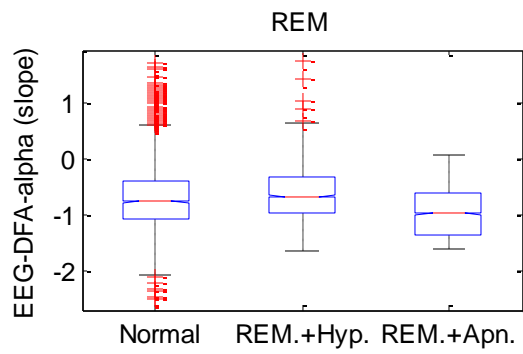
ANOVA Table					
Source	SS	df	MS	F	Prob>F
Groups	1.4323	2	0.71614	1.89	0.1599
Error	22.7338	60	0.3789		
Total	24.1661	62			



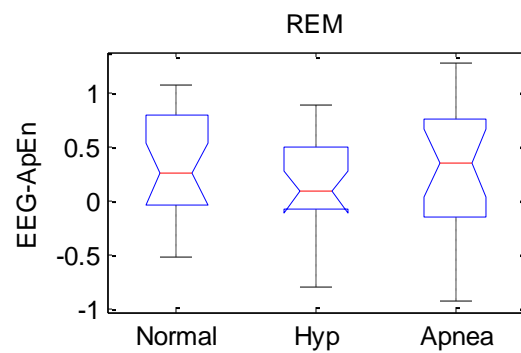
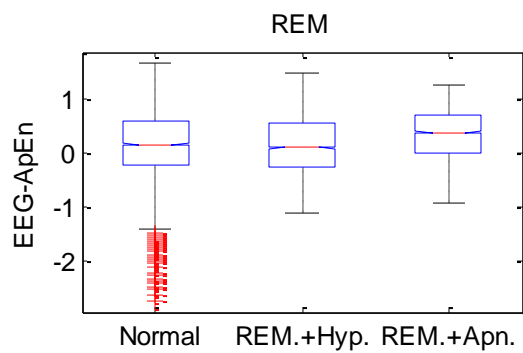
ANOVA Table					
Source	SS	df	MS	F	Prob>F
Groups	1.423	2	0.7115	1.67	0.1971
Error	25.5842	60	0.4264		
Total	27.0072	62			



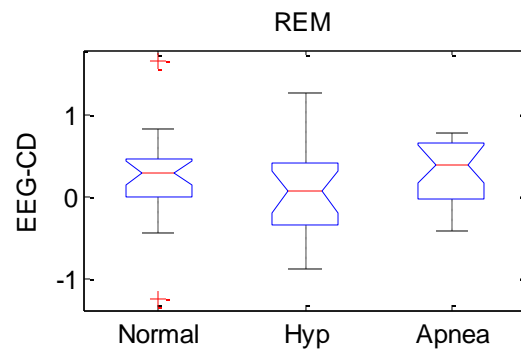
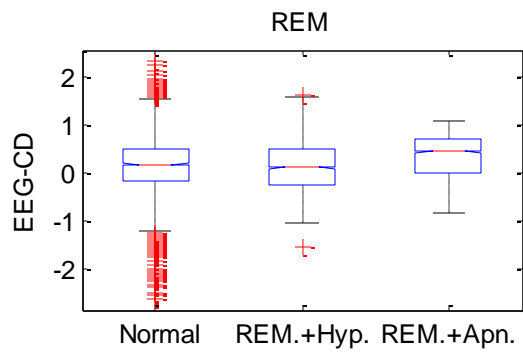
ANOVA Table					
Source	SS	df	MS	F	Prob>F
Groups	2.3601	2	1.18004	2.68	0.0769
Error	26.4441	60	0.44074		
Total	28.8042	62			



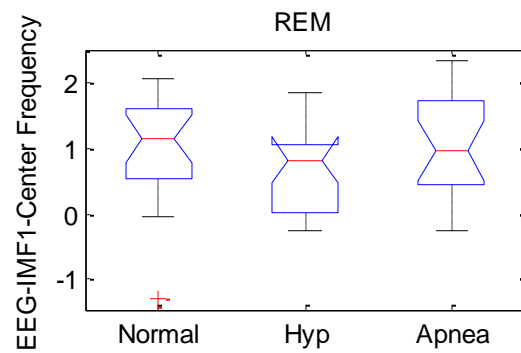
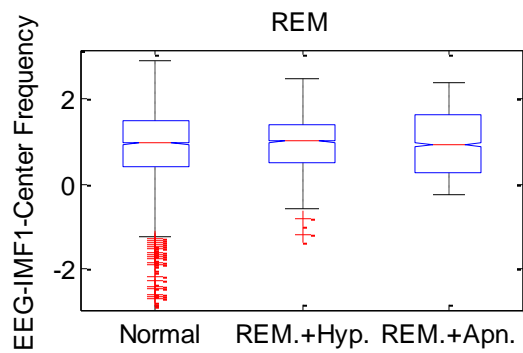
ANOVA Table					
Source	SS	df	MS	F	Prob>F
Groups	3.107	2	1.5535	5.98	0.0043
Error	15.5776	60	0.25963		
Total	18.6846	62			



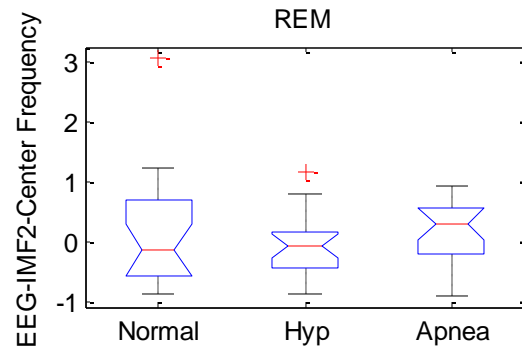
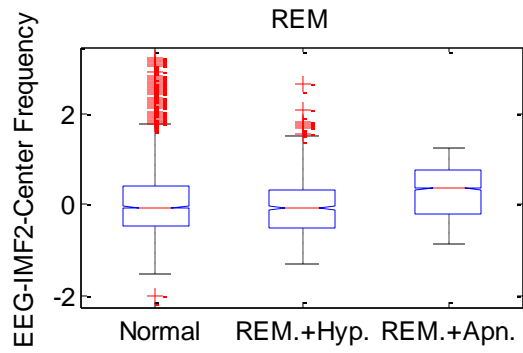
ANOVA Table					
Source	SS	df	MS	F	Prob>F
Groups	0.3471	2	0.17356	0.71	0.4975
Error	14.7434	60	0.24572		
Total	15.0905	62			



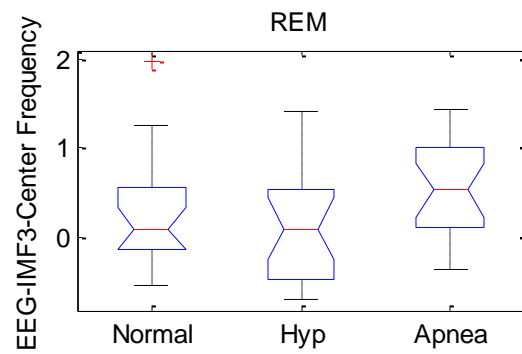
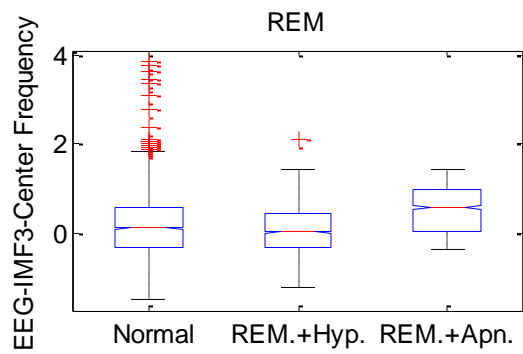
ANOVA Table					
Source	SS	df	MS	F	Prob>F
Groups	0.5449	2	0.27245	1.1	0.3379
Error	14.7966	60	0.24661		
Total	15.3415	62			



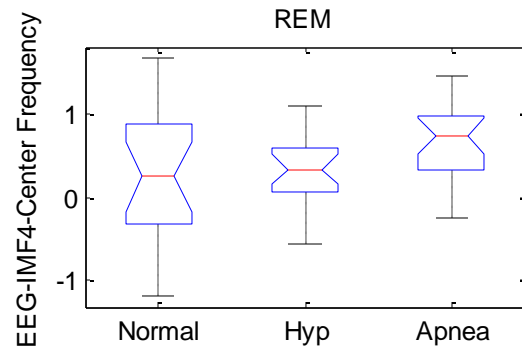
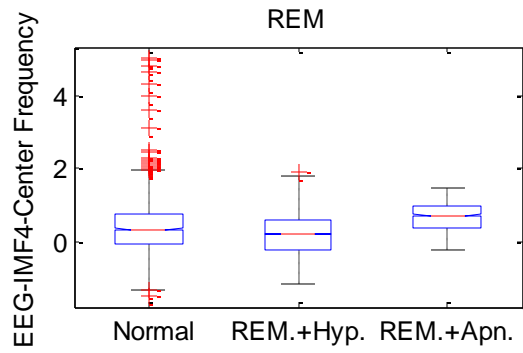
ANOVA Table					
Source	SS	df	MS	F	Prob>F
Groups	1.2453	2	0.62263	1.07	0.3484
Error	34.8123	60	0.5802		
Total	36.0575	62			



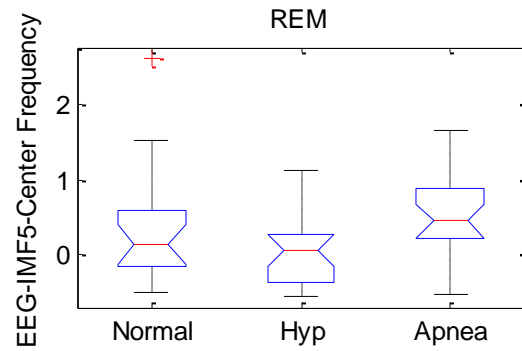
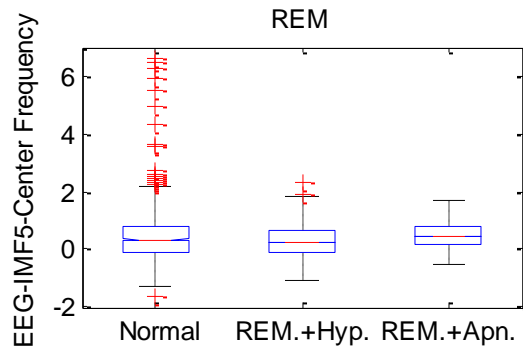
ANOVA Table					
Source	SS	df	MS	F	Prob>F
Groups	0.571	2	0.2855	0.59	0.5588
Error	29.1489	60	0.48581		
Total	29.7199	62			



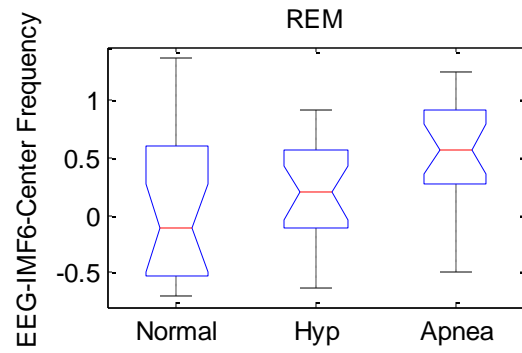
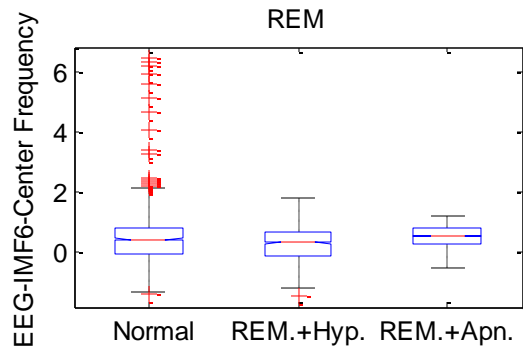
ANOVA Table					
Source	SS	df	MS	F	Prob>F
Groups	1.8355	2	0.91774	2.74	0.0729
Error	20.1218	60	0.33536		
Total	21.9573	62			



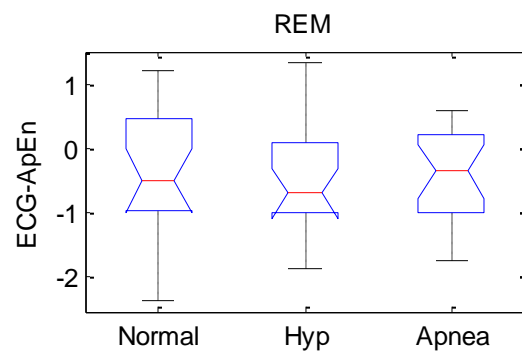
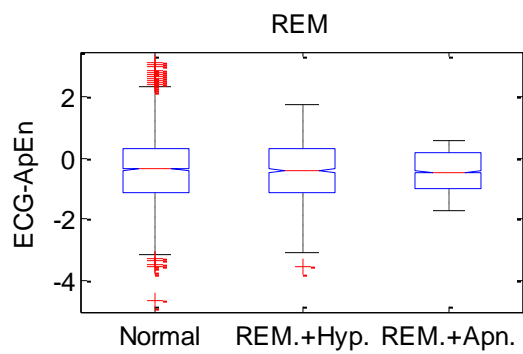
ANOVA Table					
Source	SS	df	MS	F	Prob>F
Groups	2.028	2	1.01401	2.91	0.062
Error	20.8859	60	0.3481		
Total	22.9139	62			



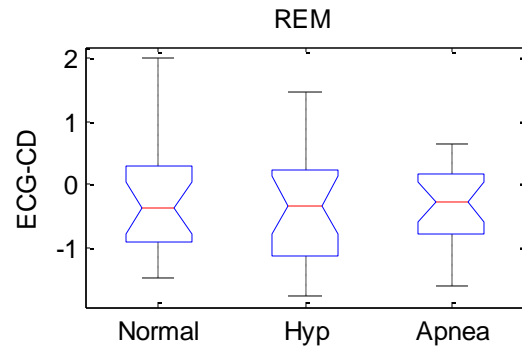
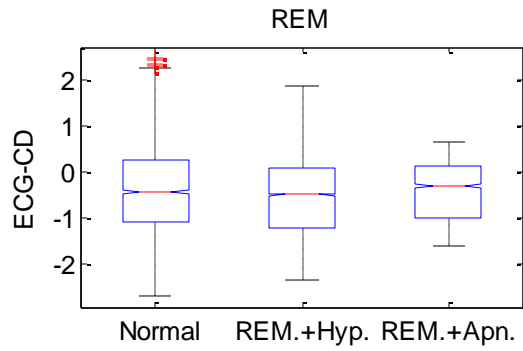
ANOVA Table					
Source	SS	df	MS	F	Prob>F
Groups	2.8167	2	1.40835	3.95	0.0244
Error	21.3719	60	0.3562		
Total	24.1886	62			



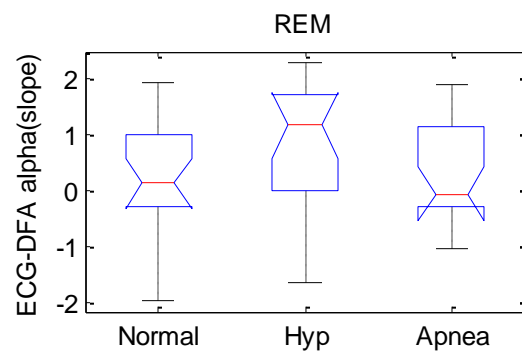
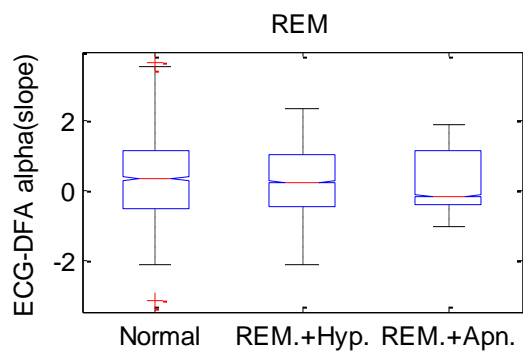
ANOVA Table					
Source	SS	df	MS	F	Prob>F
Groups	2.5529	2	1.27647	4.51	0.015
Error	16.992	60	0.2832		
Total	19.545	62			



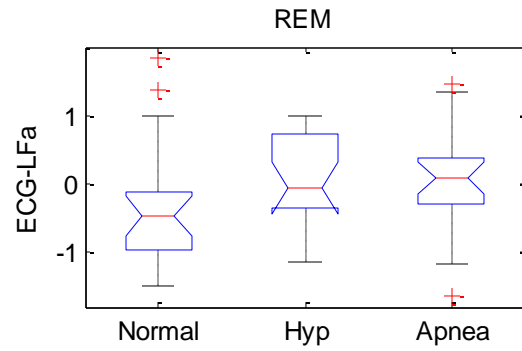
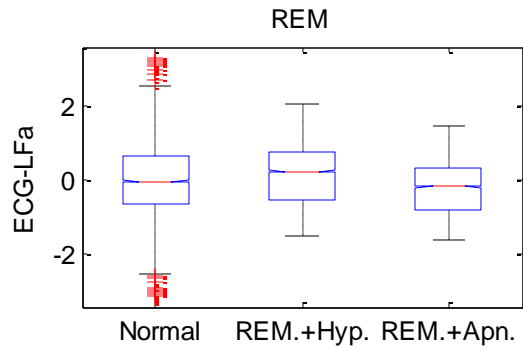
ANOVA Table					
Source	SS	df	MS	F	Prob>F
Groups	0.1606	2	0.0803	0.09	0.9097
Error	50.8412	60	0.84735		
Total	51.0018	62			



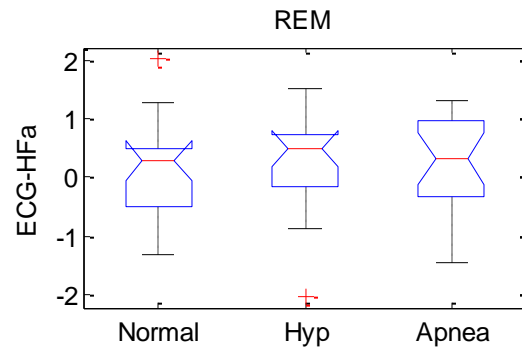
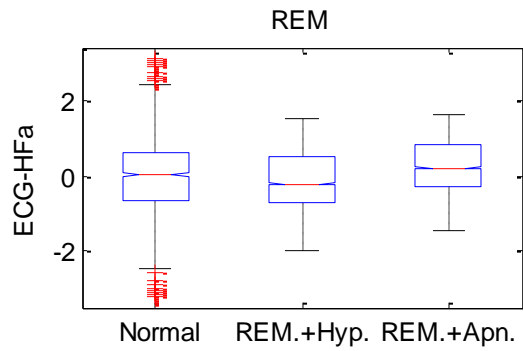
ANOVA Table					
Source	SS	df	MS	F	Prob>F
Groups	0.4227	2	0.21136	0.32	0.7255
Error	39.3028	60	0.65505		
Total	39.7255	62			



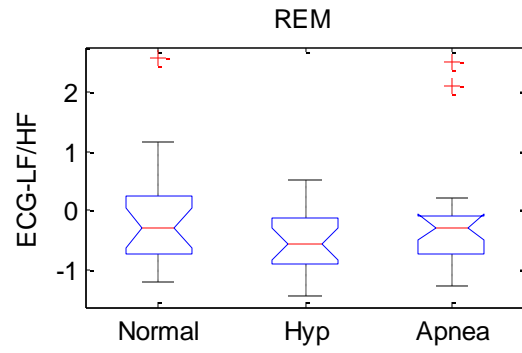
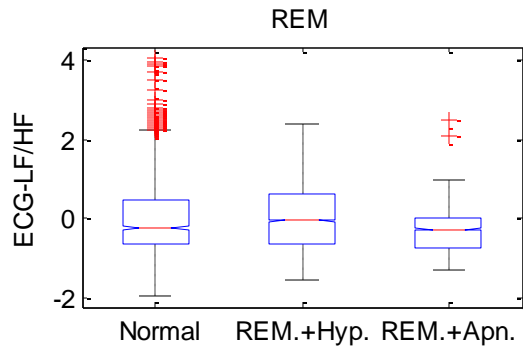
ANOVA Table					
Source	SS	df	MS	F	Prob>F
Groups	4.4877	2	2.24387	2.12	0.1291
Error	63.5399	60	1.059		
Total	68.0276	62			



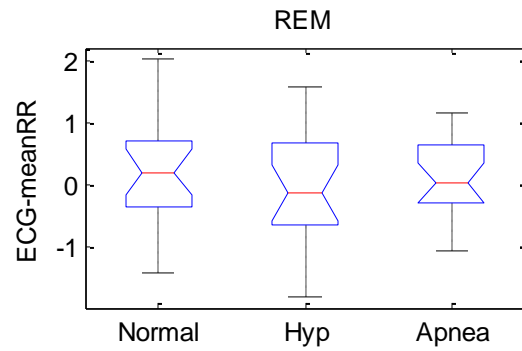
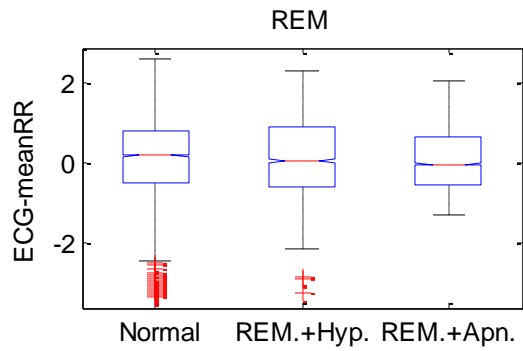
ANOVA Table					
Source	SS	df	MS	F	Prob>F
Groups	2.3485	2	1.17423	1.98	0.1475
Error	35.649	60	0.59415		
Total	37.9975	62			



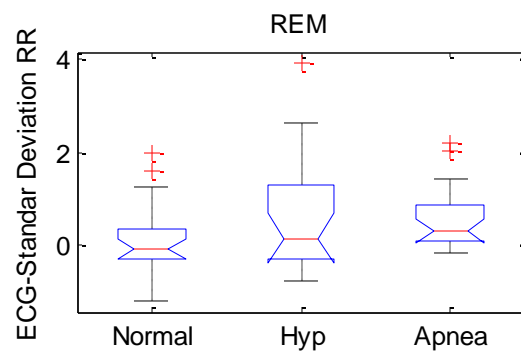
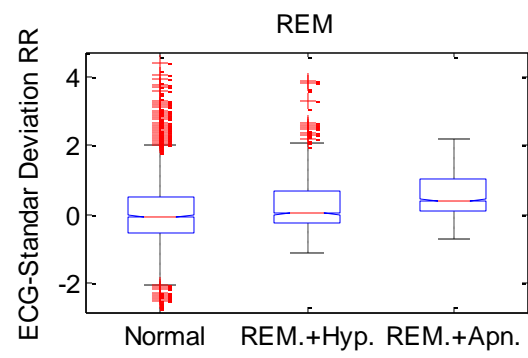
ANOVA Table					
Source	SS	df	MS	F	Prob>F
Groups	2.2654	2	1.1327	1.86	0.1638
Error	36.4516	60	0.60753		
Total	38.717	62			



ANOVA Table					
Source	SS	df	MS	F	Prob>F
Groups	2.4861	2	1.24303	2.06	0.1364
Error	36.2048	60	0.60341		
Total	38.6909	62			



ANOVA Table					
Source	SS	df	MS	F	Prob>F
Groups	0.7926	2	0.39629	0.57	0.5685
Error	41.7032	60	0.69505		
Total	42.4957	62			



ANOVA Table					
Source	SS	df	MS	F	Prob>F
Groups	3.7637	2	1.88183	2.14	0.1261
Error	52.6599	60	0.87767		
Total	56.4236	62			

Vita

Edson Estrada was born on July 8, 1979 in Chihuahua Chihuahua, México. The youngest of four children of Mario Estrada and María Meneses, he finished his undergraduate studies at the Instituto Tecnológico de Chihuahua in 2002 obtaining the title of Electrical Engineer with a minor in Digital Systems. In fall 2002, he moved to the border region of Cd. Juarez and El Paso, Texas and enrolled in Electrical and Computer Engineering where he rapidly got involved in pursuing biomedical engineering and started his research in automatic sleep stage classification and biosignal processing. He received his Master of Science degree in Electrical and Computer Engineering from the University of Texas at El Paso in 2005. In fall 2005 he joined the doctoral program.

While pursuing his degree, Dr. Estrada worked as a doctoral research assistant for the GEAR UP program under the supervision of Juliette Caire. Dr. Estrada has been the recipient of numerous awards such as the Chihuahua's government fellowship, Texas Instrument Foundation fellowship and the CONACYT scholarship. He has presented his research findings at flagship international biomedical and bioengineering conferences such as the 4th International IEEE EMBS Conference on Neural Engineering in Turkey, the 25th Southern Biomedical Engineering Conference in USA and the 20th International Conference on Electronics, Communications and Computers in Puebla, México.

Nowadays, Dr. Estrada is working as a full time professor at the Universidad Autónoma de Ciudad Juárez in the Institute of Biomedical Sciences. In his short term plans he intends to pursue a postdoctoral fellowship at an internationally reputable biomedical engineering program.

Permanent address: 14512 Las Palomas Dr. El Paso, TX 79928

This dissertation was typed by Edson Fco. Estrada Meneses